4-2-2015

Function and Regulation of the Postsynaptic Exchange Factor, Kalirin-7

Megan B. Miller
University of Connecticut, miller.meganb@gmail.com

Function and Regulation of the Postsynaptic Exchange Factor, Kalirin-7

Megan B. Miller, Ph.D.

University of Connecticut, 2015

Abstract

Through studies of a single RhoGEF, Kalirin-7, the work presented herein provides insight into several of the key mechanisms underlying postsynaptic neurotransmission in the central nervous system. Much of this work has focused on the significance of non-enzymatic functions of Kal7, highlighting the importance of spatial and temporal control of multi-domain proteins and the postsynaptic protein/ lipid interactome. Our work on *Kalrn* promoter usage and phosphorylation (Chapters 5 & 6) expands upon our understanding of synaptic protein diversity and regulation. Additionally, *Kalrn* promoter switching has implications for the poorly-understood mechanisms by which cytoskeletal dynamics and membrane trafficking are coordinated at the postsynaptic density (PSD). Combined with our biochemical characterization of the Sec14 domain (Chapter 4), our exploration of *Kalrn* promoter usage also touches upon the importance of synaptic lipid metabolism. Thus, by enhancing our knowledge of the functions and regulatory mechanisms of Kal7, we highlight the extraordinary intricacies of postsynaptic signaling and the necessity for precise control of multiple cellular events. Furthermore, we provide a large body of evidence to support the notion that large, multi-domain proteins serve diverse roles at the synapse, which are crucial for normal brain function.

Function and Regulation of the Postsynaptic Exchange Factor, Kalirin-7

Megan Bridget Miller

B.S., The Ohio State University, 2005

Ph.D., University of Connecticut, 2015

A Dissertation

Submitted in Partial Fulfillment of the

Requirements for the Degree of

Doctor of Philosophy

at the

University of Connecticut

2015

APPROVAL PAGE

Doctor of Philosophy Dissertation

Function and Regulation of the Postsynaptic Exchange Factor, Kalirin-7

Presented by:

Megan B. Miller, B.S., Ph.D.

Major Advisor _____
Betty A. Eipper, Ph.D.

Associate Advisor _____
Kimberly L. Dodge-Kafka, Ph.D.

Associate Advisor _____
Eric S. Levine, Ph.D.

Associate Advisor _____
Richard E. Mains, Ph.D.

University of Connecticut

2015

Acknowledgments

First and foremost, I would like to thank my outstanding thesis advisors, Dr. Betty Eipper and Dr. Richard Mains. They have shown me unrivaled support and guidance every step of the way, while still allowing me to pursue my own intellectual curiosities. Looking back, I think one of the greatest lessons they have taught me is the value of an open-minded and enthusiastic approach to science. One would be hard-pressed to find two people who love what they do more than Dick and Betty. In addition to being excellent scientists, Dick and Betty are also model mentors. Their dedication to the well-being and career development of their trainees is apparent. Because of them, I feel confident in my ability to pursue interesting questions with the highest level of integrity, and for that I am beyond appreciative.

I must also thank all of the other members of my lab for their support and comradery along the way. I feel extremely fortunate to have been a part of such a positive and enriching group. I would especially like to thank Yanping Wang and Darlene D'Amato for their incredible technical support and Dr. K.S. Vishwanatha who was integral to the biophysical studies presented in this dissertation. I would also like to thank my thesis committee members, Dr. Levine and Dr. Dodge-Kafka, for their honest feedback over the years. Thanks also to Dr. Yi Wu and the people at the KECK Neuroproteomics facility at Yale for their continued support and ongoing collaborations.

Of course none of this would have been possible without the UConn Health Center Biomedical Science PhD program, the Graduate Programs Committee, the Department of Neuroscience and graduate program and all of the individuals who work so hard to assure an

excellent educational experience for students. In particular, I would like to thank Dr. Barbara Kream, Stephanie Rauch, Swapna Das and Jody Gridley for their laudable dedication.

Finally, I thank all of my friends and family for their immeasurable support and understanding over the years. To my parents, Mark and Lou Miller: I would have never had the courage to pursue this degree if it were not for the lifetime of unwavering support I have received from you. It was you who first instilled in me the value of hard work, and you have never discouraged me from chasing outlandish dreams. I owe this and all future success to you. To my sister (brother) Molly, thanks for reminding me to see the humor in life when I get too serious. You will never know how much our silly conversations or absurd brotherly memories have meant to my sanity. And lastly, to my extraordinary fiancé, Giulio Chiuini: I honestly could not have done this without you. From late-night study snacks and gentle reminders to eat vegetables to nearly constant words of encouragement and an all-too-frequent shoulder to cry on, you were ALWAYS there for me. The level support you consistently show me is beyond selfless, and I truly hope that I can somehow begin to return the favor. Words cannot begin to describe how eternally grateful I am to have you in my life. From the bottom of my heart: thank you and I love you.

Table of Contents

Chapter 1:

Introduction

The majority of excitatory synapses in the mammalian forebrain occur on micron-sized dendritic protrusions called dendritic spines (1). A single spine typically receives synaptic input from only one axon terminal, and most mature spines contain localized translation machinery as well as endocytic pathway components, making them somewhat autonomous compartments capable of rapid and localized responses to synaptic events (2).

A hallmark of dendritic spines is their ability to undergo rapid morphological alterations in response to synaptic activity (**Fig. 1-1**). Long-term potentiation (LTP) and synaptic strengthening promote spine volume increases, which are apparent within seconds and can be maintained for hours. Likewise, long-term depression (LTD) results in robust and sustained spine shrinkage (3-5). Spine size is correlated with presynaptic active zone area and post-synaptic density (PSD) size, as well as surface AMPA receptor expression, further suggesting a cooperative relationship between spine morphology and synaptic function (6). Lifelong spine turnover and activity-dependent morphological changes are collectively referred to as structural plasticity, a phenomenon thought to be the central cellular mechanism underlying learning and memory (7,8).

Aberrant spine number and/or morphology have been associated with myriad neurological and psychiatric disorders (7,9-15). Reduced spine density is observed in the prefrontal cortex of schizophrenia patients (10,15) and in affected brain regions of human patients and animal models of epilepsy (16). Early stages of Alzheimer's disease are associated with spine loss (17), whereas increased spine density has been reported in the nucleus accumbens following chronic drug administration (18). A number of neurodevelopmental disorders are associated with genetic disruptions in genes which are known to contribute to spine development and maintenance. Fragile X syndrome (FXS) results from altered

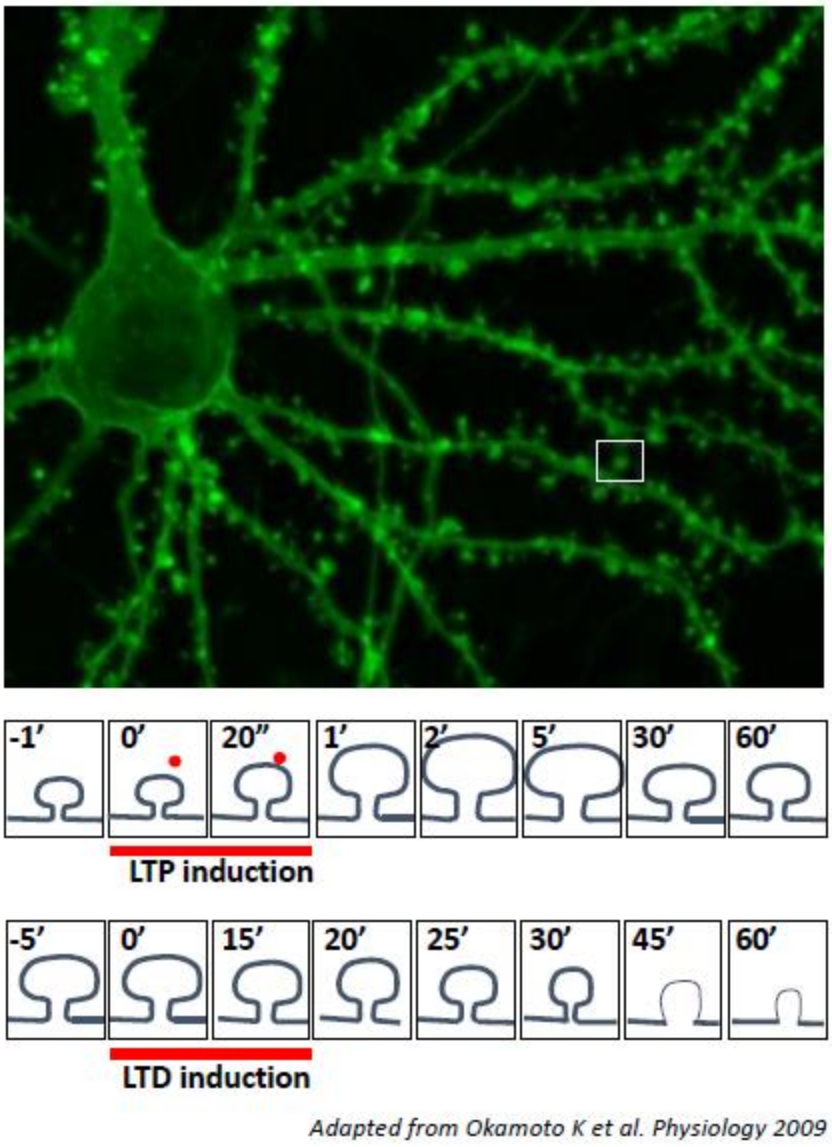

Figure 1-1. Changes in synaptic activity are correlated with rapid morphological alterations of dendritic spines. Top: A rat hippocampal neuron transfected with a membrane-targeted GFP (farnesylated-GFP) to highlight dendritic spine morphology (white box). Bottom: schematic illustrating rapid structural changes in response to induction of long-term synaptic potentiation (LTP; red dots = 2-photon glutamate uncaging onto single dendritic spine) or long-term depression (LTD; low frequency stimulation). Cartoon adapted from (5).

expression of Fragile-X mental retardation protein (FMRP), which is involved in regulating local protein synthesis within dendritic spines (19). Indeed, FSX is characterized by an overall decline in spine number, and a heightened proportion of the existing spines resemble immature filopodia and lack synaptic contacts.

Spine dynamics are controlled by RhoGTPases and their regulators

Structural plasticity of dendritic spines is mediated by rapid changes to the actin cytoskeleton (20), which are required for functional plasticity (LTP and LTD) (4,21,22). The mechanisms regulating actin dynamics are incredibly complex, but members of the Rho family of GTPases play a key roles in the process. RhoGTPases are small GTP binding proteins which cycle between an enzymatically active GTP-bound state and an inactive GDP-bound state. In spines, RhoGTPases serve as critical relays between synaptic activity and intracellular signaling events. Their numerous and diverse effectors control many biological processes, including cytoskeletal remodeling, gene transcription, and membrane trafficking (23-30). As such, RhoGTPases and their regulators are essential mediators of structural and functional plasticity. Activation of RhoGTPases is driven by guanine nucleotide exchange factors (RhoGEFs), which catalyze GDP/GTP exchange. Within spines, there are at least 10 RhoGEFs for only 4 RhoGTPases (31), alluding to the importance of tight cellular control of these proteins.

The Rho family GEFs are large, multidomain proteins which contribute to numerous cell signaling pathways. Interestingly, most RhoGEFs act downstream of multiple receptors, and synaptic transmission requires activation of multiple GEFs. Though some RhoGEFs have overlapping functions, differences in cellular, subcellular and developmental expression suggest discrete roles in cellular function. Furthermore, proper expression and function of multiple neuronal RhoGEFs is necessary for normal spine formation and synaptic function (31-35). The significance of highly converging GEF activity is not yet understood, however it is apparent that normal synapse development and plasticity requires tight spatial and temporal control of RhoGTPase activity, and attention in the field has turned

toward elucidating the complexities of how these diverse molecules cooperate to establish the anatomical substrate of synaptic plasticity.

The postsynaptic RhoGEF, Kalirin-7

Kalirin-7 (Kal7) is a neuronal RhoGEF which is highly expressed in the adult brain, where it plays a critical role in the formation and maintenance of dendritic spines (36-40). Kal7 is comprised of multiple functional domains (**Fig. 1-2**). An N-terminal, lipid-binding Sec14 domain is followed by 9 spectrin repeats, which engage in multiple protein interactions. Tandem Dbl and pleckstrin homology domains (DH, PH) make up the GEF module and contribute to the protein's enzymatic activity. The C-terminal PDZ binding motif interacts with PDZ-containing proteins, including the major postsynaptic scaffold, PSD95. Kal7 acts downstream of multiple synaptic receptors, including EphB receptors, GluN2B-containing NMDA receptors, TrkB, 5-HT2A and others (33,41-48). These studies suggest that Kal7 may serve as a crucial postsynaptic "signaling hub"; a notion which is supported by the identification of at least 20 phosphorylation sites in Kal7 isolated from rat brain (49). A Kal7 knockout ($Kal7^{KO}$) mouse line has greatly expanded our knowledge of Kal7 function. Behaviorally, $Kal7^{KO}$ animals exhibit decreased anxiety-like behavior, impaired contextual fear learning, and disrupted synaptic function (33,36,50,51). Spine density is decreased in the hippocampus of Kal7 knockout ($Kal7^{KO}$) mice, and overexpression of Kal7 in hippocampal cultures induces spine and synapse formation, even in aspiny interneurons (36,37). Chronic cocaine administration causes increased Kal7 expression, and the ability of cocaine to increase spine size and density in the mouse nucleus accumbens requires Kal7 (51). In humans, Kalirin is implicated in a number of neurological disorders characterized by aberrant spine morphology and cognitive dysfunction. Kal7 directly interacts with DISC1 (disrupted in schizophrenia) (52) and HAP1 (Huntington Associated Protein 1)(53). Genome-wide association studies link human *KALRN* to schizophrenia, ADHD, and stroke (54-57), and reduced Kalirin mRNA and protein levels were

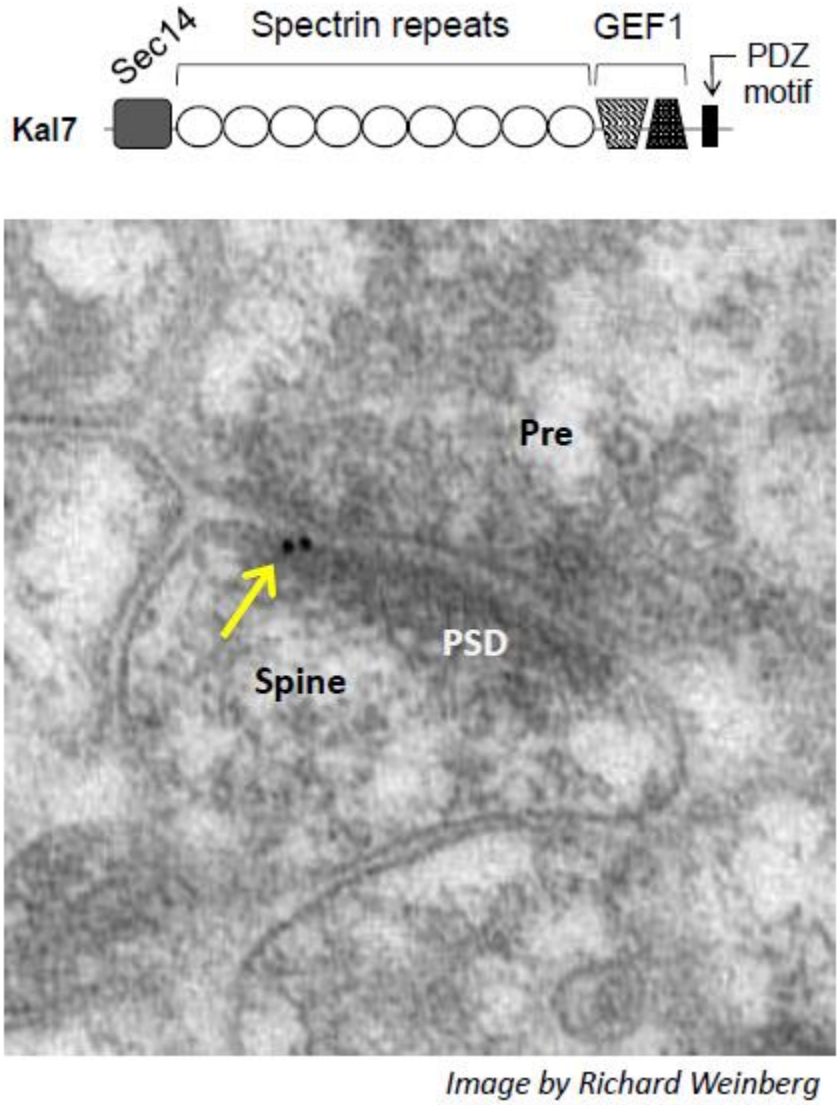

Figure 1-2. Kalirin-7 is a neuronal RhoGEF which localizes to the postsynaptic density. Top: schematic of the protein domains of Kalirin-7. Bottom: Electron micrograph through a presynaptic terminal (Pre) apposed to a dendritic spine. Yellow arrow indicates immuno-gold labeled Kal7 at the postsynaptic density (PSD). Image courtesy of our collaborator, Richard Weinberg, University of North Carolina, Chapel Hill.

found in postmortem brains of patients with schizophrenia and Alzheimer's disease (58,59). The role of Kal7 and other RhoGEFs in synaptic function is discussed in further detail in Chapter 2.

While its importance in synaptic signaling is clear, the molecular mechanisms underlying Kal7 function at the PSD are incompletely understood. Reported here are the results of our efforts to elucidate these mechanisms, focusing on protein localization, regulation of GEF activity and non-enzymatic functions.

Chapter 2

Rho GEFs in synaptic physiology and behavior

Miller MB*, Yan Y*, Eipper BA, Mains RE.

This chapter was published as a literature review in The Neuroscientist. 2013 Jun;19(3):255-73.

*Authors contributed equally

Abstract

In the mammalian brain the majority of excitatory synapses are housed in micron-sized dendritic protrusions called spines, which can undergo rapid changes in shape and number in response to increased or decreased synaptic activity. These dynamic alterations in dendritic spines require precise control of the actin cytoskeleton. Within spines, multidomain Rho guanine nucleotide exchange factors (Rho GEFs) coordinate activation of their target Rho GTPases by a variety of pathways. In this review, we focus on the handful of disease-related Rho GEFs (Kalirin; Trio; Tiam1; P-Rex1,2; RasGRF1,2; Collybistin) localized at synapses and known to affect electrophysiology, spine morphology, and animal behavior. The goal is to integrate structure/function studies with measurements of synaptic function and behavioral phenotypes in animal models.

Introduction

Rho family GTPases play essential roles in regulating the complex adjustments to the actin cytoskeleton that underlie structural plasticity in dendritic spines, making the enzymes that regulate them a critical relay system for integrating synaptic activity and intracellular signaling. Rho guanine nucleotide exchange factors (Rho GEFs) catalyze GDP/GTP exchange while Rho GTPase activating proteins (Rho GAPs) accelerate GTP hydrolysis.

The synaptic Rho GEFs are multidomain proteins capable of responding to inputs from several signaling pathways and affecting an array of downstream targets. Proper expression and function of multiple Rho GEFs is necessary for spine formation and synaptic function. While their ability to activate Rho proteins with spatial and temporal precision is critical, the unique ability of the other domains to localize the protein, interact with specific ion channels and respond to intracellular signaling proteins makes the role of each Rho GEF distinct.

A number of recent reviews provide comprehensive summaries of the many Rho GEFs with Dbl homology (DH) domains (11,27,31,60-65). We focus here on the handful of Rho GEFs known to affect behavior and synaptic function. Structurally related Rho GEFs are discussed together, with the goal of integrating structure/function studies with measurements of synaptic function and behavior.

Dual Rho GEFs (Kalirin and Trio)

Discovery and expression

Trio was first identified as an interactor with the cytosolic domain of LAR, a receptor protein tyrosine phosphatase localized to focal adhesions (66). Kalirin was first identified as an interactor with the cytosolic domain of peptidylglycine α-amidating monooxygenase, a secretory granule membrane protein (67). The proteins are 64% identical (rat Kalirin vs. rat Trio; AF232669.1 vs. XP_003753588.1) (68) and, discovered under different circumstances, would likely have been referred to as Trio- or Kalirin-1 and -2. Trio and Kalirin are notable for the presence of two Rho GEF domains of differing specificity along with a Ser/Thr kinase and multiple additional protein-protein interaction domains (**Fig. 2-1**). A single common ancestor is found in *Drosophila* (*dTrio*) and in *C.elegans* (*unc-73*). The *Drosophila* protein is 42-43% identical to both rodent Kalirin and Trio; comparisons to Unc-73 also lead to the conclusion that *Kalrn* and *Trio* arose from duplication of a common ancestor.

Kalirin and Trio are both widely expressed in the brain, primarily localized to neurons at all stages of development (39,69,70). Analysis of *dTrio* mutants highlighted its role in axon formation and

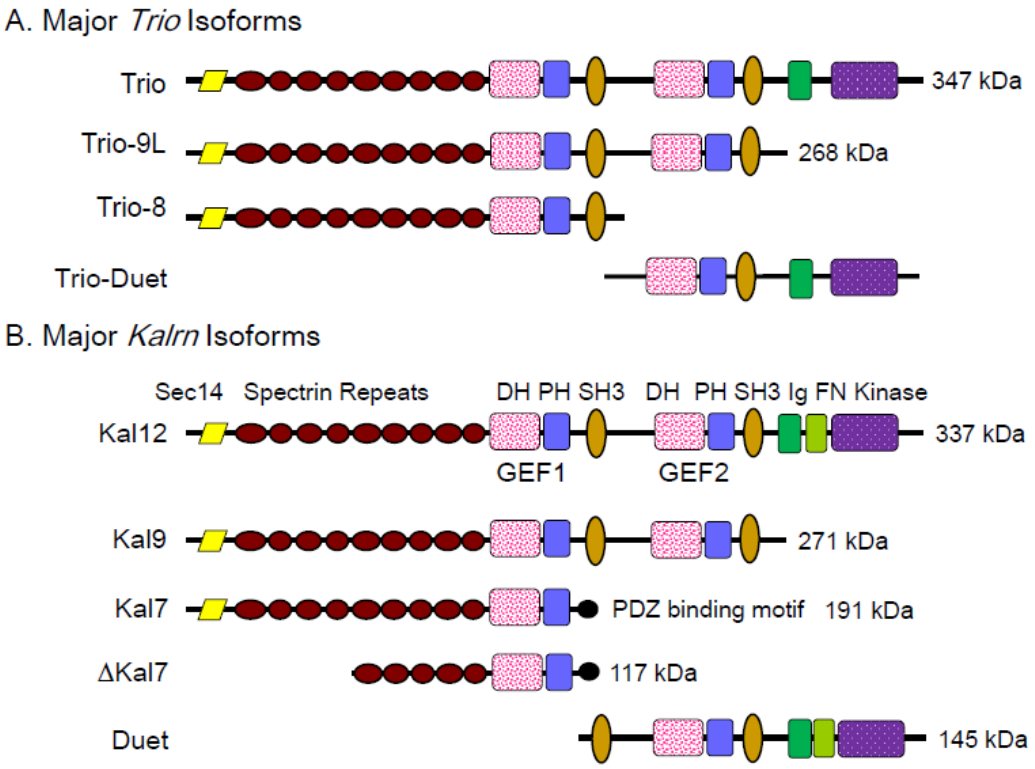

Figure 2-1. Splice Variants of Kalirin and Trio. Structural features identified in Kalirin and Trio are drawn to scale; the molecular weights of the intact proteins are indicated. Mouse *Kalrn* is on chromosome 16 and human *KALRN* is on chromosome 3. Mouse *Trio* is on chromosome 15 and human *TRIO* on chromosome 5. Only the major adult isoforms of Kalirin and Trio, which arise from alternate splicing, are shown. Some of the isoforms are very tissue-specific; Kal7 is expressed exclusively in neurons and Trio-Duet is primarily a cerebellar product, absent from cerebral cortex (71). Abbreviations used throughout all figures are: DH, Dbl-homology; PH, pleckstrin homology; SH3, Src3 homology; Ig, immunoglobulin-like; FN, fibronectin-like; PDZ-BD, PDZ binding motif.

pathfinding (72-74) Trio is most importantly expressed in cerebellar granule cells, while Kalirin is most highly expressed in long projection neurons in the cortex and hippocampus, with less expression in the cerebellum and brainstem. The developmental expression patterns of both genes are isoform- and region-specific. Expression of *Kalrn* and *Trio* is regulated independently; for example, compensatory increases in *Trio* expression have not been observed in *Kalrn* knockout mice (36).

Importantly, both genes are also expressed outside of the nervous system. Kalirin, primarily the Kal9 isoform (**Fig. 2-1A**), is expressed early in development in a wide variety of tissues throughout the body (40), primarily lung, muscle, GI epithelium and pancreas. In the adult, Kal7 is the major form in mature neurons, while Kal9 and Kal12 are found at lower levels in aorta, skeletal muscle and endocrine tissues. Kal7 is primarily expressed in postsynaptic structures such as dendritic spines, while Kal12 is especially elevated in growth cones (75) (**Fig. 2-2A**). Expression of Kal7 correlates with the onset of synaptogenesis in the cortex.

Protein structure and signaling

Both genes undergo extensive alternative splicing, yielding functionally distinct isoforms ranging from about 100 kDa to nearly 400 kDa in size (**Fig. 2-1**). For both Kalirin and Trio, GEF1 activates Rac1 and RhoG, while GEF2 activates RhoA; splice variants that include only one or the other GEF domain have been identified. Notably, the kinase domain encoded by *Kalrn* and *Trio* is absent from *dTrio* and *unc-73.* Both the Sec14 domain of Kalirin, which binds specific phosphoinositides, and its nine spectrin repeats play essential roles in its function (76). The spectrin repeat region, SH3 domains and Ig/FN domains of Kalirin and Trio interact with a wide variety of proteins including iNOS, DISC1, Arf6, afadin, PAM, and HAP1.

Recombinant Kal7 is phosphorylated by several of the protein kinases concentrated at the PSD; consistent with this, Kal7 isolated from rat brain is heavily phosphorylated (49). Several sites in Kalirin are targeted by multiple protein kinases (e.g. protein kinase A, protein kinase C, CaMKII and CKII),

leading to the suggestion that Kalirin participates in signaling pathways initiated by a variety of pathways (41,49).

Detailed examination of mutations in *unc-73* established a role for its first GEF domain in neuronal development (77) and a role for its second GEF domain in adult neuronal function (77-79). In *D. melanogaster*, a similar picture emerges; the N-terminal half of *dTrio*, which includes GEF1, is crucial to neurite outgrowth (73,74,80), while neuromuscular junction establishment and function require the GEF2 region (81,82). Liprin, a cytoplasmic binding partner of LAR, is thought to act through *dTrio* to promote correct targeting of axons, while retrograde BMP signaling from muscle to the nerve terminal acts through *dTrio* to regulate synapse development (81,82). Expression of BMP in muscle increases dTrio expression in motorneurons quite dramatically (82).

The GEF2 domain of Trio and Kalirin shares with p63RhoGEF the ability to bind to and be activated by $G\alpha_q$, placing these RhoGEFs downstream of selected G protein coupled receptors (83,84). Trio and $G\alpha_q$ co-immunoprecipitate when co-expressed in hEK293 cells (77). Acetylcholine acting through a muscarinic receptor to activate $G\alpha_q$ results in increased sphingosine kinase activation and increased levels of sphingosine-1-P in the presynaptic terminal, potentially activating Trio or Kalirin GEF2 at the same time and increasing neurotransmitter release (77-79).

Behavior

The $Trio^{-/-}$ mouse dies in late gestation (85) with spherical myofibers and major defects in secondary myogenesis. Subsequent work (86) revealed defective neuronal outgrowth, complete lack of the anterior commissure and defects in the internal capsule and corpus callosum. These defects reflect loss of the interaction of Trio with the netrin-1 receptor, Deleted in Colon Cancer (DCC), which is essential for normal Rac1 activation in axonal projections. Because of the lethality of the global $Trio^{-/-}$ knockout, cell-type specific knockouts using Cre recombinase expression driven by the nestin or GFAP promoter were created (70). Only 10% of $Trio^{nestin\text{-}KO}$ mice survived for a day; they lacked a cerebellum,

were severely ataxic and all died within 3 weeks without ever gaining significant weight. In contrast, $Trio^{GFAP\text{-}KO}$ mice appeared unaffected. Southern blot analysis demonstrated complete excision of the floxed allele in brain tissue from $Trio^{nestin\text{-}KO}$ mice (70), consistent with early expression of nestin-Cre and elimination of Trio expression in glial, as well as neuronal, lineages.

Knockout of one copy of *dTrio* results in >50% decrease in Rac1-dependent synaptic bouton numbers (82). Rac1 overexpression increases the quantal content of neuromuscular junction excitatory junction potentials (EJP), with no change in the unitary size of the quanta (82) (**Fig. 2-2B**). Likewise *dTrio* knockout decreased the quantal content of EJPs, and the EJP enhancement seen with Rac1 overexpression was largely blocked in the *dTrio* knockout. Interestingly, bone morphogenic protein (BMP) from the muscle is required for normal *dTrio* expression in the innervating neuron, and decreasing *dTrio* expression directly (as in *trio*/+ flies) or indirectly (BMP lowered) results in reduced neuromuscular junction growth; expression of *dTrio* in motorneurons, but not in the muscle, reverses the deficit. The interpretation is that the level of expression of neuronal *dTrio*, and consequent activation of Rac1, directly correlates with the size of the presynaptic terminal and thus the quantal content of the EJPs (82).

Two approaches were used to generate mouse models lacking all of the major *Kalrn* isoforms ($KalGEF1^{KO}$ and $KalSR^{KO}$) (87,88) and Kal7 was specifically targeted in another model ($Kal7^{KO}$) (36); each yielded viable homozygous knockout mice. In $KalGEF1^{KO}$ and $Kal7^{KO}$ mice, the density of hippocampal dendritic spines is decreased compared to normal (36,88). Cortical cultures prepared from $Kal7^{KO}$ mice showed almost a 50% decrease in synaptic density; in addition, Vglut1-positive puncta that were not apposed to a PSD-95 positive postsynaptic ending were observed commonly in $Kal7^{KO}$ cultures but only rarely in wildtype neurons, suggesting a role for Kal7 in synaptic maturation (36).

Although lack of Rac1 and RhoG activation in the $Kal7^{KO}$ neurons plays a major role (89), loss of other protein-protein interactions is also of importance. The first PH domain of Kalirin interacts with the juxtamembrane region connecting the final transmembrane domain of the NR2B subunit of the NMDA receptor with its cytosolic domain (33). Loss of this interaction presumably contributes to the decrease in

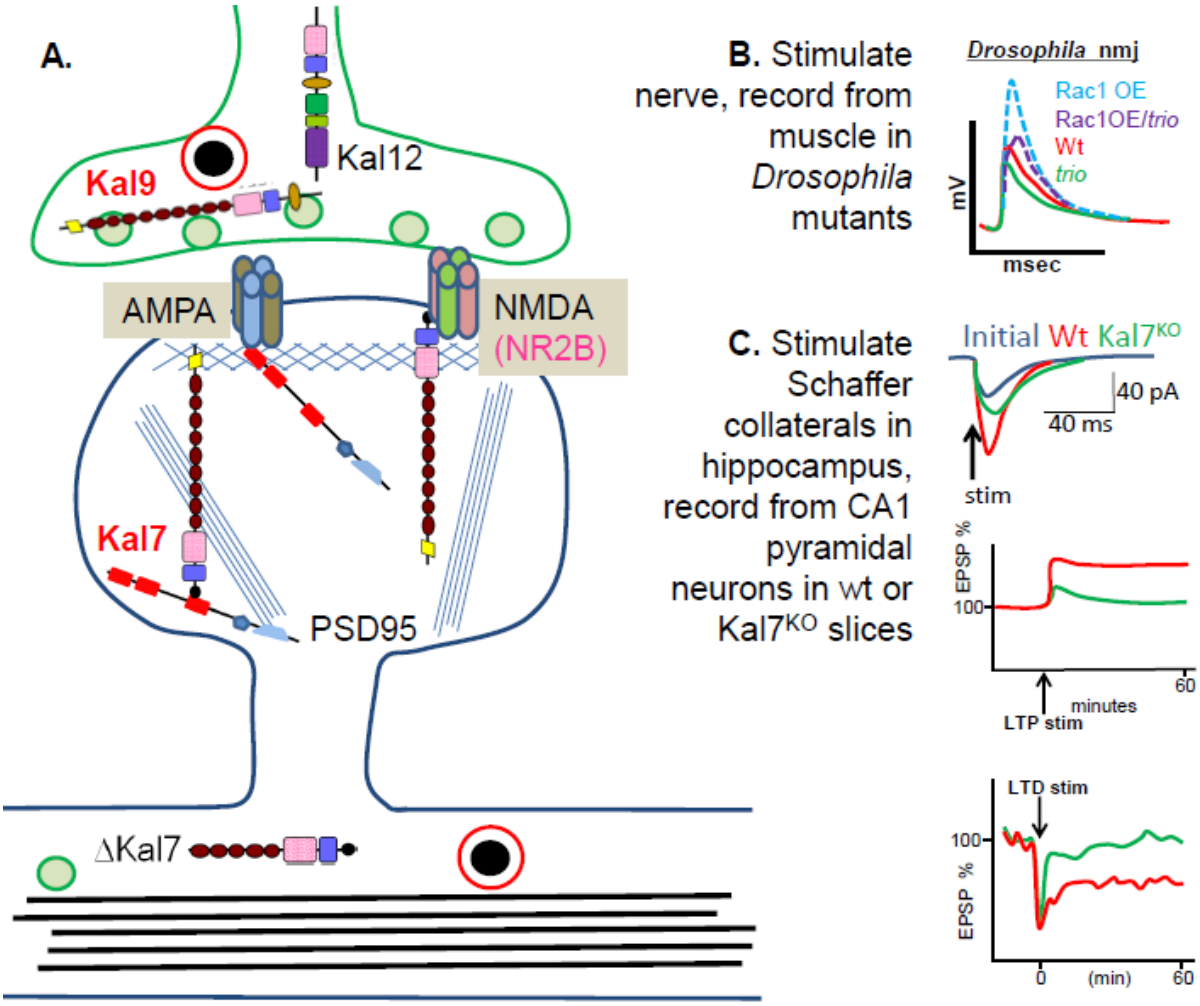

Figure 2-2. Kalirin and Trio: Synaptic Function. **A.** The major sites at which different Kalirin isoforms are localized in neurons are indicated. **B.** At the *Drosophila* neuromuscular junction, the dTrio^{KO} (green, *trio*) shows a much smaller endplate potential than the wildtype (red, Wt) (82). Over-expression of Rac1 in Wt neurons (dashed red, Rac1/Wt) enhances the endplate potential, and over-expression of Rac1 in dTrio^{KO} neurons (dashed green, Rac1/trio) compensates for the absence of *trio*. Thus both Kalirin and Trio are likely to enhance synaptic transmission in part by activating Rac1 via their GEF1 domain. **C.** The Kal7^{KO} mouse shows significantly blunted LTP in hippocampal and cortical neurons compared to wildtype (Wt) mice (green, Kal7^{KO}; red, Wt), and a similar loss of LTP is produced by pharmacological blockade of KalGEF1 (36,42). Kal7^{KO} neurons show little or no LTD.

NR2B-containing NMDA receptors observed in PSDs isolated from Kal7^{KO} mice (33,42). Genotypic differences in several of the behavioral deficits observed in Kal7^{KO} mice (conditioned place preference for cocaine and passive avoidance fear conditioning) were largely abrogated by pretreatment with ifenprodil, a selective blocker of NR2B-containing NMDA receptors, confirming the importance of the Kalirin/NR2B interaction (33). Kal7^{KO} mice show enhanced locomotor sensitization to cocaine administration (51).

A striking attribute of both the Kal7^{KO} and the KalSR^{KO} mice is the decrease in anxiety-like behavior on the elevated zero maze, along with an inability to acquire a fear-based passive avoidance task normally (36,87). Similarly, context and cued fear-based conditioning was impaired in the KalGEF1^{KO} mouse (88). Deficits in rotarod performance and in the neuromuscular junction were observed in KalSR^{KO} mice, but not in Kal7^{KO} mice; a role for Kalirin/Trio at the neuromuscular junction is consistent with observations made in *Drosophila*. Analysis of KalSR$^{KO/+}$ mice revealed a role for Kal9 in the activation of Rac1 in smooth muscle cells and in smooth muscle cell migration and proliferation (90).

Electrophysiology and synaptic function

When hippocampal LTP was recorded using a theta burst pattern paired with a depolarizing pulse in the clamped cell, pyramidal neurons in acute slices from Kal7^{KO} animals showed less than half as much potentiation as seen using wildtype slices (**Fig. 2-2C**) (36). Further studies established that the NMDA/AMPA current ratio in Kal7^{KO} mice was depressed to half in layer 2/3 cortical neurons, compared to the value in wildtype mice, which almost guarantees the LTP deficit seen in the Kal7^{KO} mice (33). The decreased amount of NR2B subunit present at the PSD and on the cell surface is presumably a direct result of the loss of Kalirin PH domain binding to the juxtamembrane domain of the NR2B subunit (33). A similar diminution in LTP was observed in KalGEF^{KO} mice vs. wildtype mice, using a high frequency stimulation paradigm to induce LTP (88). Additional electrophysiological studies demonstrated that non-NMDA receptor-dependent LTP was normal in Kal7^{KO} mice, while NMDA receptor-dependent LTD was

abolished (**Fig. 2-2C**) (42), focusing attention on NMDA receptor related deficiencies. Bath application of NPPD, a Kalirin/Trio GEF1-selective blocker, greatly decreased LTP as did the loss of the Kal7 protein, implicating the GEF1 domain in the electrophysiological changes seen in $Kal7^{KO}$ mice (42). The decreased paired pulse ratio (2^{nd} evoked EPSC not as much larger than the closely paired 1^{st} evoked EPSC as in wildtype) observed in $KalGEF1^{KO}$ mice (88) may reflect decreased levels of Kal9 and Kal12. Kal9 and Kal12 are known to occur in presynaptic terminals and growth cones (75), and their loss may underlie some of the hormone secretion abnormalities observed in the $KalSR^{KO}$ mice (87).

The $Kal7^{KO}$ mouse was studied extensively, using both hippocampal and cortical slices. Correlating with a 15% decrease in dendritic spine density, recordings from hippocampal slices showed a 50% decrease in sEPSC frequency with no change in sEPSC amplitude, as might be predicted if not all of the remaining dendritic spines are fully functional (36). Similarly, the mEPSP frequency was significantly lower in frontal cortex slices from $KalGEF1^{KO}$ mice, again with normal amplitude (91).

Disease relevance

Mutations at the *KALRN* locus have been strongly associated with schizophrenia (92) and early onset coronary artery disease (93). Loss of one copy of *Kalrn* produces mice with arterial smooth muscle cells which show reduced proliferation, migration and reduced Rac1 activation after carotid endothelial denudation (90). Alzheimer's patients have significantly less Kal7 in hippocampal extracts than non-demented patients (58). Kal7 mRNA and protein are increased in both rats and mice in response to cocaine (51,94,95); since Kal7 over-expression leads to increased dendritic spines in a number of neuronal systems (96), it is not surprising that $Kal7^{KO}$ mice do not exhibit the usual increase in nucleus accumbens dendritic spine numbers in response to chronic cocaine (51). Chronic prolonged restraint stress has the opposite effect, decreasing the level of Kal7 in the hippocampus to half the normal level (97).

T-cell lymphoma invasion and metastasis family (Tiam1 and Tiam2)

Discovery and expression

Tiam1 was identified as a T-lymphoma invasion and metastasis-inducing gene by retroviral insertional mutagenesis and encodes a GEF specific for Rac **(98,99)**. Tiam1 is widely expressed in the developing central nervous system, and expression continues at postnatal stages (E14.5 to P180), with an established role in neuronal migration and axonal extension both *in vitro* and *in vivo* **(90,100)** Kawauchi and others 2003). Subcellularly, Tiam1 is localized to dendrites and dendritic spines, where it is enriched at the PSD **(101)**. Tiam2, a closely related gene, is widely expressed in both in mouse and human brain **(102)**.

Due to its roles outside of the CNS, Tiam1 has been extensively studied in cancer research and T-cell migration (103,104). A recent study demonstrated that Tiam1-Rac1 signaling antagonizes centrosome separation during prophase and is required to balance Kinesin-5-induced forces during bipolar spindle assembly (105). These results suggest that Tiam1 controls cell division, and the disruption of Tiam1 in neuroepithelial cellssupports the observation of severe brain abnormalities in one Tiam-/- mouse line (106).

Protein structure and function

Tiam1 is a multi-domain protein with a myristoylation site at its N-terminus; two PEST sequences, a PH-CC-Ex domain (a PH domain, a putative coiled-coil region, and a conserved extra region), a Ras-binding domain and a PDZ domain precede the catalytic DH domain, which is followed immediately by a PH domain and a PDZ binding motif at the C-terminus (**Fig. 2-3A**). Tiam2, also referred to as STEF (SIF and Tiam1 like-exchange factor), lacks a myristoylation signal and PEST sequences but otherwise shares significant homology to Tiam1; portions of Tiam1 and Tiam2 are 70% identical (102,107). Knocking down Tiam1 and Tiam2 using antisense oligonucleotides or shRNAs

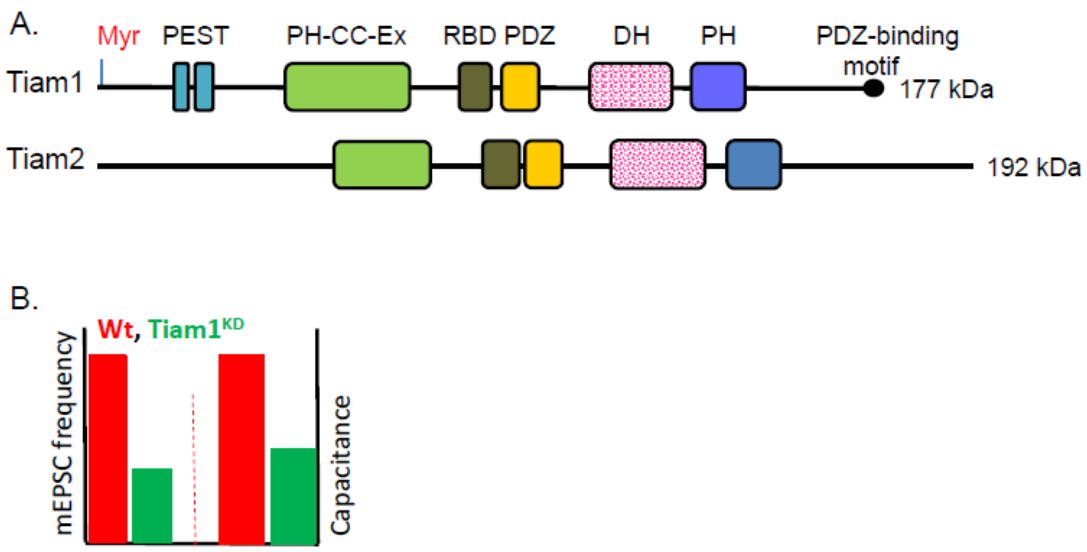

Figure 2-3. Tiam1 and Tiam2. **A.** Structure of Tiam1 (*TIAM1*, human 21q22.11) (177 kDa) and Tiam2 (*TIAM2*, human 6q25.2) (192 kDa). **B.** Tiam1 RNAi in rat hippocampal neurons results in a ~62% decrease in mEPSC frequency and a decrease in membrane capacitance compared to the control neurons, suggesting that Tiam1 knockdown results in fewer synapses and smaller cell size (32,101).

affects neurite length and morphology (108,109), suggesting that both proteins contribute to neurite outgrowth; we focus on Tiam1 because it is necessary for dendritic arbor and spine formation.

Behavior

Tiam1 knockout mouse lines were created by Malliri et al. (103) and by Yoo et al.(106). Tiam1$^{-/-}$ mice generated by ablating exon 2 grow and reproduce normally (103); these mice are primarily used in cancer biology and immunology research. The other Tiam1 knockout mouse line was generated using a Tiam1 gene-trapped embryonic stem cell line, which targets the intron separating exons 5 and 6, potentially creating a truncated Tiam-β-galactosidase fusion protein (106,110). Although no other genes are known to lie in the targeted region, these E9.5 and E10.5 Tiam$^{-/-}$ embryos exhibit anencephaly and exencephaly and do not survive beyond E13.5, indicating that Tiam1 is important for early forebrain development (106). Despite high expression levels in the brain and an obvious role in CNS function, to our knowledge there have been no behavioral or electrophysiological studies performed with homozygous or heterozygous Tiam1$^{-/-}$ animals.

Electrophysiology and synaptic function

RNAi-mediated knockdown of Tiam1 in rat hippocampal neurons dramatically reduces dendritic arborization and spine density (32,101,111) as well as frequency of spontaneous miniature excitatory postsynaptic currents (mEPSC) (**Fig. 2-3B**). Decreasing Tiam1 inhibits neuronal migration and prevents axon formation, with most neurons exhibiting smaller growth cone size and abnormal axon cytoskeletal organization (90,109,112) as well as neuronal migration (Kawauchi and others 2003). MAP1B interacts directly with Tiam1 (**Fig. 2-4**), and over-expression of Tiam1 rescues the axonal growth defects observed in MAP1B-deficient neurons. These data suggest that the MAP1-Tiam1 interaction plays an important role in Rac1 regulation and is required for axonal elongation (**Fig. 2-4**) (113).

Tiam1 over-expression induces extension of multiple axon-like neurites (109,112), and also results in increased dendritic spine density (101), further suggesting a roles in spine and axon formation. Tiam1 interacts directly with the NR1, but not any of the NR2 subunits of the NMDA receptor, and is phosphorylated in a Ca^{2+}-dependent manner following NMDA receptor stimulation. Knocking down Tiam1 expression in rat cortical neurons blocks NMDA receptor-induced increases in dendritic spine density, indicating that Tiam1-dependent Rac1 activation is required for NMDA receptor-mediated spine formation (101).

The PH-CC-Ex domain of Tiam1 interacts with the EphB2 receptor tyrosine kinase in a kinase-dependent manner. RNAi-mediated knockdown of Tiam1 expression blocks the ability of ephrin B1 to increase dendritic spine density in rat hippocampal neurons (32). Interestingly, the Tiam1 PH-CC-Ex region acts in a dominant-negative manner, probably by binding to Tiam1 interacting proteins and preventing recruitment of endogenous Tiam1 to the membrane (**Fig. 2-4**) (32,101). The crystal structure of PH-CC-Ex reveals that this region is a novel protein- and membrane-binding module, strongly binding the NMDA receptor loop I peptide (residues 591-610) and not the C-terminal tail peptide (residues 921-938) (**Fig. 2-4**) (114). This type of interaction is reminiscent of the binding of Kalirin-PH1 to the juxtamembrane domain of the cytoplasmic tail of NR2B (33).

Tiam1 also binds to partitioning-defective gene 3 (PAR-3), a member of the PAR polarity complex, which contributes to spine morphogenesis (111). PAR-3 spatially restricts Tiam1 to dendritic spines, contributing to proper spine formation (**Fig. 2-4**) (111). Finally, Tiam1 is involved in the BDNF-TrkB signaling pathway. Tiam1 is required for BDNF-induced spine morphogenesis and neurite extension; BDNF-activated TrkB directly binds to and activates Tiam1 by phosphorylating Tyr^{829}, and a point mutation at this residue blocks BDNF-induced morphological changes (115,116). In maturing postnatal cerebellar granule cells, BDNF up-regulated expression of Tiam1 and the NR2C NMDA receptor via the TrkB-Erk cascade. This up-regulation is blocked not only by inhibition of signaling

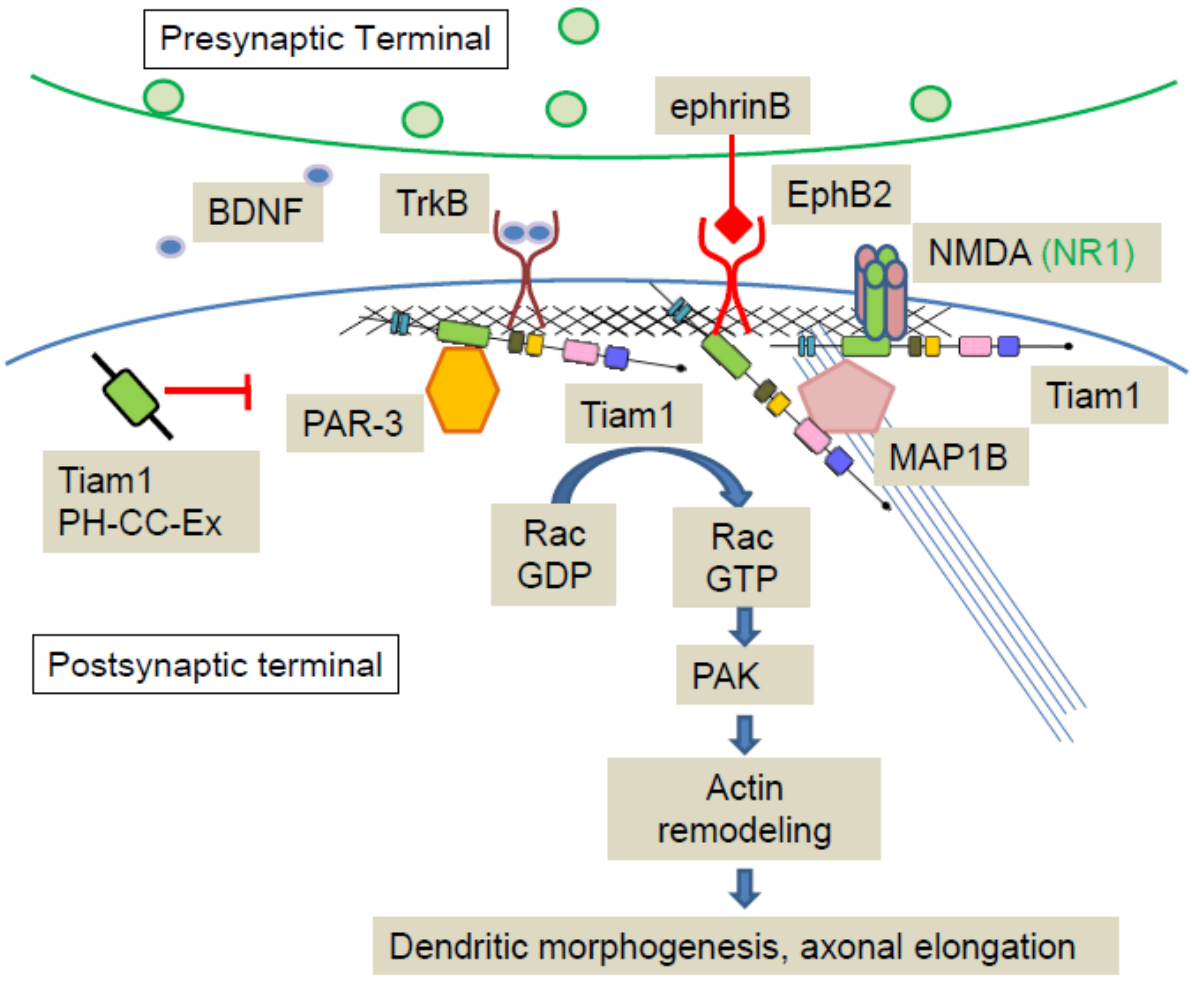

Figure 2-4. Tiam1: Synaptic Functions. Schematic illustrates proposed signaling mechanisms of Tiam1 at the synapse. Tiam1 interacts with many postsynaptic proteins including the NMDA receptor, EphB, MAP1B, PAR-3 and TrkB, which controls dendritic morphogenesis and axon elongation.

pathways, but also by suppression of the Etv1/Er81 transcription factor using Etv1 siRNA (**Fig. 2-4**) (117).

Disease relevance

In hippocampal neurons, Tiam1 is activated and recruited to membranes following exposure to amyloid beta peptide (Aβ), and thus may be involved in Alzheimer's disease pathology (118,119). In addition to the roles of Tiam1 in the nervous system, Tiam1$^{-/-}$ mice are resistant to Ras-induced skin tumors, suggesting that Tiam1 is a critical regulator of tumor formation and invasion (103,120)**.**

Phosphatidylinositol (3,4,5)-trisphosphate-dependent Rac Exchange Factor Family (P-Rex1 and P-Rex2)

Discovery and expression

Two gene family members have been characterized in human (*PREX1, PREX2*) and mouse (*Prex1, Prex2*) (**Fig. 2-5A**). P-Rex1 was purified from neutrophil cytosol on the basis of its phosphatidylinositol(3,4,5)trisphosphate [PI(3,4,5)P_3]-sensitive Rac GEF activity (121); Rac activation in these cells plays an essential role in chemotaxis, phagocytosis and reactive oxygen species (ROS) formation. The Rac GEF activity of purified P-Rex1 was also shown to be stimulated by the addition of recombinant $G\beta_1\gamma_2$ (121) (122). The effects of PI(3,4,5)P_3 and Gβγ on Rac activation are synergistic, leading to the concept that P-Rex1 could serve as a coincidence detector for the simultaneous activation of both signaling pathways. P-Rex2, which was identified by homology, is 59% identical to P-Rex1. As for P-Rex1, PI(3,4,5)P_3 and Gβγ exert a synergistic effect on the ability of P-Rex2 to activate Rac1 (123).

Northern blot analysis of human tissue reveals high levels of P-Rex1 mRNA in neutrophils, with slightly lower levels in brain (121,124). P-Rex1 mRNA expression in brain is readily detected from E13 through adulthood, with levels highest from E17 through P7 (125). Based on Western blot analysis, P-

Rex1 expression is widespread, but highest in the cerebellum (124). *In situ* hybridization reveals a complex and rapidly changing pattern for P-Rex1, with expression in cerebral cortex, trigeminal ganglion and dorsal root ganglia readily apparent at E12 (124). In the adult, expression of P-Rex1 is most notable in layers II/III of the cortex and in the Purkinje cell layer of the cerebellum. In tissue sections and cultured neurons, endogenous P-Rex1 protein localizes to the shafts of neurites (125). As hippocampal neurons differentiate in culture, P-Rex1 localizes to the distal part of the axon and axonal growth cones; expression of exogenous P-Rex1 enlarges axonal, but not dendritic, growth cones (126).

P-Rex2 mRNA is most highly expressed in heart, skeletal muscle and placenta, but is also present in adult brain (123). Western blots reveal similar levels of P-Rex2 in brain and lung (124); *in situ* hybridization and immunostaining identify cerebellar Purkinje cells as the major site of P-Rex2 expression in adult brain, with lower levels in frontal cortex, striatum, amygdala and hippocampus.

Protein structure and function

The catalytic Dbl homology domain of P-Rex occurs near its N-terminus, followed by a PH domain, two DEP (Disheveled, EGL-10, Pleckstrin) domains, two PDZ domains and an inositol polyphosphate 4-phosphatase-like domain **(Fig. 2-5A)**. $PI(3,4,5)P_3$ binds to the PH domain while Gβγ subunits interact with the DH domain (**Fig. 2-5B**); binding of either $PI(3,4,5)P_3$ or Gβγ stimulates the ability of P-Rex to activate Rac, with a synergistic effect of the two activators. P-Rex1 activates Rac1 and Rac3 (Rac1B), a neuron-specific Rho GTPase (126).

Intact P-Rex1 is 60-fold less active than its isolated DH/PH domain; the DEP and PDZ domains play a role in keeping P-Rex1 inactive. $PI(3,4,5)P_3$ increases the activity of the isolated DH/PH domain of P-Rex1, but has a far greater effect on the activity of full-length P-Rex1. Gβγ seems to require only the DH domain to activate P-Rex1; as for $PI(3,4,5)P_3$, the effect of Gβγ on Rac activation is substantial (122). The ability of the Gβγ dimer released upon GPCR stimulation to activate P-Rex1 depends on its Gγ subunit (127). A yeast two-hybrid screen using the tandem DEP domains of P-Rex1 and a human brain

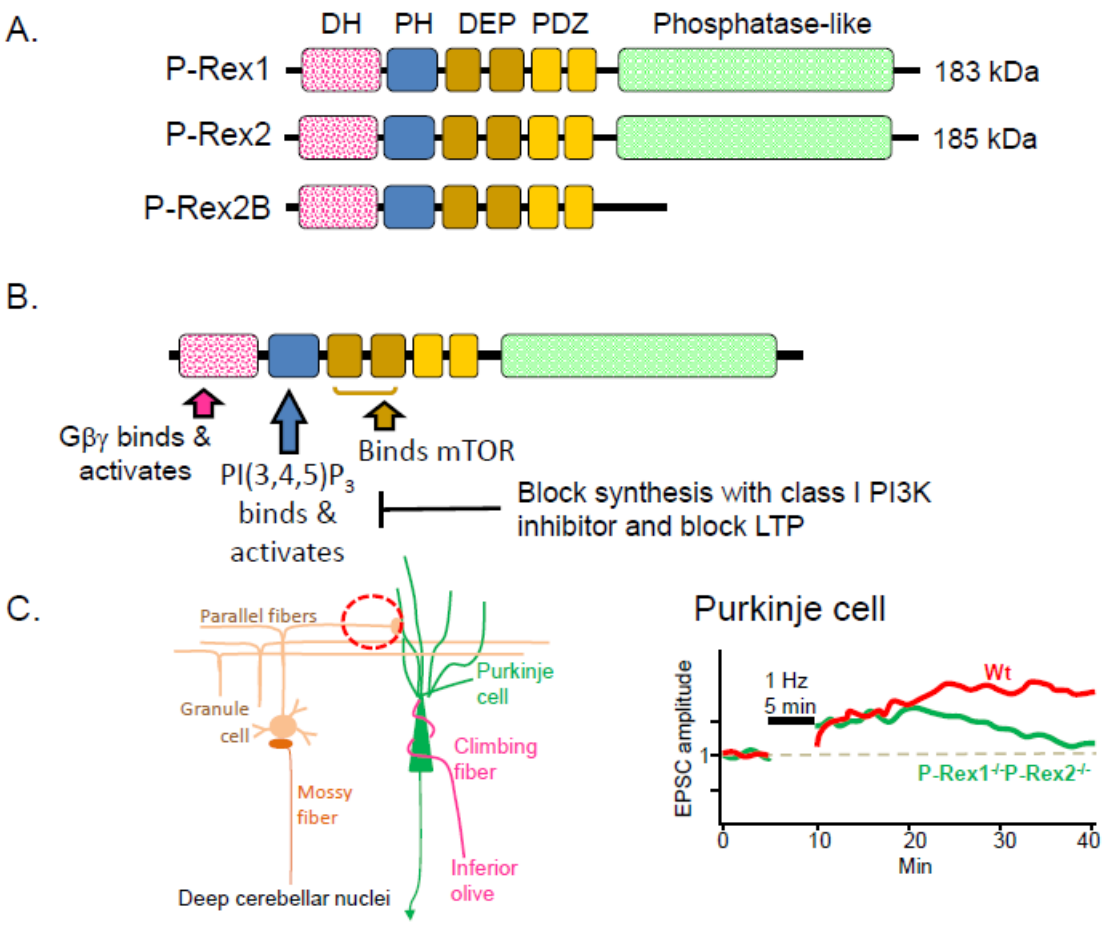

Figure 2-5. P-Rex1 and P-Rex2. **A.** Human P-Rex1 (*PREX1*, 20q13.13) (185 kDa) accounts for 0.1% of the cytosolic protein in neutrophils and is also highly expressed in brain (121). Human P-Rex2 (*PREX2*, 8q13.2) (183 kDa) is not expressed in neutrophils, but is highly expressed in skeletal muscle, heart and placenta. Mouse P-Rex1 and P-Rex2 are on Chr2 and 1, respectively. In addition to a DH and adjacent PH domain, both full-length proteins include two DEP (Disheveled, EGL-10, Pleckstrin) domains, two PDZ domains and an inositol polyphosphate 4-phosphatase-like domain; the phosphatase domain is absent from P-Rex2B, a 980 amino acid splice variant expressed only in the heart (124). **B.** Key signaling pathways known to affect P-Rex1 function are identified, along with some of its major downstream targets in the nervous system. The DEP and PDZ domains play a role in protein-protein interactions and membrane targeting; phosphorylation of P-Rex1 by PKA disrupts these interactions and diminishes the ability of Gβγ to bind to and activate P-Rex1 (130). **C.** The cell types involved in the parallel fiber Purkinje cell synapses examined electrophysiologically are illustrated (red dashed circle). Parallel fiber stimulation causes LTP at wildtype synapses; while P-Rex1$^{-/-}$P-Rex2$^{-/-}$ mice produce a similar response immediately after stimulation, the response is not sustained (131).

cDNA library identified the C-terminal region of mammalian target of rapamycin (mTOR), including its serine/threonine kinase domain, as an interactor (**Fig. 2-5B**) and both P-Rex1 and P-Rex2 have been identified as components of the mTORC2 complex (128). Phosphorylation of P-Rex1 by PKA alters its intramolecular interactions and prevents its binding and activation by Gβγ (129).

The activation of Rac1 and Rac2 in neutrophils triggers a variety of responses including chemotaxis, generation of ROS and secretion of azurophilic granules. It is striking that the absence of P-Rex1 has quite distinct effects on these responses (132). The ability of unprimed or tumor necrosis factor α-primed P-Rex1$^{-/-}$ neutrophils to produce ROS in response to formyl-Met-Leu-Phe (fMLP) is only slightly diminished; in contrast, the ability fMLP to stimulate ROS production by lipopolysaccharide-primed neutrophils is almost entirely eliminated (132).

The GEF activity of P-Rex1, which is expressed endogenously in PC12 pheochromocytoma cells, is activated by NGF, resulting in increased membrane ruffling and cell motility (125). Along with the DH domain, the PDZ and phosphatase-like domains of P-Rex1 play essential roles in its ability to stimulate membrane ruffling. PC12 cell migration in response to NGF is greatly increased upon expression of exogenous P-Rex1; the process is dependent on activation of Rac1. Deletion of the DH domain of P-Rex1 (ΔDH-P-Rex1) yielded a dominant negative variant of P-Rex1, which blocks NGF-induced PC12 cell migration.

Behavior

P-Rex1, P-Rex2 and P-Rex1/P-Rex2 knockout mice have been characterized. P-Rex1$^{-/-}$ mice are viable and healthy, perform normally in tests of motor behavior, and are slightly smaller than wildtype mice (124,132) P-Rex2$^{-/-}$ mice are viable and fertile although females have lower than normal body weight (124). The brains of P-Rex2$^{-/-}$ mice show no major anatomical defects, but Purkinje cell dendritic structure is abnormal. Rotarod performance in adult female P-Rex2$^{-/-}$ mice is somewhat compromised, while male performance is less affected (124). Basic sensory motor functions and gait are normal. P-

Rex1$^{-/-}$/P-Rex2$^{-/-}$ mice are viable and fertile, with sex-specific changes in body weight. Brain anatomy is grossly normal, with disordered Purkinje cell dendrites, as observed in the P-Rex2$^{-/-}$ mouse brain. The motor behavior of male and female P-Rex1$^{-/-}$/P-Rex2$^{-/-}$ mice is more impaired than that of P-Rex2$^{-/-}$ mice, with substantial deficits in rotarod performance, open field behavior, beam walking and gait (124). Deficits worsen with age and are more pronounced in females than in males.

Electrophysiology and synaptic function

The prevalence of P-Rex1 and P-Rex2 in cerebellar Purkinje cells, the altered Purkinje cell dendritic morphology and altered motor function observed in mice lacking both P-Rex proteins identified parallel fiber/Purkinje cell synapses as a likely site at which to observe alterations in synaptic transmission (**Fig. 2-5C**). LTD at these synapses, which can be evoked by co-stimulation of parallel fiber and climbing fiber inputs, involves increased phosphorylation of AMPA receptor GluR2 subunits, which promotes their internalization and decreases the response to transmitter release (131). The parallel fiber-Purkinje synapse is essential for the eye-blink reflex.

LTP at these same synapses can be evoked by stimulating the parallel fibers alone; although less well understood than LTD, it is clear that LTP involves phosphatase-mediated reversal of GluR2 phosphorylation and decreased AMPA receptor internalization. Consistent with a role for P-Rex, inhibition of PI3K abolishes LTP entirely. Synthesis of NO is required for LTP at these synapses and NO donors can evoke LTP. P-Rex1 and P-Rex2 are activated by PI(3,4,5)P_3, the product of Class I PI3Ks, which are essential for the induction of hippocampal LTP and NMDA receptor evoked increased surface expression of GluR1-containing AMPA receptors in hippocampal neurons.

Sagittal slices from the cerebellar vermis of P21-P28 mice, were used (131); despite the altered dendritic morphology observed in P-Rex1$^{-/-}$/P-Rex2$^{-/-}$ mice, synaptic transmission, short-term plasticity and passive membrane properties were unaltered. LTP was induced at parallel fiber Purkinje cell synapses by stimulating at 1 Hz for 5 min. In wildtype mice, this triggers an increase in parallel fiber EPSC

amplitude that lasts over 30 min; with no change in paired-pulse ratio, the effect is thought to be post-synaptic (**Fig. 2-5C, red**). In the P-Rex1$^{-/-}$/P-Rex2$^{-/-}$ mice, EPSC amplitude shows an initial increase but this increase is not sustained (**Fig. 2-5C, green**). Parallel fiber LTP can also be evoked by exogenous NO donors; the initial response of P-Rex-deficient slices to an exogenous NO donor resembles the wildtype response, but potentiation is not sustained. Hence, P-Rex family enzymes are required for the maintenance of cerebellar LTP.

Disease relevance

PREX1 maps to a Type 2 diabetes mellitus susceptibility locus. Insulin is known to activate PI3K, yielding PI(3,4,5)P_3 and muscle cells that lack Rac1 are known to exhibit impaired insulin-stimulated GLUT4-translocation. Although Rac1 does not promote GLUT4 translocation when insulin levels are saturating (100 nM), it does at physiological levels of insulin (1-10 nM). In the absence of insulin, expression of exogenous P-Rex1 in adipocytes has no effect on GLUT4 trafficking; however, the effect of insulin on GLUT4 trafficking is enhanced. Pre-treating adipocytes with a PI3K inhibitor decreases the ability of P-Rex1 to enhance the actions of insulin (130).

Ras-guanine nucleotide-releasing factor family (RasGRF1 and RasGRF2)

Discovery and expression

Although initially identified due to their sequence homology to yeast CDC25, a potent Ras GEF, the mammalian Ras-guanine nucleotide-releasing factors (RasGRFs) are large, multidomain proteins containing both Ras GEF and Rac GEF domains. *RASGRF1* (mouse chromosome 9, human 15) is paternally imprinted and expressed only after birth. *RASGRF2* (mouse chromosome 13, human 5) is not imprinted, but its expression is developmentally regulated; low early in development, expression increases around postnatal day 10 in the rat and remains high in adulthood. Both RasGRF1 and RasGRF2 are predominantly expressed in neurons of the adult brain, although RasGRF2 is also highly expressed in

other tissues (133,134). In addition to the two full-length proteins, smaller alternatively spliced transcripts have been identified; some have unique developmental expression patterns and differential effects on downstream signaling, suggesting diverging physiological roles (see (135) for review). Our discussion here will focus on the full-length gene products, which have been studied in more detail.

Protein structure and function

Full length RasGRF proteins contain an N-terminal PH domain followed by a coiled coil domain, a Ca^{2+}/calmodulin-binding IQ domain, the tandem DH/PH domains common to Dbl family Rho GEFs, a Ras exchange motif (REM), and a Ras GEF domain (CDC25) (**Fig. 2-6A**). *In vitro* and *in vivo* studies have shown that both full-length RasGRFs are capable of activating Ras family members as well as the Rho GTPase Rac1. The IQ domain of RasGRF1 binds calmodulin in a Ca^{2+}-dependent manner, leading to increased GEF activity in cells (136), but not *in vitro* (137). A RasGRF2 mutant lacking the IQ domain altogether is still able to activate Ras, but does not result in activation of its downstream effector, Erk (138). These results have not been entirely reconciled, but the hypothesis that RasGRF activity requires proper protein localization and assembly of downstream networks prevails. The N-terminal PH and CC domains may also be involved in protein localization. RasGRF1, but not RasGRF2, contains a "Neuronal domain (ND)", which lets RasGRF1 associate with NMDA-type glutamate receptors through a direct interaction (**Fig. 2-6A**); the ND interacts directly with the cytosolic tail of the NR2B subunit (139) (**Fig. 2-7**). Disruption of this interaction results in reduced Erk activation in cultured hippocampal neurons, while leaving NMDA receptor-mediated current intact following bath application of NMDA receptor agonists (139).

A role for RasGRF1 has also been identified in Ca^{2+}-dependent signaling downstream of various GPCRs and receptor tyrosine kinases. PKA-mediated phosphorylation and activation of RasGRF1 is also necessary for Erk activation following stimulation of exogenous $G\square_s$-coupled $5\text{-}HT_7$ serotonin receptors

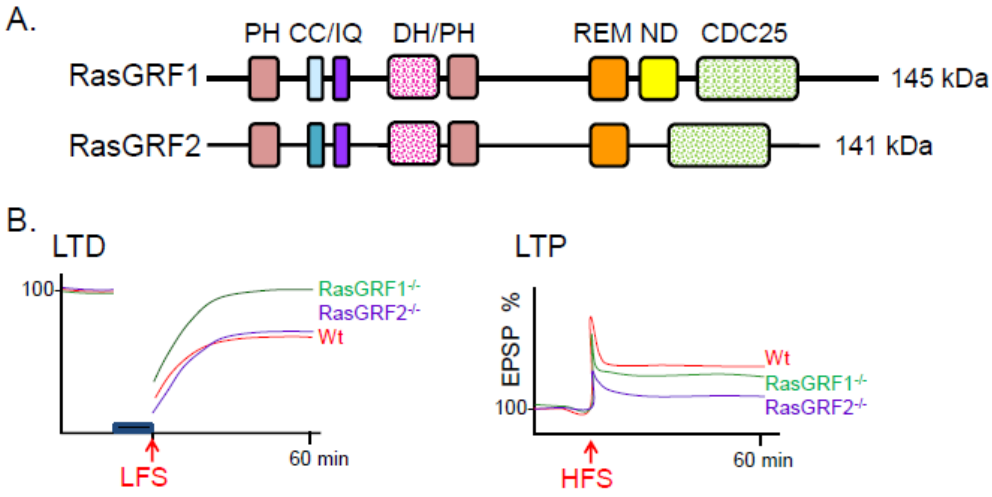

Figure 2-6. RasGRF1 and RasGRF2. **A.** RasGRF1 and RasGRF2 are encoded by separate genes (*RASGRF1* and *RASGRF2*), respectively located on chromosomes 15 and 5 in human (Chromosomes 9 and 13 in mouse). Key features of RasGRF1 and RasGRF2 are identified: CC, coiled coil; IQ, Ca^{2+}/calmodulin-binding domain; REM, Ras exchange motif; ND, neuronal domain; CDC25, Ras GEF domain. **B.** Electrophysiological recordings revealed significantly impaired LTP but normal LTD in slices from the hippocampus of P25 and older RasGRF2$^{-/-}$ mice, while LTD but not LTP was disrupted in hippocampal slices from RasGRF1$^{-/-}$ mice (141).

in HEK-293 cells (140). Stimulation of TrkA receptors, dopamine receptors and muscarinic acetylcholine receptors also results in RasGRF1 activation. The mechanisms and consequences of these interactions have not been fully elucidated, but all appear to require RasGRF1 phosphorylation, most at Ser^{916}, as well as its Ca^{2+}-dependent association with calmodulin (140,142-144).

Behavior

The availability of several transgenic mouse lines has established the physiological significance of the RasGRF family. Phenotypically, mice lacking RasGRF1 ($RasGRF1^{-/-}$) are smaller than their wildtype littermates, and behavioral tests have revealed impaired fear conditioning in $RasGRF1^{-/-}$ mice. Normal performance on hippocampal memory tasks was seen in mice lacking both the full-length RasGRF1 and a less studied splice variant of RasGRF1, p55-GRF1; however numerous studies using mice lacking only the full-length RasGRF1 isoform have shown impaired hippocampal-dependent memory (141,145-147). Locomotor sensitization and conditioned place preference for cocaine are significantly reduced in $RasGRF1^{-/-}$ mice, while both are exacerbated in animals over-expressing RasGRF1 (148). RasGRF1 may also be involved in CB1 (endocannabinoid) receptor sensitization and tolerance to Δ9-THC, since $RasGRF1^{-/-}$ mice have altered gene expression profiles following chronic Δ9-THC exposure (149). Visual phenotypes, including deficient photoreception, have also been observed and likely arise from RasGRF functions in the retina (150). $RasGRF2^{-/-}$ mice grow and reproduce normally (151) and most reported phenotypes of single and combined knockout strains have indicated RasGRF2 involvement in immune mechanisms.

Electrophysiology and Synaptic Function

Using theta burst stimulation, Brambilla et al. showed impaired LTP in the amygdala of $RasGRF1^{-/-}$ mice, though hippocampal LTP appeared normal (145). They also observed elevated basal field activity in both amygdala and hippocampal slices (145). Furthermore, recordings from cultured

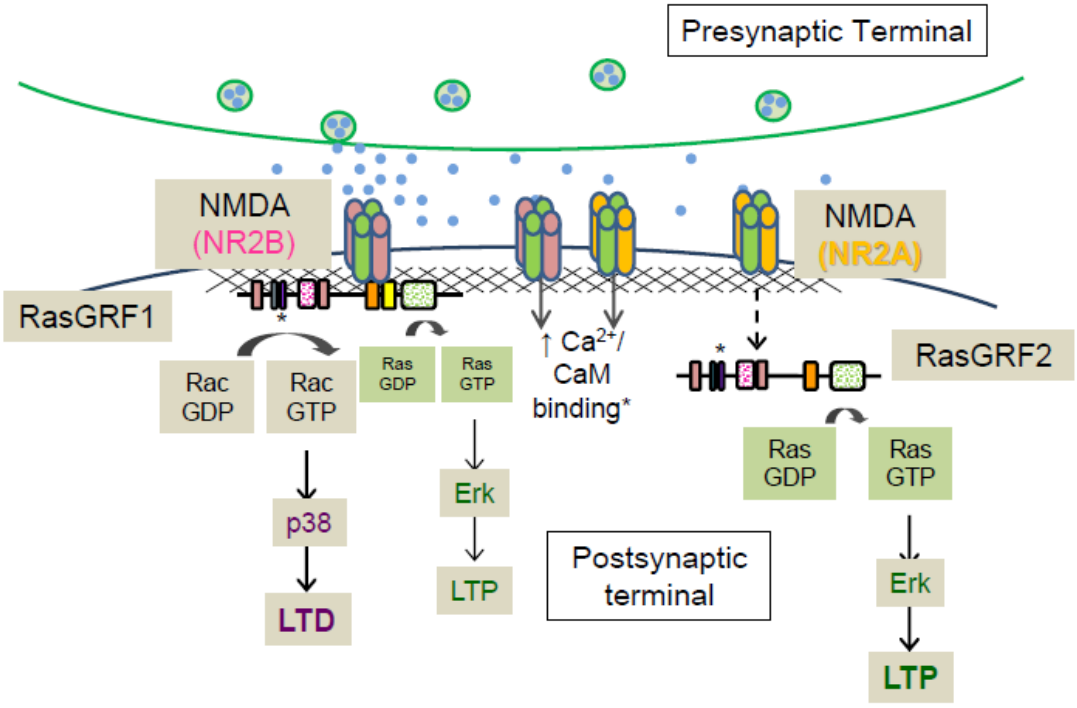

Figure 2-7. Distinct roles for RasGRF family members in NMDA-mediated long term plasticity. Schematic illustrates proposed signaling mechanisms of the major RasGRF family members, RasGRF1 and RasGRF2. While both proteins are known to contribute to NMDA receptor-mediated Erk activity *in vivo*, data from biochemical and electrophysiological experiments suggest that RasGRF1 acts downstream of NR2B-containing NMDA receptors and signals predominantly through Rac and p38 to promote LTD in hippocampal slices. RasGRF2, however, signals almost exclusively through Ras and Erk following activation of NR2A-containing NMDA receptors to promote LTP.

neurons and acute brain slices revealed hippocampal hyperexcitability in RasGRF1$^{-/-}$ mice, and convulsant drug administration studies have shown increased seizure susceptibility in these animals (152).

Although the RasGRF proteins are structurally similar (**Fig. 2-6A**), diverging roles in synaptic function are apparent. Both RasGRF1 and RasGRF2 act downstream of NMDA receptors. While both RasGRFs are known to contribute to neuronal Ras/Erk signaling *in vivo*, evaluation of Erk activity following NMDA stimulation in acute hippocampal brain slices from knockout animals revealed larger deficiencies in NMDA receptor-mediated Erk activation in RasGRF2$^{-/-}$ mice than in RasGRF1$^{-/-}$ mice (141). Conversely, hippocampal slices from RasGRF1$^{-/-}$ mice show reduced NMDA receptor-mediated activation of the Rac effector p38 MAP kinase, while recordings from RasGRF2$^{-/-}$ slices are indistinguishable from wildtype (**Fig. 2-7**).

Although basal synaptic transmission appears to be normal in hippocampal slices from mice (P25-36) lacking both RasGRF1 and RasGRF2, expression of both LTP and LTD is blunted in hippocampal slices from adult animals; this deficit is not seen in P14-18 brains (141). Electrophysiological analysis of single knockout brains revealed that hippocampal LTD, but not LTP, is disrupted in RasGRF1$^{-/-}$ mice, while LTP, but not LTD, is impaired in RasGRF2$^{-/-}$ mice (141) (**Fig. 2-6B**). Further manipulation suggests that these effects are mediated by different NMDA receptor subtypes. APV blockade of NMDA receptors blocks NMDA-mediated activation of Erk, but not p38, while selective blockade of NR2B-containing NMDA receptors with ifenprodil prevents NMDA-mediated p38 activation with no effect on Erk activation. Thus, electrophysiological and biochemical studies using knockout animals suggest that RasGRF2 signals predominantly through the Ras/Erk pathway in response to NR2A-containing NMDA receptor activation and contributes to LTP induction. Conversely, RasGRF1 contributes mostly to NMDA receptor-dependent LTD via Rac/p38 activation downstream of NR2B-containing NMDA receptor activation (139,141) (**Fig. 2-7**).

Furthermore, cortical Ca^{2+}-permeable AMPA receptor currents are reduced in RasGRF1$^{-/-}$ and 2$^{-/-}$ knockout animals and are abolished in double knockout animals. Both RasGRF proteins co-

immunoprecipitate with the GluR1 subunit, but not the GluR2 subunit, of the AMPA receptor in lysates from cortical brain slices following bath application of AMPA (153). Tian et al. also showed that RasGRF expression is required for Ras/Erk signaling following activation of Ca^{2+}-permeable AMPA receptors in the adult brain (153).

Disease relevance

Increased RasGRF1 expression is seen in the striatum, cortex and cerebellum following chronic cocaine, amphetamine or THC administration (148,149,154-156). Furthermore, RasGRF1$^{-/-}$ mice display decreased locomotor sensitization and conditioned place preference for cocaine (148). RasGRF1 may also be involved in CB1 cannabinoid receptor adaptation and drug tolerance following THC administration (149,155). RasGRF1$^{-/-}$ mice and non-human primates expressing dominant negative forms of RasGRF1 are significantly less susceptible to L-dopa-induced dyskinesias associated with dopamine replacement therapies (157), and mice lacking both full-length isoforms have higher susceptibility to cerebral ischemia.

Collybistin.

Discovery and expression

Collybistin [*Arhgef9*; human *hPEM2* (Posterior End Mark-2), *ARHGEF9*] was discovered in a yeast two hybrid screen for gephyrin interactors (158); gephyrin, a scaffolding protein, plays an essential role in the postsynaptic clustering of $GABA_A$ and glycine receptors, both of which are ligand gated inhibitory ion channels. The collybistin gene is located on the X chromosome. In the rat, alternative splicing generates collybistin transcripts that encode functionally distinct proteins (**Fig. 2-8A**). Some lack the SH3 domain that precedes the catalytic DH/PH domain and three different C-termini (CB1, CB2, CB3) have been identified; $CB2_{SH3+}$ and $CB3_{SH3+}$ are the major splice variants in the rat (159). Two promoters generate hPEM2, producing slightly different sequences that precede the SH3 domain (159).

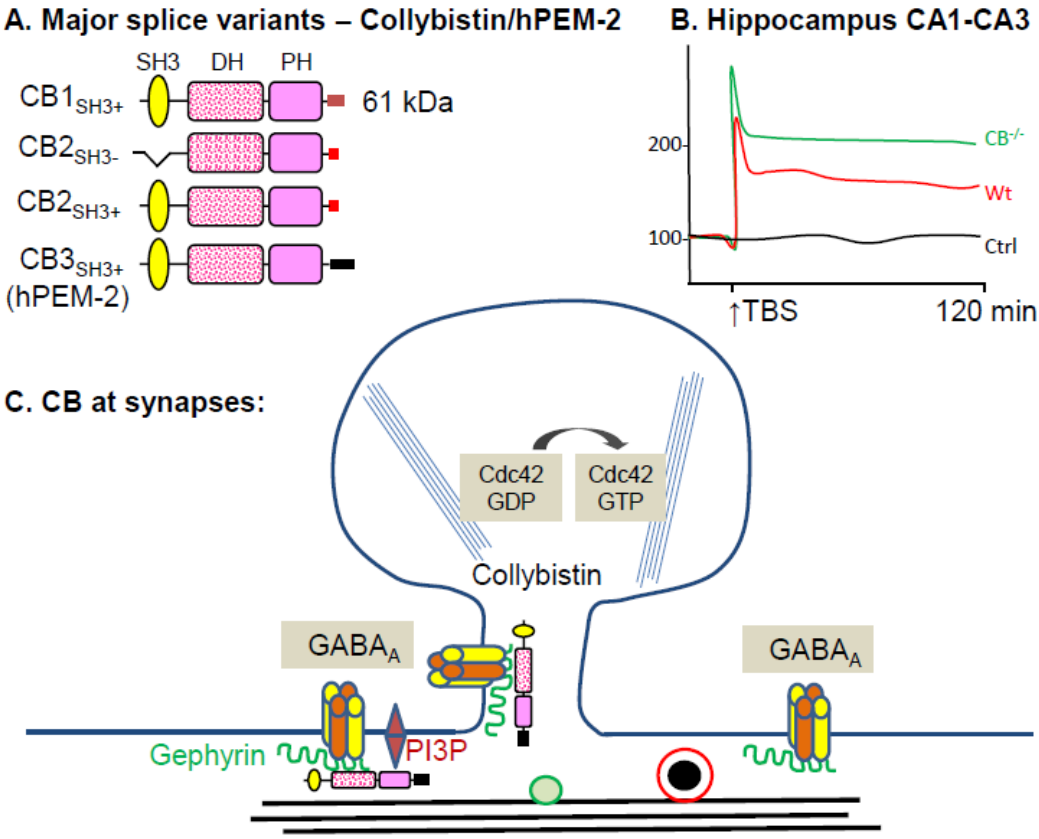

Figure 2-8. Collybistin structure and synaptic function. **A.** The major splice variants of rat collybistin (CB; Arhgef9) are shown; the human homologue, hPEM-2 (*ARHGEF9)* has alternate promoters, but does not have similar splice variants (159). **B.** Slices prepared from collybistin$^{-/-}$ mice show exaggerated hippocampal LTP; theta-burst stimulation was applied to fibers from CA3 neurons and fEPSPs were recorded in the stratum radiatum of the CA1 region (160). The genotypic difference was abrogated in the presence of picrotoxin, a $GABA_A$ receptor blocker, which increased potentiation only in wildtype slices. **C.** Collybistin localizes the scaffolding protein gephyrin, which in turn clusters $GABA_A$ and the group of GlyR receptors (as depicted).

Collybistin transcripts are highly expressed in neurons throughout the adult brain and spinal cord, with little expression outside of the nervous system. Collybistin is expressed in all cerebellar neurons, with highest levels in Purkinje cells (161). Expression of collybistin is upregulated during the time of major neuronal differentiation and synaptogenesis and it is thought to play a role in post-mitotic neurons (27,161). Collybistin immunostaining is strong in dendrites, with very little in cell body (162); Collybistin is detected at only a subset of gephyrin-positive inhibitory synapses containing all major $GABA_AR$ subunits (Patrizi and others 2011).

Protein structure and signaling.

The DH domain of collybistin activates Cdc42, but does not activate Rac1 or RhoA; this domain is involved in binding gephyrin (27,31) (162). The SH3 domain of collybistin interacts with neuroligin-2, a transmembrane protein that interacts with presynaptic neurexins localized at GABAergic synapses (110), and the PH domain binds selectively with the phosphoinositide PI3P (Patrizi and others 2011). Initial comparisons of collybistin variants with and without the SH3 domain suggested an inhibitory role for this region: $CB2_{SH3-}$ forms a ternary complex with gephyrin and Cdc42 while $CB2_{SH3+}$ does not (162). Other work argues that all four major isoforms of Collybistin concentrate at GABAergic synapses (110).

Collybistin plays a role in localizing gephyrin, which is thought to form a scaffold beneath the plasma membrane that contributes to the anchoring of receptors. Gephyrin, which interacts with microtubules, actin filaments and many additional proteins, plays an essential role in the formation of postsynaptic $GABA_A$ and glycine receptor clusters. The PH domain of collybistin is essential for gephyrin clustering and for interaction with PI3P, but Cdc42 activation by collybistin does not appear to be essential (162).

In collybistin$^{-/-}$ mice, a subset of the GABAergic synapses fail to form normally, but glycinergic synapses are unaffected. The effect on $GABA_A$ receptors is both subtype and region-specific: γ2-containing $GABA_A$ receptor levels drop in the basolateral amygdala and hippocampus, but not in the

brainstem or cerebellum (160). In affected areas, the absence of collybistin results in a decrease in the density of gephyrin clusters at postsynaptic densities and in decreased staining for the γ2 and α2 subunits of the $GABA_A$ receptor. Why the effects are so regionally specific is not yet clear.

Behavior

Given its role in inhibitory receptor clustering, it is not surprising that collybistin$^{-/-}$ mice have significantly fewer $GABA_A$ receptor clusters in the amygdala and hippocampus than wt mice (160). Surprisingly, spinal cord and brainstem Gly receptors are properly assembled (162). The number of postsynaptic gephyrin puncta was dramatically decreased in the CA1 region of the hippocampus, while the decreases were evident but much less striking in other regions such as the amygdala; paradoxically, the number of VIAAT puncta (presynaptic marker for GABA terminals) was normal (160) (163).

Consistent with loss of $GABA_A$ receptor clusters in the amygdala and the hippocampus, Collybistin$^{-/-}$ mice have impaired spatial learning, reduced exploratory behavior, and increased anxiety-like behavior (160). Time spent in the open arm of the elevated plus maze was dramatically reduced. The Barnes maze is learned well by wildtype mice, but not by Collybistin$^{-/-}$ mice. Motor performance was normal in Collybistin$^{-/-}$ mice, consistent with normal glycinergic inhibition (160).

Electrophysiology and neuronal function

Electrophysiological recordings from collybistin$^{-/-}$ mice have been carried out *in vitro* and *in vivo* (160). The frequency and amplitude of GABAergic miniature inhibitory postsynaptic potentials (mIPSPs) in CA1 pyramidal neurons were both decreased in Collybistin$^{-/-}$ mice. As expected, the field EPSP slope in CA1 is dramatically increased in wildtype mice in the presence of picrotoxin and only a blunted increase is seen in CB$^{-/-}$ mice (consistent with loss of necessary clustering of $GABA_AR$) (163). LTP induction using theta-burst stimulation of the CA3-CA1 hippocampal collateral pathway produces an enhanced response in Collybistin$^{-/-}$ mice (**Fig. 2-8B**); the difference between genotypes is eliminated by

picrotoxin, again consistent with diminished GABA function in $CB^{-/-}$ mice. A low frequency stimulation paradigm that produces LTD in wildtype mice does not do so in $Collybistin^{-/-}$ mice.

Disease relevance

Harvey et al. (159) identified a mutation in the SH3 domain of collybistin when examining 32 hereditary hyperekplexia (excessive startle response) patients; the child with the mutation survived until age 4 but suffered from tonic seizures provoked by tactile stimulation and was severely mentally retarded. Expression of $CB3_{SH3+}$ bearing this mutation results in loss of endogenous gephyrin clusters and mislocalization of $GABA_A$ receptors (160). Expression of $CB2_{SH3+}$ mutated at the same site does not support gephyrin localization to the cell surface (162). Loss of function mutations in the *ARHGEF9* gene lead to mental retardation and refractory epilepsy in both boys and heterozygous girls (159).

Chapter 3

Non-enzymatic domains of Kalirin7 contribute to spine morphogenesis through interactions with phosphoinositides and Abl

Xin-Ming Ma*, Megan B. Miller*, K. S. Vishwanatha, Maegan J. Gross, Yanping Wang,

Thomas Abbott, TuKiet T. Lam, Richard E. Mains, Betty A. Eipper

** Equal first authors*

This chapter was published in its present form in Molecular Biology of the Cell;

2014 May; 25(9):1458-71.

Abstract

Like several Rho GDP/GTP exchange factors (GEFs), Kalirin7 (Kal7) contains an N-terminal Sec14 domain and multiple spectrin repeats. A natural splice variant of *Kalrn* lacking the Sec14 domain and four spectrin repeats is unable to increase spine formation; our goal was to understand the function of the Sec14 and spectrin repeat domains. Kal7 lacking its Sec14 domain still increased spine formation, but the spines were short. Strikingly, Kal7 truncation mutants containing only the Sec14 domain and several spectrin repeats increased spine formation. The Sec14 domain bound phosphoinositides, a minor but crucial component of cellular membranes, and binding was increased by a phosphomimetic mutation. Expression of KalSec14-GFP in non-neuronal cells impaired receptor-mediated endocytosis, linking Kal7 to membrane trafficking. Consistent with genetic studies placing *Abl*, a non-receptor tyrosine kinase, and

the *Drosophila* ortholog of *Kalrn* into the same signaling pathway, Abl1 phosphorylated two sites in the fourth spectrin repeat of Kalirin, increasing its sensitivity to calpain-mediated degradation. Treatment of wildtype mouse, but not $Kal7^{KO}$ mouse, cortical neurons with an Abl inhibitor caused an increase in linear spine density. Phosphorylation of multiple sites in the N-terminal Sec14/spectrin region of Kal7 may allow coordination of the many signaling pathways contributing to spine morphogenesis.

Introduction

Genetic linkage studies identified *KALRN* as a risk factor for schizophrenia, attention deficit hyperactivity disorder, early onset coronary artery disease and stroke (164-167). Kalirin7 (Kal7), a Rho GDP/GTP exchange factor (RhoGEF) for Rac1 and RhoG, is the most abundant isoform of the *Kalrn* gene in the adult brain and is localized to the postsynaptic side of excitatory synapses (168). Knockout and over-expression studies revealed important roles for Kal7 in dendritic spine formation and synaptic function (42,168-173) and *KALRN* has been implicated in neurological disorders associated with aberrant dendritic spine density and morphology (174,175).

Although the GEF domain and Class 1 PDZ-binding motif are identical in Kal7 and ΔKal7, a natural splice variant (**Fig. 3-1A**), the full-length protein is essential for dendritic spine formation (176). Since Kal7 includes a Sec14 domain and four spectrin repeats absent from ΔKal7 (**Fig. 3-1A**), the aim of this study was to determine how these domains contribute to spine formation. *TRIO* shares the same overall architecture as *KALRN* (177), as do *Drosophila trio* and *C. elegans unc-73*, paralogs of *KALRN* and *TRIO* (**Fig. 3-1B**) (178,179). Three other RhoGEFs, *Mcf2*, *Mcf2l* and *Puratrophin-1* (Purkinje cell atrophy associated protein-1; *Plekhg4*) also include a Sec14 domain (**Fig. 3-1C**) (180-182). Natural splice variants of *Mcf2* and *Mcf2l* lack the Sec14 domain, as is the case for the ΔKal7 isoform of *Kalrn*. Yeast Sec14p, the founding member of this family, binds phosphatidylinositol and phosphatidylcholine, mediating their transfer between membranes and coordinating Golgi complex lipid metabolism and

protein transport (183-185). The Sec14 domains of Mcf2 and Mcf2l play a role in protein localization and regulation of GEF activity (182).

The nine spectrin repeats of Kal7 form nested structures, giving this region an extended, rod-like structure (186); many of the proteins that interact with Kalirin do so by binding to this region (187-191). At least one spectrin-like domain is predicted in the region between the Sec14 and GEF domains of Mcf2 and Mcf2l (**Fig. 3-1C**). The multiple tandem spectrin repeats of erythrocyte spectrin and skeletal muscle dystrophin provide essential mechanical support and flexibility to the overlying plasma membrane (192-194). In neurons, controlled calpain-mediated proteolysis of αII-spectrin contributes to dendritic outgrowth and synaptic remodeling (195-197). Phosphorylation of a single Tyr in αII-spectrin alters its function by decreasing its sensitivity to proteolytic cleavage by mu-calpain (195,198).

Kal7 acts downstream of multiple receptors, including ionotropic receptors (NMDA receptors), receptor tyrosine kinases (EphB2, ErbB and PDGFβ) and G protein coupled receptors (endothelin receptor and $5HT_{2a}$ receptor) (169,172,199,200). Consistent with its role in multiple spine morphogenesis pathways, Kal7 isolated from rat brain is extensively phosphorylated (201). Thr^{79}, situated near the putative lipid-binding pocket of the Kalirin Sec14 domain, can be phosphorylated by CaMKII, protein kinase A and protein kinase C, and is phosphorylated *in vivo* (201). Several phosphorylation sites were identified within the first four spectrin repeats of Kalirin and Fyn, a non-receptor tyrosine kinase, was shown to phosphorylate Tyr^{591} in spectrin repeat 4 *in vitro* (201). Although axon guidance studies placed *Abl*, another non-receptor tyrosine kinase, and the *Drosophila* orthologue of *Kalrn* into the same pathway (202,203), the underlying mechanism has not been elucidated. Utilizing primary neuronal cultures and examining the properties of the Sec14 and spectrin repeat regions of Kal7, we sought to determine the roles of these non-catalytic domains in controlling the ability of Kal7 to stimulate spine formation and affect spine morphology.

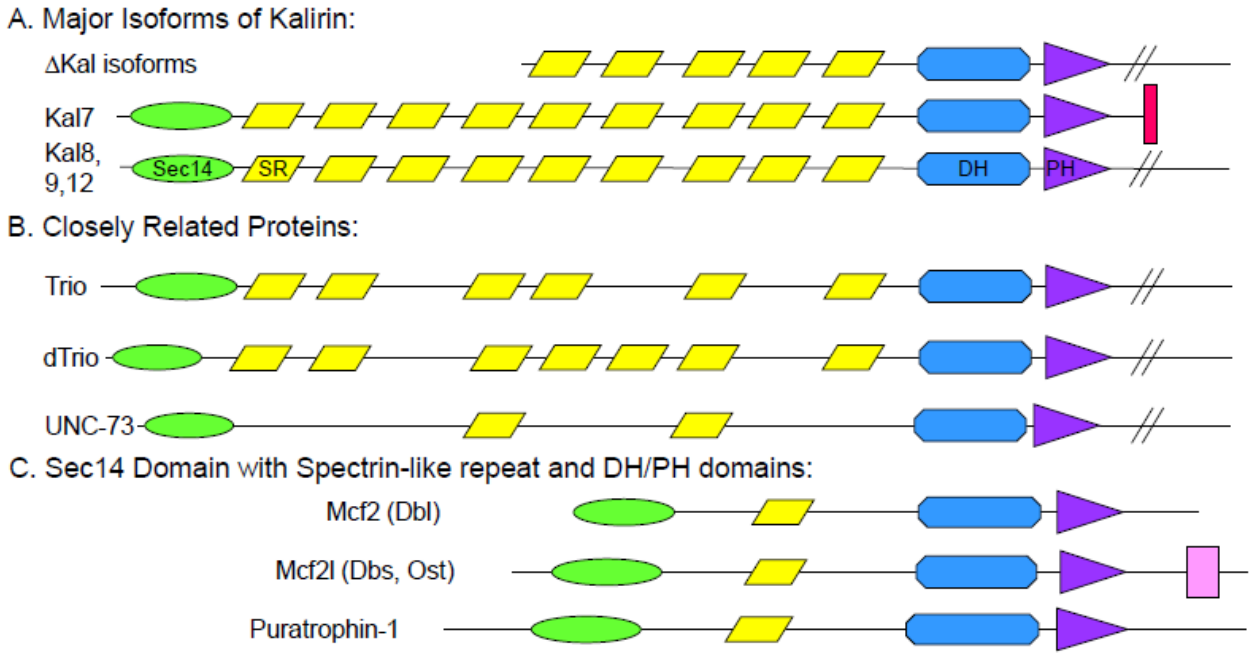

Figure 3-1. RhoGEFs encoded by the *Mus musculus* genome with putative Sec14 and spectrin repeat domains. The N-terminal region of each protein is drawn approximately to scale. (**A**) Major isoforms of mouse *Kalrn*. The presence of nine spectrin repeats (SRs) was experimentally verified (Vishwanatha et al., 2012). The longer isoforms (Kal8, Kal9, Kal12) contain additional domains (SH3, GEF2, kinase). (**B**) The N-terminal region of a single splice variant of *Trio* and the *Kalrn/Trio* ortholog in *C. elegans* and *D. melanogaster* is shown with predicted SRs. (**C**) A single splice variant of each additional *Mus musculus* RhoGEF with a predicted Sec14 domain is shown. Sec14, CRAL_TRIO domain – green oval; SR, spectrin-like repeat – yellow parallelogram; DH, Dbl homology domain – blue polygon; PH, pleckstrin homology domain – purple triangle; SH, Src Homology 3 domain – pink rectangle; PDZ binding motif - red bar. *Kalrn*, A2CG49; *Trio*, Q0KL02; *Drosophila trio A*, Q7KVD1; *unc-73A*, O61528; *Mcf2*, A2AEU1; *Mcf2l*, Q64096; *Puratrophin-1* (*Plekhg4*), mFLJ00068.

Results

Kal7 and ΔKal7 differ in their effects on spine density, spine length and synapse formation

Although ΔKal7 and Kal7 are equally active RhoGEFs and have identical PDZ-binding motifs, exogenous Kal7 expressed in cultured cortical neurons localizes to spine-like dendritic protrusions, while ΔKal7 localizes more diffusely, with less staining apparent in spines (176). Levels of Kal7 protein are much greater than levels of ΔKal7 in mouse and rat cortex (171,204-206) and hippocampus (171) and neither protein shows any tendency to oligomerize (176,186). To determine which aspects of spine morphogenesis were most affected by the absence of the Sec14 and first four spectrin repeat regions, we quantified the effects of Kal7 and ΔKal7 on synaptic cluster density and location, the association of spines with pre-synaptic endings, spine length and spine area; different proteins are known to contribute differently to control of these parameters (207-209).

Dissociated rat neurons were nucleofected with vectors encoding Myc-tagged Kal7 or ΔKal7 at the time of plating and kept in culture for 20 days (DIV20) before fixation and analysis. Exogenous Kalirin was visualized using monoclonal antibody to Myc and presynaptic endings were identified using antibody to the endogenous vesicular glutamate transporter, Vglut1 (**Fig. 3-2**). Based on Myc staining, neurons expressing similar levels of the two proteins were compared. Neurons expressing MycΔKal7 extended more MAP2-positive processes than neurons expressing MycKal7, but the processes were shorter (**Fig. 3-2A, B;** not quantified). MycKal7 was primarily localized (about 70% of total signal) to the tips of dendritic spines (**Fig. 3-2A, C**). In agreement with our previous report (210), nearly all MycKal7-positive puncta were apposed to presynaptic Vglut1-positive puncta. In contrast, much of the MycΔKal7 was uniformly distributed throughout the cell soma and diffuse staining was observed in the dendritic shaft (**Fig. 3-2B, D**); about 50% of the MycΔKal7 staining was in spines. Some MycΔKal7-

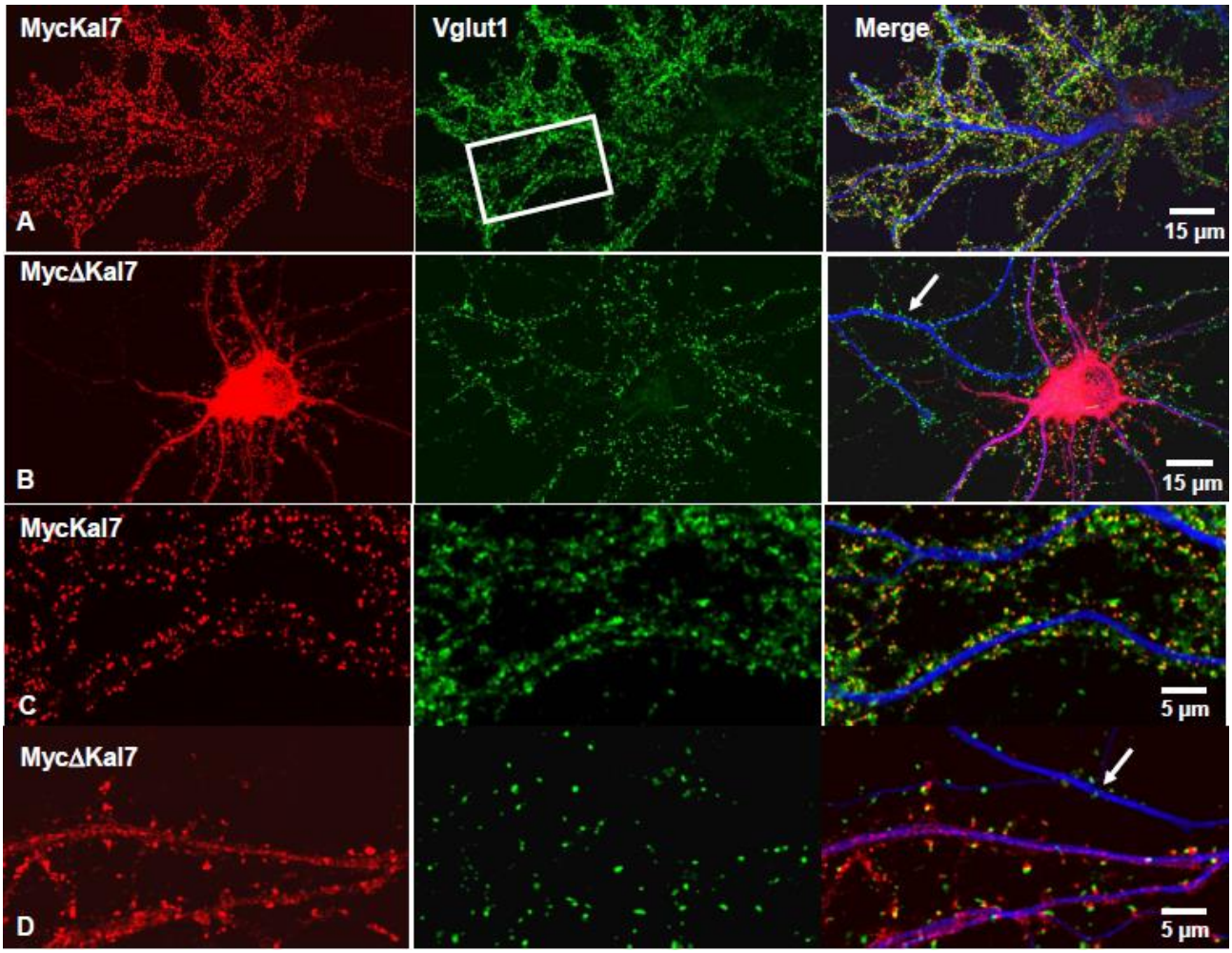

Figure 3-2. MycKal7 and MycΔKal7 differ in their effects on spine and synapse formation. Hippocampal neurons were transfected with vector encoding MycKal7 (**A**, **C**) or MycΔKal7 (**B**, **D**) at the time of plating (P0). Neurons were fixed at DIV20 for double immunostaining with antibodies to Myc (red), Vglut1 (green: a marker for excitatory presynaptic terminals) and MAP2 (blue: a marker for dendrites). (**C**) is a higher power image from the boxed dendrites of (**A**). The arrows in (**B**) and (**D**) show a Myc-negative, non-transfected dendrite. In earlier studies using similar protocols, we established that levels of exogenous MycKal7 were only slightly higher than levels of endogenous Kal7 (210).

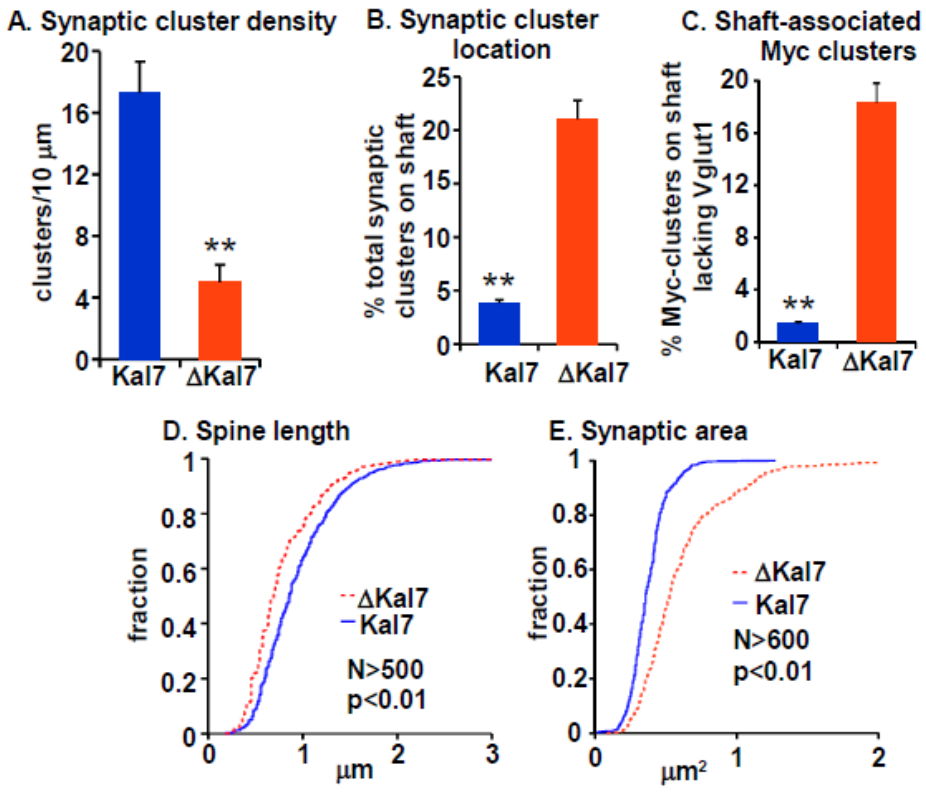

Figure 3-3. Quantification of spine morphology in neurons expressing MycKal7 or MycΔKal7. Hippocampal neurons expressing MycKal7 or MycΔKal7 as described in **Fig. 3-2** were analyzed. Myc-positive and Vglut1-positive clusters were manually traced in at least 10 neurons for each group; criteria for inclusion are described in Methods. Myc-clusters were identified as spine-associated or shaft-associated. (**A**) Juxtaposed or overlapping Myc/Vglut1 clusters on spines or the dendritic shaft are referred to as synaptic clusters; data are reported as clusters/10 µm. Synaptic cluster density was significantly higher in neurons expressing MycKal7 than in neurons expressing MycΔKal7 (17.3±2.0 vs. 5.0±1.1 per 10 µm dendrite; $p<0.01$; t-test); error bars show standard error of the mean. (**B**) Myc-staining along dendrites within 100 µm of the cell soma was quantified using Metamorph and identified as spine-associated or shaft-associated. Shaft-associated synaptic clusters were plotted as a percentage of total synaptic clusters; shaft-associated synaptic clusters were more common in neurons expressing MycΔKal7 ($p<0.01$; t-test). (**C**) Shaft-associated Myc-clusters that lacked an apposed Vglut1 cluster were plotted as a percentage of total shaft-associated Myc-clusters; this percentage was higher in neurons expressing MycΔKal7 ($p<0.01$; t-test). Spine length (**D**) was significantly longer in neurons expressing MycKal7 than in neurons expressing MycΔKal7 ($p<0.01$; Kolmogorov-Smirnov). The area occupied by each Myc/Vglut1 cluster was quantified (**E**) and was significantly smaller in neurons expressing MycKal7 than in neurons expressing MycΔKal7 ($p<0.01$; Kolmogorov-Smirnov).

positive clusters along MAP2-positive dendrites were localized at the tips of dendritic spines, juxtaposed to Vglut1-positive puncta, but many occurred along the dendritic shaft (**Fig. 3-2D**).

Synaptic cluster density was determined by counting the number of Myc-positive puncta juxtaposed to Vglut1-positive puncta per unit dendrite length. Both spine and shaft clusters were counted. Synaptic cluster density was three-fold higher in neurons expressing MycKal7 than in neurons expressing MycΔKal7 (**Fig. 3-3A**). We then compared the proportion of total synaptic clusters associated with the dendritic shaft rather than a dendritic spine (**Fig. 3-3B**). In neurons expressing MycKal7, shaft synapses made up fewer than 5% of the total synaptic clusters, while over 20% of the total synaptic clusters on MycΔKal7-expressing neurons were associated with the shaft. Furthermore, while shaft-associated Myc-positive puncta formed by MycKal7 were almost always juxtaposed to a Vglut1-positive punctum, about 20% of the Myc-positive clusters formed by MycΔKal7 on the dendritic shaft lacked a Vglut1-positive presynaptic ending (**Fig. 3-3C**). Essentially every spine-associated Myc-positive punctum was juxtaposed to a Vglut1-positive punctum (**Fig. 3-2C, D**).

Since a Myc/Vglut1-positive cluster defines the juncture of the dendritic spine with its presynaptic ending, the distance (< 5 μm) between a Myc/Vglut1-positive cluster and the adjacent dendritic shaft was taken as the measure of spine length (**Fig. 3-3D**). Neurons expressing MycΔKal7 had slightly shorter spines than neurons expressing MycKal7 (0.79 ± 0.02 μm vs. 0.95 ± 0.02 μm; $p < 0.01$). The total area encompassed by the synaptic cluster (postsynaptic Myc staining and the adjacent presynaptic Vglut1 staining) was quantified as a measure of synaptic area (**Fig. 3-3E**). Although the spines formed in neurons expressing MycΔKal7 were shorter, their synaptic cluster areas were substantially larger than in neurons expressing MycKal7 (0.61 ± 0.01 μm^2 vs. 0.37 ± 0.01 μm^2, respectively; $p < 0.01$).

Taken together, these data indicate that the N-terminal Sec14/spectrin repeat region of Kal7 contributes to synaptic cluster density, location and area, to dendritic spine length and to the interaction of

presynaptic endings with their postsynaptic targets. We sought to further evaluate the roles of the Sec14/spectrin region by expressing truncated proteins in neurons.

The Sec14 domain of Kalirin plays a role in determining dendritic spine length

To explore the role of the Sec14 domain in neurons, both Kal7 lacking this domain (HA_2ΔSec14Kal7; see diagram at top of **Fig. 3-4**) and MycKal7 were co-expressed with GFP in cortical neurons (**Fig. 3-4A, B**). Dendritic spine density was not significantly different in neurons expressing ΔSec14Kal7 and MycKal7 (**Fig. 3-4D**), and both MycKal7 and ΔSec14Kal7 were largely localized to the tips of dendritic protrusions. However, dendritic spines formed in response to expression of ΔSec14Kal7 were shorter than those formed in response to MycKal7 (**Fig. 3-4E**); in both cases, most of the protrusions terminated in bulbous heads.

When expressed alone, the Sec14 domain of Kalirin (KalSec14-GFP) was diffusely distributed throughout the soma, dendritic shaft and dendritic protrusions (not shown). Even when expressed at low levels, expression of KalSec14-GFP had a detrimental effect on neuronal survival; since expression of KalSec14-GFP declined rapidly, cultures nucleofected at the time of plating were fixed on DIV13. The protrusions formed in neurons expressing KalSec14-GFP were less numerous, but longer than those present in neurons expressing MycKal7 or ΔSec14Kal7 (**Fig. 3-4C, D, E**). Although not essential for the formation of dendritic spines, our data indicate that the Sec14 domain of Kalirin plays a role in determining protrusion length.

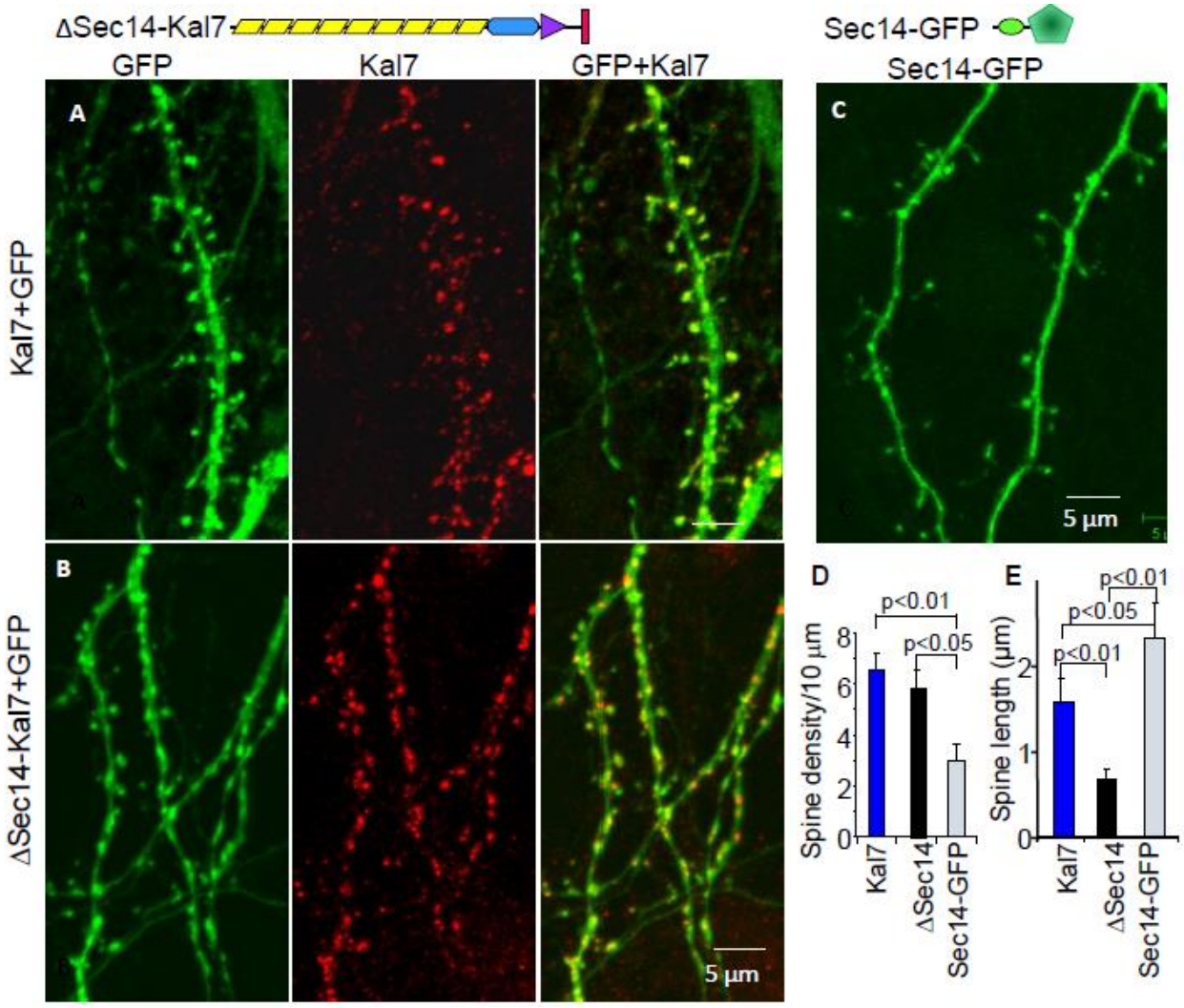

Figure 3-4. The Sec14 domain of Kal7 plays a role in determining spine length. Diagrams illustrating the proteins expressed appear at the top. Hippocampal neurons prepared from P0 rat embryos were doubly transfected with vectors encoding MycKal7 and GFP (**A**) or HA_2-ΔSec14-Kal7 and GFP (**B**) or transfected with vector encoding a KalSec14-GFP fusion protein (**C**) at the time of plating. Neurons were visualized for GFP and Myc (HisMycKal7) or HA (HA_2-ΔSec14-Kal7) (red) at DIV13, a time at which endogenous Kal7 is barely detectable (171). Spine density (**D**) was indistinguishable in neurons expressing Kal7 and ΔSec14-Kal7 but was significantly lower in Sec14-GFP expressing neurons (t-test); synaptic density is lower here than in **Fig. 3-3** because synapse formation is not complete in DIV13 neurons. Quantification of spine length (**E**) revealed that ΔSec14-Kal7 produced significantly shorter spines than MycKal7 ($p<0.01$), while Sec14-GFP produced aberrantly long spines ($p<0.05$).

N-terminal fragments of Kal7 stimulate the formation of dendritic spines

Kal4, a minor *Kalrn* splice variant (transcript levels in adult mouse cortex = 5.76 ± 0.17% that of Kal7), contains only the Sec14 domain and five spectrin repeats (**Fig. 3-5, top**). Both MycKal4 and MycKalSolo, which contains the Sec14 domain and all nine spectrin repeat regions of Kalirin, lack a GEF domain and PDZ binding motif (**Fig. 3-5, top**). To evaluate the role of the N-terminal region of Kalirin in spine morphology, these Myc-tagged proteins were co-expressed with GFP in primary rat neurons and fixed after 18DIV. Like MycKal7, MycKalSolo and MycKal4 were largely localized to puncta at the tips of dendritic protrusions (**Fig. 3-5C** and **D**). In both cases, Myc-positive puncta were closely juxtaposed to presynaptic Vglut1 positive puncta, indicating that the aberrantly shaped protrusions generated in response to expression of MycKalSolo or MycKal4 attracted pre-synaptic endings (**Fig. 3-5E** and **F**). Notably, the PDZ-binding motif was essential for postsynaptic localization of exogenous Kal7 at earlier developmental timepoints, when dendritic filopodia predominate (211); endogenous Kal7 and many of the other constituents of mature synapses are not expressed at this stage.

As expected, expression of MycKal7 increased spine formation approximately three-fold over the GFP control; in contrast, expression of MycΔKal7 had no effect on spine density (**Fig. 3-6A)**. Expression of MycKal4 or MycKalSolo stimulated the formation of dendritic protrusions, although not to the same extent as the full-length molecule (**Fig. 3-6A**; $p < 0.05$ for MycKal4 and MycKalSolo vs. GFP).

To quantify differences between the morphology of the protrusions formed in response to expression of MycKalSolo or MycKal4 or MycKal7, synaptic area and spine length were determined as described in **Fig. 3-3**. Synapses formed in response to MycKal4 were smaller than those formed by the full-length protein (0.45 ± 0.01 vs. 1.04 ± 0.02 μm^2 for Kal7, $p<0.01$), and synapses formed in response to MycKalSolo were intermediate in size (0.73 ± 0.01 μm^2), larger than Kal4 ($p<0.01$) and smaller than Kal7 ($p<0.01$) (**Fig. 3-6B)**. The protrusions formed in response to MycKal4 (1.06 ± 0.02 μm) were substantially shorter than those formed in response to MycKalSolo (1.24 ± 0.02 μm, $p<0.01$) and neither truncated form of Kal7 stimulated the formation of spines that were as long as those formed in response to

MycKal7 (1.54 ± 0.02 μm, $p<0.01$) (**Fig. 3-6C)**. Although the morphology of the dendritic protrusions and synaptic clusters formed in response to expression of N-terminal fragments of Kalirin lacking a GEF domain and a PDZ-binding motif was aberrant, the postsynaptic and presynaptic proteins needed to form functional synapses accumulated in or near them. Like full-length Kal7, MycKalSolo and MycKal4 co-localized with the postsynaptic density marker, NR1, as well as with PSD95 and ionotropic glutamate receptor subunit GluR1 at spine tips (PSD95 and GluR1, data not shown).

Although analytical ultracentrifugation revealed no tendency for the spectrin repeat regions of Kalirin to oligomerize (186), our earlier studies demonstrated interactions between Kal7 and its fifth spectrin repeat as well as the presence in cortical cytosol of Kal7 in heterogeneous higher molecular weight complexes (176). To determine whether localization of MycKalSolo and MycKal4 to spine tips required the presence of endogenous Kalirin, we expressed these proteins in cortical neurons prepared from mice lacking all of the isoforms of *Kalrn* (205). In the absence of any endogenous Kalirin proteins, MycKalSolo and MycKal4 still localized to small puncta juxtaposed to Vglut1-positive presynaptic endings (**Fig. 3-6E** and **F**). Difficulty expressing these truncated proteins and in maintaining healthy cultures of *Kalrn* knockout neurons precluded more detailed analysis of morphological differences and synapse formation.

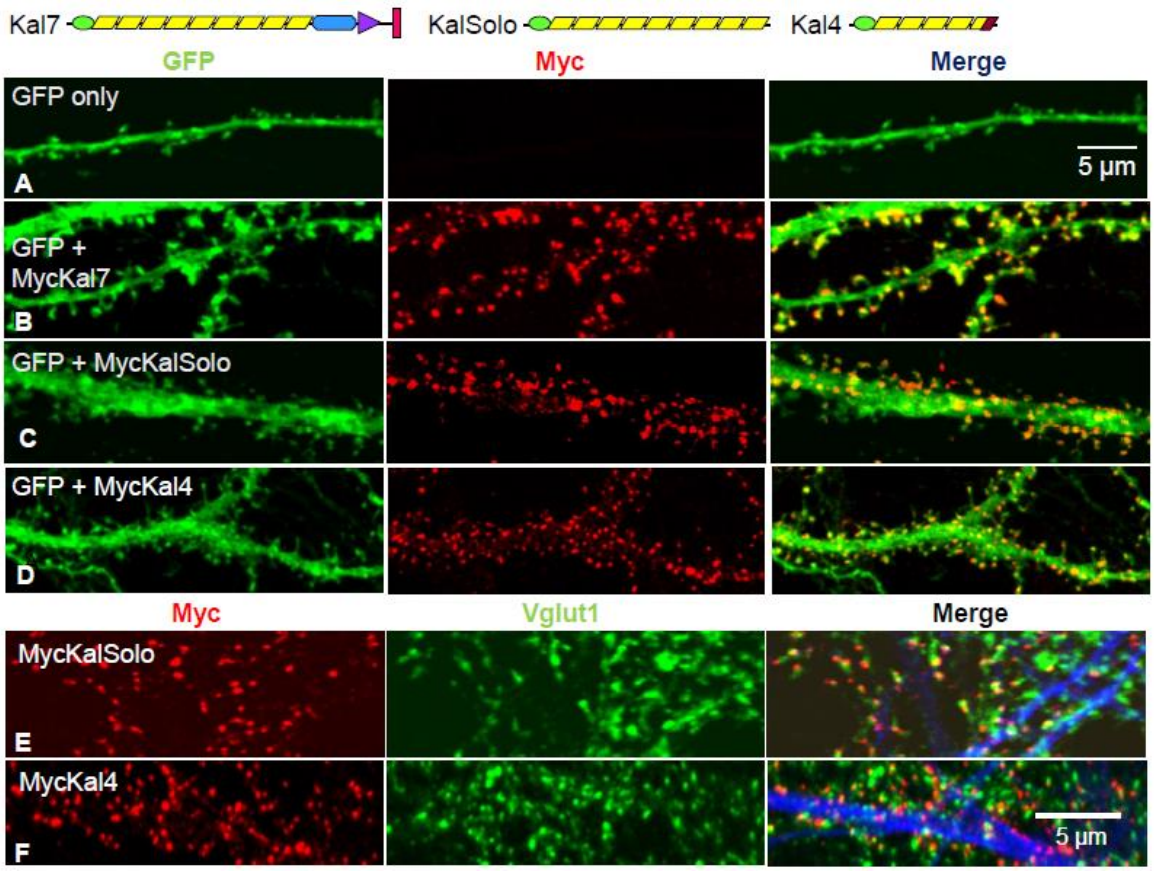

Figure 3-5. Expression of Kalirin constructs lacking the GEF and PDZ binding domains causes spine formation. Diagrams illustrating the proteins expressed appear at the top. Cortical neurons were transfected with vector encoding GFP only (**A**) or doubly transfected with vectors encoding GFP and MycKal7 (**B**), MycΔKal7 (not shown), MycKalSolo (**C**) or MycKal4 (**D**) at the time of plating. Neurons were visualized for GFP (green) and Myc (red) at DIV18. Cortical neurons expressing MycKalSolo (**E**) or MycKal4 (**F**) were stained simultaneously with antibodies to Myc (red), Vglut1 (green) and MAP2 (blue); for both, most Vglut1 puncta were juxtaposed to Myc puncta.

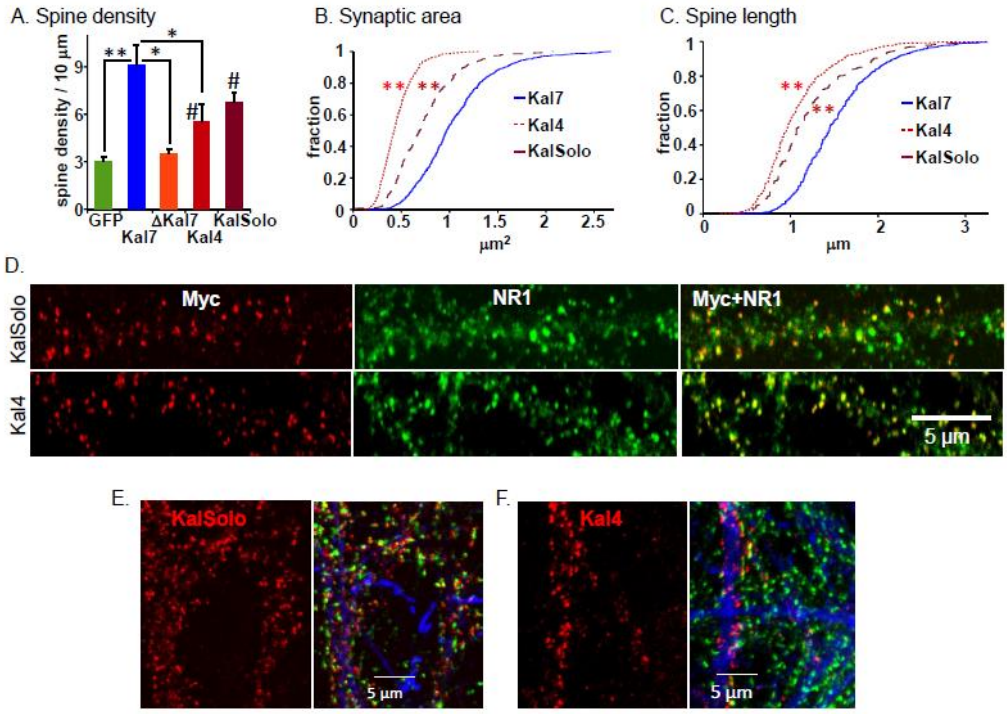

Figure 3-6. Neurons expressing MycKalSolo or MycKal4 form spines with aberrant morphology. (**A**) Spine-like protrusions along dendrites (at least 10 neurons in each group) within 100 µm of the cell soma were quantified using MetaMorph as described; one way analysis of variance (ANOVA) followed by Dunnett's test - *, $p < 0.05$; ** $p< 0.01$; #, $p<0.05$ compared to GFP and ΔKal7. MycΔKal7 did not differ from GFP in its ability to induce spine formation. Myc-positive and Vglut1-positive clusters on the dendritic shaft were included in the measurements for hippocampal neurons reported in **Fig. 3-3**; for the cortical neurons shown here, Myc-positive clusters on the dendritic shaft were excluded. Synaptic (Myc/Vglut1 cluster) area (**B**) and spine length (**C**) were quantified using Metamorph; data are displayed as a Kolmogorov-Smirnov distribution: (**B**) Kal7 larger than KalSolo and KalSolo larger than Kal4 (all $p<0.01$, **, Kolmogorov-Smirnov); (**C**) Kal7 larger than KalSolo and KalSolo larger than Kal4 (all $p<0.01$, **, Kolmogorov-Smirnov). (**D**) DIV 20 cortical neurons expressing MycKalSolo or MycKal4 (as described in **Fig. 3-5**) were stained simultaneously with antibodies to Myc (red) and NR1 (green); antibody specific to MAP2 was included to verify the identity of dendrites (not shown). Antisera to PSD95 and GluR1 produced staining patterns similar to those shown for NR1 (data not shown). (**E-F**) Cortical neurons prepared from E20 total Kalirin knockout embryos were nucleofected with vectors encoding MycKal7 (not shown), MycKalSolo or MycKal4; Myc (red), Vglut1 (green) and MAP2 (blue) were visualized simultaneously in cultures fixed on DIV19. As observed in primary neurons from wildtype rats, MycKalSolo and MycKal4 localized to spine-like structures; Vglut1 positive endings were juxtaposed to the small puncta formed by MycKalSolo and MycKal4.

KalSec14 forms an independent domain that interacts with phosphoinositides in a phosphorylation-dependent manner

Since neuronal expression demonstrated a role for the Sec14 domain in Kal7 function, we sought to uncover the underlying mechanism. The tissue-specific use of alternate *Kalrn* promoters appends peptides ranging in length from 5 to 38 amino acids to the N-terminus of the Sec14 domain (204,212). A GST-KalSec14 fusion protein was previously used to demonstrate its lipid binding abilities (Schiller et al., 2008); to eliminate potential interference from the N-terminal GST tag, we cleaved GST from purified KalSec14 (produced from the A-promoter) and included a short epitope tag on its C-terminus (**Fig. 3-7A**). Two residues in the Sec14 domain (Thr^{79} and Ser^{83}) can be phosphorylated by protein kinase A, protein kinase C and CaMKII, and both sites are phosphorylated in Kal7 isolated from mouse striatum [(201) and unpublished]. Based on the structures of yeast Sec14p and the Sec14 domain of neurofibromin 1, both phosphorylation sites should lie just outside of the putative lipid binding pocket (183,213). To determine whether phosphorylation of the Sec14 domain of Kalirin at either of these sights might alter its ability to bind lipids, we also purified KalSec14 in which Thr^{79} or Ser^{83} was mutated to Glu ($T^{79}E$) or Asp ($S^{83}D$), respectively, to try to simulate phosphorylation.

The structure of purified KalSec14 was evaluated using circular dichroism. Consistent with its identification as an independent domain, analysis of the spectrum revealed a protein that was 71% α-helix, 19% β-sheet and 10% unfolded (**Fig. 3-7A**). We used thermal denaturation to determine whether the isolated KalSec14 domain adopted a stably folded structure (**Fig. 3-7B**); cooperative unfolding was observed, with a

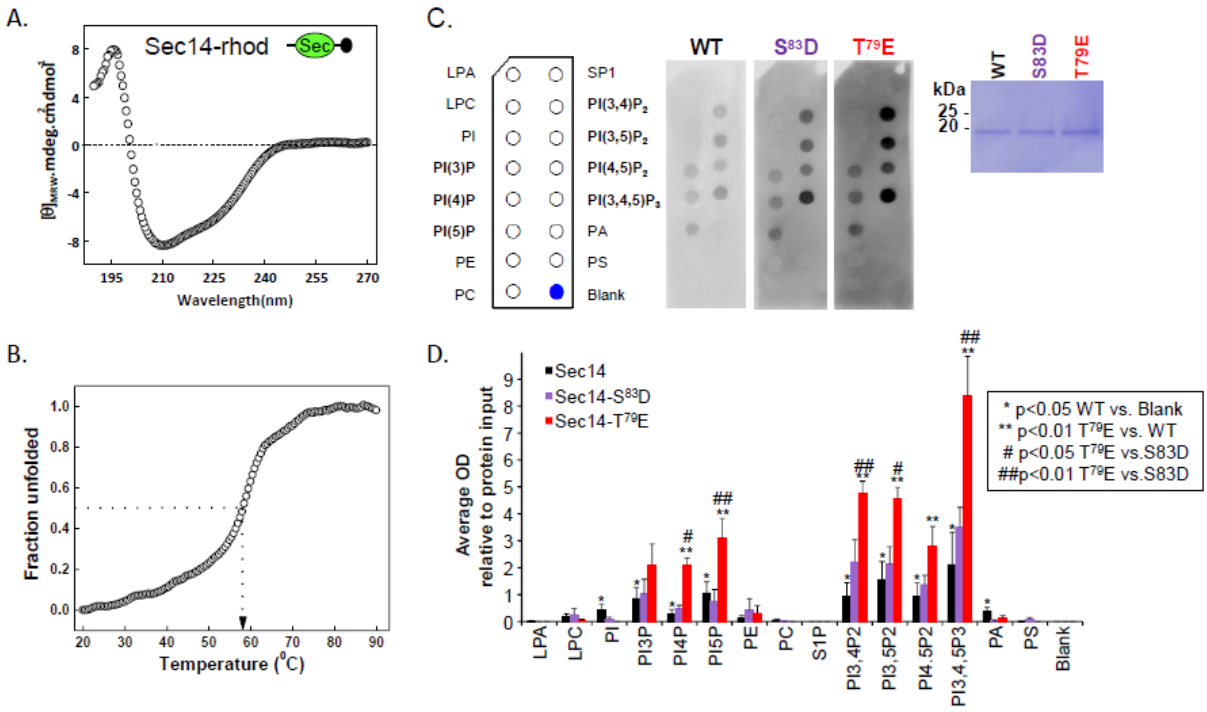

Figure 3-7. (Legend on following page)

Figure 3-7. The Sec14 domain of Kalirin interacts with phosphoinositides. (**A**) The circular dichroism spectrum (average of 6 determinations) of purified rhodopsin-tagged KalSec14 [inset illustrates location of epitope tag (black circle)] was evaluated from 190 to 270 nm; the spectrum obtained for KalSec14/$T^{79}E$ was indistinguishable (not shown). (**B**) Cooperative unfolding was observed in a thermal denaturation study of KalSec14; the transition temperature observed was 58$\pm$1^{o}C for WT-KalSec14 and 57$\pm$1^{o}C for KalSec14/$T^{79}E$ (**C**) Purified WT-KalSec14, KalSec14/$T^{79}E$ and KalSec14/$S^{83}D$ (1 □g/mL) [inset: Coomassie stained membrane demonstrating the purity of the recombinant proteins] were incubated with PIP strips as described in Methods; bound protein was visualized using antibody to the rhodopsin epitope tag. The lipids on the PIP strips are identified. (**D**) Data from five experiments were quantified; after background subtraction and normalization to the binding of WT-KalSec14 to PI(3,4,5)P_3, data were averaged; error bars represent standard error of the mean. No significant binding was observed to lysophosphatidic acid (LPA), lysophosphatidylcholine (LPC), phosphatidylethanolamine (PE), phosphatidylcholine (PC), sphingosine-1-phosphate (SP1) or phosphatidylserine (PS). WT-Sec14 exhibited significant binding to each of the phosphatidylinositides (*, $p<0.05$ WT vs. Blank; Holm-Sidak multiple comparisons test). Compared to WT-Sec14 and Sec14/$S^{83}D$, Sec14/$T^{79}E$ exhibited enhanced binding to each phosphorylated phosphatidylinositide except PI3P (** and ##, $p<0.01$ Sec14/$T^{79}E$ vs. WT and Sec14/$S^{83}D$, respectively; Holm-Sidak multiple comparisons test). After background subtraction and averaging, data for Sec14/$S^{83}D$ did not differ significantly from WT.

melt temperature of 58±1ºC. The KalSec14/T79E protein had similar properties (71% α-helix, thermal melt midpoint 57±1ºC).

We used PIP strips to assess the ability of purified KalSec14, KalSec14/T79E and KalSec14/S83D to interact with specific lipids. KalSec14 exhibited significant binding to each of the phosphorylated phosphatidylinositides, but not to major phospholipids like phosphatidylethanolamine, phosphatidylcholine or phosphatidylserine (**Fig. 3-7C**). KalSec14/T79E and KalSec14/S83D also exhibited a preference for phosphatidylinositides. Compared to the wildtype protein, KalSec14/T79E showed enhanced binding to each phosphorylated phosphatidylinositide except PI(3)P (**Fig. 3-7D**). Lipid binding by KalSec14/S83D did not differ significantly from that of WT-KalSec14. Taken together, our data suggest that Kal7 interacts with cellular membranes through KalSec14-mediated phosphatidylinositide binding. Furthermore, this interaction may be modulated by the phosphorylation status of KalSec14 and by alterations in cellular PIP levels. Since the phosphatidylinositides play a crucial role in membrane trafficking events, we evaluated the effect of KalSec14 expression on receptor-mediated endocytosis using a transferrin uptake assay.

KalSec14 expression reduces transferrin uptake in neuroendocrine cells

Expression of MycKal7, but not MycΔKal7, was previously shown to inhibit transferrin receptor-mediated endocytosis in non-neuronal cells (176), raising the possibility that the inhibition could be due to the Sec14 domain or the first 4 spectrin repeats. We used a similar system to evaluate the effect of the KalSec14 domain on transferrin endocytosis (**Fig. 3-8**). We expressed GFP or KalSec14-GFP and assessed uptake of fluorescently-tagged transferrin by serum-starved neuroendocrine cells. After a 5-min incubation with fluorescently-tagged transferrin (Tf-546), cells were rinsed in serum-free medium and fixed. As in neurons, KalSec14-GFP was diffusely distributed and expression at high levels or for long periods of time had a deleterious effect on cell morphology. To avoid the disruptive effects of expressing

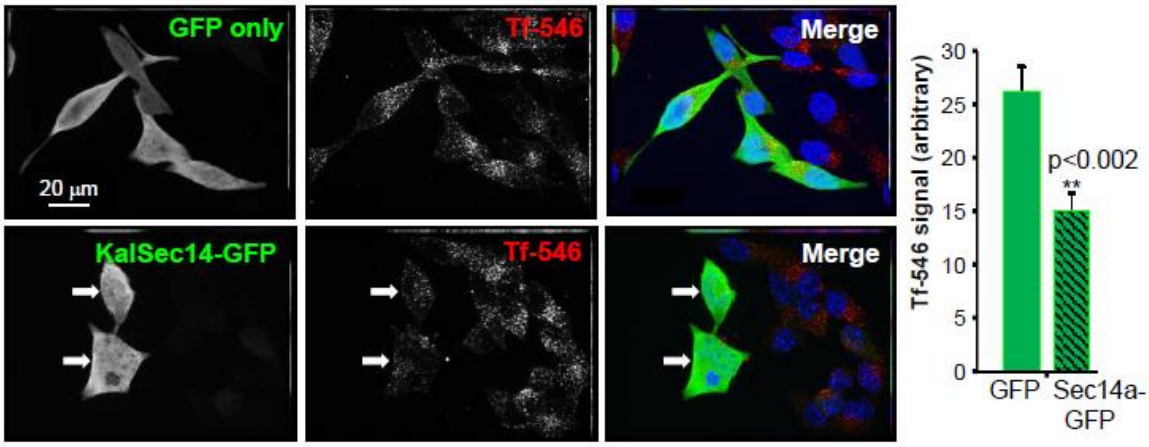

Figure 3-8. KalSec14-GFP disrupts receptor-mediated endocytosis in AtT-20 corticotrope tumor cells. (**Left**) 63X images showing Alexafluor-546-Transferrin uptake (red) by AtT-20 corticotrope tumor cells expressing either GFP (top) or KalSec14-GFP (bottom). Cells were exposed to AlexaFluor546-Tf for 5 min approximately 24 hours after transfection, and were then fixed, stained and imaged. Scale bars, 20 µm. (**Right**) Quantification of internalized 546-Tf. Data were collected using MetaMorph; values were normalized to cell size and relative to GFP control cells (n = 8 for GFP and 12 for Sec14-GFP; error bars, +/- SEM; **, $p<0.002$). Results were confirmed in an independent experiment.

high levels of KalSec14-GFP, less DNA was used in the transfection and the exogenous protein was visualized with a GFP antibody. Fluorescence microscopy revealed a significant reduction in Tf-546 internalization in cells expressing KalSec14-GFP when compared to GFP control cells (**Fig. 3-8**), indicating that exogenous KalSec14 interfered with constitutive membrane trafficking. Whether this effect is directly dependent on the lipid binding ability of KalSec14 or modulated by phosphorylation remains to be determined.

Kalirin SR4:6 is phosphorylated by Abl1

Our goal was to identify the features unique to the N-terminal portion of Kal7 that make this region important for spine formation, but its tight association with the cytoskeleton and lack of solubility complicated the search for interactors. The *Drosophila* ortholog of *Kalrn, dTrio,* was identified in a screen for heterozygous enhancers of lethality caused by mutations in *Abl* (203), and flies with mutations in *dTrio* and *Abl* exhibited similar deficits in axonal growth (202). Extending these observations to vertebrates is difficult, since gene duplication created two dual RhoGEFs, *Kalrn* and *Trio*, both equidistant in sequence from *Drosophila trio* (206). Additionally, human and other vertebrate genomes encode two *ABL* non-receptor tyrosine kinases, *ABL1* and *ABL2* (214-216). Several observations led us to ask whether Kalirin might be phosphorylated by Abl1. First, Kalirin plays an essential role in pathways activated by the PDGFβ receptor (200), and PDGFβ receptor engagement in hippocampal neurons activates Abl1 and inhibits NMDA receptor current (217). Second, the spectrin skeleton is thought to form a point of convergence between pathways controlled by Tyr phosphorylation and pathways controlled by intracellular Ca^{2+} (198). A phospho-Tyr was identified in SR7 of Kal7 isolated from adult mouse brain, and Tyr residues in SR4 (Tyr^{591}) and in the PDZ-binding motif (Tyr^{1653}) are phosphorylated *in vitro* by Fyn, a non-receptor tyrosine kinase (201).

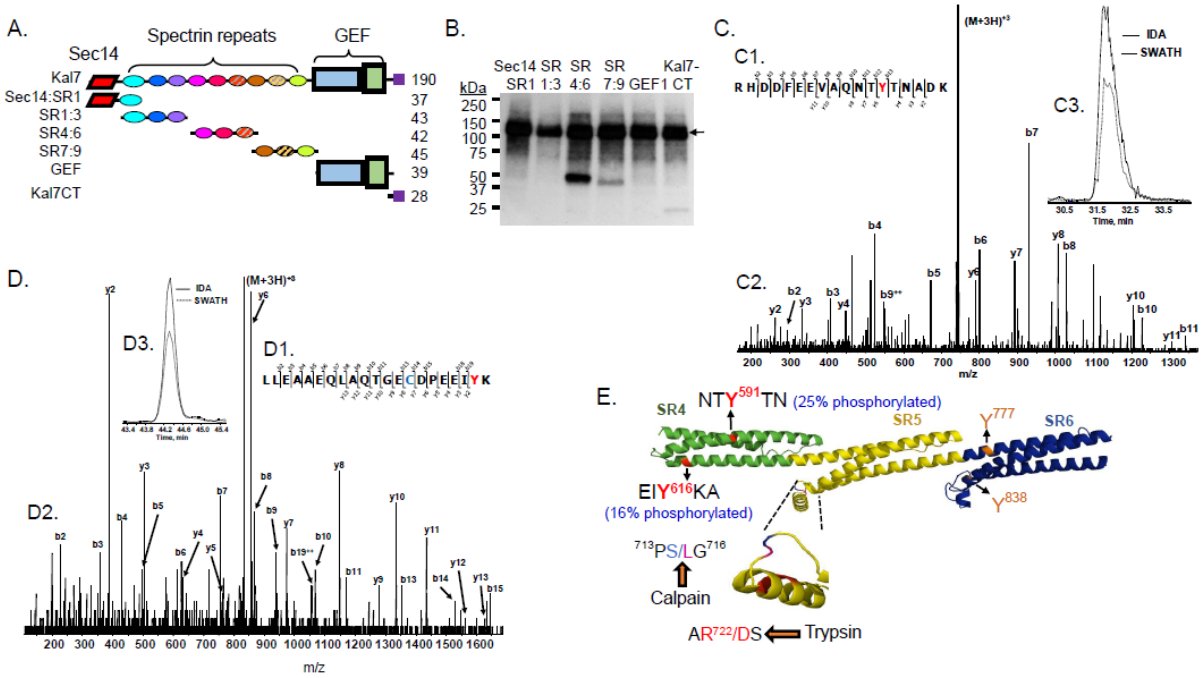

Figure 3-9. Phosphorylation of Kal SR4:6 by Abl1. (**A**) The purified fragments of Kalirin (0.5 µM) shown in the diagram were each exposed to recombinant Abl1 (10 nM) along with 5 µM ATP and 0.75 µCi [^{32}P-γ] ATP at 32°C for 30 min. (**B**) The reactions were stopped by boiling each sample into Laemmli sample buffer; after SDS-PAGE and transfer to a PVDF membrane, phosphorylated proteins were visualized by autoradiography (3 h exposure). In addition to autophosphorylated Abl1 (135 kDa; arrow), KalSR4:6 was phosphorylated; less extensive phosphorylation of KalSR7:9 and Kal7-CT was also detectable. (**C** and **D**) The reaction was scaled up as described in Methods and phosphorylated SR4:6 recovered from a silver stained 4-15% acrylamide gel was subjected to in-gel digestion with trypsin followed by LC-MS/MS identification of phosphorylated Tyr residues. Sites are identified using the NP_114451.2 numbering scheme for *Kalrn*. MS/MS fragmentation patterns for the Tyr^{591} (**C**) and Tyr^{616} (**D**) peptides are shown. Manual verification and the site of Tyr modification (red Y) are illustrated in **C1** and **D1**. The b- and y-ion series peak assignments are shown (**C2** and **D2**). Extracted Ion Chromatograms of the parent ion (M+2H)$^{+2}$ for the IDA and SWATH runs were retention time aligned (**C3** and **D3**). Note that the Cys (blue) in the Tyr^{616} peptide was acrylamide gel modified (propionamide). **(E)** Model illustrates the location of the four Tyr residues in KalSR4:6. For each Tyr, % Phosphotyrosine (shown in parenthesis) was calculated relative to the sum of all of the peptides containing that Tyr residue (phosphorylated or not). The protease-sensitive insert in the B-C loop of SR5 (inset) contains the only predicted calpain cleavage site (186).

The purified fragments of Kal7 shown in **Fig. 3-9A** were incubated with recombinant Abl1 and [^{32}P-γ]ATP for 30 min. Autoradiography after SDS-PAGE revealed preferential phosphorylation of SR4:6 by Abl1 (**Fig. 3-9B**); no phosphorylation of Sec14:SR1, SR1:3 or the GEF region was detected and phosphorylation of SR7:9 and GST-Kal7-CT was much less extensive than phosphorylation of SR4:6. Similar experiments utilizing recombinant Abl2 indicated that it does not phosphorylate Sec14:SR1, SR1:3 or SR4:6 (data not shown).

Tryptic digestion and high resolution LC-MS/MS analysis of recombinant SR4:6 phosphorylated by Abl1 identified two Abl1 phosphorylation sties in SR4,Tyr^{591} (**Fig. 3-9C**) and Tyr^{616} (**Fig. 3-9D**). Tyr^{591} is also phosphorylated by Fyn, but Abl1, unlike Fyn, does not extensively phosphorylate Tyr^{1653}, which sits in the PDZ-binding motif of Kal7 and is contained in Kal7-CT (**Fig. 3-9B**). The extent to which Abl1 phosphorylated Tyr^{591} and Tyr^{616} under the conditions tested was determined by quantifying all of the peptides that contained the Tyr of interest; based on this analysis, both Tyr^{591} and Tyr^{616} were extensively phosphorylated (25% and 16%, respectively), while no detectable phosphorylation of Tyr^{777} or Tyr^{838} (both located in SR6) occurred (**Fig. 3-9E**). Based on the structure predicted for SR7:9 (http://zhanglab.ccmb.med.umich.edu/I-TASSER/), Tyr^{591} is located at the interface between helices A and B of SR4 and introduction of a negative charge at this position would be expected to perturb the structure.

Abl1 phosphorylation of KalSR4:6 increases calpain-mediated proteolysis

Both the formation of new spines and the remodeling of existing spines require changes in the existing cytoskeleton; endoproteolytic cleavage of cytoskeletal proteins is known to contribute to this process. Calcium-mediated activation of mu-calpain and ERK-mediated activation of m-calpain are known to contribute to this remodeling process (197,218-220). KalSR4:6 was previously shown to contain a trypsin-sensitive site in the B-C loop of SR5 (AR^{722}/DS) (**Fig. 3-9E**) (186). We tested the

hypothesis that phosphorylation of KalSR4:6 by Abl1 alters its sensitivity to calpain-mediated proteolysis *in vitro*. KalSR4:6 that had been incubated with γ-^{32}P-ATP and Abl1 and KalSR4:6 incubated under the same conditions but without Abl1 were exposed to increasing concentrations of mu-calpain. SDS-PAGE revealed that ^{32}P-labeled KalSR4:6 phosphorylated by Abl1 (**Fig. 3-10A, left**) was more sensitive to mu-calpain-mediated degradation than the non-phosphorylated protein (**Fig. 3-10A, right**). The only predicted calpain cleavage site in KalSR4:6 (PS^{714}/LG) is located in the same loop that contains the previously identified trypsin-sensitive site (186).

We next asked whether KalSR4:6 in which Tyr^{591} or Tyr^{616} had been replaced by a negatively charged amino acid (Glu), exhibited a similar increase in calpain sensitivity. SDS-PAGE analysis of purified KalSR4:6/Y^{591}E and KalSR4:6/Y^{616}E revealed that each migrated more slowly than KalSR4:6, suggesting a major effect of each point mutation on the properties of the protein, even during SDS polyacrylamide gel electrophoresis (**Fig. 3-10B, left**). Consistent with this conclusion, KalSR4:6/Y591/E was more sensitive to calpain-mediated degradation than the wildtype protein, with nearly complete degradation after incubation with 50 ng of calpain (**Fig. 3-10B, right**). Mutation of Tyr^{616} to Glu had a lesser effect on sensitivity to mu-calpain (**Fig. 3-10B, right**). Preferential Abl1-mediated phosphorylation of Tyr^{591} vs. Tyr^{616} and a more powerful effect of Tyr^{591} phosphorylation on sensitivity to calpain cleavage were confirmed by analyzing the stability of Abl1-phosphorylated KalSR4:6/Y^{591}E and KalSR4:6/Y^{616}E (data not shown).

Inhibition of Abl alters spine morphology

The role of the BCR/ABL fusion protein in cancer led to the development of compounds that inhibit ABL1/ABL2 without affecting other non-receptor tyrosine kinases (214,215). We exposed DIV18 cortical neurons prepared from wildtype mice to one of these inhibitors (GNF-5) for 6 h and then quantified dendritic protrusion density and length; membrane targeted farnesylated GFP (fGFP) was

expressed to facilitate the analysis (**Fig. 3-10C**). Drug treated and control neurons were fixed and stained for GFP and filamentous actin. The density of actin-rich dendritic protrusions on the dendrites of wildtype cortical neurons increased significantly following GNF-5 treatment, with no effect on protrusion length (**Fig. 3-10C**). Based on its effects on KalSR4:6, phosphorylation of Kal7 by Abl1 may target it for cleavage by calpain. If so, inhibition of Abl1 would be expected to stabilize Kal7; the ability of Kal7 to stimulate the formation of dendritic spines could account for the observed increase in protrusion density.

We next asked whether cultures prepared from $Kal7^{KO}$ cortices responded differently to GNF-5 treatment (**Fig. 3-10D**). When DIV18 cortical neurons from $Kal7^{KO}$ mice were exposed to the same level of GNF-5, protrusion density was unaffected. Although GNF-5 was without effect on dendritic protrusion length in wildtype neurons, $Kal7^{KO}$ neurons responded to drug treatment with an increase in protrusion length (**Fig. 3-10D**). The fact that GNF-5 had distinctly different effects on the dendritic protrusions formed by wildtype and $Kal7^{KO}$ neurons is consistent with the conclusion that Kal7 plays an important role in Abl-mediated effects on spine morphology. The ability of Kal7 to promote spine maturation (171) may limit the formation of long, filopodia-like protrusions; lacking this maturation factor, the protrusions formed by $Kal7^{KO}$ neurons may be more likely to elongate.

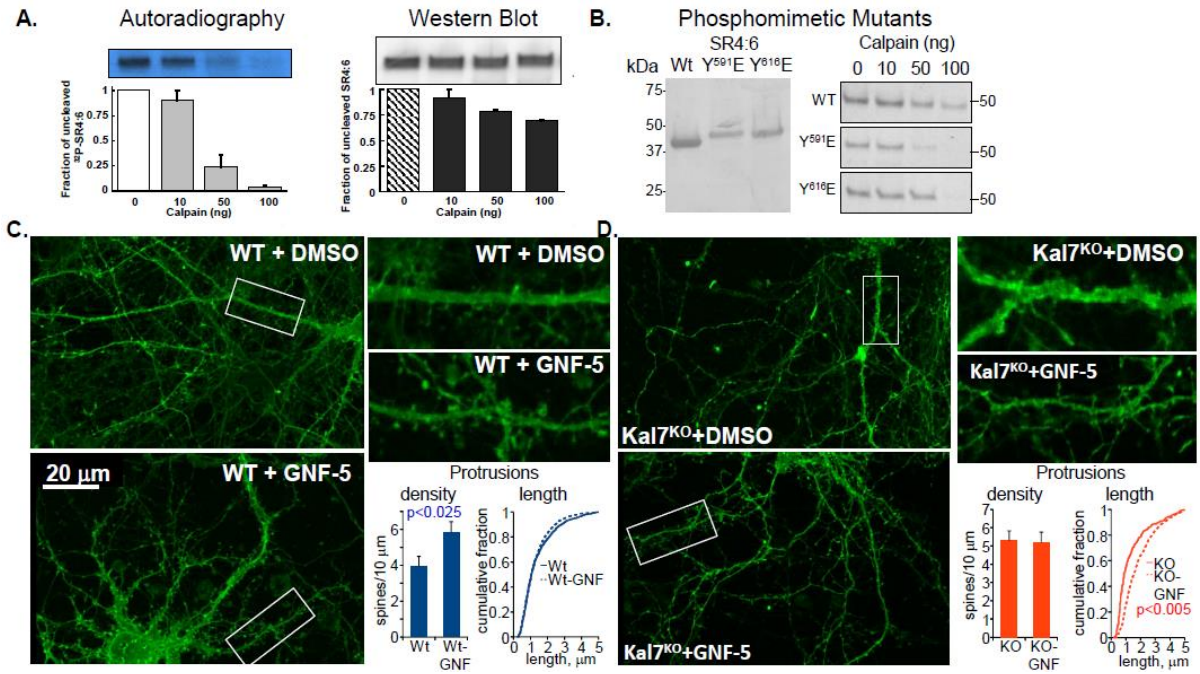

Figure 3-10. (Legend on following page)

Figure 3-10. Phosphorylation of KalSR4:6 by Abl1 increases its sensitivity to calpain. (**A**) KalSR4:6 phosphorylated with γ-^{32}P-ATP by Abl1 or exposed to the same conditions in the absence of ATP and Abl1 was exposed to the indicated amount of mu-calpain for 60 min at 37^{o}C. Digested samples were fractionated by SDS-PAGE and transferred to PVDF membranes; ^{32}P-labeled KalSR4:6 was visualized by autoradiography (**Left**) and unlabeled KalSR4:6 was visualized by Western blot (**right**) using an antibody to SR4:7 (JH2580) (221). The amount of intact KalSR4:6 remaining was quantified; error bars show range of duplicate experiments. (**B**) Purified recombinant KalSR4:6 and KalSR4:6 with a phosphomimetic mutation at position 591 (SR4:6/Y^{591}E) or at position 616 (SR4:6/Y^{616}E) was fractionated by SDS-PAGE, transferred to a PVDF membrane and visualized with Coomassie Brilliant Blue; mutation of either Tyr residue altered the mobility of the protein during electrophoresis. The purified proteins (1 µg each) were exposed to the indicated dose of mu-calpain as described above; the reaction was stopped and the SDS-PAGE fractionated products were visualized with Coomassie; mutation of either site increased the calpain sensitivity of the protein. (**C, D**) DIV18 cortical neurons from WT (**C**) and Kal7^{KO} (**D**) mice were exposed to medium containing 10 µM GNF-5 in DMSO, or an equivalent volume of DMSO, for 6 h and fixed. Images were coded and scored by a blinded observer. GNF-5 increased the dendritic protrusion density in WT but not Kal7^{KO} neurons (**C**), while increasing the protrusion length in Kal7^{KO} but not WT neurons (**D**). N=9-14 WT neurons, 6-8 Kal7^{KO} neurons; N=1187-1652 WT protrusions, 306-838 Kal7^{KO} protrusions.

Discussion

Spine morphology, a key determinant of excitatory synaptic transmission, is regulated by the actin cytoskeleton (208,209,222-225). The Sec14 and first four spectrin repeats of Kal7 contribute to control of synaptic cluster area and location, trans-synaptic communication, spine density and spine length. Long-term potentiation in hippocampal slice preparations, control of spine head size and spine formation by cortical neurons in response to ephrinB require the GEF activity of Kal7 (42,172), but spine formation does not. The ability of the Sec14 and spectrin repeat regions of Kalirin to modulate spine formation and size provides sites at which diverse signaling pathways can regulate these processes.

The Sec14 domain of Kal7 and spine length

Kal7 lacking only its Sec14 domain (ΔSec14Kal7; diagram, **Fig. 3-4**) produced the normal number of spines, but the spines were short. Consistent with this, expression of the isolated Sec14 domain increased spine length without increasing spine formation. Sec14 domains occur in only ~20 murine proteins (183,226); some bind small, hydrophobic ligands while others interact with small GTPases and their GEFs and GAPs. The Sec14 domains of Mcf2 and Mcf2l are involved in intramolecular interactions and bind phosphoinositides (180-182). The ability of similar lipid binding proteins to move lipids between membranes is suited to a role in changing cell morphology (227).

Both GST-KalSec14 and KalSec14-rhodopsin bound multiple phosphatidylinositides and not the more prevalent phospholipids. Thr^{79}, predicted by homology modeling to be in an α-helix that stabilizes the lipid binding pocket, can be phosphorylated by multiple synaptic protein kinases, and is phosphorylated *in vivo* (201). Its replacement with a phosphomimetic mutation enhanced Sec14 binding to most of the phosphatidylinositides. Although different phosphatidylinositides are localized to different compartments, KalSec14-GFP was diffusely distributed when expressed in neurons or in neuroendocrine cells, and prolonged or high level expression was toxic.

When expressed in fibroblasts, Kal7, but not ΔKal7, blocked the uptake of transferrin (176); the transferrin/transferrin receptor complex is bound by the AP2 complex and internalized in a clathrin-mediated process (228). Expression of KalSec14-GFP diminished transferrin uptake, linking Kalirin to membrane trafficking. Internalization of transferrin by its receptor is blocked when plasma membrane levels of PtdIns(4,5)P_2 are rapidly reduced (228). The diminished levels of NR2B on the surface of $Kal7^{KO}$ neurons could reflect the role of the Kal7 Sec14 domain in membrane trafficking. AMPA receptor clustering at the PSD is affected by phosphatidylinositides (229) and phosphoinositide-3-kinase activation affects spine and synapse formation (230).

Spine length is decreased by repeated stimulation of cultured neurons with NMDA or by blocking $GABA_A$ receptors and increased by short-term treatment with tetrodotoxin (231,232). Loss of SynCAM 1, a synaptic adhesion molecule (233), and ablation of PSD95 (234) increase spine length. Over-expression of the actin binding domain of α-actinin-2, which binds NMDA receptor subunits NR1 and NR2B (235), increases spine length without altering spine density.

The spectrin repeats of Kal7, Abl and spine formation

Unlike ΔKal7, which did not increase spine formation, expression of ΔSec14Kal7 (diagram, **Fig. 3-1A**) increased spine density as much as Kal7. Fragments of Kal7 composed only of SRs were often insoluble, so we examined proteins that included the N-terminal Sec14 domain and four (Kal4) or nine (KalSolo) SRs. Their effects on spine density, length and area were graded. Although the spines that formed in response to Kal4 and KalSolo were shorter, with smaller synaptic areas than spines formed in response to Kal7, post-synaptic markers (PSD-95, GluR1, NR1) accumulated at their tips and pre-synaptic endings were juxtaposed.

Over-expression of α-actinin-2, with its SRs and PDZ-binding motif, increases both spine length and density (236). Hippocampal neurons deficient in Septin7 have abnormally long spines (237). Septin7

forms a complex with ERK3 and MK5 and is localized at the spine base. Interestingly, the SR region of Kalirin interacts with MK5, which phosphorylates a Ser in the SH3-binding motif in SR3 (238), perhaps contributing to the effects of Kalirin on spine length.

The molecular basis underlying the genetic association of *dTrio* and *dAbl* has never been clarified (202,203,239). *Abl1* and *Abl2/Arg*, mammalian homologues of *dAbl*, are both expressed in neurons (215,216,240). Abl proteins localize to sites of actin remodeling and multiple receptor tyrosine kinases interact with and are phosphorylated by Abl (214). We focused on Abl1 because it phosphorylated a site in SR4, but SR7:9 was phosphorylated by Abl2. Like Kal7, Abl1 localizes to the PSD, where it phosphorylates PSD-95 (215,217,240). Activation of Abl can be triggered by receptor tyrosine kinases, chemokine receptors, oxidative stress and interactions with regulatory proteins (215). Abl1 phosphorylates two Tyr residues (Tyr^{591} and Tyr^{616}) in the fourth SR of Kalirin; Kal7 isolated from mouse brain is phosphorylated on Tyr^{591} (201).

Phosphorylation of Tyr^{591} produced a substantial change in the conformation and protease sensitivity of KalSR4:6. Controlled proteolysis plays an essential role in long-term potentiation (218) and in spine morphogenesis (220,241,242). Specifically, calpain inhibitors block LTP *in vitro* and *in vivo* (241). Phosphorylation of a single Tyr in αII-spectrin reduces its susceptibility to calpain-mediated proteolysis (195,196). In contrast, phosphorylation of KalSR4:6 by Abl1 increased its sensitivity to calpain cleavage. The site phosphorylated by Abl1 is conserved in Kalirin and Trio. Although well-conserved in Kalirin, the protease-sensitive loop in KalSR4:6 is not present in Trio. Phosphorylation of Kal7 at Tyr^{591} could also affect its localization or its ability to interact with other proteins. The third SR of Kalirin contains an SH3-binding motif, raising the possibility that it could interact with the SH3 domain of Abl1. The interaction of Abl1 with F-actin and G-actin (214) could then contribute to the ability of Kal4 and KalSolo, which lack a GEF domain, to increase spine formation.

Highly selective inhibitors of Abl1/Abl2 were developed to treat chronic myeloid leukemia (214,215). We were able to demonstrate an increase in the density of dendritic protrusions 6 h after the

addition of GNF-5 to primary cultures of cortical neurons. Notably, since GNF-5 inhibits Abl1 and Abl2 (both of which are expressed in these neurons), both Abl1 and Abl2 may contribute to the observed changes in protrusion density. To our knowledge, this is the first time the neuronal effects of this class of Abl inhibitors have been evaluated. The fact that protrusion density was not increased when $Kal7^{KO}$ neurons were exposed to GNF-5 establishes a role for Kal7 in the response. Stabilization of Kal7 in response to inhibition of Abl1 phosphorylation of Tyr^{591} and/or Tyr^{616} could contribute to the observed increase in protrusion density.

Materials and Methods

Primary neuronal cultures and transfection

Cultures were prepared from postnatal day 0 (P0; cortical or hippocampal) Sprague Dawley rats or embryonic day 20 (E20; cortical) $KalSR^{KO/KO}$ mice as described (170,171). In $KalSR^{KO/KO}$ mice, elimination of exon 13 in the spectrin repeat region ablates production of all major isoforms of Kalirin (205). Freshly dissociated neurons (1-2 x 10^6 neurons) were nucleofected using program O-003 (Amaxa Gmbh, Germany) with the vectors described below. Nucleofected neurons were kept in Neurobasal A (embryonic) or Neurobasal (P0) maintenance medium for up to 3 weeks as described (168). The vectors encoding HisMycKal7, HisMycΔKal7, HisMycKalSolo, HisMycKal4, HA_2ΔSec14Kal7 (starts EEWIELRL-) and KalSec14-GFP (ends -LDYNH) (176) and farnesylated-GFP (fGFP) (243) were described. The pGEX6P1-KalSec14 vectors included the rhodopsin epitope (*italicized*) at the COOH-terminus (M^{1}VLSG – LRLSL^{172}*GATETSQVAPA*) (Kalirin numbering: AAF66018.1, GI:7650388).

Immunocytochemistry

Immunostaining of cultures was performed as described (210). Neurons were fixed with 4% paraformaldehyde in phosphate buffered saline (PBS). After permeabilization with 0.20% Triton X-100 in blocking buffer [1% BSA, 5% normal goat and/or donkey serum in PBS, pH7.4] followed by incubation for 50 min in blocking buffer at room temperature, cells were doubly or triply stained with appropriate primary antibodies overnight at 4°C. Primary antibodies were visualized with appropriate secondary antibodies: Cy3-donkey anti-mouse, FITC-donkey anti-rabbit, FITC-donkey anti-rat and FITC-donkey anti-guinea pig IgG were from Jackson ImmunoResearch Laboratories, Inc. (West Grove, PA); Alexa Fluor 633-goat anti-rabbit and anti-mouse IgG were from Molecular Probes (Eugene, OR). Images were obtained using a Zeiss LSM510 confocal microscope. Hoechst nuclear stain (Invitrogen, Grand Island, NY) and TRITC-phalloidin (Sigma-Aldrich, St. Louis, MO) were used where indicated.

Antibodies

Rabbit antibodies to the following antigens were used: Kal7 (affinity-purified JH2958, 1:200) (Penzes et al., 2000), MAP2 (1:500, AB5622, Millipore, Billerica, MA) and Myc (1:100, #39688, Abcam). Mouse monoclonal antibodies to the following antigens were used: PSD95 (clone28/43, 1:300, UC Davis, NeuroMab Facility), NR1 (1:300, #556308, BD Pharmingen), MAP2 (1:500, #1406, Sigma), Myc (9E10, 1:20). Guinea pig antibody to Vglut1 (1:3000, AB5909, Millipore, Billerica, MA) and rat antibody to GFP (1:1000, Nacalai Tesque, Kyoto, Japan) were used where indicated.

GNF-5 Treatment

Sparsely plated WT or Kal7$^{KO/KO}$ cortical neurons were nucleofected with vector encoding fGFP at plating and grown on cover slips for 18 days. On DIV18, neuronal maintenance medium was removed

entirely and replaced with maintenance medium containing 10 µM GNF-5 (diluted from a 10mM stock in DMSO) or control (1 µl/mL DMSO). Plates were returned to the incubator for 6 hours and cells were then fixed with 4% paraformaldehyde in phosphate buffered saline. Cultures were stained for GFP using a rat primary antibody and FITC-labeled secondary antibody and for filamentous actin using TRITC-phalloidin (Sigma-Aldrich).

Transferrin uptake

AtT-20 corticotropic tumor cells plated on glass cover slips in 4-well dishes were transfected 24 hours later with vectors encoding EGFP or KalSec14-GFP; 24 hours after transfection, cells were serum starved for 30 min, then incubated with 0.25 mg/mL with Alexafluor-546-tagged Transferrin (Invitrogen) in serum-free medium for 5 minutes at 37°C/ 5% CO_2. Cells were then quickly rinsed with serum-free medium and immediately fixed with 4% paraformaldehyde in phosphate buffered saline. Coverslips were stained using the GFP antibody and Hoechst (Invitrogen) nuclear stain.

Image analysis and quantification

Spine density and synaptic clusters were quantified by a blinded observer after the scale bar for the image was calibrated using Metamorph (Molecular Devices, Sunnyvale, CA) as described (171). Briefly, for initial quantification of spine density and synaptic clusters (**Figs. 2 - 6**), a stack of images (Z step, 0.3 µm) was acquired using a 63X objective (2.5 digital zoom factor) and dendrites were visualized in 3-dimensions using the Zeiss LSM Image Browser. Synaptic clusters were manually traced using Metamorph. Spine density and synaptic clusters were counted and cluster size was measured after images were calibrated and thresholds were set to ensure that all interesting structures were included in the analysis. Quantifications were performed using Metamorph and were limited to dendrites within 100 µm

of the soma. The length of each traced spine was measured using Metamorph. Data are presented as average ± SEM. The effects of MycΔKal7, MycKalSolo and MycKal4 were compared to those of GFP and MycKal7; comparisons were made amongst neurons displaying similar levels of Myc signal.

For analysis of transferrin uptake by AtT-20 cells and for analysis of the effects of GNF-5 () on neuronal morphology, images were taken using an Axiovert 200M epifluorescence microscope and a 63X oil objective. Image processing was done using AxioVision software, with identical settings within experiments. Images used for analysis were compressed Z-stack series, with Z-steps of 0.55±0.07 and 0.40+0.08 μm for Tf uptake and GNF-5 (Sigma-Aldrich, St. Louis, MO) treatment, respectively. To measure transferrin uptake, Metamorph was used to trace individual cells and determine average 546-Tf (red) signal. Intensity values were averaged within groups and then compared. Images from GNF-5-treated neurons were coded and analyzed by a blind observer. For each neuron, dendritic protrusions within 100 μm of the cell soma and < 5 μm in length were counted and protrusion density per 10 □m of dendrite was calculated. Protrusion length was determined by measuring the distance between the point where the protrusion met the shaft and the tip of the protrusion. After all data were collected, images were de-coded and data were averaged within groups.

Preparation and Analysis of Sec14-rhodopsin

A pGEX-6P vector encoding the Sec14 domain of rat Kalirin (M^{1}VLSG – LRLSL^{172}*GATETSQVAPA*) with a rhodopsin epitope tag at the C-terminus (*TETSQVAPA*) (244) was constructed and verified by sequence analysis (sites are identified using the U88157.1 numbering scheme for *Kalrn*). Protein expression and purification were carried out essentially as described (186). Briefly, the GST-fusion protein from a 500 ml culture was bound to a 5 ml GSTrap-4B column (GE Healthcare, Piscataway, NJ), eluted by overnight cleavage with GST-HRV3C protease (GenWay Biotech, Inc., San Diego, CA) and purified by chromatography on a Q-Sepharose column (5 mm x 40 mm) equilibrated with

20 mM NaTES, pH 8.0 at a flow rate of 0.5 ml/min; proteins were eluted with a linear gradient to 500 mM NaCl in the same buffer over 180 min. The purity of the KalSec14-rhodopsin was over 93% as assessed by staining with Coomassie Brilliant Blue R250. pGEX-6P vectors encoding two phosphomimetic mutants of KalSec14-rhodopsin were constructed; Thr^{79} was mutated to Glu (Sec14/T^{79}E) and Ser^{83} was mutated to Asp (Sec14/S^{83}D). Vector sequences were verified, and mutant proteins were purified in a similar manner. Protein concentrations were determined by measuring absorbance at 280 nm (using the molar extinction coefficient calculated from tryptophan and tyrosine content). A Jasco J-715 spectropolarimeter with a thermostated cell housing was used as described (186); spectra were recorded between 190 and 270 nm. Secondary structure analyses were carried out using CDSSTR (245) with the reference database available in DICHROWEB (http://dichroweb.cryst.bbk.ac.uk/html/home.shtml). Thermal unfolding profiles were determined by raising the temperature from 20 to 90^{o}C at a rate of 1^{o}C/min.

Lipid binding

PIP strips (Echelon Bioscience, P-6001) were blocked with 3% fatty acid free BSA (Sigma-Aldrich, A6003) in Tris buffered saline containing 0.1% Tween-20 (TTBS) for 1 hr at RT and then incubated with 1 μg/ml purified Sec14 protein (wildtype or mutant) diluted in blocking solution for 1 hr at RT. PIP strips were washed 3 times in TTBS and visualized using a mouse monoclonal antibody to the rhodopsin tag and an HRP-conjugated anti-mouse secondary antibody. Signals were quantified using a GeneGnome digital imaging system and identical exposure times. Following background subtraction, densitometric data for all three proteins were normalized to the signal obtained for wildtype Sec14 binding to PI(3,4,5)P_3, its preferred interactor. Across experiments, normalized values were averaged within groups and represented as relative values +/- SEM. Note that in earlier PIP strip binding studies (176) GST was not removed from the N-terminus of the Sec14 domain (M^{1}VLSG – LLSRL^{186}).

Abl1 Phosphorylation of KalSR4:6

Purified KalSR4:6 (1.0 µM in a final volume of 25 µl) was incubated with recombinant mouse Abl1 (100 nM) and 2 mM ATP for 1 h at 32ºC, as recommended by the supplier (SignalChem, Richmond, Canada). Denatured samples were loaded onto a 4-15% acrylamide gel (Bio-Rad) and visualized using the SilverSNAP stain (Pierce); control KalSR4:6 (no Abl1) and Abl1 phosphorylated KalSR4:6 were excised, destained and subjected to in-gel tryptic digestion (Promega, Cat#V51111) at the Yale/NIDA Neuroproteomics Center. Peptides extracted with 80% acetonitrile, 0.1%TFA were dried under vacuum, dissolved in 70% formic acid and immediately diluted with 50 mM potassium phosphate buffer at 25ºC. Information Dependent Acquisition (IDA) and SWATH acquisitions were carried out on an AB SCIEX Triple TOF™ 5600 coupled with a Waters nanoACQUITY UPLC system. Digests (5µl) were loaded onto a Waters Symmetry® C18 180µm x 20mm trap and separated on a nanoACQUITY 1.7um BEH300 C18 (75µm x 150mm) column. Peptide separations were performed at 500 nl/min with Buffer A (0.1% formic acid) and Buffer B (CH_3CN containing 0.1% formic acid). A linear gradient (70 min) was run with 1% buffer B at initial conditions, 35% buffer B at 70 min, 95% buffer B at 70.33 min, and column re-equilibration for 20 min. IDA runs were carried out at high sensitivity with resolution ~16-18K in the MS/MS (w/max of 30 MS/MS per cycle) at 0.05 sec/scan and TOFMS scan of 0.25sec. SWATH acquisition was carried out over the mass range of 400-1250 with setting at 26 Da scan window with 1Da overlap (i.e.400-425, 424-450, etc.) for a total of 34 SWATH windows per cycle. Acquired LC MS/MS data were analyzed using Analyst (v.2.5) and PeakView (v.2.0, AB SCIEX). Protein identification and site modification assignment utilized MASCOT (Matrix Science) searches; modification sites of interest were manually verified. Skyline (246) was utilized to obtain precursor ion quantitation from SWATH data on the various modification sites. Peak intensities for all peptides containing the site of interest (phosphorylated or not) were summed and used to calculate % Tyrosine phosphorylation. Sites were identified using the NP_114451.2 numbering scheme for *Kalrn*.

Sensitivity to cleavage by calpain I (Sigma) was tested using KalSR4:6 phosphorylated by Abl1 as well as purified KalSR4:6, KalSR4:6/Y^{591}E and KalSR4:6/Y^{616}E. For preparation of radiolabeled KalSR4:6, recombinant protein (0.5 µM in a final volume of 25 µl) was incubated with Abl1 (10 nM), 5 µM ATP, 0.75 µCi/ml ^{32}P-ATP as described above. The entire reaction mixture was then incubated with varying doses of calpain in 25 mM sodium **3-(N-Morpholino)propanesulfonic acid (**MOPS), pH 7.2 containing 1µM $CaCl_2$ for 60 min at 37ºC. After SDS-PAGE and transfer to a PVDF membrane, radiolabeled products were identified by autoradiography; unlabeled proteins were identified by Western blot analysis using an antibody to SR4:6 (JH2580).

Statistical analyses

Analyses were performed with Students t-test or JMP6 software (SAS Institute, Cary, NC) using one way analysis of variance (ANOVA) followed by Dunnett's test to assess statistical significance between groups; *$p< 0.05$ or **$p<0.01$ was considered statistically significant. The lipid binding data were compared using two-way ANOVA with repeated measures for the four sets of measurements (Holm-Sidak multiple comparisons test; GraphPad Prism or SigmaPlot).

Acknowledgments

This work was supported by grants from the NIH (DK-32948, DA-15464, DA-23082 and P30 DA018343) and by support from the Scoville Endowment and the Janice and Rodney Reynolds Endowment. We thank Darlene D'Amato for incomparable technical assistance, Laura Urbanski for her assistance with the calpain studies, Kathrin Wilczak and Mary LoPresti for assistance with sample preparation, Lisa Chung for help with pTyr quantitation and Dr. Prashant Mandela for assistance with the $KalSR^{KO}$ mice.

Author Contributions

X.M.M., M.B.M., K.S.V. and Y.W. conducted the experiments

M.J.G. analyzed neuron images

T.A. and T.T.L. conducted Mass Spec experiments and analysis

M.B.M., X.M.M., R.E.M., and B.A.E. wrote the manuscript

Author Institutions (if other than UConn Health Center)

T.T.L. and T.A. are affiliated with W.M. Keck Facility, Yale University, New Haven, CT

Chapter 4

Kalirin promoter usage determines the presence of an amphipathic helix which enhances Sec14 domain-mediated membrane interactions

Megan B. Miller, K.S. Vishwanatha, Richard E. Mains, Betty A. Eipper

This chapter was submitted for publication in the Journal of Biological Chemistry in its present form. It is currently undergoing minor revisions for resubmission.

Abstract

Previous studies revealed an essential role for the lipid-binding Sec14 domain of Kalirin (KalSec14), but its mechanism of action is not well understood. Since alternative promoter usage appends unique N-terminal peptides to the KalSec14 domain, we used biophysical, biochemical and cell biological approaches to examine the two major products, bKalSec14 and cKalSec14. Promoter B encodes a charged, unstructured peptide, while promoter C encodes an amphipathic helix (Kal-C-helix) with striking biological function. Both bKalSec14 and cKalSec14 interact with lipids in phosphatidylinositol phosphate (PIP) strip and liposome flotation assays, with significantly greater binding by cKalSec14 in both assays. Disruption of the amphipathic face of the Kal-C-helix in cKalSec14$_{KKED}$ eliminates its increased liposome binding. While cKalSec14 shows significantly reduced binding to liposomes lacking PIPs or cholesterol, liposome binding by bKalSec14 and cKalSec14$_{KKED}$ is not affected. When expressed in AtT-20 cells, bKalSec14-GFP shows diffuse localization, while cKalSec14-GFP localizes to the *trans*-Golgi Network (TGN) and secretory granules. The amphipathic C-helix is sufficient for this localization. When AtT-20 cells are treated with a cell-permeant derivative of the Kal-C-helix (Kal-C-helix-Arg9), we observe a substantial increase in secretion of a product stored in mature secretory granules with no effect

on basal secretion; a cell-permeant control peptide lacking the ability to interact with PI(4)P (Kal-C-helix$_{KKED}$-Arg9), does not have this effect. Together, our data reveal major functional implications for Kalirin promoter usage and identify a novel, amphipathic helix-mediated lipid sensing mechanism for cKalSec14.

Introduction

Kalirin is a Rho family GDP/GTP exchange factor (GEF) with widespread cell signaling functions. Alternative splicing of the *Kalrn* gene gives rise to multiple isoforms which are developmentally regulated and tissue-specific. Kalirin7 (Kal7), found exclusively in the nervous system, is the major isoform in the adult brain and is essential for synaptic structure and function (33,36,37,42,43,247). Kal9 and Kal12 are expressed throughout development, both within and outside of the nervous system. Kal9/12 are crucial for normal neurite outgrowth, endocrine and bone homeostasis, and smooth muscle cell migration (205,248-250). Kalirin proteins have multiple functional domains, with major splice variants differing at their C-termini. Kal7, -9, and -12 share identical N-terminal Sec14 domains, which are followed by nine spectrin repeats and tandem Dbl and pleckstrin homology domains (GEF1), activating Rac1 and RhoG (**Fig. 4-1A**). Only Kal7 terminates in a PDZ binding motif. Kal9 and Kal12 have a second GEF domain (GEF2), which activates RhoA, and Kal12 includes a putative kinase domain.

In addition to its GEF domains, essential roles for the non-enzymatic domains of Kalirin have been identified (76,251). Of particular interest is the N-terminal Sec14 domain (Fig. 4-1A and B).Yeast Sec14p, which catalyzes the exchange of phosphatidylcholine and phosphoinositide between cellular membranes, is required for normal post-Golgi trafficking and lipid metabolism (252-254). Based on sequence analysis, Sec14 domains have been identified in dozens of mammalian proteins, as well as hundreds of proteins from other eukaryotic organisms. Sec14 domains bind to a diverse set of small lipid ligands, including phosphatidylcholine, phosphoinositides, squalene, tocopherols and retinaldehyde. As

such, members of the "Sec14 superfamily" have diverse biological functions, including roles in lipid transport, membrane trafficking and cytoskeletal regulation (255). The Sec14 domain of α-Tocopherol transfer protein (α-TTP) binds both phosphoinositides and α-tocopherol, with a single point mutation in its phosphoinositide binding cleft causing severe vitamin E deficiency and ataxia (256). Sec14 domain mutations are also associated with retinal degeneration and cancer (257,258).

While some Sec14 superfamily members consist almost entirely of the Sec14 domain, many are larger, multi-domain GTPase regulatory proteins. The Sec14 domain of p50RhoGAP targets it to endosomes and mediates interaction with Rab11 (259). Disruption of the Sec14 domain in truncated isoforms of two other Rho GEFs (Dbl and Dbs/Ost) causes altered localization of the proteins and their effector, Cdc42 (260). The Sec14 domain of Kalirin interacts with phosphoinositides, but not with other more prevalent membrane lipids (76,251). Furthermore, cultured hippocampal neurons expressing a Kal7 mutant lacking only its Sec14 domain form abnormally short spines (251).

Sequence homology among Sec14 superfamily members is typically low, but their structures are remarkably similar (256,261,262) (**Fig. 4-1C**). Alternating α-helix and β-sheet motifs create a lipid binding pocket with a hydrophobic core (CRAL_TRIO domain; named for **c**ellular **r**etin**al**dehyde binding protein and Trio, a homologue of Kalirin). Upstream of the lipid binding pocket, some Sec14 family members also have a 4-helix subdomain, commonly referred to as a CRAL_TRIO_N domain (**Fig. 4-1B**). Recent phylogenetic analysis of the Sec14 superfamily places the Sec14-containing RhoGEFs in an intermediate position, between those that have the N-terminal domain and those that do not (263).

Alternative promoter usage generates isoforms of Kalirin in which its CRAL_TRIO domain is preceded by four very different sequences encoded by Ex1A, Ex1B, Ex1C or Ex1D (**Fig. 4-1A**). While Ex1B and Ex1C are not identified as CRAL_TRIO_N domains, their conservation and unique features suggested that they could affect the function of the CRAL_TRIO domain. Ex1A, which includes only four amino acids, would not be expected to form a functional domain. Here, we show that alternate promoter usage affects Sec14 domain lipid binding, subcellular localization and function.

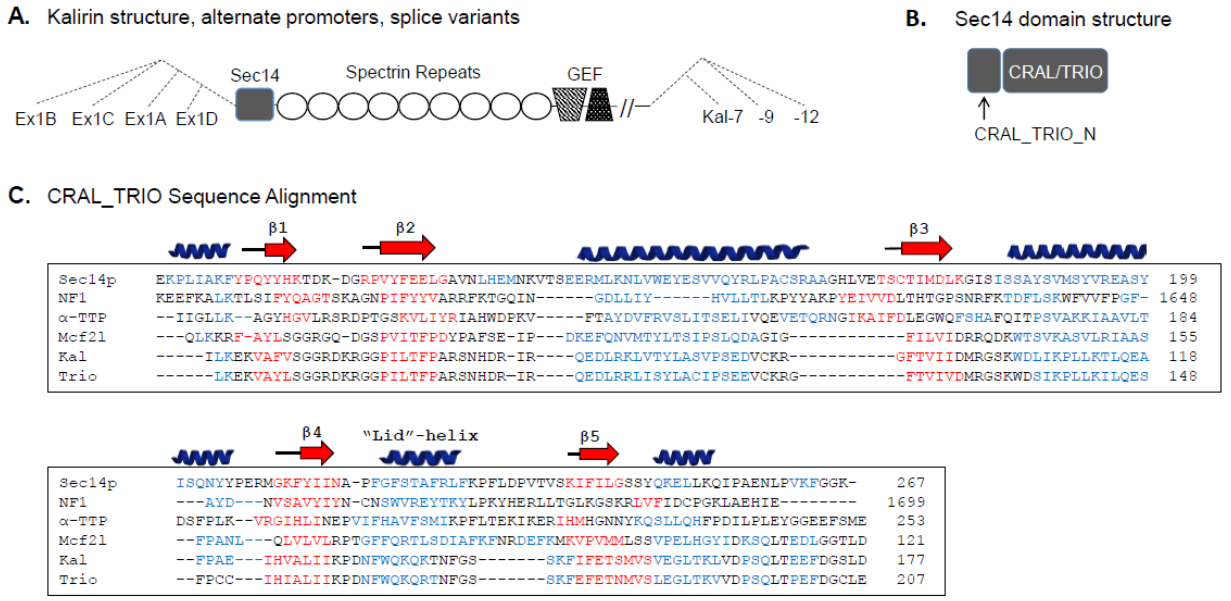

Figure 4-1. Kalirin and the Sec14 superfamily. **A.** Schematic illustrating use of four different *Kalrn* promoters, which encode alternate first exons (Ex1A, Ex1B, Ex1C, Ex1D); the CRAL_TRIO domain begins in exon 2, which is common to transcripts initiated at each of these promoters. Alternative splicing generates transcripts encoding Kal7, Kal9 and Kal12, which each terminate with exons encoding unique 3'-untranslated regions. **B.** Sec14 superfamily members include a CRAL_TRIO domain, which typically binds hydrophobic ligands; some Sec14 superfamily members include a CRAL_TRIO_N domain. **C.** Multiple sequence/structural alignment for several CRAL_TRIO domains; residues known or predicted to form α-helices (blue) and β-sheets (red) are identified. Structures are known for yeast Sec14p (ID:6323725; PDB ID-1AUA; helices and β-strands shown above the alignment), neurofibromin 1 (NF1) (ID:119600680; PDB ID-3P7Z) and α-tocopherol transfer protein (α-TTP) (ID:4507723; PDB ID-1OIP). Secondary structures for the CRAL_TRIO regions of Kalirin (ID:295054252), Mcf2l (ID:341940943; also known as Dbs and Ost) and Trio (ID:257051075) were predicted using the Phyre2 modeling program (www.sbg.bio.ic.ac.uk/phyre2/). Dashes were inserted to optimize alignment; GenBank number of the final residue shown for each protein is given at the end.

Experimental Procedures

Protein expression and purification

KalSec14 variants were expressed and purified using a pGEX-6P vector system, as described previously (251,264). Constructs were designed using the rat *Kalrn* sequence (U88157.1 numbering scheme; Ex1A) and verified by sequence analysis. GST fusion proteins were bound to a 5 ml GSTrap-4B column (GE Healthcare, Piscataway, NJ) and eluted by overnight cleavage with GST-HRV3C protease (GenWay Biotech, Inc., San Diego, CA). Purification was accomplished using a Q-Sepharose column (5 mm x 40 mm) equilibrated with 20 mM NaTES, pH 8.0 at a flow rate of 0.5 ml/min. Proteins were eluted over 180 min with a linear gradient to 500 mM NaCl in the same buffer. Proteins used for PIP strips included a rhodopsin tag at their C-terminus (265). For liposome assays, the rhodopsin tag was removed and proteins were extended to include the first helix of spectrin repeat 1 (EFP199), since this was found to improve protein solubility and stability.

Circular Dichroism

CD experiments were done as reported previously (264). CD spectra were recorded using Jasco J715 spectropolarimeter (Jasco, Easton, MD) calibrated with d (+)-10-camphor-sulphonic acid ammonium salt, with a thermostated cell housing and 1 mm path length cell at 20C. Recombinant Sec14 proteins (6 µM) or synthetic peptides (20 µM) were prepared in buffer (20mM NaTES, 150mM NaCl, pH 7.0) and far UV CD spectra recorded between 190-260nm. An average of three runs was recorded for each protein sample. Synthetic peptides (Biomatik USA, LLC, Wilmington, Delaware; > 90% purity) used in these studies included: Kal-b (PPEGASEEGGAADSD), Kal-c (TDRFWDQWYLWYLRLLRLLDRG), Kal-c_{KKD} (DRFKDQKYLWDLRLLRLLDRG); one tryptophan residue was left in the mutant peptide to enable tryptophan fluorescence measurement. Peptides were solubilized in 1mM HCl and stored at -20ºC.

PIP Strips

PIP strips (Echelon Bioscience, P-6001) were used according to the manufacturer's instructions, as reported previously (251). Briefly, strips were blocked with 3% fatty acid free BSA (Sigma-Aldrich, A6003) in Tris buffered saline containing 0.1% Tween-20 (TTBS) for 1 hr at RT and then incubated with 1 µg/ml of the indicated rhodopsin-tagged Sec14 protein for 1 hr at RT. PIP strips were rinsed thoroughly and protein binding was visualized using a mouse anti-rhodopsin monoclonal antibody and an HRP-conjugated anti-mouse secondary antibody. Signals were quantified using a GeneGnome digital imaging system and identical exposure times. Following background subtraction, densitometric data were normalized to the signal obtained for cSec14-rhodopsin binding to PI(4)P, consistently the darkest spot across groups.

Liposome preparation and flotation assays

The following synthetic and natural lipids were purchased from Avanti Polar Lipids, Inc. (Alabaster, Alabama): DOPC (18:1, 850375), DOPE (18:1, 850725), DOPS (18:1, 840035), D-*myo*-PI(3,4,5)P_3 (P-3916), D-*myo*-PI(4)P (P-4016), brain PI(4)P (840045), cholesterol (700000P), and LissRhod PE (18:1, emission 571 nm, 810150). All powdered lipids were dissolved in chloroform or a mixture of chloroform, methanol and water (20:9:1), per manufacturer instructions. Liposomes were prepared essentially as described by Avanti. To start, lipid stocks were mixed in the desired proportions, dried under nitrogen gas, and lyophilized overnight. Lipid mixtures were reconstituted to a final concentration of 1 mM in HN buffer (20 mM HEPES, 150 mM NaCl, pH 7.4). Mixtures underwent five freeze-thaw cycles with vigorous vortexing between each. Using a mini-extruder, unilamellar liposomes were prepared by passing lipid mixtures 21 times through polycarbonate membranes of 100 nm pore size. Hydrated lipid mixtures were stored at -20^{0}C for up to one month; liposomes were freshly prepared for each experiment.

Liposome flotation assays were conducted on a density gradient in a manner similar to previous reports (266). Accudenz (Accurate Chemical and Scientific Corp., Westbury, New York) solutions (80% and 20%) were prepared in HN buffer. Unilamellar liposomes (50 µl) were combined with 0.5 µg of purified protein and incubated at room temperature for 30 min. The entire liposome/protein mixture was combined with 50 µl of 80% Accudenz at the bottom of an ultracentrifuge tube and carefully mixed to completion by pipetting up and down. The resulting mixture was carefully over-layered with 250 µl of 20% Accudenz and then with 50 µl of HN buffer. Samples were centrifuged at 55,000 rpm at 4^0C for 30 min in a TL-100 ultracentrifuge using a Beckman TLS 55 swinging bucket rotor. Gradients were then divided into four 100-µl fractions, which were carefully collected from the bottom of the tube using gel loading micro-pipet tips. Each fraction was analyzed for liposome and protein content using spectrophotometry (546 excitation/571nm emission) and Western blot analysis, respectively. At least 90% of the Lissamine Rhodamine PE marker was recovered in the top fraction.

For analysis of protein content, equal aliquots of each gradient fraction were denatured in 1X Laemmli sample buffer, fractionated on 4–15% acrylamide gels and transferred to PVDF membranes. Western blot analysis was conducted using either a mouse GST antibody [for PI(4)P-Grip GST] or a rabbit KalSec14 antibody [CT 302; (248)] and mouse or rabbit HRP-tagged secondary antibodies. SuperSignal West chemiluminescent substrate (Thermo Scientific) and a GeneGnome digital imaging system were used to visualize blots, with exposures adjusted to be in the linear range. After background subtraction, bands were quantified and data were represented as a proportion of total protein recovered.

Tryptophan Fluorescence

The tryptophan blue shift assay was conducted by incubating 2 µM synthetic peptide (Kal-c or Kal-c_{KKD} peptide) with 20 µM liposomes (diameter, 100 nm), either with or without 8% PI(4)P in HN buffer, at room temperature for 45 min. Control reactions were incubated without liposomes. Intrinsic fluorescence was measured using a F2500 spectrofluorimeter (Hitachi, Japan) with a thermostated cell

holder and a 1 cm path length quartz cuvette. Slit widths with a nominal bandpass of 10 nm were used for both excitation and emission beams. Fluorescence emission spectra were recorded from 300 to 400 nm after excitation at 280 nm; the blue shift graphs were constructed using averaged values from three continuous scans.

Cell culture and transfection

AtT-20 mouse corticotrope tumor cells were maintained at 37^0C in a 5% CO_2 atmosphere in DMEM-F12 cell culture medium containing 10% fetal calf serum (Hyclone), 10% NuSerum (Corning), penicillin/streptomycin, and 25 mM HEPES. Transient transfections were performed in serum-free Optimem medium using Lipofectamine 2000 (Invitrogen, Carlsbad, CA) at 2 µl per µg DNA. To reveal differences in late/recycling endocytic trafficking, cells were treated with a low dose of nocodazole (10µM) in growth medium for a short time (30 min) prior to fixation; this dose of nocodazole has been shown to disrupt microtubule-dependent endosomal trafficking without completely disrupting the TGN (267). New DNA vectors: bKalSec14-GFP and cKalSec14-GFP (both end with $-LDYNH^{162}$), Kal-C-helix-GFP (Ex1C appended to N-terminus of EGFP), and Kal C-$helix_{KKED}$-GFP (WWWY→KKED). PEAK-His.Myc-Kal7a (251) was used as a template to introduce a silent mutation (Nru1 site) at nt93 (Genbank AAT39517.1 numbering) using site-directed mutagenesis with the QuikChange Kit (Stratagene). The Kal-a front without the HisMyc tag was created by PCR using this vector and a reverse primer including the Nru1 site. The Kal-b and Kal-c fronts were created using rat brain cDNA with sequence-specific forward primers and the common reverse primer introducing the Nru1 site. All three fronts were cut with BamH1 and Nru1 and inserted into pEGFP-rKalSec14 (251) cut with Bgl2 and Nru1. The $A^{206}K$ substitution in EGFP-N2 was also produced using the QuikChange kit (268). All Kal-Sec14 sequences end with $LRLSL^{172}$ fused to EGFP. Long synthetic oligonucleotides were hybridized to create the amphipathic wildtype Kal-c front (MTDRFWDQWYLWYLRLLRLL) and the mutant Kal-c_{KKED} front

(MTDRF**K**DQ**K**YL**ED**LRLLRLL) flanked by restriction sites for Sac2 and BamH1; these fragments were then inserted into pEGFP-N2($A^{206}K$). All constructs were verified by DNA sequencing.

Immunocytochemisty.

Cell cultures were fixed in 4% paraformaldehyde, permeabilized with 0.075% Triton X-100 and blocked with 2mg/mL BSA. Primary antibodies used for immunostaining include rat anti-GFP (NacalaiTesque, Kyoto, Japan, 1:1000), rabbit-anti-TGN38 [JH 1479, 1:1000, (269)] and rabbit-anti-ACTH [Kathy,(269)]. TRITC-Phalloidin (Sigma) was used to visualize filamentous actin.

Cell-Permeant peptides

To investigate the biological activity of the amphipathic Kal-C-helix, we designed a cell-permeant peptide in which the C-helix is followed by nine arginine residues (C-helix-Arg9; TDRFWDQWYLWYLRLLRLLD-RRRRRRRRR). A control peptide in which four of the hydrophobic residues were replaced with charged residues (underlined) was also designed ($C\text{-helix}_{KKED}$-Arg9; TDRFKDQKYLEDLRLLRLLD-RRRRRRRRR). Synthetic peptides (Biomatik USA, LLC; >90% purity) were dissolved in DMSO, yielding stock concentrations of 2 mM.

Live Cell Imaging

AtT-20 cells were plated at low density on poly-L-lysine-coated glass-bottom MatTek dishes and grown in serum-containing DMEM/F12 for 2 days. At least 24 hr before imaging, cells were transfected with the indicated plasmids as described above. Prior to imaging, cells were allowed to acclimate to imaging medium (DMEM/F12 air without phenol red) at 37^0C for at least 20 min. While on a stage warmer held at 37^0C, cells were imaged using a Nikon Eclipse TE300 inverted epifluorescence microscope with a 40X/0.60 Plan Fluor air objective and associated NIS-Elements software. Live cell

imaging was performed at a rate of 1 frame per 20s for 30-40 minutes. After at least 10 min of baseline imaging, a 10 μM working solution of either C-helix-Arg9 or control peptide in imaging medium was added to the cells on the stage warmer, producing a final concentration of 5 μM peptide in imaging medium. A final concentration of 10 μM peptide was also tested and gave similar results.

Secretion Experiments

Secretion experiments were conducted as reported previously (270). Briefly, AtT-20 cells were plated at high density in 12- or 6-well dishes and maintained for two days in normal growth medium. Prior to treatment, cells were equilibrated in an air incubator in complete serum free medium lacking bicarbonate (CSFM-air); CSFM-air consists of DMEM/F-12 containing insulin/transferrin/selenium (ITS), 25 mM HEPES, pH 7.4, and 50 μg/mL bovine serum albumin. Cells were incubated in pre-warmed CSFM-air at least twice for exactly 30 min at 37^0C; these samples of medium allowed us to assess "basal" secretion. After the final period of "basal" secretion, cells were incubated in CSFM-air medium containing either a low concentration of secretagogue ($BaCl_2$, 0.5 mM), 5 μM cell-permeant peptide (either WT C-helix or mutant control), or both 5 μM cell-permeant peptide and 0.5 mM $BaCl_2$. After 30 min, medium was collected (stimulated secretion) and cells were homogenized in SDS lysis buffer [0.5% (w/v) SDS, 50 mM Tris.HCl, pH 8.0, 1 mM dithiothreitol, 2 mM EDTA,50 mM NaF], which was immediately boiled for 5 min. Protease inhibitors were added to all samples immediately following collection. Samples were separated using SDS-PAGE and protein content was evaluated by Western Blot analysis. A rabbit antibody to prohormone convertase 1 (PC-1 [JH 888, (271)] was used to evaluate secretion. Data are presented as fold change over basal.

Results

Alternative promoter usage creates two structurally distinct KalSec14 domains

Full-length Kalirin transcripts are initiated at one of four promoters, termed A, B, C and D (Fig. 4-1A); transcripts generated from the different promoters encode four to 38 amino acids which precede exon 2. Proteins which extend from the N-terminus to a specified point beyond the end of the CRAL_TRIO domain [which extends from the 16th residue of exon 2 (I^{20}LK) to SLD^{159}] are referred to as aKalSec14, bKalSec14, cKalSec14 or dKalSec14. In this study, we focused our attention on the proteins produced from promoters B and C, the major promoters used in neurons (95); previous studies focused only on promoter A product (37). Though similar in length, the sequences and predicted structures of the initial peptides encoded by promoters B and C are remarkably different (**Fig. 4-2A and B**). While the Kal-b peptide is negatively charged and predicted to be unstructured, the Kal-c peptide is highly hydrophobic, with 15/27 residues having hydrophobic properties, and predicted to form an α-helix. In fact, a helical wheel projection predicts that the Kal-c peptide forms a nearly perfect amphipathic helix (**Fig. 4-2B**). Synthetic Kal-b and Kal-c peptides were used to confirm these structural predictions using circular dichroism. As predicted, the Kal-b peptide was unstructured (i.e. a random coil), while the Kal-c peptide had spectral properties characteristic of a helical protein (high at 190 nm, minima at 208nm and 222nm, Fig. **4-2C**).

Since the Kal-c peptide includes three tryptophan residues, we took advantage of the characteristic spectral shift in tryptophan fluorescence emission that occurs as a function of solvent polarity to assess its interaction with membranes (**Fig. 4-2D**). A significant change in both fluorescence intensity and emission maxima was observed upon mixing Kal-c peptide with unilamellar liposomes. A mutated version of the Kal-c peptide (Kal-c_{KKD}) was designed to disrupt its amphipathic nature by replacing three hydrophobic residues with three polar residues (WWY→KKD; Fig. 4-2B). Kal-c_{KKD}, which is predicted to adopt a helical structure with greatly reduced amphipathic moment, exhibited the features expected of a helical structure when examined by circular dichroism **(Fig. 4-2C**). However, Kal-

c_{KKD} failed to show any changes in either fluorescence intensity or emission maxima following the addition of unilamellar liposomes (**Fig. 4-2D**). Similar constructs were used as controls in later experiments. Given the unique features of the Kal-b and Kal-c peptides, which immediately precede the lipid-binding CRAL_TRIO domain of Kalirin (**Fig. 4-1**), we decided to investigate functional differences between bKalSec14 and cKalSec14.

Promoter usage alters lipid interactions by KalSec14 variants

Like many other Sec14 family members, KalSec14, binds to phosphoinositides (PIPs) (251). Here, we used PIP strips (Echelon) to evaluate the lipid binding capabilities of bKalSec14 and cKalSec14. Rhodopsin-tagged bKalSec14 and cKalSec14 were expressed and purified, as described previously for aKalSec14 (251) (**Fig. 4-3A**). While bKalSec14-rhod showed some binding to phosphoinositides, we saw significantly more binding by cKalSec14-rhod to almost all PIPs (Fig. 4-3B, C). Neither protein interacted appreciably with the other lipids tested. We found previously that aKalSec14-rhod (**Fig. 4-2A**) binds specifically to phosphoinositides, with the most binding to PI(3,4,5)P_3 (251). Interestingly, cKalSec14-rhod showed the most binding to PI(4)P, suggesting that promoter usage contributed to both the affinity and specificity of KalSec14-lipid interactions.

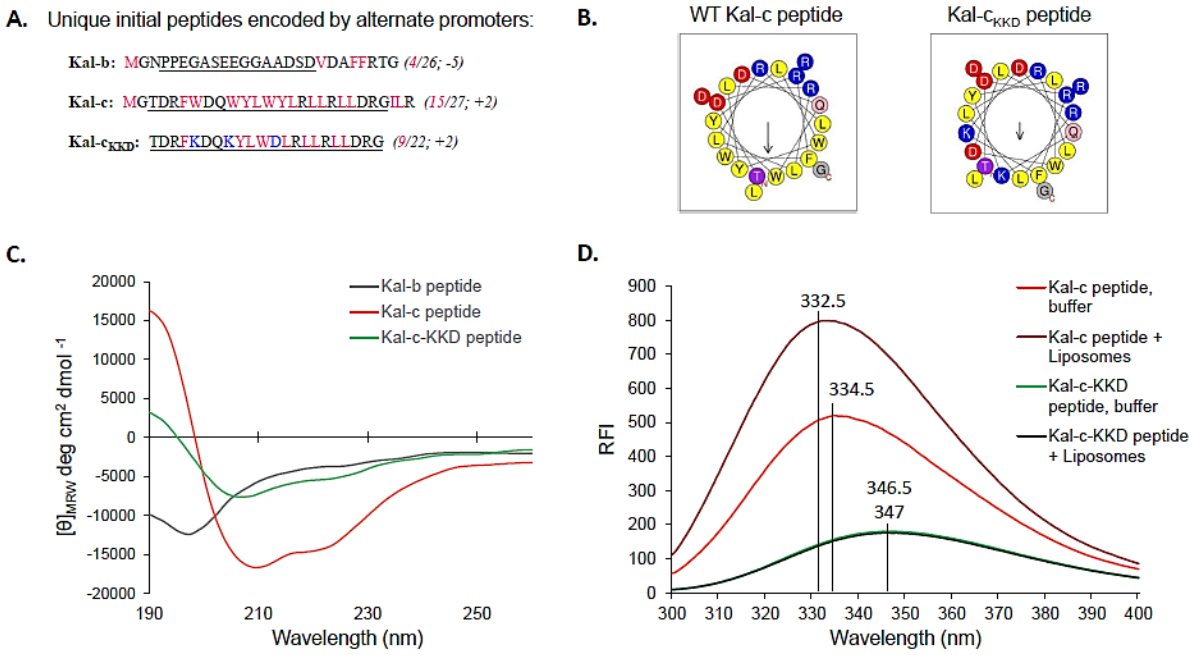

Figure 4-2. Kalirin promoter C encodes an amphipathic helix. **A.** Peptide sequences generated by transcripts initiated from rat promoters A, B and C are shown. Hydrophobic residues are shown in pink; in parentheses, number of hydrophobic residues/total number of residues and net charge predicted. Underlining indicates the synthetic peptides (Kal-b, Kal-c, Kal-c_{KKD}) used for structural studies. In the Kal-c_{KKD} peptide, residues shown in blue were mutated in order to maintain helicity but disrupt the amphipathic nature of the helix. **B.** Helical wheel projections for the synthetic peptides were obtained using HeliQuest with an 18 amino acid analysis window (http://heliquest.ipmc.cnrs.fr/); Kal-b is not predicted to form an α-helix (Quick2D, Max-Planck Institute for Developmental Biology Bioinformatics Toolkit). Yellow, hydrophobic residues; red, negatively charged; blue, positively charged. Arrows point to the hydrophobic face, with the length of the arrow indicative of the calculated hydrophobic moment. **C.** CD spectra for Kal-b, Kal-c and Kal-c_{KKD} peptides are shown. **D.** Tryptophan fluorescence measurements for Kal-c and Kal-c_{KKD} peptides with and without liposomes. As expected for an amphipathic helix, λ_{max} for the Kal-c peptide showed a blue shift in the presence of liposomes (from 334.5 to 332.5 nm). λ_{max} for Kal-c_{KKD} shifted by only 0.5 nm in the presence of liposomes, from 347 vs 246.5. RFI = relative fluorescence intensity.

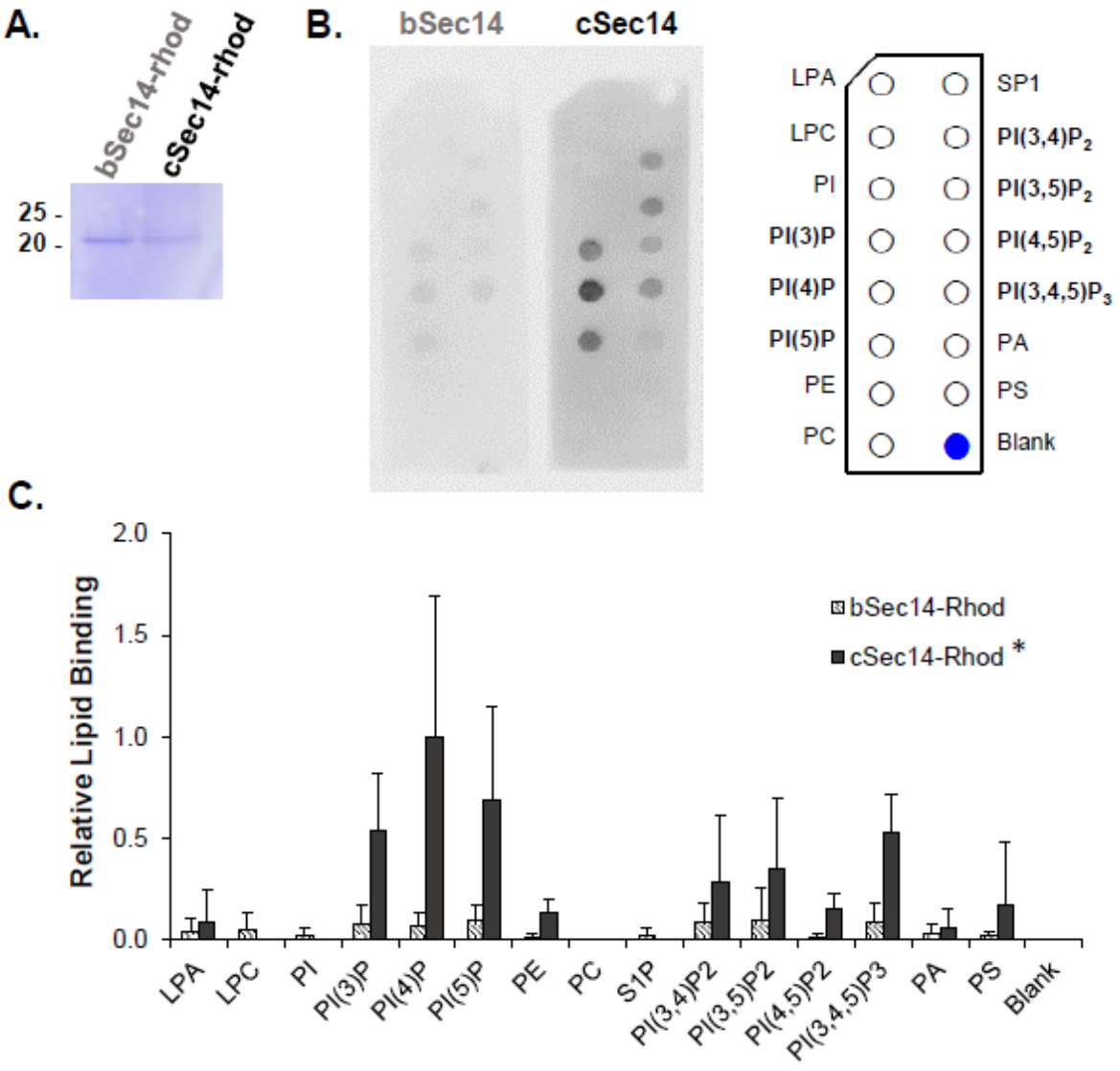

Figure 4-3. The bSec14 and cSec14 domains of Kalirin exhibit differential binding to PIP strips. **A.** Coomassie stained membrane showing purified bSec14-rhod and cSec14-rhod. **B**. The bSec14-rhod and cSec14-rhod domains bound to PIP strips were quantified using an antibody to the epitope tag. The lipids on the PIP strips are identified in the schematic to the right. **C.** Group data from 2-4 experiments shown as spot intensity relative to cSec14-rhod binding to PI(4)P, its preferred interactor; error bars = standard deviation. cSec14 binding to PIPs was significantly higher than bSec14 binding; *$p<0.02$ by 2-way ANOVA.

cKalSec14-GFP localizes to the TGN in neuroendocrine cells

The phosphoinositides are a critically important class of cell signaling lipids which are known to have somewhat discrete subcellular localization [for review see (272,273)]. As such, phosphoinositide binding often contributes to effector protein localization to specific subcellular compartments. Since PI(4)P is enriched in the membranes of the *trans*-Golgi network (TGN), we wondered if promoter usage influenced protein localization. To test this, we expressed KalSec14-GFP-fusion proteins in a well-characterized neuroendocrine cell line (AtT-20s). While bKalSec14-GFP was diffusely distributed in these cells (Fig. 4-4A), cKalSec14-GFP localized to the perinuclear region **(Fig. 4-4B**); in cells expressing higher levels of cKalSec14-GFP, diffuse staining throughout the cytosol became more pronounced. cKalSec14-GFP co-localized extensively with staining for TGN38, a marker for the *trans*-Golgi network (**Fig. 4-4B**). In some transfected cells, we also observed cKalSec14-GFP localization at the tips of processes, where mature secretory granules accumulate; secretory granules were identified by staining with an antibody to adrenocorticotropic hormone (ACTH), which is synthesized and stored in these cells. PI(4)P is found in the membranes of post-Golgi vesicles, including secretory granules (272).

The perinuclear region of AtT-20 cells that contains the Golgi and *trans*-Golgi network is also enriched in late endosomes (274). To better distinguish the TGN from late endosomes, we treated cKalSec14-GFP-expressing cells for a short time with a low concentration of nocodazole to destabilize microtubules and disrupt microtubule-dependent endosomal trafficking; as expected, TGN38 staining, while more fragmented than in control cells, remained concentrated in the perinuclear region (**Fig. 4-4D**). We found that most of the cKalSec14-GFP signal was still associated with TGN38-containing compartments (**Fig. 4-4D, yellow arrows**), indicating that it was localized to the TGN. While a few cKalSec14-GFP positive puncta were visible throughout the cell after nocodazole treatment (white arrowhead), our data indicate that only a small fraction of the cKalSec14-GFP was associated with endosomes.

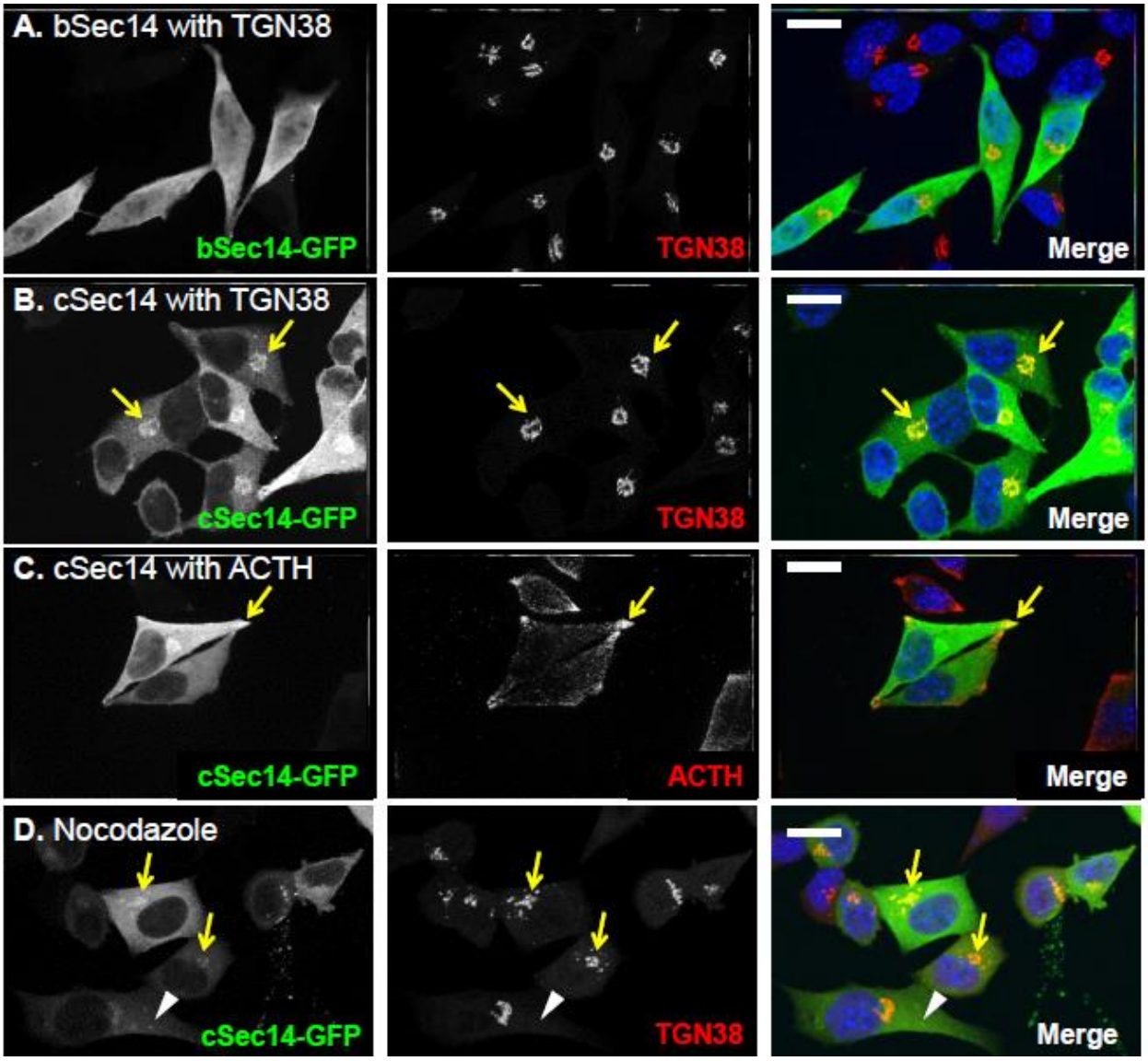

Figure 4-4. Differential localization of bSec14 and cSec14 GFP fusion proteins in AtT-20 cells. Immunostaining of AtT-20 cells transiently transfected with vectors encoding bSec14-GFP or cSec14-GFP. **A.** bSec14-GFP was diffusely localized, while cSec14 colocalized with the TGN marker, TGN38 (**B**; yellow arrows), and occasionally with ACTH (**C**; yellow arrows), a marker for the mature secretory granules which accumulate at the tips of cellular processes. **D.** Cells were treated with a low dose of nocodazole (10 µM) for a short time (30 min) to disrupt the microtubule-dependent trafficking of late/recycling endosomes into the perinuclear region (274). Much of the cSec14-GFP continued to co-localize with TGN38 (yellow arrows), but some cSec14-GFP-positive vesicular structures that lacked TGN38 could be identified (white arrowheads). In the merged images, green = GFP, red = TGN38 (panels A, B, D) or ACTH (panel C), blue = Hoechst. Scale bar = 20µm.

The Kal-C helix alone localizes to the TGN

We next wondered if the amphipathic Kal-C helix were sufficient to localize GFP to the TGN area. To test this, we transfected AtT-20 cells with expression vectors encoding GFP fusion proteins in which the wild type or mutant C-helix preceded GFP (Kal-C helix-GFP and Kal-C helix$_{KKED}$-GFP). Remarkably, we found that Kal-C helix-GFP localized to the TGN region in AtT-20 cells (**Fig. 4-5A**). Furthermore, disruption of the amphipathic nature of the helix was sufficient to prevent this localization, since Kal-C-helix$_{KKED}$-GFP was diffusely distributed throughout the cytosol (**Fig. 4-5B**).

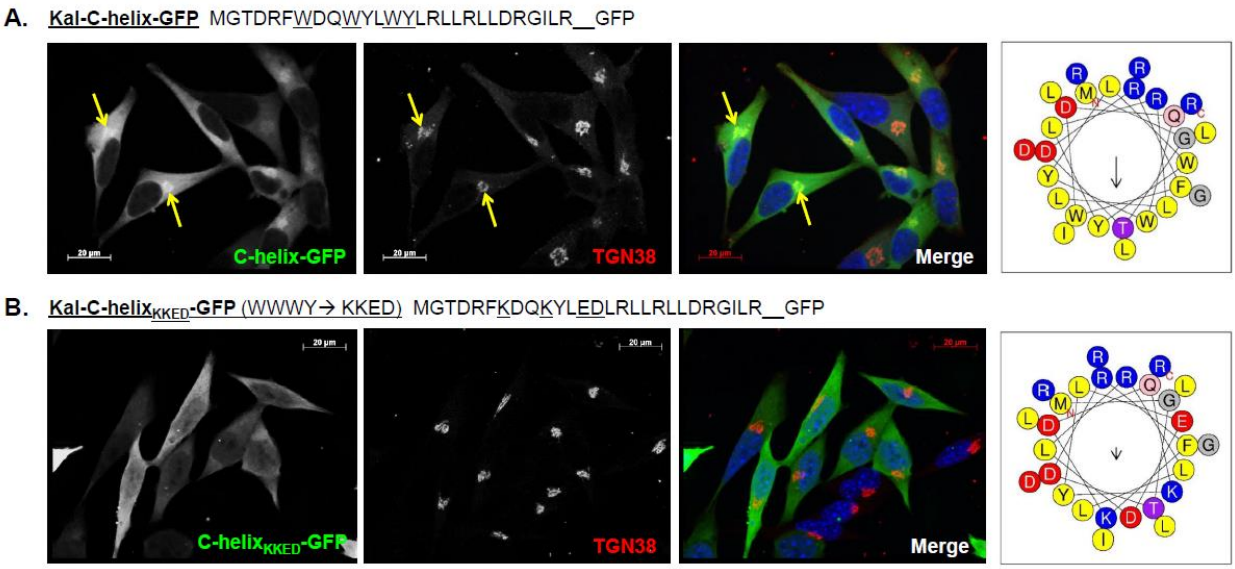

Figure 4-5. The amphipathic C-helix of Kalirin is sufficient to localize GFP to the TGN area in AtT-20 cells. **A.** Immunostaining of AtT-20 cells transiently transfected with GFP fused to the C-helix of Kalirin. **B.** Immunostaining of AtT-20 cells transiently transfected with GFP fused to Kal-C-helix$_{KKED}$; mutations were introduced to maintain helicity but eliminate the amphipathic nature of the helix. Helical wheel projection diagrams (HeliQuest) for the two peptides are shown to the right. In the merged images, green = GFP, red = TGN38, blue = Hoechst. Scale bar = 20µm.

The Amphipathic Kal-C helix is essential for cKalSec14 lipid interactions

To further evaluate the role of the Kal-C helix in KalSec14-mediated lipid interactions, we utilized a liposome binding assay. Synthetic and natural lipids were combined in proportions that mimic the membranes of the TGN (266,275). The resulting "Golgi Mix" consisted of 52% DOPC, 20% DOPE, 5% DOPS, 15% Cholesterol, 8% PI(4)P, and trace amount of fluorescent lipid. Lipids were dried, reconstituted and extruded through a 100 nm pore diameter filter. Unilamellar liposomes were incubated for 30 min with purified KalSec14; KalSec14 bound to liposomes was separated from free KalSec14 based on its decreased density using an Accudenz gradient (**Fig. 4-6A**). After centrifugation, liposomes and any protein bound to them were recovered from the top of the gradient. Using this approach, over 90% of fluorescently tagged unilamellar liposomes were recovered in the top fraction (fraction 1), as assayed by spectrophotometry for the fluorescent lipid (**Fig. 4-6B**). When liposomes were combined with PI(4)P-Grip-GST (Echelon, positive control protein), we found over 90% of the protein in the top fraction (Fig. 4-6C, D). When PI(4)P-Grip-GST was loaded onto an Accudenz gradient without liposomes, no protein was detectable in the top fraction (**Fig. 4-6C, D**).

The liposome binding abilities of purified bKalSec14, cKalSec14 and cKalSec14$_{KKED}$ (helix mutant) were compared (**Fig. 4-6E**). All three proteins showed significant binding to liposomes (**Fig. 4-6E, F**). Consistent with the PIP strip assays, we found significantly more cKalSec14 in the liposome fraction than bKalSec14 (**Fig. 4-6E, F**). This difference could be due to conformational differences of the putative lipid binding pocket due to inclusion of different N-terminal peptides (Figures 4-1 and 4-2). We found that disruption of the Kal-C-helix was sufficient to abolish the difference in liposome binding between bKalSec14 and cKalSec14 (Fig. 4-6E, F), so that cKalSec14$_{KKED}$ behaved like bKalSec14. These data indicate that the N-terminal amphipathic helix in cSec14 serves to enhance the ability of this domain to interact with membranes, and that this increase was likely due to interactions mediated by the amphipathic helix itself.

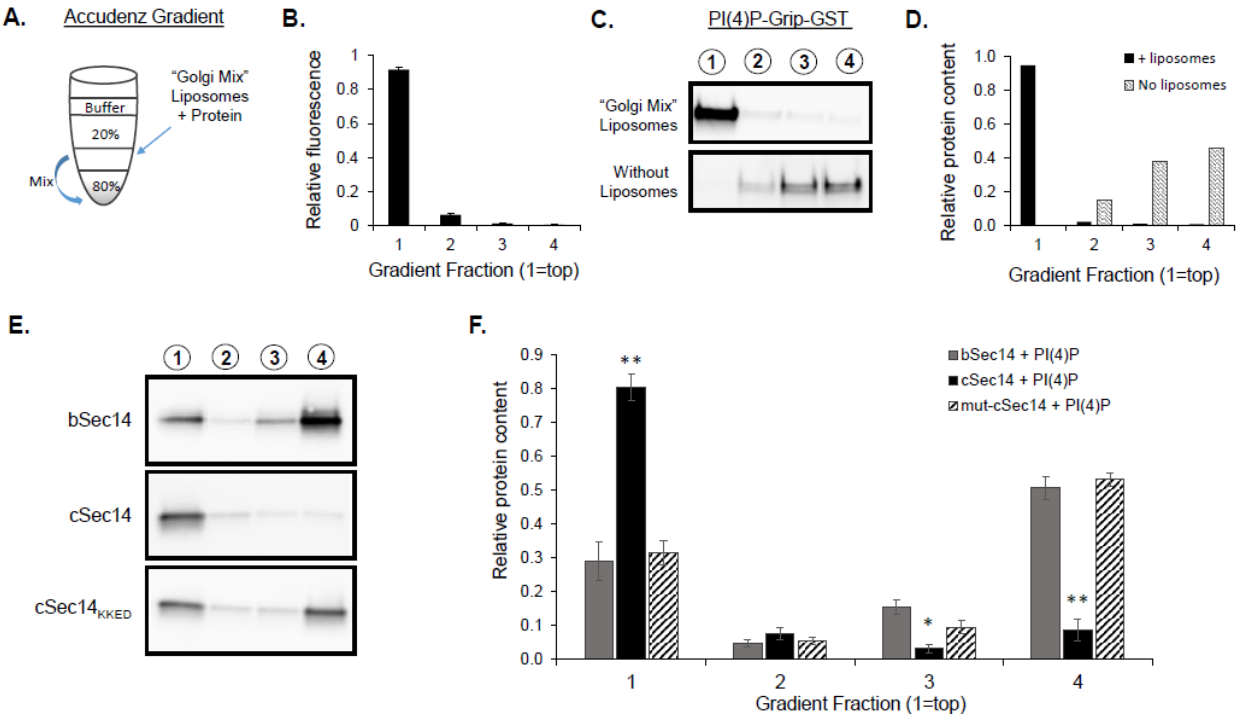

Figure 4-6. Liposome binding assays reveal an important role for the amphipathic C-helix in KalSec14membrane interactions. **A.** Schematic illustrating Accudenz gradients used for the liposome flotation assays conducted in Figs. 6 and 7. The indicated liposome/protein mix (50µl) was combined with 50µl of 80% Accudenz, then overlayered with 250µl of 20% Accudenz and 50µl of buffer. Gradients were centrifuged in a swinging bucket rotor for 30 min, and 100-µl fractions were removed and analyzed for lipid and protein content. **B.** Relative lipid fluorescence in gradient fractions; spectrophotometry data from 21 separate gradients were averaged, showing >90% of the lipid was found in the top fraction of the gradient after centrifugation. **C.** Purified PI(4)P-Grip-GST (positive control) was analyzed on gradients in the presence (top) or absence (bottom) of "Golgi-mix" liposomes; gradient fractions are indicated above each lane. Protein content, detected using a GST antibody, was quantified as shown in **D. E.** Representative blots from liposome assays with KalSec14 variants. cSec14 bound significantly more to "Golgi mix" liposomes than bSec14, and this difference was eliminated when the C-helix was mutated to disrupt its amphipathic nature; group data are shown in **F**. Error bars = S.E.M; n = 4-6 experiments per protein. Asterisks indicate significant difference from bSec14 + PI(4)P liposomes by 2-way ANOVA; **p < 0.001, *p < 0.02.

Membrane interactions by cKalSec14 require phosphoinositides and cholesterol

Since our PIP strip data indicated that KalSec14 bound specifically to phosphoinositides, we wanted to determine whether PIP content affected the KalSec14-liposome interaction. When flotation assays were conducted with liposomes lacking PIPs **(Fig. 4-7A**), we found that cKalSec14 binding was reduced by 85%, completely eliminating the difference between bKalSec14 and cKalSec14 (**Fig. 4-7B**, green hashed bars). This suggested that cKalSec14 membrane interactions were sensitive to PIP content. Although bKalSec14 binding appeared slightly reduced in the absence of PIPs, data from 6 separate experiments did not reach statistical significance. Since several Sec14 proteins bind lipids other than phospholipids and Golgi/TGN membranes are enriched in cholesterol (276), we wondered if the interaction of KalSec14 with liposomes was sensitive to cholesterol content. cKalSec14 binding was significantly reduced when cholesterol was excluded from the liposomes (**Fig. 4-7B**, red hashed bars), though to a lesser extent than was seen in the absence of PIPs. bKalSec14 binding was not significantly affected by cholesterol content. Interestingly, removing both PI(4)P and cholesterol from liposomes was not sufficient to abolish completely the interaction of either protein with liposomes (**Fig. 4-7**, blue hashed bars), suggesting that other lipids also contribute to the KalSec14-membrane interaction.

To determine the role of the amphipathic C-helix in liposome interactions, we conducted the same experiments with the Kal-C-helix mutant protein, cKalSec14$_{KKED}$. Remarkably, this protein did not display the same sensitivity to lipid content that was seen with cKalSec14; neither the PI(4)P nor cholesterol content of the liposomes affected cKalSec14$_{KKED}$ binding to liposomes (**Fig. 4-7**). Together, our liposome data suggest that the amphipathic Kal-C-helix is a lipid sensor, which enhances KalSec14-mediated membrane interactions in a lipid-specific manner.

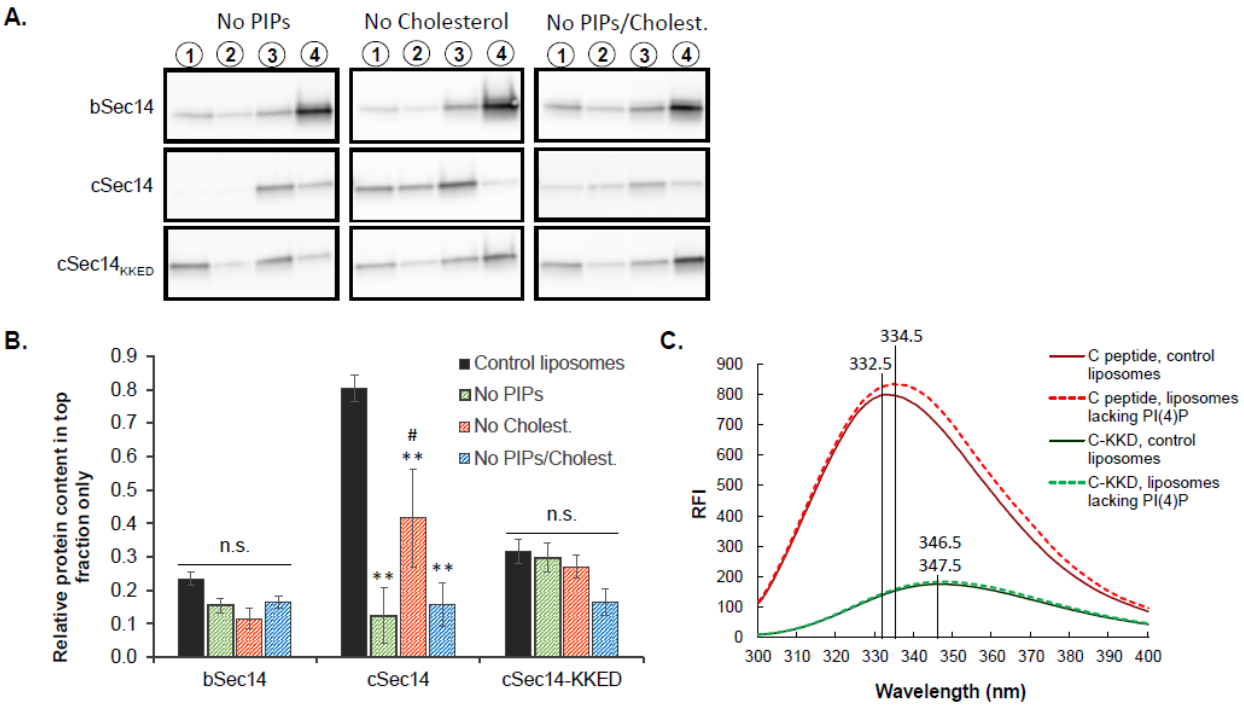

Figure 4-7. cSec14/liposome interactions require phosphoinositides and cholesterol. **A.** Representative blots from flotation assays using liposomes of different lipid content. **B.** Group data showing protein content of the top fraction only for each condition. Values are relative to total protein recovery from each gradient. Data for control Golgi Mix liposomes (GM, black bars) are the same data shown in Fig. 4-6F, fraction 1. Error bars = S.E.M; n = 5-6 experiments for No PIP and No Cholesterol conditions, n = 3 experiments for No PIP/Cholest. condition. All statistics by 2-way ANOVA; ** $p < 0.001$ vs. control GM (black bars); $^{\#}p < 0.02$ vs. No PIP condition (green hashed bars); n.s. = not statistically significant. **C.** Compared to buffer alone (see **Fig. 4-2D**), incubation of Kal-c peptide with liposomes lacking PI(4)P showed an increase in intensity; the λ_{max} for Kal-c peptide rose from 332.5 to 334.5 nm (identical to buffer alone, **Fig. 4-2D**) when PI(4) was eliminated from the liposomes. The λ_{max} for Kal-c_{KKD} peptide shifted only slightly (346.5 to 347.5) when PI(4)P was eliminated from liposomes. Both values were within 0.5 nm of the buffer only condition (347.0) in **Fig. 4-2D**, and all values were considerably right-shifted when compared with λ_{max} values for the wildtype Kal-c peptide.
Liposome conditions as in **Fig. 4-6**.

We returned to tryptophan fluorescence to determine whether the Kal-C-helix interacted directly with PI(4)P. We observed a 2 nm blue shift in the maximal emission wavelength of the wildtype Kal-C-helix peptide when incubated with liposomes containing PI(4)P vs. liposomes lacking any PIPs **[Fig. 4-7C**, λ_{max} 334.5 nm without PI(4)P and 332.5 nm with PI(4)P]. PI(4)P had no effect on the emission spectrum of the mutant Kal-C-helix peptide, Kal c_{KKD} (**Fig. 4-7C**). These data led us to conclude that the amphipathic helix encoded by Ex1C interacts with PI(4)P. When appended to the CRAL_TRIO domain of Kalirin, this amphipathic helix creates a bipartite lipid-binding domain.

The Amphipathic Kal-C-helix promotes secretion in AtT-20 cells

The *trans*-Golgi Network serves as the cellular hub for protein sorting and transport, as well as secretory granule assembly. These processes are tightly controlled by a myriad of protein and lipid interactions, many of which are mediated by the phosphoinositides (PIPs). TGN-enriched PI(4)P, for example, aids in recruiting effector proteins necessary for Golgi vesicle budding (277). Since our data show that the amphipathic Kal-C-helix engages in PI(4)P-dependent membrane interactions and localizes to the TGN, we hypothesized that it played a role in Golgi-mediated trafficking events.

To test this hypothesis, we utilized a cell-permeant version of the amphipathic Kal-C-helix (Kal-C-helix-Arg9). In contrast to transiently expressing Kal-C-helix-GFP, as in Figure 4-5, this strategy allowed us to evaluate acute effects of the C-helix and eliminate limitations associated with low transfection efficiency. In order to verify that the peptide was able to penetrate cell membranes, we used time-lapse imaging to visualize cSec14-GFP distribution before and after application of peptide. As shown in Figure 4-4, cSec14-GFP localized to the TGN when transiently expressed in AtT-20 cells. We observed robust disruption of this localization within 6 min of introducing 5 μM of Kal-C-helix-Arg9 (**Fig. 4-8A**). There was no effect on cSec14-GFP localization following treatment with a control peptide [mutant R7-Kal7CT(96)] (**Fig. 4-8B**).

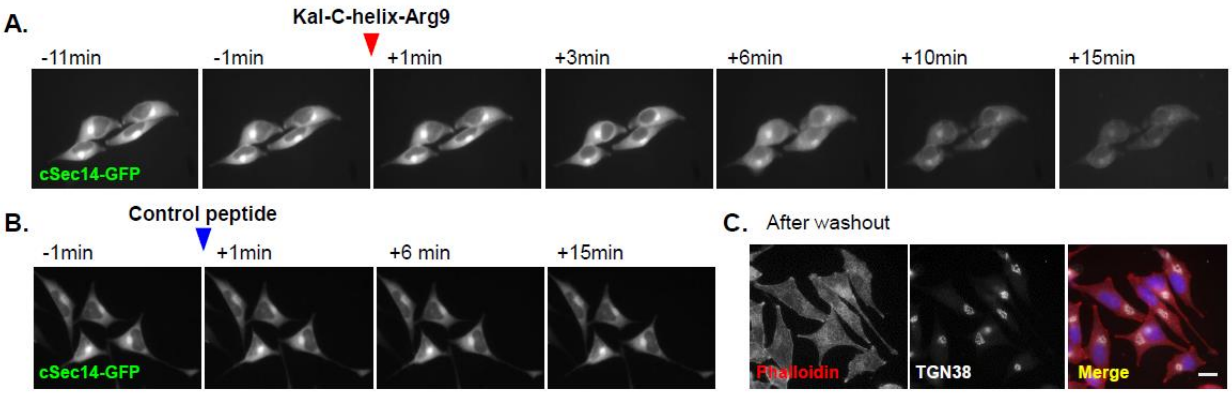

Figure 4-8. Cell permeant Kal-C-helix peptide. **A**. Time-lapse imaging of cSec14-GFP-expressing AtT-20 cells before and after treatment with Kal-C-helix-Arg9 peptide (red arrow). cSec14-GFP localization was disrupted and fluorescence intensity declined. **B**. Treatment with inactive control peptide (blue arrow) had no effect on cSec14-GFP localization or fluorescence intensity, indicating that the loss of signal intensity in **A** was not due to bleaching. **C.** AtT-20 cells treated with 5 µM Kal-C-helix-Arg9 peptide for 30 min were rinsed and returned to normal growth medium. Cells were fixed 72 hours later and stained for filamentous actin (phalloidin, red), TGN38 (white) and Hoechst (blue). After washout, treated cells were indistinguishable from control cells, with the usual number of dividing cells (not shown). Scale bar = 20 µm.

Continued treatment with Kal-C-helix-Arg9 resulted in a marked reduction in total fluorescence intensity, which was not observed in the control condition and thus not due to bleaching. This decrease was likely due to intracellular degradation of the displaced cSec14-GFP. Importantly, Kal-C-helix-Arg9 was not toxic under these conditions, since cells appeared morphologically normal and continued to divide after washout of the peptide (**Fig. 4-8C**). These experiments demonstrated that Kal-C-helix-Arg9 penetrated cell membranes and disrupted TGN localization of cKalSec14-GFP.

AtT-20 cells, immortalized mouse anterior pituitary corticotropes, synthesize proopiomelanocortin (POMC); endoproteolytic cleavage of POMC by prohormone convertase 1 (PC1) leads to the production of adrenocorticotropic hormone (ACTH), β-endorphin and other products that are stored in secretory granules for release in response to secretagogue stimulation (271). AtT-20 cells have been used extensively to study secretory pathway function, making them an excellent model system for evaluating the effects of the Kal-C-helix on cell function. Autoproteolytic cleavage of proPC1 (87 kDa) in the endoplasmic reticulum produces an 81 kDa N-terminally truncated product that is cleaved into a more active C-terminally truncated product (63-kDa PC1) only in mature secretory granules [Fig. 4-9A, bottom (271,278)]. The 81 kDa intermediate is secreted basally while the 63 kDa product is stored in mature secretory granules and released only in response to secretagogues like $BaCl_2$. Basal and stimulated secretion were monitored by quantifying release of 81 kDa and 63 kDa PC1 (**Fig. 4-8D**). Duplicate wells of AtT-20 cells were first equilibrated in CSFM; sequential 30 min collection periods allowed us to assess basal and stimulated secretion and the effect of the cell permeant peptides on each. Cell permeant peptide (5μM C-helix-Arg9 or C-helix$_{KKED}$-Arg9), $BaCl_2$ (0.5mM) or both cell permeant peptide and $BaCl_2$ were added as indicated, and cell extracts were prepared after the final collection (**Fig. 4-8E**, top).

Compared to basal levels, secretion of 63 kDa PC1 increased more than 5-fold in response to Kal-C-helix-Arg9 (**Fig. 4-9Aii, B**). In comparison, $BaCl_2$, a known secretagogue, increased 63 kDa PC1 secretion around 8.5-fold (**Fig. 4-9Ai, B**). When Kal-C-helix-Arg9-treated cells were subsequently stimulated with $BaCl_2$, secretion was further stimulated (**Fig. 4-9Aii, B**). When cells were treated with both Kal-C-helix-Arg9 and $BaCl_2$, secretion levels were comparable to those achieved with $BaCl_2$ alone

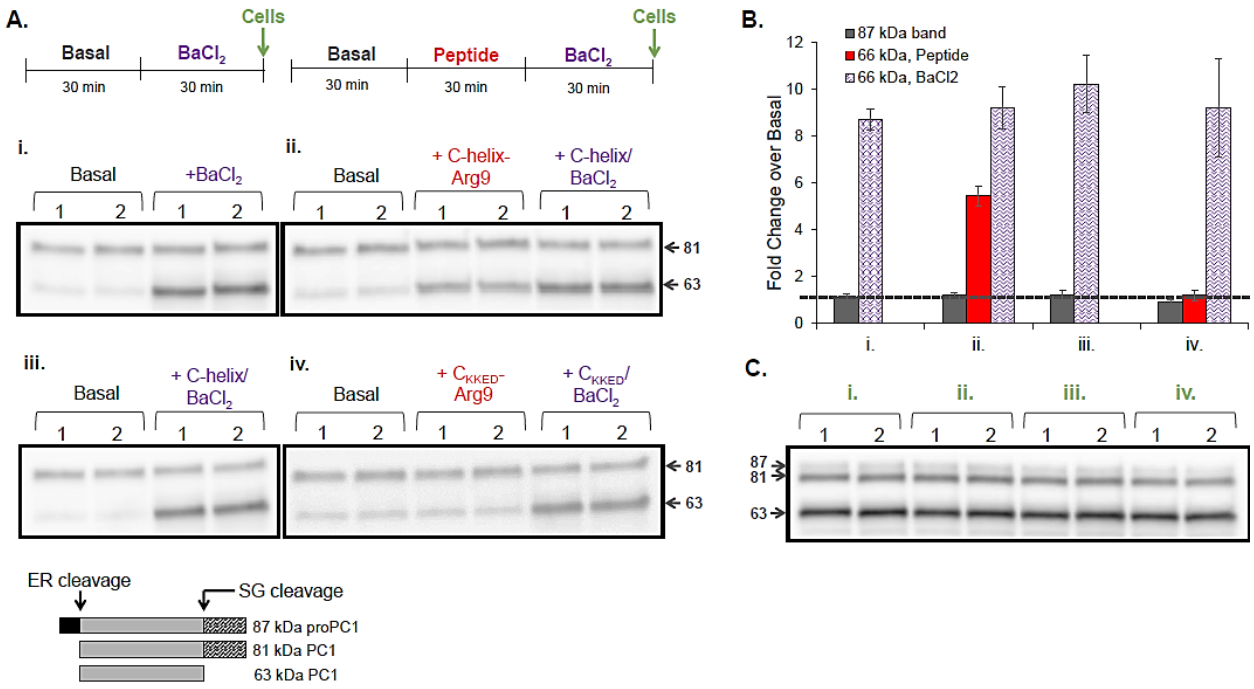

Figure 4-9. Kal C-helix stimulates secretion by AtT-20 cells. **A.** Secretion of PC1 products was monitored to measure basal and stimulated secretion by AtT-20 cells following 30 min of treatment with Kal-C-helix-Arg9 peptide, Kal-C-helix$_{KKED}$-Arg9 control peptide and/or $BaCl_2$, as indicated. After two 30 min washes to allow acclimation to serum-free medium, basal secretion was evaluated for 30 min. In duplicate, AtT-20 cells were then treated with one of four paradigms: 0.5 mM $BaCl_2$ alone (Ai.); 5 µM Kal-C-helix-Arg9 alone, followed by Kal-C-helix-Arg9 with 0.5 mM $BaCl_2$ (Aii.); 5µM Kal-C-helix-Arg9 and 0.5 mM $BaCl_2$ (Aiii.); or 5 µM Kal-C-helix$_{KKED}$-Arg9 alone, followed by Kal-C-helix$_{KKED}$-Arg9 and 0.5 mM $BaCl_2$ (Aiv.). Medium samples were separated by SDS-PAGE and evaluated for PC1 protein content. The 81 kDa form of PC1 is secreted basally, while the 63 kDa form is stored in mature secretory granules and released in response to secretagogues like $BaCl_2$ (278). Addition of the Kal-C-helix-Arg9 peptide, but not the control peptide, stimulated secretion of 63 kDa PC1; secretion of 81 kDa PC1 was not affected by either peptide or by $BaCl_2$. A diagram of PC1 cleavage products is shown at the bottom. **B.** Group data showing medium levels of 81 kDa and 63 kDa PC1 as fold change over basal (dashed line) under the four paradigms. X axis labels correspond to conditions in **A**. n = 4-6 from 3 separate experiments. **C.** Western blot showing PC1 content in cell lysates harvested after the indicated treatment paradigm.

(**Fig. 4-9Aiii, B**). Incubation with Kal-C-helix$_{KKED}$-Arg9 control peptide had no effect on secretion (**Fig. 4-9Aiv, B**), signifying a specific effect of Kal-C-helix-Arg9. Importantly, secretion of 81 kDa PC1 was not affected by $BaCl_2$ or by either Kal-C-helix peptide (**Fig. 4-9A, B**), indicating that Kal-C-helix-Arg9 interacted specifically with the regulated secretory pathway. AtT-20 cells are "professional" secretory cells and a 30 min exposure to secretagogue releases only a small proportion of the total cell content. As such, we did not observe significant differences in PC1 cell content between conditions (**Fig. 4-9C**), further demonstrating that Kal-C-helix-Arg9 treatment did not cause a generalized release of cell content.

Discussion

As important mediators of cytoskeletal regulation, the Rho family GEFs have major roles in cell motility, morphology, and polarity [for review see (31,35)]. Often large, multi-domain proteins, it is likely that many of these proteins are highly specialized molecules, capable of integrating multiple cellular signaling events. Furthermore, the sheer number of GTPase regulatory proteins has made it clear that normal cell signaling relies on their tight spatial and temporal control. In the present study, we describe a potential mechanism by which Kalirin may integrate cytoskeletal regulation and secretory pathway function in a promoter-specific manner. At the same time, we add to knowledge of the Sec14 superfamily of lipid binding proteins and characterize a novel amphipathic helix-mediated mechanism for altering Sec14 domain lipid sensing and function.

Kalrn promoter C usage generates an amphipathic helix that binds PI(4)P

The existence of multiple *Kalrn* promoters was reported previously (95), but their functional significance was not evaluated. Each promoter contributes an initial protein-coding exon that precedes the lipid-binding CRAL_TRIO domain of Kalirin. Given that a CRAL_TRIO_N domain precedes the CRAL_TRIO domain in many Sec14 superfamily members (263), we explored the hypothesis that *Kalrn*

promoter usage was of functional significance. While *Kalrn* promoter B usage generates a charged peptide that is unstructured, *Kalrn* promoter C usage generates a hydrophobic peptide that forms an amphipathic helix which interacts with membranes. A peptide similar to the one generated from rat *Kalrn* promoter C was identified only in mammals and is highly conserved (perfect conservation in over two dozen mammalian sequences examined). A peptide similar to the one generated from rat *Kalrn* promoter B was found in all vertebrates; although its sequence is much less well conserved, its length and hydrophilic nature are conserved.

Membrane binding amphipathic helices are used in many ways, generally adopting an orientation parallel to the plane of the membrane. The amphipathic helix buried within the core of Arf-GDP is exposed as a result of the conformational change that occurs when GTP replaces GDP (279). Amphipathic lipid packing sensors (ALPS motifs), which are generally unfolded until they interact with membranes, have a hydrophobic face rich in bulky residues, with the opposing face free of charged residues (280,281). The Kal-C-helix has a hydrophobic face rich in bulky residues, but its opposing face is highly charged. While ALPS motifs often recognize lipid-packing defects and areas of membrane curvature, we saw no indication that the ability of cKalSec14 to interact with liposomes was curvature sensitive. Strikingly, the Kal-C-helix alone, without the CRAL_TRIO region of the Sec14 domain, localized GFP to the TGN area, and disrupting the amphipathic nature of the helix eliminated its ability to do so.

Kalrn promoter usage affects KalSec14-mediated membrane interactions

Here, we report marked differences in the properties of the Sec14 domains generated from the two major *Kalrn* promoters used in the brain. Using both PIP strips and liposome binding assays, we showed that bKalSec14 and cKalSec14 differed in their ability to interact with lipids. While recombinant bKalSec14 and cKalSec14 both interacted with multiple phosphoinositides on PIP strips, neither pattern reproduced the lipid specificity of aKalSec14 (251) or GST-Sec14 (76). To further evaluate KalSec14

membrane interactions, we altered the lipid content of the liposomes. We found that cKalSec14, but not bKalSec14, interactions were highly sensitive to lipid content. The superiority of liposome binding of cKalSec14 over bKalSec14 was abolished in liposomes lacking PI(4)P. The fact that cholesterol enhanced the binding of cKalSec14 to liposomes without affecting the binding of bKalSec14 may reflect its ability to cluster PI(4,5)P_2 (282). Remarkably, cKalSec14 lipid sensitivity was ablated by disrupting the amphipathic nature of the Kal-C-helix (cSec14$_{KKED}$), revealing an amphipathic helix-mediated lipid sensing mechanism.

Expression in AtT-20 cells revealed differential subcellular localization by bKalSec14 and cKalSec14. bKalSec14-GFP was diffusely distributed, while cKalSec14-GFP colocalized with markers for the *trans*-Golgi Network and secretory granules. Consistent with the importance of the ability of cKalSec14 to interact with PIPs, PI(4)P levels are enriched in Golgi membranes (283). To our knowledge, this is the first demonstration of a Sec14 superfamily member that uses an amphipathic helix that acts as a lipid sensor in conjunction with its lipid-binding CRAL_TRIO domain. Several Sec14 superfamily members are known to bind multiple lipid ligands. Yeast Sec14p binds phosphatidylcholine (PC) and phosphatidylinositol (PI), and both interactions are necessary for normal function (254). The Sec14 domain of α-tocopherol transfer protein (α-TTP) has distinct binding sites for α-tocopherol (vitamin E) and PIPs, and disruption of PIP binding impairs cellular α-tocopherol transport (256). How the lipid binding Kal-C-helix and the lipid-binding CRAL_TRIO domain of Kalirin interact is not yet clear.

The amphipathic Kal-C-helix promotes secretion

The multiple roles of phosphoinositides in cytoskeletal organization, membrane trafficking and secretion (272,273) suggest many ways in which the ability of the Kal-C-helix to bind PI(4)P could affect cell function. Since prolonged expression of cKalSec14-GFP clearly had an impact on cell morphology, we used a cell permeant Kal-C-helix to explore its acute effects. Although we focus here on its effects on

secretion, changes in cytoskeletal organization were also observed, as would be expected for a peptide that binds PIPs (284). Secretion of mature 63 kDa PC1, which is stored in regulated secretory granules and normally released only in response to secretagogue stimulation, was increased six-fold in cells exposed to the cell permeant Kal-C-helix peptide; the mutant Kal-C peptide was without effect on PC1 secretion. The fact that secretion of 81 kDa PC1, which is not stored in mature secretory granules, was unaffected focusses our attention on the proteins and lipids uniquely involved in the regulated secretory pathway (282). Interacting with multiple proteins, $PI(4,5)P_2$ plays an essential role in regulated secretion; an indirect effect of the Kal-C-helix that produced an increase in $PI(4,5)P_2$ levels could contribute to the response observed. PI(4)P negatively regulates interaction of the $p150^{Glued}$ subunit of the dynein/dynactin motor with the retromer complex, facilitating unloading of retromer-dependent cargo (283); disruption of this step in membrane trafficking could indirectly affect secretory granule release.

Early studies using adrenal chromaffin cells revealed a requirement for normal phosphoinositide metabolism for Ca^{2+}-dependent catecholamine secretion (285). Regulated secretion from PC12 cells requires the generation of $PI(4,5)P_2$ from PI(4)P by phosphatidylinositol-4-phosphate 5-kinase (PtdInsP5K) (286). Increased plasma membrane $PI(4,5)P_2$ content increases the readily releasable pool of secretory vesicles in chromaffin cells (287) and the major neuronal PtdInsP5K, phosphatidylinositol phosphate kinase type Iγ (*PIPK1γ)*, is essential for vesicle release from nerve terminals and chromaffin cells (288,289). The priming step that precedes Ca-triggered vesicle fusion involves a phosphatidylinositol transfer protein. Like other Sec14 superfamily members, KalSec14 may function as a lipid transport protein.

Given the importance of $PI(4,5)P_2$ in regulating secretion, one possible explanation for our results is that the Kal-C-helix promotes phosphorylation of PI(4)P. This model would be consistent with studies on yeast Sec14p suggesting that the Sec14-phosphatidylinositol interaction encourages PI phosphorylation by presenting the lipid to PtdIns 4-OH kinase (254). This hypothesis is supported by data showing reduced PI(4)P content and significantly impaired secretory pathway function in Sec14p-deficient yeast (253). Interestingly, secretion deficits can be rescued by restoring PI(4)P content (253).

One might speculate that the amphipathic Kal-C-helix uses a similar mechanism to promote $PI(4,5)P_2$ synthesis and induce secretion. Additionally, direct modulation of both calcium and potassium channels by PIPs has been demonstrated (290), making it plausible that some combination of activation of calcium channels and inactivation of potassium channels could contribute to the increased secretion seen upon application of Kal-C-helix-Arg9.

How promoter usage and Sec14 domain interactions affect the function of full-length Kalirin proteins is currently under investigation. In addition to its Sec14 domain, Kalirin may interact with membrane lipids through the interaction of its spectrin repeat region with sorting nexins 1 and 2 (SNX1 and SNX2) (291). Members of the SNX-BAR subfamily of sorting nexins use their phosphoinositide-binding PX domain and a curvature sensitive BAR domain to tie cargo sorting to membrane tubulation during endocytic trafficking. Since molecular interactions and localization greatly influence the signaling cascades to which a protein contributes, it is possible that alternate promoter usage creates Kalirin subpopulations, which are segregated for action in discrete signaling cascades.

Acknowledgments

We thank Darlene D'Amato and Yanping Wang for their help with cell culture, biochemistry and molecular biology and the UCHC Biophysical Core for providing access to essential equipment. This work was supported by a grant from the National Institutes of Health, DK-032948.

Author contributions

Sec14 sequence alignments were compiled by K.S.V. and B.A.E.

All experiments were conducted by M.B.M, with great technical assistance from K.S.V.

The manuscript was written by M.B.M., K.S.V., R.E.M., and B.A.E.

Chapter 5

Alternate promoter usage generates two subpopulations of Kalirin-7

Megan B. Miller, Yanping Wang, Taylor Larese, Yi Wu, Richard E. Mains, Betty A. Eipper

Abstract

Kalirin (Kal) is a dual Rho GDP/GTP exchange factor (GEF) which is highly expressed in the central nervous system (CNS). Alternative splicing generates 3 major Kalirin isoforms, which are developmentally regulated and essential in CNS development. While Kal9 and Kal12 are crucial for normal neurite outgrowth, Kal7 plays important roles in dendritic spine formation and synaptic plasticity. Full-length Kalirin includes four unique, alternate initial exons (Ex1A, 1B, 1C, 1D), but little is known about the expression and functional significance of the distinct initiation sites. *Kalrn* promoter usage is developmentally regulated, varying across brain regions. Ex1B is used early in development, with Ex1C becoming the major isoform in the adult hippocampus. Promoters A and D are rarely used in the brain. Subcellular fractionation and an antibody to the Ex1C peptide (an amphipathic helix which binds to phosphoinositides, Kal-C-helix) demonstrated that the PSD is enriched in C-helix-containing Kal7 (cKal7), with little cKal7 found in the cytosol. In primary neuronal cultures, Kal-C-helix staining is localized to dendritic spines, juxtaposed to Vglut1 puncta. Both bKal7-GFP and cKal7-GFP localize to dendritic spines, increasing spine number in neuronal cultures; cKal7-GFP forms significantly smaller postsynaptic sites. Interestingly, promoter usage also affects GEF activity; bKal7 has significantly more GEF activity for Rac1 than cKal7. Since the amphipathic C-helix interacts with PI(4)P and contributes to Sec14 domain-mediated membrane interactions *in vitro*, a cell-permeant Kal C-helix peptide was tested on neurons. C-helix peptide treatment resulted in AMPAR internalization and reduced dendritic spine length, suggesting a role in postsynaptic membrane trafficking.

Introduction

Glutamatergic synapses are characterized by the presence of a postsynaptic, electron-dense region known as the postsynaptic density (PSD). Though less than a square micron in size, the PSD is comprised of hundreds of proteins which, together, dictate postsynaptic responses to excitatory neurotransmission. Classes of proteins found at the PSD include neurotransmitter receptors, molecular scaffolds, cytoskeletal proteins, cell trafficking machinery and an abundance of signaling molecules required for synaptic function (292,293). Among the PSD signaling molecules are dozens of kinases, phosphatases, and regulators of GTPase activity, many of which have apparently overlapping functions. The reasons for such a high degree of redundancy are not yet understood, but it is clear that tight spatial and temporal control over PSD-associated signaling molecules is key to proper synaptic function.

Kalirin-7 (Kal7) is a PSD-localized Rho family GDP/GTP exchange factor (GEF) for Rac1. Through its GEF activity, Kal7 promotes actin polymerization and structural plasticity of dendritic spines. It also engages in direct interactions with a number of other important synaptic proteins, including PSD95 and GluN2B, and contributes to actin dynamics (36,37,41,42). As such, Kal7 plays a crucial and well-established role in synaptic structure and function. Genetic ablation of Kal7 ($Kal7^{KO}$) results in decreased dendritic spine density and substantially impaired structural and functional plasticity (36,42). Behaviorally, $Kal7^{KO}$ animals display impaired fear learning, decreased anxiety-like behavior and heightened sensitivity to cocaine (36,51,294).

Through alternative splicing, the *Kalrn* gene encodes several longer isoforms, Kal9 and Kal12, both of which include a second GEF domain for RhoA. Both isoforms are expressed in the brain throughout development, with significant expression also seen in muscle, heart, bone and other tissues (205,248-250). Kal9/12 are crucial for normal neurite outgrowth and, in addition to Kal7-mediated phenotypes, mice lacking all isoforms of Kalirin ($KalSR^{KO}$) have markedly impaired neuromuscular and neuroendocrine function (205,295). Outside of the nervous system, animals deficient in Kalirin

expression display decreased bone mass, and diminished protection in a model of neointimal hyperplasia (atherosclerosis) (249,250).

In addition to alternative splicing, the use of multiple promoters adds further diversity to the protein products generated from the *Kalrn* gene (95,296). Full-length Kalirin transcripts are generated from four distinct initiation sites, termed B, C, A and D, each of which encodes a single, unique initial exon (Ex1A, 1B, 1C, 1D; **Fig. 5-1**). Interestingly, the peptides encoded by these initial exons differ substantially in sequence and structure (**Table 5-2**). Importantly, the Ex1C peptide forms an amphipathic helix which binds directly to phosphoinositide-4-phosphate [PI(4)P], a lipid with essential roles in mediating membrane/receptor trafficking in all cells, including neurons. Ex1B encodes a charged and unstructured peptide, which does not engage in PIP interactions. Our recent work revealed a role for these initial peptides in controlling membrane interactions by the N-terminal Sec14 domain of Kalirin (this thesis, Chapter 4). However, very little is known about the physiological relevance of alternate promoter usage in the mammalian nervous system. Here, we identify striking developmental regulation of *Kalrn* promoter usage in the rodent brain and reveal functional consequences of promoter usage on Kal7 localization and synaptic function. This work also provides further support for the importance of strict spatial and temporal regulation of postsynaptic signaling.

Materials and Methods

RNA extraction and polymerase chain reaction

Fresh tissue was collected from cortex, hippocampus and striatum of C57BL/6 mice at the indicated developmental stages, ranging from embryonic day 16 (E16) through postnatal day 28 (P28), and adult (>P80). RNA was prepared using Trizol (Invitrogen) following the manufacturer's instructions, except that the isopropanol precipitation step was lengthened to overnight at -20°C.

qRT-PCR. cDNA was prepared using iScript reverse transcriptase (BioRad) and random primers. Reaction mixtures were heated to 65°C for 5 minutes, then chilled on ice for 5 minutes prior to following the manufacturer's reverse transcription protocol. Real-time PCR was performed using an Eppendorf Realplex2 machine and Sybr-Green (BioRad), with the following parameters: 95°C for 2 min, then 40X 95°C for 15 sec, 55°C for 15 sec, 68°C for 40 sec. Primer sequences and calculated melting temperatures are listed in Table 5-1 and were validated previously (95). Data were analyzed using the relative cycle threshold (ΔCt) method with respect to GAPDH, which remains constant across development (not shown). Results are presented as average exponentiated ΔCt values from 3-4 biological replicates per group +/- standard error of the mean.

Long-range PCR. cDNA was prepared using Superscript III reverse transcriptase (Invitrogen) and Oligo-dT primers (Qiagen); the mRNA, Oligo-dT and buffer were heated at 65°C for 5 min, chilled on ice to add dithiothreitol and enzyme, then incubated at 50°C for 30 min, 55°C for 30 min, and finally denatured at 70°C for 15 min. PCR was performed with the Expand Long Template PCR system from Roche using Buffer 1 (1.75 mM $MgCl_2$). The PCR program was 92C, 2 min; [61C 30 sec; 68C, 15 min; 92C 10 sec] x 10; [65C 30sec, 68C 15 min, 92C, 15 sec] x 40; finally, analysis on a 1% agarose gel. Primers are listed in Table 5-2; Expected product lengths are as follows: Exon 1 (B or C) vs. Exon 13 = 2.0 kb, Exon 1 (B or C) vs. Kal7 = 5.0 kb, Exon 1 (B or C) vs. DH2 = 5.8 kb.

Target	Oligo	Sequence	T_m (°C)	Product length (nt)
qPCR				
GAPDH	Forward	TTGTCAGCAATGCATCCTGCACCACC	61	119
	Reverse	CTGAGTGGCAGTGATGGCATGGAC	61	
Kal Exon 1A	Forward	CAGGGCAGCCATAAATGGTTTTATCTG	58	121
Kal Exon 1B	Forward	GTGGACGCCTTTTTCCGGACAG	59	116
Kal Exon 1C	Forward	CTTGCTTCGGCTTCTGGATCGAG	59	117
Kal Exon 1D	Forward	CTTTGTTTCTTCCTCACTGCAGCGG	59	120
Kal Exon 3	Reverse	CCTCGCTTGTCACGCCCCC	60	
Long-Range PCR				
Kal Exon 1B	Forward	ACTCGGACGTGGACGCCTTTTTCCGGAC	66	See text
Kal Exon 1C	Forward	GTATCTCCGCTTGCTTCGGCTTCTGGATCG	66	
Kal7 specific	Reverse	CATGTCCCAGGCTGCGCGCTAAACGTAAG	66	
Kal DH2	Reverse	TAGTCCTTCTCTGTCTGTACCAGCTCATTCAGGAC	66	

Table 5-1. PCR primers. Shows target, sequence, melt temperature (T_m °C), and product size (nucleotides) for all forward and reverse primers used for qPRC and Long-range PCR.

Antibodies

Antibodies used for Western blotting: Affinity purified rabbit polyclonal to spectrin repeat (4-7) of Kalirin (JH2581) (247), affinity purified rabbit polyclonal to Kal Sec14 (CT302) (248), affinity purified rabbit polyclonal to Kal C-helix (CT38) (248), affinity purified rabbit polyclonal to Kal7 (JH2959) (248), mouse monoclonal to PSD-95 (clone K28/43; NeuroMab Facility, University of California, Davis, Davis, CA), mouse monoclonal to GAPDH (Millipore) mouse antibody to Myc epitope tag [9E10, (297)], mouse monoclonal to NR2B (clone 59/20; NeuroMab), mouse monoclonal to NR1 (catalog no. 556308; BD Biosciences), mouse monoclonal to GluR1 (catalog no. ab31232; Abcam),

Primary antibodies used for immunostaining include rat anti-GFP (NacalaiTesque, Kyoto, Japan), mouse monoclonal to PSD95 (clone 28/43, 1:300; NeuroMab), and guinea pig antibody to Vglut1 (AB5909; Millipore). Primary antibodies were visualized with appropriate secondary antibodies: Cy3-donkey anti-mouse and fluorescein isothiocyanate (FITC)-donkey anti-rat immunoglobulin G (IgG) were from Jackson ImmunoResearch Laboratories (West Grove, PA); Alexa Fluor 633-goat anti-guinea pig IgG was from Molecular Probes (Eugene, OR).

Subcellular fractionation

Mouse forebrain tissue was dissected and homogenized in 10 volumes of Buffer A (10 mM HEPES, pH 7.4, 320 mM sucrose, 2 mM EDTA, 5 mM NaF, 1 mM sodium orthovanadate, 1 mM PMSF, and protease inhibitor cocktail). Subcellular fractionation of lysates was conducted as described previously (33). Briefly, homogenates were centrifuged for 10 min at 1000 x g to remove insoluble material, and the supernatant was centrifuged again at 14,000 x g for 15 minutes to yield a pellet (P2 = crude synaptosomes) and supernatant (S2 = soluble material). The S2 fraction was centrifuged again at 100,000 x g for 15 minutes, giving rise to a pellet (P3) enriched in endoplasmic reticulum and Golgi apparatus, and a supernatant (S3) containing cytosolic proteins. P3 was solubilized in sodium

dodecyl sulfate lysis buffer (SDS- LB; 50mM Tris [pH 7.6], 1% SDS, 130mM NaCl, 5mM EDTA, 50mM NaF, 10mM Na_3PO_4) and both solubilized P3 and S3 were used for immunoprecipitation. The crude synaptosomal fraction (P2) was homogenized in Buffer B (2 mM HEPES, pH7.4) and then further processed to generate purified postsynaptic densities (PSDs). In short, the resuspended P2 fraction was loaded onto a sucrose gradient (1.2M, 1.0M, 0.8M sucrose in 10 mM HEPES, pH7.4) and centrifuged at 80,000 x g for 120 min. Material that accumulated at the 1.0M/1.2M interface was collected (crude PSD fraction), diluted with two volumes of Buffer C (10 mM HEPES, pH7.4) and centrifuged at 435,000 x g for 15 min to pellet the PSDs. The final PSD pellet was solubilized in SDS-LB and used for immunoprecipitation.

Immunoprecipitation and Western blot analysis

Samples were immunoprecipitated essentially as described previously (33). Cytosolic (S3), ER/Golgi (P3, solubilized in SDS-LB) and PSD fractions (after addition of a 10-fold weight excess of NP-40 over SDS) were tumbled overnight at 4°C with protein A resin and affinity purified rabbit antiserum JH2581 (247), which recognizes the spectrin repeat 4 to 7 region of Kalirin. Following incubation, unbound protein was removed and the resin was washed twice with TMT buffer (20 mM Na-TES, 10 mM mannitol, pH 7.4, 1.0% Triton X-100). Bound protein was eluted by boiling into 1× Laemmli SDS sample buffer. Bound proteins were fractionated using SDS-PAGE and transferred to PVDF membranes. Membranes were immunoblotted using indicated antibodies.

Rac1 biosensor and Rac activation assay

A FRET biosensor for activated Rac1 (Dora-Rac1) (298) was used to evaluate Rac1 activation in cells expressing Kal7 variants resulting from use of the indicated promoters. The sensor contains an N-terminal FRET donor (Cerulean3) linked to a Rac binding domain derived from PAK (PBD), which is

connected via an extended linker peptide to the FRET acceptor (Venus), which has Rac1 linked to its C-terminus. A Myc epitope tag was included at the N-terminus to facilitate quantification of protein expression by western blot analysis. To conduct the assay, pEAK-Rapid cells (a HEK-293 derivative) were plated at medium-high density onto poly-L-lysine (Sigma) coated, glass-bottom 24-well dishes with black walls (In Vitro Scientific); cells were maintained in growth medium (DMEM/F12, 10% FCS, 25 mM HEPES, containing Pen/Strep) and were kept in a 5% CO_2 incubator. When cultures were about 70% confluent, cells were transfected using TransIT-2020 (Mirus, Madison WI) using a ratio of 1.5 µl reagent/µg DNA. Each well was co-transfected with 0.2 µg of the Dora-Rac1 biosensor and 0.05 to 0.5 µg of pEAK-Kal7 (pEAK-aKal7, pEAK-bKal7, pEAK-cKal7). Empty pEAK-HisMyc carrier DNA was used to bring the total transfection suspension to 0.7 µg per well. After transfection, cultures were kept in normal growth medium for 29-30 hours, at which point growth medium was replaced with DMEM lacking phenol red, Na-pyruvate and vitamins (US Biological) and cells were allowed to acclimate to room temperature for 15-20 minutes. FRET ratios were read for each well using an EnSpire 2300 Multilabel Plate Reader (Perkin Elmer, Waltham MA). Wells were excited at 420 nm and fluorescence spectra were collected from 440 to 600 nm. After subtracting the spectra from a biosensor-only control well, relative Kal7-mediated Rac1 activation was determined by dividing the 525-nm (Venus) emission peak by the 475-nm (Cerulean3) emission peak. After reading the emission spectra, cells were harvested and protein expression levels were determined by Western blot analysis using antibodies to Kal7 (JH2959) and the Myc-tag on the biosensor. As expected, biosensor expression levels were the same in all wells and Kal7 expression levels increased linearly with increasing vector concentration. The FRET ratio (525/475) for each condition was plotted against the amount of Kal7 DNA used for transfection and against the observed protein expression level; similar answers were obtained using both approaches.

Primary neuronal culture and transfection

Primary rat hippocampal neuron cultures were prepared from embryonic day 18 (E18) Sprague–Dawley rats as described (96,251,299). Neurons for immunostaining were dissociated and plated at medium to high density in plating medium (DMEM + 10% FCS + pen/strep and fungizone) on poly-L-lysine-coated coverslips. Neurons expressing farnesylated-GFP (fGFP; (300)) were nucleofected at plating using program O-003 (Amaxa, Cologne, Germany). Kal7-GFP transfections were carried out two days after plating using 0.7µl Lipofectamine 2000 transfection reagent (Life Technologies) per µg DNA. Non-transfected neurons for BS^3 crosslinking experiments were plated onto plastic tissue culture dishes at similar density.

Expression vectors

The pEAK vector (251) was used to accommodate the rat aKal7, bKal7, and cKal7 inserts without an epitope tag. The pEGFP-N2 vector (Clontech) was used directly, and the farnesylated EGFP vector has been described [fGFP (300)]. To facilitate construction of expression vectors encoding the bKal7 and cKal7 NH_2-termini, a silent *Nru1* mutation was inserted at nt 93 of aKal7(Spec9-GFP); EGFP is located in an exposed loop in the 9^{th} spectrin repeat (251). All constructs were verified by DNA sequencing.

Cell permeant peptides

The cell-permeant Kal-C-helix (C-helix-Arg9; TDRFWDQWYLWYLRLLRLLD-RRRRRRRRR) and control (C-$helix_{KKED}$-Arg9; TDRFKDQKYLEDLRLLRLLD-RRRRRRRRR) peptides (Biomatik USA, LLC; >90% purity) were described previously (Miller, PhD Thesis, Chapter 4).

Both peptides were dissolved in DMSO to create 2-mM stock solutions. Rat hippocampal cultures were treated with 5μM cell permeant peptide diluted in half fresh/ half conditioned neuronal maintenance medium for 20 minutes at 37˚C, 5% CO_2. For immunocytochemistry, neurons were transfected with fGFP immediately after dissociation, plated onto coverslips at medium density, treated with peptide at 17DIV and fixed in 4% paraformaldehyde in PBS 20 minutes later. Neurons used for BS^3 crosslinking were plated onto plastic dishes and treated with cell permeant peptide at 25 DIV.

Immunocytochemistry and imaging

Neuronal cultures were fixed in 4% paraformaldehyde in PBS, permeabilized with 0.075% Triton X-100 and blocked with 2mg/mL BSA, then doubly or triply stained with primary antibodies overnight at 4°C, as indicated. All images were obtained using a Zeiss (Jena, Germany) Axiovert 200M microscope using a 63X oil objective and AxioVision software (Carl Zeiss Microscopy, LLC, Thornwood, NY, USA). Optical sectioning was achieved with the Zeiss ApoTome module, and 3 sections of 0.4 μm each were compressed for each image.

Image analysis

Spine density and synaptic clusters were analyzed using MetaMorph image analysis software (Molecular Devices, Sunnyvale, CA) as described (96,251). Briefly, representative dendritic segments within 150μm of the cell soma were measured and spines/synaptic clusters were counted manually. A line was drawn from the dendritic shaft to the tip of the spine head to measure spine length; dendritic protrusions under 5μm in length were considered dendritic spines. Postsynaptic cluster area was determined by manually tracing GFP puncta. Length and area measurements were calibrated using a representative scale bar and data from each image (1 neuron / image) were averaged. All images were coded and scored by a blinded observer. After de-coding, data were compared across groups and represented as average values ± SEM.

BS^3 Crosslinking

Neuronal surface proteins were cross-linked using membrane-impermeable bis-(sulfosuccinimidyl) suberate (BS^3) (Thermo Scientific) and a protocol adapted from previously established methods (33,301). Immediately following peptide or control treatment, cultured rat hippocampal neurons were rinsed twice in ice cold artificial cerebrospinal fluid (ACSF; in mM: 26 HEPES [7.4], 125 NaCl, 2.3 KCl, 2 $CaCl_2$, 2 $MgSO_4$, 1.26 KH_2PO_4, 10 Glucose). The final wash volume was replaced with 2mM BS^3 crosslinking solution in ACSF, and plates were rocked gently on a shaker for 40 minutes at 4°C. To stop the reaction, a 1M glycine solution was added to the crosslinking solution to give a final concentration of 15 mM. After several minutes, the cultures were washed again with 5 mM glycine in ACSF. Cells were scraped into SDS-LB with protease inhibitors, then heated to 55˚C for 10 min and centrifuged for 20 min at 20,000 rpm at room temperature. Supernatants were saved and protein concentrations were determined using a bicinchoninic acid assay (BCA; Thermo Scientific) per the manufacturer's instructions. Protein (25 µg) from each sample was used for Western blot analysis. Discrete bands at the expected molecular weight for each protein of interest were quantified as a measure of internal protein concentration. Crosslinked proteins appeared as diffuse, high molecular weight signal, which was not present in the "No BS^3" control condition. After background subtraction, the ratio of surface/ internal receptor expression was calculated and compared across groups.

Results

Full-length Kalirin expression is initiated at one of four alternate promoters, resulting in four unique initial exons (Ex1A, 1B, 1C, 1D), which precede the start of the common lipid-binding, Sec14 domain (exons 2-5) (**Fig. 5-1**). Notably, the unique peptides resulting from the alternate promoters are remarkably different in sequence and predicted structure (**Table 5-2**). Ex1A was identified first and

encodes a short, hydrophilic peptide (Ex1A-peptide); although not well conserved evolutionarily, similarly short sequences were identified in the bactrian camel, Chinese hamster and African elephant. Mouse Ex1B encodes a 25 amino acid peptide (Ex1B-peptide), which is negatively charged and unstructured (see Chapter 4). An identical peptide is encoded by human *Kalrn* Ex1B and highly homologous peptides were identified in other mammals. A homologous (negatively charged, few hydrophobic residues) Ex1B-peptide was identified in lower vertebrates. The Ex1C-peptide forms an amphipathic helix, with its hydrophobic residues aligning at one face of the helix, while the charged residues align at the other. The amphipathic C-helix interacts with phosphoinositides and enhances KalSec14-mediated membrane interactions (Chapter 4). The Ex1C-peptide is remarkably well-conserved in mammals with identical sequences in 100+ species. Interestingly, despite the presence of a *Kalrn* gene, no Ex1C homolog could be identified in lower animals, suggesting a specific role in more evolved nervous systems. Identified in mouse, rat and human, Kal Ex1D encodes the longest initial peptide (38 amino acids); as for the Ex1C-peptide, the Ex1D-peptide is positively charged and could adopt a helical structure. Notably, neither the invertebrate homologs of *Kalrn* (*dTrio* and *Unc-73*) nor the mammalian paralog of *Kalrn* (*Trio*) encode peptides that correspond to any of the Kalirin Ex1-peptides. Rather, sequence homology is first apparent at the start of the Sec14 domain encoded by Kal Exon 2.

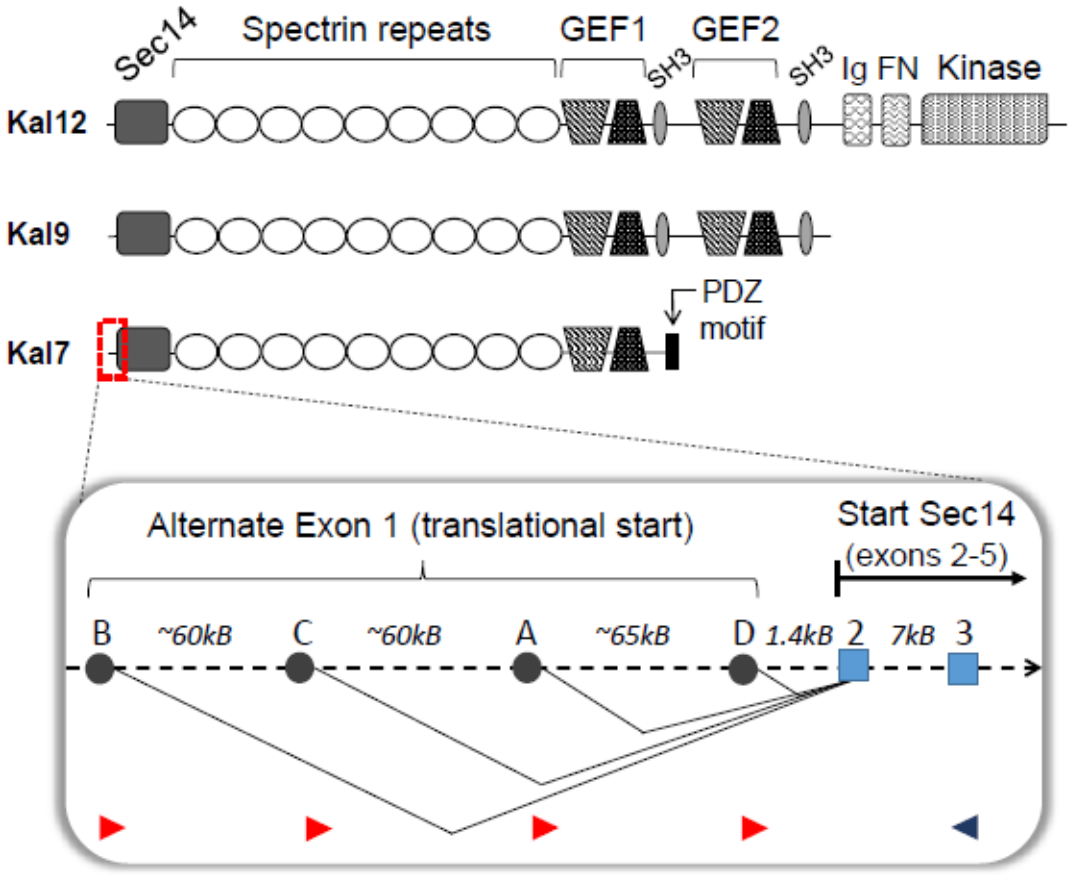

Figure 5-1. Major full-length Kalirin splice variants and promoter diagram. **A.** Developmentally regulated and tissue specific alternative splicing of the *Kalrn* gene gives rise to three major full-length Kalirin (Kal) proteins, Kal12, Kal9 and Kal7. Protein domains are indicated. **B.** Diagram of alternate promoters present in the rat *Kalrn* gene. Promoters are separated by large introns (57-65 kb) located 1.4 to 180 kb upstream of common exon 2; a similar arrangement is seen in other species, including human. qPCR primer locations for Figure 5-2 are indicated; red arrowheads show location of Exon 1 specific forward primers, blue arrowhead shows the location of the common reverse primer in Exon 3.

Exon 1	Peptide sequence (mouse)	charge	Properties	Conservation
A	MGVLSG *(mouse)* MMPSRR *(African elephant)* MGMLLVL *(Chinese hamster)*	0 +2 0	Very short	Poorly conserved
B	MNPP EGAAEEGGAADS DVDAFFRTG *(mouse)* MNPP EGAAEEGGAADS DVDAFFRTG *(human)* MNPA EGAAEEGAVPDS EVDAFFRTG *(Budgie, bird)* MNPAA EGAAEEGAVPDS EVDAFFRTG *(Anolis, lizard)* MNS A E APEDGPNDS DTDAFFKTG *(Danio, fish)* M.....EG AEET AKDSADITAFYRSG *(Xenopus, amphibian)*	-5 -5 -5 -5 -5 -3	Charged, hydrophilic, unstructured	Well conserved in mammals, moderately in vertebrates
C	MTDRFWDQWYLWYLRLLRLLDRGILR *(mouse)* MTDRFWDQWYLWYLRLLRLLDRGILR *(human)* - Identical in 100+ mammals - Not found in birds, lizards, fishes, amphibians	+2 +2	Highly hydrophobic, amphipathic helix	Extremely well conserved in mammals, not found in lower species
D	MGFERAYLKELKTELENKVVSLKSEFFLVFVSSSLQRR *(mouse)*	+2	Mostly hydrophilic	Not in other species
E (human)	MENITSSIFDVISKGKVAPTFSYW *(human)*	0	Mostly hydrophilic	Not in other species

Table 5-2. Peptide sequences, structural/ biophysical properties and evolutionary conservation of each initial peptide. Green = interior Met; Blue = charged residue; Pink = hydrophobic; Gray = not matched. Accession numbers for sequences: aKal, XM_006522372; bKal, XM_006522368.1; cKal, BC157950.1; dKal, XM_001001454.1. Other "A": African elephant XP_010591303.1; Chinese hamster XP_007639189.1. Other "B": human XP_006713879.1; budgie XP_005153849.1; Anolis, XP_008107705.1; Danio XP_009302722.1; Xenopus AAH88976.1. Other "C": Peptides resembling the mouse Ex1C-peptide were identified only in mammals, with over 100 exact matches in GenBank, including human EAW79419.1; sperm whale XP_007118801.1; bactrian camel XP_006189909.1; prairie vole XP_005344933.1; armadillo XP_004465866.1; rhesus monkey EHH16131.1; ferret XP_004745470.1; hedgehog XP_007528965.1; rabbit XP_002716592.1. Human "E": EAW79418.1.

Kalrn promoter usage is developmentally regulated and varies across brain regions

To evaluate the physiological significance of *Kalrn* promoter usage, we used qPCR to assess transcript levels in three mouse brain regions across development. RNA was collected from cortex, hippocampus and striatum from postnatal day 1 (P1) through P28. Cortical and hippocampal RNA was also collected from embryonic day 16 (E16) mice. Unique forward primers which recognize each initial exon were paired with the same reverse primer to common exon 3 (**Table 5-1, Figure 5-1**) (95). Transcript levels with respect to GAPDH are shown in Figure 5-2. We found that *Kalrn* promoter usage in the mouse brain is developmentally regulated and varies across brain regions. Ex1B (**Fig. 5-2, A-C**, blue lines) was highly expressed at early developmental time points, making up nearly 100% of all embryonic *Kalrn* transcripts in the cortex and hippocampus. Ex1C (**Fig. 5-2, A-C**, orange lines) expression was not detectable embryonically, but increased postnatally in all three brain regions. Interestingly, a developmental switch from Ex1B to Ex1C was observed at P8 in the hippocampus, with Ex1C comprising nearly 75% of the *Kalrn* transcripts in this tissue by P28 (**Fig. 5-2B**). Conversely, Ex1B remained the predominant isoform in the cortex throughout development (**Fig. 5-2A**), and Ex1B and Ex1C transcript levels in the striatum were equivalent after P8 (**Fig. 5-2C**). Notably, although PCR products of the correct size were detected for all primer sets (95), these results indicate that promoters A and D are not used appreciably in the brain throughout development. While panels A-C in Figure 5-2 highlight differences in promoter usage across brain regions, panels D and E illustrate the developmental regulation of Ex1B and Ex1C. Alternative: In order to determine whether the transcripts initiated at these four promoters accounted for most of the *Kalrn* transcripts present, we analyzed the same samples using a primer set in Exon 10 (spectrin repeat 5); when normalized to GAPDH, the Exon 10 transcript levels were approximately equal to the sum of the Ex1A to Ex1D transcript levels for all ages in all three tissues (not shown).

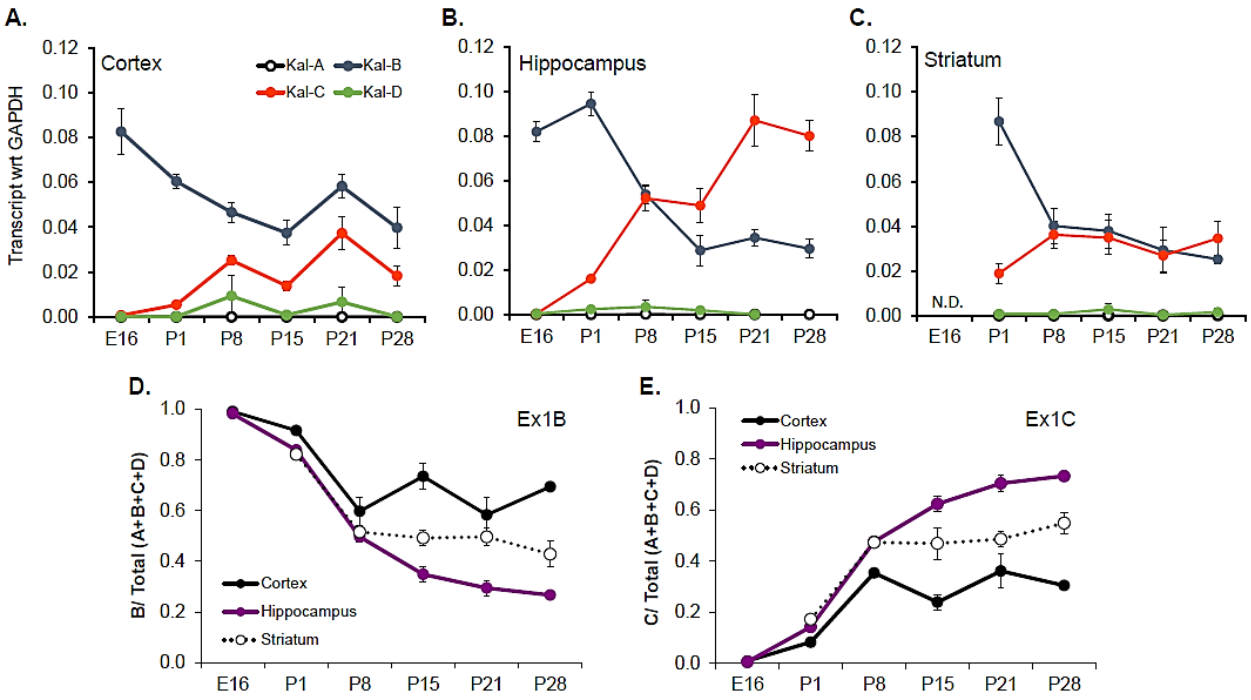

Figure 5-2. Developmental regulation of *Kalrn* promoter usage. **A-C.** qPCR data showing *Kalrn* Exon 1 (Ex1) transcript levels in the cortex (A), hippocampus (B) and striatum (C) across development. Data are shown as group averages (ΔCt with respect to GAPDH) ± SEM. Black lines = Ex1A, blue lines = Ex1B, orange lines = Ex1C, green lines = Ex1D. **D-E.** The same data shown in A-C, plotted to highlight developmental regulation. Ex1B (D) and Ex1C (E) transcript levels are shown as a proportion of total (A+B+C+D) full-length Kalirin transcript across brain regions.

Promoters B and C with major splice variants

Expression of the three major Kalirin splice variants, Kal7, Kal9 and Kal12, is also developmentally regulated (248). Like Kal Ex1B, Kal9 and Kal12 expression is highest early in development and then declines postnatally. The Kal Ex1C expression profile resembles that of Kal7, which is not present embryonically, but becomes the major isoform in the adult brain. To rule out the possibility that *Kalrn* B- and C-promoters are used only with specific splice variants, we conducted long-range PCR reactions using adult mouse cDNA; forward primers specific for the B- and C-promoters were paired with reverse primers specific to either Kal7 (reverse primer in the PDZ motif) or Kal9/12 (reverse primer in the DH domain of GEF2)(**Fig. 5-3A**). We did not attempt to distinguish Kal9 and Kal12 transcripts, since adult expression of each is relatively low. Using this strategy with mouse cortical cDNA, we found products of the expected size from all primer pairs, indicating that the unique peptides encoded by Ex1B and Ex1C are present in Kal7 (denoted bKal7 and cKal7) and Kal9/12 (**Fig. 5-3B**). Similar results were found previously using rat cDNA (296). Since the bKal and cKal isoforms differ in mass by only 972 Da, they cannot be separated by SDS-PAGE.

cKal7 is enriched at the postsynaptic density

To evaluate the expression and localization of endogenous bKal7 and cKal7, we developed an antibody (CT38) which specifically recognizes the Ex1C-peptide (**Fig. 5-4A**). The Ex1C-peptide antibody successfully recognizes cKal7 expressed in HEK cells, with no reactivity observed to bKal7 (**Fig. 5-4B**). The Ex1C-peptide antibody is only about a third as efficient at recognizing cKal7 as a previously-reported antibody raised to the Sec14 domain, CT302 (**Fig. 5-4A-B**) (248). Attempts to develop an antibody to the unstructured Ex1B-peptide were unsuccessful.

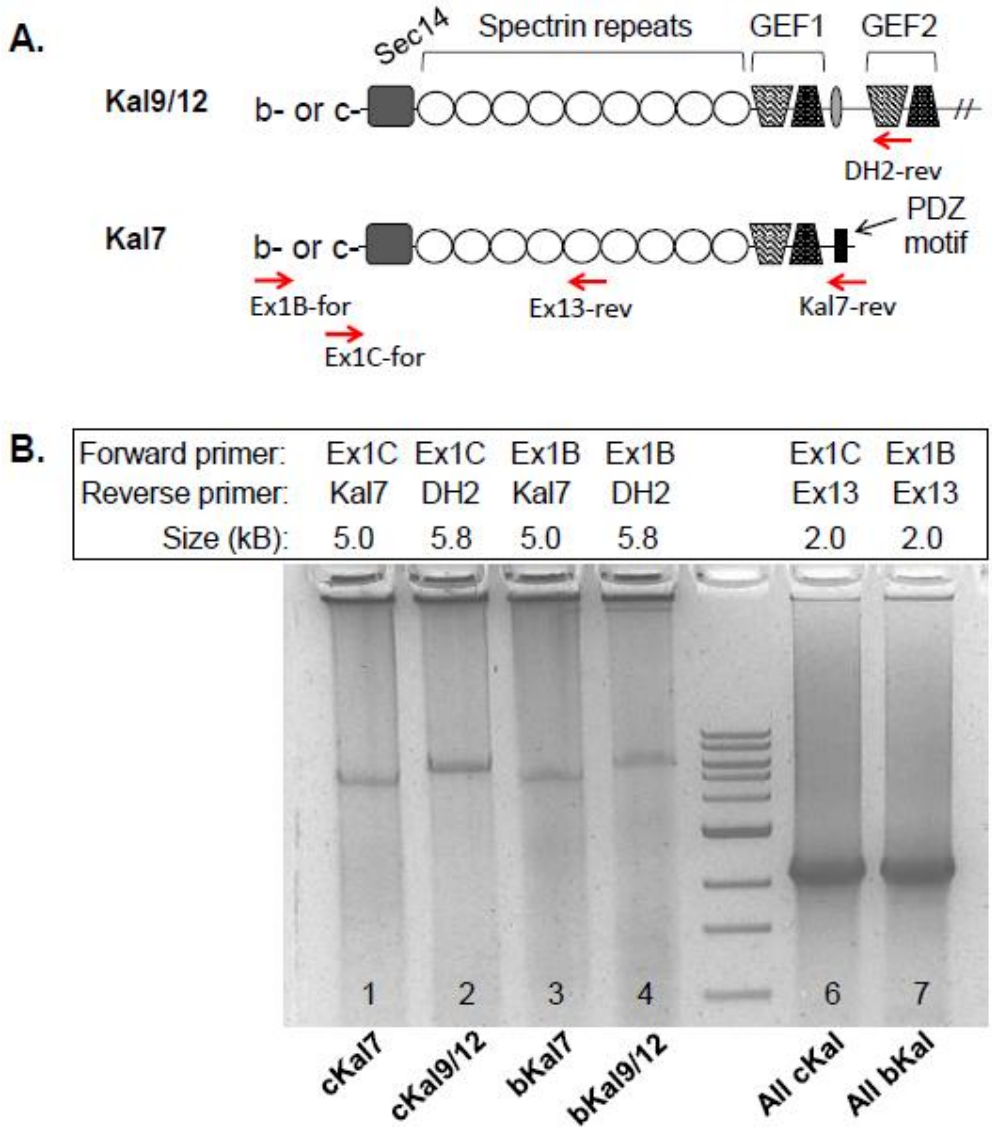

Figure 5-3. Long-range PCR showing major promoters and splice variants. **A.** Diagram showing forward (for) and reverse (rev) primer locations, red arrows. Each forward primer was paired with each reverse primer. **B.** DNA gel showing major PCR products resulting from the primer pairs indicated at the top of each lane. Products from Ex1C forward primer to each reverse primer are in lanes 1 (Kal7-rev), 2 (DH2-rev) and 6 (Ex13 rev). Products from the Ex1B forward primer are in lanes 3 (Kal7-rev), 4 (DH2-rev) and 7 (Ex13 rev). Lane 5 is a molecular weight marker (top to bottom: 10, 6, 3, 2, 1 kb). Product size and identity are indicated at the bottom of each lane.

To determine cKal expression levels and subcellular localization, we performed a series of immunoprecipitation (IP) experiments following subcellular fractionation of adult mouse forebrain lysates into soluble (S2) and postsynaptic density-enriched fractions (PSD); the success of the subcellular fractionation and immunoprecipitation protocols was verified using antisera to GAPDH (a soluble protein) and PSD-95 (a marker for the PSD) (**Fig.4C**). Total Kalirin protein was precipitated with an antibody recognizing the spectrin repeat region (SR4-7), which is common to all Kalirin isoforms (affinity purified JH2581; **Fig. 5-4A**). Bound and unbound fractions were subjected to Western blot analysis using the Sec14 antibody (CT302) or the new, Ex1C-peptide antibody (CT38). Consistent with previous findings, the Sec14 antibody detected all three of the major Kalirin isoforms in the soluble fraction, and Kal7 was enriched in the PSD fraction (**Fig. 5-4C**, Sec14). Remarkably, when the same bound fractions were blotted with the Ex1C-peptide antibody, a robust Kal7 band was observed in the PSD fraction, but crossreactivity was not detected in the soluble (S2) fraction (**Fig. 5-4C**, Ex1C). The lack of Ex1C-peptide-containing Kalirin in the soluble fraction suggests that its amphipathic helix may play a role in localizing the protein to the PSD.

Since the Ex1C-peptide localizes to the *trans*-Golgi network (TGN) in non-neuronal cells (Chapter 4), we further separated the S2 fraction into a cytosolic fraction (S3) and an endoplasmic reticulum (ER)/ Golgi-enriched fraction (P3); Kalirin immunoprecipitated from these fractions using the spectrin repeat antibody was analyzed in the same way. As expected, all three Kalirin isoforms were present in both the cytosolic and ER/ Golgi fractions (**Fig. 5-4D**). When the same samples were probed with the Ex1C-peptide antibody, we observed a clear Kal7 band in the ER/Golgi fraction, but none of the cytosolic Kalirin was detected by this antibody (**Fig. 5-4D**). These experiments suggest that the C-helix interacts with ER/Golgi membranes in neurons, as in non-neuronal cells.

In order to estimate the fraction of the Kal7 in the cytosol, ER/Golgi and PSD-enriched fractions accounted for by cKal7, a calibrator sample was used. An identical amount of lysate from HEK cells expressing cKal7 (as in **Fig. 5-4B**) was analyzed alongside immunoprecipitated Kalirin samples from

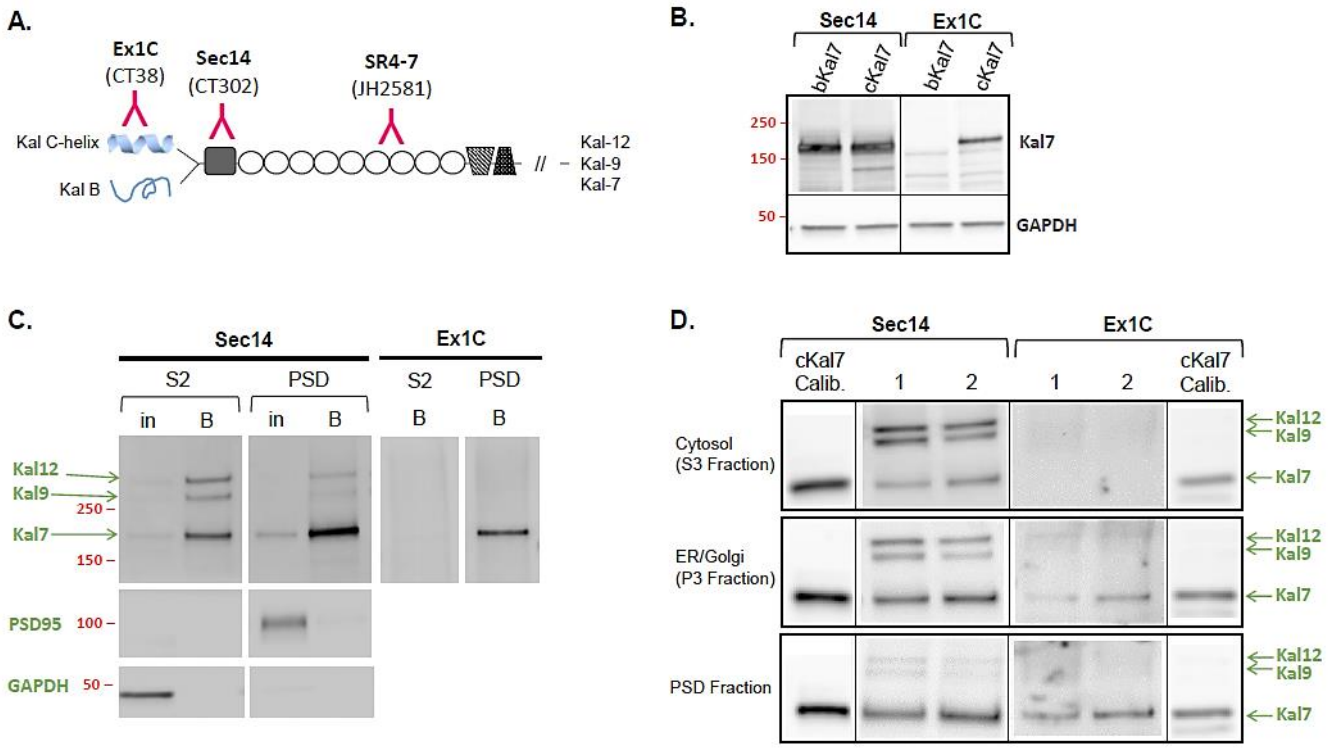

Figure 5-4. Subcellular localization of cKal7. **A.** Kal protein diagram showing epitope locations for the antibodies used: the SR4:7 and Sec14 antibodies recognize all full-length Kalirin isoforms; the Ex1C-peptide antibody only recognizes Kalirin isoforms resulting from the C-promoter. All antibodies were affinity-purified. **B.** Western blot of cell lysates from HEK cells expressing either bKal7 or cKal7. Samples were analyzed in duplicate and probed with the Sec14 antibody or the Ex1C-peptide antibody, as indicated. Molecular weights are indicated on the left; GAPDH is shown as a loading control. **C.** Western blots of immunoprecipitated samples from a representative experiment. Input (in) and bound (B) fractions are shown for using the Sec14 antibody to demonstrate immunoprecipitation efficiency (typically 80-90%). Molecular weights and Kalirin isoforms are indicated on the left. PSD95 and GAPDH bands are shown to demonstrate efficacy of the subcellular fractionation protocol. Separate aliquots of the same bound samples were visualized using the Ex1C-peptide antibody. **D.** Immunoprecipitated (bound) samples from cytosolic (S3) and ER/ Golgi Fractions. Identical samples were analyzed in duplicate and blotted for either Sec14 or Ex1C-peptide. **E.** cKal7 expressed in exogenously in pEAK cells was used as a Calibrator (Calib.); identical aliquots of immunoprecipitates prepared using the SR4:7 antibody were fractionated along with aliquot of the Calibrator samples and visualized with the Sec14 antibody or with the Ex1C-peptide antibody. Images were quantified using SynGene and the Sec14/Ex1C-peptide ratio for the Calibrator was used to estimate how much of the Kal7 was cKal7. Similar results were observed across 3 separate experiments.

each fraction (**Fig. 5-4D**); the calibrator sample and the immunoprecipitates were visualized together using antisera to the Sec14 domain or to the Ex1C-peptide. Using the ratio of the calibrator band intensities when blotted with the Sec14 domain antibody vs the Ex1C-peptide antibody (CT302/CT38 band density; typically between 2.3 and 2.8) we estimated that approximately 23-26% of the PSD-localized and ER/Golgi-localized Kal7 in the mouse forebrain was cKal7, with the amphipathic C-helix at its N-terminus. The remainder was presumably bKal7, with the unstructured Ex1-B peptide at its N-terminus. Given that our forebrain samples contained predominantly cortical tissue, these estimates were consistent with our qPCR data (**Fig. 5-2A**). Despite the fact that our long-range PCR data show C promoter usage among Kal9/12 transcripts, we were unable to reliably detect these higher molecular weight isoforms with this antibody. We never observed Ex1C peptide signal above background levels in S3 fractions.

Endogenous cKalirin localizes to dendritic spines

We next used the Kal Ex1C-peptide antibody to visualize cKal localization in cultured neurons using immunocytochemistry. Rat hippocampal neurons were transfected at plating with a farnesylated-GFP construct (fGFP), which targets the plasma membrane to enable easy visualization of dendritic spines. After 22 DIV, neurons were fixed and co-labeled with antibodies to the Ex1C-peptide (CT38, red), the vesicular glutamate transporter 1 (Vglut1, blue), and GFP (green). The vast majority of the Ex1C-peptide signal was apparent as punctate staining localized to the tips of dendritic spines and juxtaposed to Vglut1 puncta, which are indicative of presynaptic terminals (**Fig. 5-5**, yellow arrowheads). Ex1C-peptide staining was also observed in the soma (**Fig. 5-5**, white arrowheads in merged image), consistent with its ER/Golgi localization, as seen biochemically (**Fig. 5-4**).

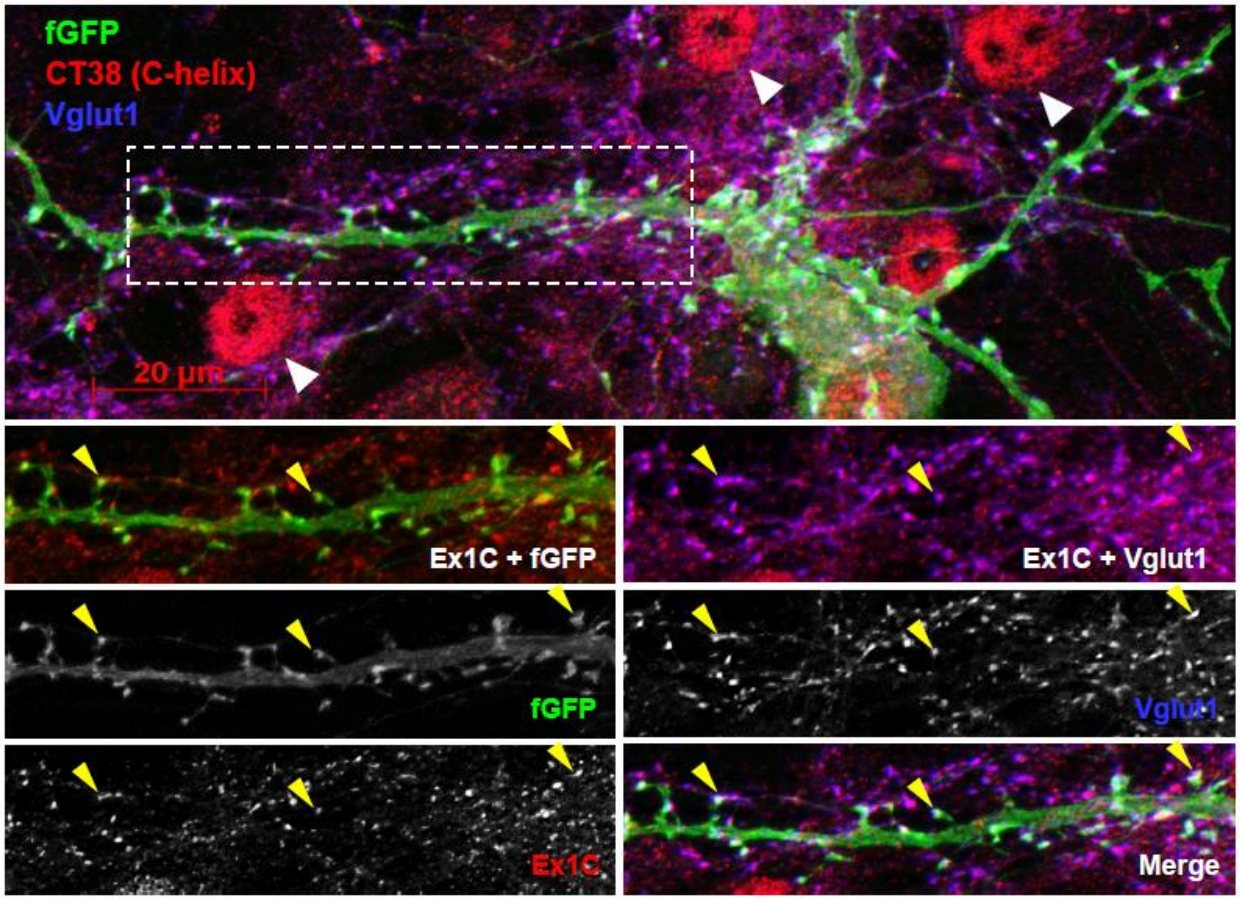

Figure 5-5. Localization of endogenous cKal by immunocytochemistry. Rat hippocampal neurons (22 DIV) expressing farnesylated-GFP (fGFP) were immunostained with antibodies to Ex1C-peptide (CT38, red), Vglut1 (blue) and GFP (green). The representative image shown is a compressed Z-stack taken with a 63X oil objective. Bottom images show single and double channels of the boxed area in the top image. The green and red merged image highlights Ex1C-peptide localization to the tips of dendritic spines. The red and blue merged image highlights Ex1C-peptide apposition to presynaptic terminals, visualized by Vglut1 staining. Individual channels are shown in grey scale, as indicated. Yellow arrowheads point to discrete spines; white arrowheads point to cell somas; Scale bar = 20µm.

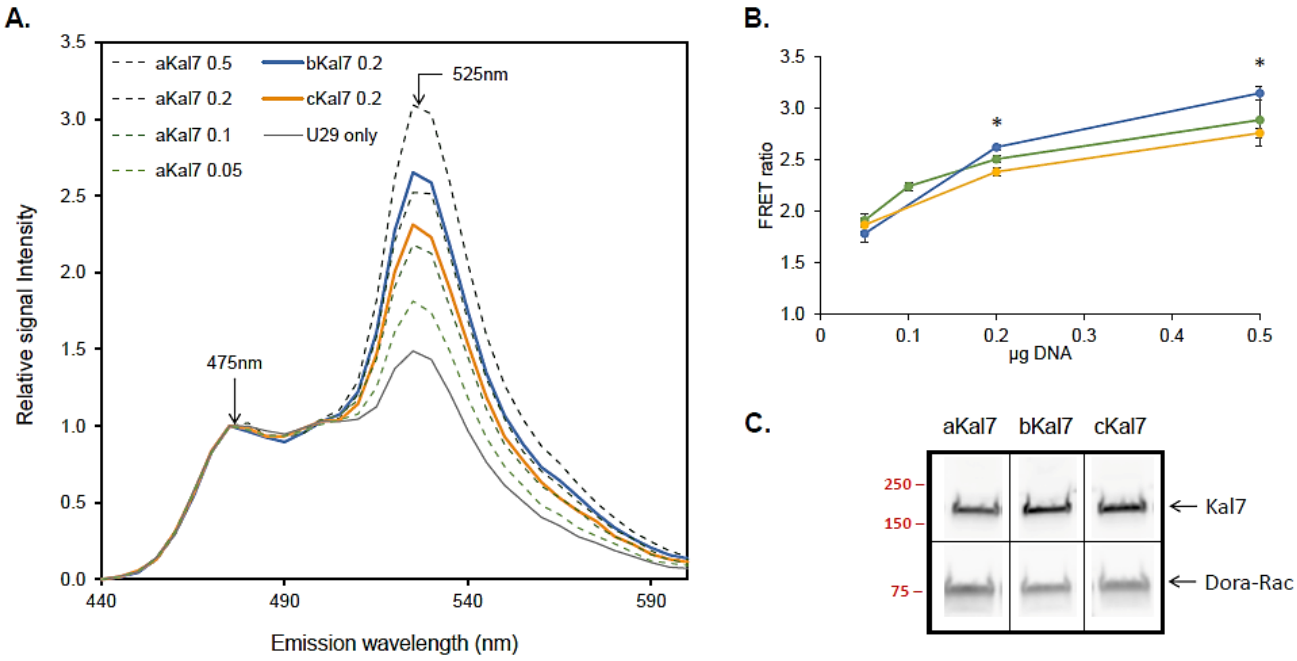

Figure 5-6. Differences in GEF activity by bKal7 and cKal7. **A.** Representative emission spectrum, with signal intensity normalized to that of the FRET donor emissions wavelength, 475nm. Curves are an average of two wells per condition. Grey line = biosensor only, with no exogenous GEF expression; hashed lines show aKal7 standard curve; data for the middle concentration (0.2µg DNA) of bKal7 (blue) and cKal7 (yellow) are shown. **B.** Bar graph showing group data as FRET ratios (252/475) over amount of transfected DNA for aKal7 (green), bKal7 (blue) and cKal7 (gold); n = 4 replicates from two experiments for each. * $p < 0.005$ for bKal7 vs cKal7. **C.** Western blot of cell lysates from a representative Rac1 activation assay showing equal expression of Kal7 isoforms (0.5µg DNA each) and Dora-Rac1 biosensor across groups.

Promoter usage affects Kal7 GEF activity

One of the major biological roles of Kal7 is to coordinate the cytoskeletal dynamics underlying structural growth, maintenance and plasticity in dendritic spines. Through its enzymatic GEF domain, Kal7 activates the small GTPase, Rac1, which promotes actin polymerization. We used a Rac1 biosensor (Dora-Rac1) in a cell-based Rac1 activation assay to evaluate the GEF activity of bKal7 and cKal7. We compared the activity of these isoforms to the activity of aKal7, the only isoform used in exogenous expression systems, until now. pEAK-Rapid cells (a HEK derivative) were transfected with vector encoding Dora-Rac1 and varying amounts of vector encoding each Kal7 isoform; carrier DNA was used to keep the total amount of DNA constant. The following day, emission spectra were recorded and FRET ratios were calculated by dividing the FRET acceptor emission peak (525nm, Venus) by the donor peak (475nm, Cerulean3; **Fig. 5-6A**). For all constructs, we observed an increase in Rac1 activation with increasing concentrations of Kal7 DNA (**Fig. 5-6A, B**). Interestingly, bKal7 induced nearly 7% more FRET than cKal7, on average. Since a two-fold increase in Kal7 expression results in a FRET ratio increase of approximately 15% (average of all constructs), this observation suggests that bKal7 is nearly 50% more active than cKal7.

bKal7 and cKal7 have different effects on postsynaptic structure

Given that Kal7 GEF activity is essential for normal synapse formation and maintenance, we wondered if bKal7 and cKal7 differed in their ability to promote synaptogenesis. To assess this issue, we expressed exogenous bKal7-GFP or cKal7-GFP in DIV15 rat hippocampal neurons; immature neurons were selected to mimic the time at which expression of Kal7 normally increases and expression from the *Kalrn* C-promoter is initiated (**Fig. 5-2**). As expected, both proteins localized primarily to postsynaptic sites, juxtaposed to the presynaptic marker Vglut1 (**Fig. 5-7**). Neurons transfected with soluble EGFP are shown for comparison. In order to determine whether bKal7 and cKal7 differed in their ability to localize to these immature spines, GFP signal intensity was quantified in spines and in dendrites and the ratio of

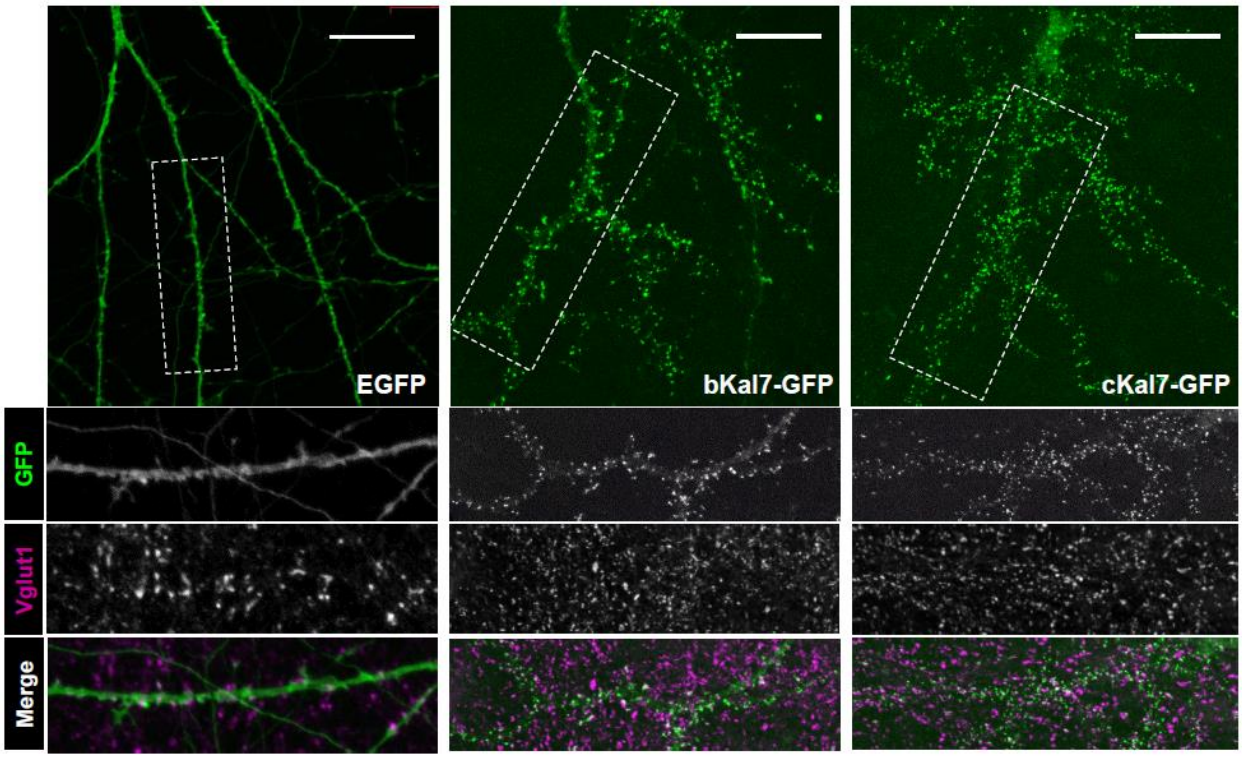

Figure 5-7. Exogenous expression of bKal7-GFP and cKal7-GFP in primary neuronal cultures. Rat hippocampal neurons were transfected with vector encoding either EGFP, bKal7-GFP or cKal7-GFP at 2DIV, then fixed and immunostained at 15DIV. Images are compressed Z-stacks of 3 focal planes at 63X magnification. In all cases, cell somas are located just above the pictured dendrites. Boxed areas are expanded below with Vglut1 signal shown. Green = GFP, purple = Vglut1, scale bars = 20µm.

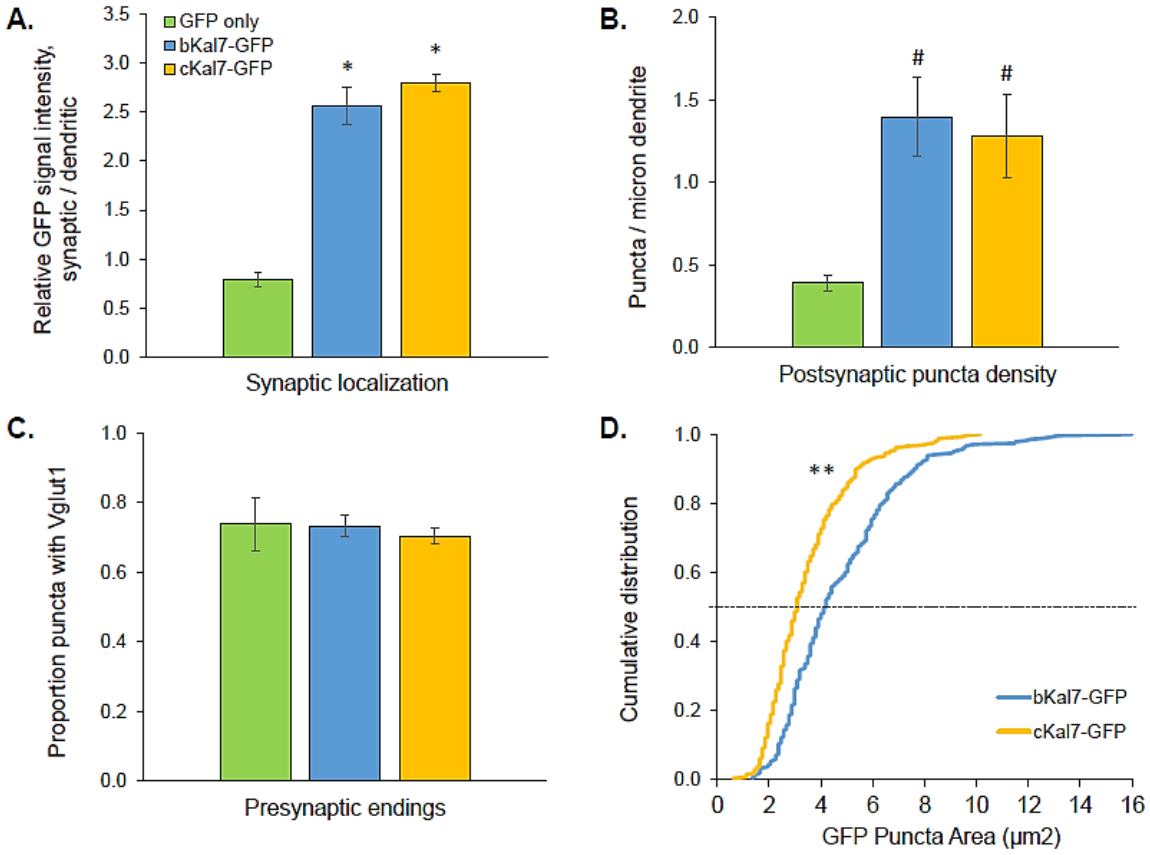

Figure 5-8. Quantification of EGFP, bKal7-GFP and cKal7-GFP localization. **A.** GFP signal intensity was measured with metamorph following manual identification of synaptic and dendritic areas. Intensity measurements from multiple areas (at least 5 discrete areas for dendrites and dozens for synapses) were averaged for each cell. The ratio of synaptic GFP signal intensity over dendritic shaft GFP signal intensity is displayed as a measure of synaptic localization. *$p < 0.005$ vs EGFP control. **B.** Linear density of postsynaptic sites was measured by counting GFP puncta (bKal7 and cKal7 conditions) or PSD95 staining (GFP control cells; not shown). Data are represented as puncta per micron of dendrite. $^{\#}p<0.01$ vs. EGFP control. **C.** Quantification showing the proportion of postsynaptic puncta (based on GFP or PSD staining, as in B) with an apposed presynaptic ending. **D.** Cumulative distribution plot of postsynaptic area obtained by measuring bKal7-GFP and cKal7-GFP puncta size (276 and 435 individual puncta, respectively); ** $p<0.005$ based on Kolmogorov-Smirnov test. For all panels, green bars = EGFP control, blue = bKal7, gold = cKal7; data resulted from analysis of at least two dendrites from each of 5, 7 and 9 cells for EGFP, bKal7-GFP and cKal7-GFP, respectively.

puncta/spine intensity to dendritic intensity was calculated (**Fig. 5-8A**). Higher ratios for bKal7-GFP and cKal7-GFP vs. GFP demonstrated their enrichment at synaptic sites.

Linear density of GFP-positive puncta along dendrites was similar in bKal7- and cKal7-expressing neurons, and both isoforms of Kal7 caused a robust increase in the number of puncta compared with the EGFP control (**Fig. 5-8B**). Increases of similar magnitude have been shown previously following expression of exogenous myc-tagged aKal7 (myc-aKal7) (96,251). The process by which filopodia mature into mature spines with a PSD apposed to a functional presynaptic ending involves many steps. We did not observe any difference across groups in the number of GFP-positive puncta apposed to Vglut1-positive puncta (**Fig. 5-8C**), indicating that bKal7 and cKal7 are equally able to attract presynaptic endings. In addition to synapse number, the size and shape of synaptic contacts bear functional significance. Interestingly, we found that the cKal7-GFP positive puncta were significantly smaller than those produced by bKal7-GFP (**Fig. 5-8D**). This result is consistent with the idea that cKal7 is a less active GEF than bKal7 (**Fig. 5-6**).

The Ex1C peptide promotes glutamate receptor endocytosis and spine shrinkage.

bKal7 and cKal7 share >98% sequence homology, differing only in their small, N-terminal peptides, and yet we have provided clear evidence for functional divergence. It stands to reason that the initial peptides themselves may engage in physiologically significant interactions which contribute to the function of full-length Kal7. Our biochemical characterization (See Chapter 4) of the initial peptides revealed that the Ex1C encodes an amphipathic helix which directly interacts with phosphoinositide-4-phosphate [PI(4)P] and enhances membrane interactions by the Sec14 domain. Conversely, Ex1B encodes a charged and unstructured peptide, which does not interact with membranes. Furthermore, cSec14-GFP, but not bSec14-GFP, localizes to the trans-Golgi network (TGN) in cultured AtT-20 cells, and this interaction can be disrupted by treating cells with a cell-permeant Ex1C peptide (Kal C-helix-

Arg9; Chapter 4). We utilized the same cell-permeant peptide to determine acute effects of the Kal Ex1C-encoded amphipathic helix on neuronal structure and function.

The phosphoinositides (PIPs), including PI(4)P, are crucial mediators of membrane and receptor trafficking in all cells. For this reason, we wondered if the Ex1C peptide interacted with postsynaptic membrane trafficking machinery. We treated 25DIV rat hippocampal neurons for 20 minutes with 5μM of cell-permeant Ex1C peptide (Kal C-helix-Arg9). Parallel cultures were treated with a control peptide, in which four of the hydrophobic residues were replaced with charged residues (WWWY→KKED; C-helix$_{KKED}$-Arg9). The mutant peptide still forms an α-helix, but it is no longer amphipathic in nature and does not interact with PI(4)P (Chapter 4). After treatment, cultures were rinsed in ice cold artificial cerebrospinal fluid (ACSF) and surface receptors were cross-linked with BS^3, as done previously (33,301). Cells were homogenized in 1% SDS and lysates were separated by SDS-PAGE. After immunoblotting, cross-linked receptors appeared as high molecular weight complexes, which were absent in lanes containing control samples for which BS^3 was not added (**Fig. 5-9**). Signal which appeared as a single band at the expected molecular weight was considered internalized receptor. Percent surface expression was calculated by dividing the high molecular weight signal by the total (internal + cross-linked). We observed a significant decrease in surface expression of the GluR2 AMPA receptor subunit in cultures treated with Kal C-helix-Arg9 compared with those treated with the control peptide or vehicle (DMSO) only (**Fig. 5-9B, D**). We saw the same trend for the GluR1 subunit, but data from four samples did not reach statistical significance (**Fig. 5-9A, D**). These data indicate that the Ex1C peptide promotes AMPAR internalization in cultured hippocampal neurons. The same treatment did not have a significant effect on surface expression of GluN1, an NMDA receptor subunit, but BS^3 crosslinking of this receptor was not as robust (**Fig. 5-9C, D**). We were unable to attain quantifiable GluN2B crosslinking using this protocol.

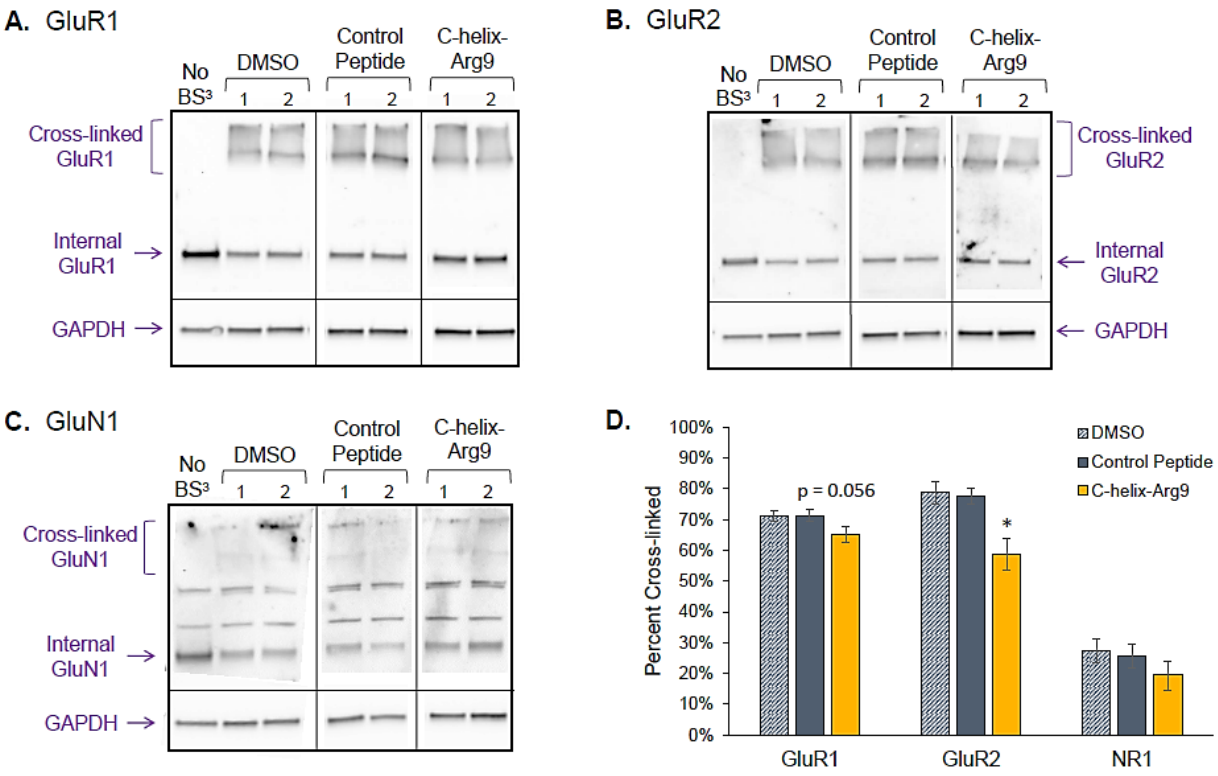

Figure 5-9. Glutamate receptor surface expression. **A.** Western blot of cross-linked lysates from 25DIV neuronal cultures showing cross-linked and internal GluR1. Duplicate samples are run for each condition. As expected, we did not observe high molecular weight signal in the "No BS3" lane. **B.** and **C.** show the same samples evaluated for GluR2 and GluN1, respectively. **D.** Quantification of receptor surface expression as percent cross-linked over total signal. * $p < 0.01$ vs control peptide.

We next evaluated the effect of C-helix-Arg9 treatment on dendritic spine number and morphology. Rat hippocampal neurons were transfected at plating with farnesylated GFP (fGFP) and grown in culture for 17 days. Cultures were treated for 20 minutes with 5μM of either Kal C-helix-Arg9 or control (C-helix$_{KKED}$-Arg9) peptide. Neurons were then fixed, stained and analyzed for changes in dendritic spine number and morphology (**Fig. 5-10**). Compared with the control group, we observed a small but significant reduction in dendritic spine length following treatment with Kal C-helix-Arg9 **[Fig. 5-10C**; 1.74μm (C-helix) vs 1.88μm (control) at 50%; 2.43 vs 2.69 at 85%]. Linear spine density, however, did not differ with treatment (**Fig. 5-10D**). Control-treated cultures never differed significantly from untreated cultures (not shown). Together, these experiments suggest that the Ex1C peptide present in cKal7 promotes AMPAR internalization and spine shrinkage in cultured neurons.

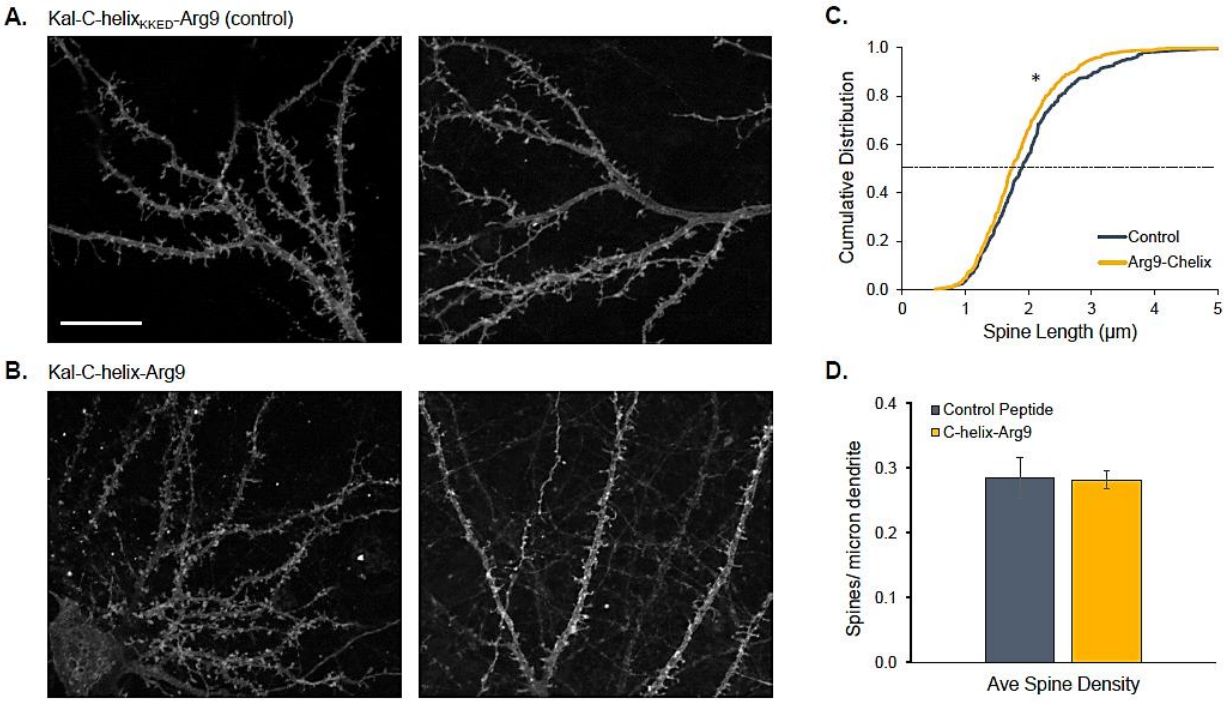

Figure 5-10. Kal C-helix peptide treatment affects spine morphology. **A.** and **B.** Representative images of 17DIV rat hippocampal neurons treated with cell-permeant control (panel **A**, C-helix$_{KKED}$-Arg9) or Kal Ex1C peptide (panel **B**, C-helix-Arg9). Neurons were transfected at plating with fGFP and immunostained with a GFP antibody to enable easy morphological analysis (shown in grey scale). Duplicate images for each group are shown; scale bar = 20µm and applies to all images. **C.** Cumulative distribution plot of dendritic spine length for control and C-helix-Arg9 treated neurons. * $p < 0.5$ via Klomogorov-Smirnov; $n > 415$ spines from 10-12 neurons. **D.** Linear spine density for each group given in average spines per micron dendrite.

Discussion

Alternate promoters

By multiple accounts, alternative promoter usage serves as a major source of genetic and proteomic diversity, rivaling that of alternative splicing (302,303). The most recent estimates suggest that nearly half of all protein-coding genes in the human genome have multiple promoter sequences (304,305) and that many of them are conserved in the mouse genome (306). We demonstrate here that alternate promoters add to the diversity of *Kalrn* transcripts in a developmentally-regulated and region-specific manner. For some genes, differential promoter usage results in alternate 5' untranslated regions (UTRs) with no change in the protein coding region. Other genes utilize alternate promoters in a manner similar to *Kalrn*. The protocadherin (*Pcdh*) genes, which encode a family of cell surface proteins expressed in the brain, each have more than a dozen alternative initiation exons which splice to a common C-terminus (307). Interestingly, *Pcdh* promoter choice affects 3' alternative splicing of the gene and isoforms are differentially expressed in different cell types (307). Although our long-range PCR experiments show that the two major Kalirin promoters (Ex1B and Ex1C) are used for both Kal7 and Kal9/12, we have not been able to visualize Kal9/12 protein using the Ex1C peptide antibody. Thus, while mRNA transcript from Ex1C→Kal9/12 was observed, we cannot rule out the possibility that Ex1C is more commonly expressed with Kal7.

Given the frequency of alternate promoters in the human genome, it is not surprising that aberrant promoter usage has been associated with many disease conditions, both within and outside of the nervous system (302,305). In fact, several studies suggest that genes with alternate promoters are more likely to be associated with disease (305,308). Brain derived neurotrophic factor (BDNF) utilizes multiple promoters in a tissue-specific manner, and promoter usage is altered in the rat brain after kainic acid induced seizures (309). A single nucleotide polymorphism (SNP) in the promoter region of the 5-HT2A serotonin receptor affects promoter activity and is associated with multiple psychiatric disorders (310).

Interestingly, genetic linkage studies have identified several SNPs within the promoter region of *KALRN*. Two SNPs, one just upstream from Ex1B (rs12637456) and another between Ex1B and Ex1C (rs9289231) are associated with coronary artery disease (93,311,312). Three SNPs, one in the promoter region (rs17286604) and two located just after exon 3 (rs11712039 and rs11712619) have been identified as risk factors for ischemic stroke (55,57). Whether these SNPs alter *KALRN* promoter usage and isoform expression will be of interest in future studies.

Identification of two sub-populations of Kal7

bKal7 and cKal7 differ only in their N-terminal 25-26 amino acids, yet our data indicate substantial functional significance for the different isoforms. Biochemical and histological experiments revealed that both bKal7 and cKal7 localize to dendritic spines, suggesting the presence of two sub-populations of Kal7 within these compartments. This notion is consistent with the results from a study utilizing serial section electron microscopy and immunogold labeling to visualize Kal7 localization within dendritic spines (313). The authors identified Kal7 particles in both synaptic (closely associated with the PSD) and extrasynaptic microdomains, which differentially contributed to PSD size and spine volume. While synaptically-localized Kal7 was only weakly correlated, the number of extrasynaptic Kal7 particles was strongly correlated with increased PSD area and increased spine volume (313). Providing a potential mechanism for these observations, our data suggest that bKal7 is more cytosolic (i.e. not restricted to the PSD) than cKal7, which is found only in the PSD or with membranes. Since the dynamic actin pools underlying structural plasticity are mostly extrasynaptic (314,315), this model would suggest that bKal7 is more suited to affect cytoskeletal dynamics within spines. Indeed, our data show that bKal7 has significantly higher GEF activity and forms larger spines than cKal7 when exogenously expressed. Collectively, our data suggest bKal7 may play a greater role in modulating actin rearrangements within dendritic spines.

Notably, until now, every study employing exogenous expression of Kalirin has utilized aKal7, although promoter A is rarely used in the rodent brain. Given that our data reveal clear promoter-specific effects on Kal7 localization and function, a switch to Ex1B and/or Ex1C-driven Kalirin expression would be prudent.

A novel link between actin dynamics and membrane trafficking

In addition to cytoskeletal demands, the expression of structural and functional synaptic plasticity requires on-demand trafficking of membrane proteins and lipids to and from the surface (2,316), a process which itself requires actin. Despite this fact, the mechanisms by which actin dynamics and membrane trafficking are coordinated within spines remain enigmatic. The results of this study suggest that cKal7 may play a role in integrating these processes. Membrane interactions mediated by the Sec14 domain of Kalirin are enhanced by inclusion of the amphipathic Ex1C-helix, which directly binds to PI(4)P and possibly other phosphoinositides (PIPs) (Chapter 4). PIPs are a class of highly regulated membrane lipids which play crucial roles in cellular trafficking (272,273). Though much remains to be understood about their roles at the PSD, their importance for postsynaptic function is clear. NMDA receptor stimulation causes phosphatidylinositol-(3,4,5)-trisphosphate (PIP_3) accumulation in the plasma membrane (317), where it aids in AMPA receptor stabilization (318). The role of PI(4,5)P_2 in modulating ion channel function is well-documented (290), and metabolism of this lipid by the lipid phosphatase, synaptojanin 1, is required for proper AMPA receptor internalization (319). Furthermore, aberrant phosphoinositide metabolism is implicated in Autism and Down's Syndrome pathology (320-322). Though little is known about its specific roles in spines, PI(4)P is an obligate precursor to all other PIP species, and its function is crucial for post-Golgi trafficking.

Our experiments with a cell-permeant peptide revealed that acute exposure to the amphipathic Ex1C-helix (Kal-C-helix-Arg9) resulted in a net increase in AMPAR internalization, which was associated with decreased spine length. Importantly, a control peptide which does not interact with PIPs

did not have the same effect. The specific mechanism for these effects is not yet clear. One possibility is that the peptide disrupts neuronal PIP metabolism. An alternative explanation is that C-helix-Arg9 interferes with endogenous cKal7 interactions at the synapse. The later interpretation is supported by our observation that C-helix-Arg9 treatment disrupts cSec14-GFP localization in AtT20 cells (Chapter 4). In either case, it is clear that the amphipathic helix encoded by Kal Ex1C is biologically relevant and further studies aimed at elucidating its role in postsynaptic membrane trafficking are warranted.

Acknowledgements

We thank Darlene D'Amato her enormous laboratory support and help with the molecular biology. This work was supported by a grant from the National Institutes of Health, DK-032948.

Author Contributions

M.B.M. conducted most of the experiments

Y. Wang conducted the long-range PCR

T.L. contributed to image quantification/analysis

Y. Wu designed the Dora-Rac1 biosensor and provided extensive technical advice

B.A.E. developed the Kal-C-Helix antibody and the cell permeant peptides

R.E.M. developed expression vectors, long-range PCR protocols and analyzed promoter information

M.B.M., R.E.M. and B.A.E. jointly designed experiments and wrote the manuscript

Chapter 6

Kalirin-7 phosphorylation is tissue-specific and responsive to cocaine

Megan B. Miller, Yan Yan, Drew D. Kiraly, Thomas Abbott, Tukiet T. Lam,

Chris Colangelo, Betty A. Eipper, Richard E. Mains

Abstract

Kalirin-7 (Kal7) is a synaptic RhoGEF with crucial roles in postsynaptic signaling and implications in addiction, schizophrenia and other disorders characterized by synaptic dysfunction. Previous work has demonstrated that Kal7 is highly phosphorylated, suggesting its involvement in multiple signaling pathways and revealing a likely mechanism for its regulation. Here, we use quantitative mass spectrometry (SWATH) to evaluate potential changes in Kal7 phosphorylation in the rat brain in response to cocaine exposure. Adult male rats were treated either acutely or chronically with saline or cocaine, and Kal7 phosphorylation status was evaluated in the nucleus accumbens (NAc) and prefrontal cortex (PFC). We found that Kal7 phosphorylation is differentially regulated by treatment and brain region. In total, 26 phosphorylation sites were identified across the entire molecule, including 5 tyrosine residues. 10 of the sites were highly phosphorylated (50% or higher) in one or both brain regions. At baseline, 25 of 26 residues were phosphorylated in both the NAc and the PFC, but phosphorylation levels differed between the regions at 12/26 sites. Overall, phosphorylation levels were higher in the PFC than in NAc. Cocaine altered phosphorylation levels at 4 sites in the NAc, all of which were clustered around the GEF domain. In the PFC, cocaine induced changes in phosphorylation levels at 5 sites, most of which were clustered toward the N-terminus. The exception was Tyr1342, which is located in the GEF domain and was the only residue regulated by cocaine in both the NAc and PFC.

Expanding upon previous work, our findings suggest that Kal7 is phospho-regulated in a region- and experience-dependent manner.

Introduction

Drugs of abuse hijack the brain's normal reward circuitry and chronic use frequently results in addiction, a pathological condition resulting from long-lasting synaptic and molecular changes. Principally driven by dopamine (DA), the reward pathway is a highly complex system, involving multiple cell types in multiple brain regions (323). Dopamine neurons in the ventral tegmental area (VTA) project to GABAergic medium spiny neurons (MSNs) in the nucleus accumbens (NAc), which provide inhibitory feedback to the VTA. Glutamatergic neurons in the prefrontal cortex (PFC) innervate the NAc and also engage in bi-directional communication with VTA DA neurons.

Cocaine, a psychomotor stimulant and potent inhibitor of DA reuptake, is one of the most commonly used illicit drugs. While physiological and behavioral responses to acute cocaine are likely mediated mostly by hyperactivity of mesolimbic and mesocortical DA release, it is clear that glutamatergic transmission from the PFC is a major player in the addictive behaviors that follow repeated exposure to cocaine. Prolonged cocaine exposure results in strengthening of glutamatergic inputs to the NAc, which are required for normal acquisition of sensitization and drug seeking behaviors (323-325). In fact, addiction is now widely considered to be a form of sub-cortical learning, with underlying mechanisms akin to better studied forms of plasticity, like hippocampal LTP and LTD (326-328). As such, glutamate receptors, protein kinases and other crucial components of excitatory synapses have emerged as crucial players in addiction pathology.

Kalirin-7 (Kal7) is a multi-functional guanine nucleotide exchange factor (GEF) for Rac1 and RhoG, Rho family small GTP binding proteins, and has been identified as a postsynaptic signaling hub due to its involvement in many synaptic signaling pathways. Kal7 localizes to the postsynaptic density of excitatory synapses, where it plays a crucial role in dendritic spine formation and plasticity (36,51). Kal7

activity is required for proper signaling through ligand gated ion channels (e.g., NMDA and AMPA receptors), receptor tyrosine kinases (e.g., EphB, PDGFR), G protein coupled receptors (e.g., 5-HT2A) and adhesion proteins (e.g., N-cadherin) (41,42,44,46). Developmentally, Kal7 expression begins postnatally, around the time of synaptogenesis, and Kal7 becomes the major *Kalrn* isoform in the adult brain (248). Expression is highest in pyramidal neurons of the cortex and hippocampus, with significant levels also observed in medium spiny neurons (MSNs) of the striatum and nucleus accumbens (39,94). Consistent with its role in dendritic spine morphology, Kal7 expression is elevated in the nucleus accumbens following chronic cocaine exposure, and cocaine-induced increases in MSN spine density require Kal7 (51). $Kal7^{KO}$ mice display increased locomotor sensitization and impaired place preference following chronic cocaine administration (51). In a self-administration paradigm, $Kal7^{KO}$ animals display higher rates of self-administration than controls (294). Furthermore, in withdrawn rats, normal increases in AMPA receptor surface expression and spine density are ameliorated when Kalirin is knocked down (45).

Further attesting to its role as a signaling hub, Kal7 is phosphorylated by multiple PSD-localized kinases. Using mass spectrometry to directly measure phosphorylation, we previously identified 22 unique phosphorylation sites in Kal7 from the mouse brain (49). Here, we used mass spectrometry and quantitative SWATH data analysis to identify changes in Kal7 phosphorylation in the PFC and NAc following acute and chronic cocaine administration.

Methods

Animal Treatment

Adult male Sprague Dawley rats purchased from Charles River and allowed to acclimate for one week were split into three groups of six or seven. Animals were weighed (average 260 $\pm$ 5 gm) and each animal received an intraperitoneal injection every day for the next seven days; immediately after each

injection, animals were placed singly into clean cages without food, water or bedding (with orange scent), where they remained for 45 minutes before being returned to their home cage. Animals in the Saline group received 1.0 ml saline each day. Cocaine was dissolved in phosphate buffered saline (4 mg/ml). Animals in the Acute Cocaine group received six daily injections of saline; on Day 7 they received a single 20 mg/kg injection of cocaine and were sacrificed 30 minutes later. Animals in the Chronic Cocaine group received seven daily injections of 20 mg/kg cocaine and were sacrificed 30min after the final injection.

Tissue (prefrontal cortex and nucleus accumbens) was harvested from coronal sections using a tissue punch, weighed, sonicated in 10 volumes of SDS-P lysis buffer (50 mM Tris, 1% SDS, 130 mM NaCl, 10 mM Na pyrophosphate, 50 mM NaF, 5 mM EDTA, pH 7.6) containing 1 mM PMSF, 1 mM orthovanadate and one PhosSTOP tablet (Roche)/10ml and heated at 95C for 5 min. Samples were then centrifuged at 14,000 x g for 15 minutes; supernatants were transferred to new tubes, aliquots were taken for protein determination and stored at -80C. Protein concentration was determined using the bicinchoninic acid assay (Pierce) with bovine serum albumin as a standard and ranged from 7 to 10 mg/ml.

Immunoprecipitation

Immunoprecipitation was carried out with slight modifications of the protocol described previously (49) using affinity-purified antibody to the Sec14 domain of Kalirin (248). For each sample, 0.8 volumes of 10% NP-40 (Pierce, SurfActs) treated with orthovanadate and PhosSTOP was added to an aliquot containing 2 mg protein; samples were allowed to tumble in the cold room for 20 min and then centrifuged at 4C for 15 min at 14,000 x g to remove any insoluble material. Supernatants were then further diluted with 3.5 volumes TM-P (20 mM Na TES, 10 mM mannitol, 5 mM EDTA, 50 mM NaF, 10 mM Na pyrophosphate, pH 7.4) containing 1 mM orthovanadate, 1 tablet PhosSTOP/10 ml and Calbiochem Phosphatase Inhibitor Cocktail I. Each sample then tumbled overnight at 4C with ~3 □g

affinity-purified CT302 antibody and 10 □l Protein A beads that had been washed with TM-P-IPT buffer (TM-P buffer containing 1% TX-100). Beads were pelleted and washed twice with TM-P-IPT buffer and once with TM-P buffer. Bound protein was eluted by boiling the beads in Laemmli sample buffer treated with orthovanadate and Calbiochem Phosphatase Inhibitor Cocktail I. Samples fractionated on 10-lane BioRad 4-15% gels were visualized using the Pierce SilverSNAP kit; each band of Kal7 was excised and frozen until processing for mass spectroscopic analysis. Simultaneous analysis of 50, 100 and 200 ng bovine serum albumin confirmed the recovery of about 200 ng (1 pmol) Kal7 from 2 mg total protein (0.01% total protein).

Identification and quantitative analysis of phosphorylation sites

Immunopurified Kal7 samples were cleaved using in-gel tryptic digestion (V51111; Promega, Madison WI) and subjected to information-dependent acquisition and SWATH acquisition, as described (248). Skyline (329) was employed for precursor ion quantitation using SWATH data for the various phosphorylation sites (248). The approach to estimating the extent of phosphorylation at each site was the method described by Baucum et al (330), bearing in mind the cautions about absolute values due to ionization efficiencies (330). Depending on the peptide, various modifications were identified, most notably cysteine and methionine oxidation and variable tryptic cleavage. Modifications were verified by manual inspection of the raw mass spectra for every phosphorylation site. The area under the curve for the m, m+1 and m+2 ions were calculated for each sample for all variants of each phosphorylated peptide (with all Cys, Met and tryptic variations included), and the ratio (phosphorylated/[phosphorylated + nonphosphorylated]) was calculated for the m, m+1 and m+2 ions for each sample. The data are expressed as the ratio of phosphorylated/total recovered peptide and statistical analyses were performed using a one-way ANOVA (SigmaPlot), as in (330). Sites are numbered using AF230644_1 for rat cKal7.

Results

Adult male Sprague-Dawley rats were subjected to one of three treatment paradigms: Saline, Acute Cocaine and Chronic Cocaine (**Fig. 6-1A**). Animals were sacrificed 30 minutes after the final injection, and tissue from the prefrontal cortex (PFC) and nucleus accumbens (NAc) was homogenized in buffer containing multiple phosphatase inhibitors. Kalirin was then isolated from homogenates by immunoprecipitation and SDS-PAGE (**Fig. 6-1B,C**). Kal7 bands were carefully cut from the gel and processed for analysis by mass spectrophotometry.

Using information-dependent, SWATH acquisition, we identified a total of 26 phosphorylated residues in Kal7 isolated from the rat brain (**Fig. 6-2, Table 6-S1**). Figure 6-3 shows examples of how potentially ambiguous sites of phosphorylation were resolved by further fragmentation of each peptide. For example, the peptide containing T79 was initially identified as that peptide with [+80] in M/z, indicating phosphorylation. Then the y9-y12 ions demonstrated that the Tyrosine and Serine residues were not phosphorylated (no [+80]), and the b3 and b4 ions demonstrated that T79 was unambiguously phosphorylated in about 75% of the recovered peptides from both the NAC and the PFC. The pattern for S271,S276 was more complex, since some peptides had a y5 ion [+80] (indicating that S276 was phosphorylated) and some did not; some peptides gave a y8 ion without a phosphate, indicating that S271 was phosphorylated.

Phosphorylation sites were identified across the molecule, occurring in the Sec14 domain, the spectrin repeat region, the GEF domain and the PDZ motif. All but one site (Tyr616) was identified in both the PFC and NAc. Interestingly, tyrosine phosphorylation was far more common in Kalirin (5/26 sites) than is typical of the average phosphoprotein, in which phosphotyrosine accounts for only 2% of the phosphorylated residues (331-333). Fourteen of the 26 sites reported here were previously identified in the mouse brain, and an additional two sites were identified in MycHisKal7(a) expressed transiently in HEK cells or using *in vitro* kinase assays [(49) **Table 6-1**]. The remaining 10 sites are new to this study.

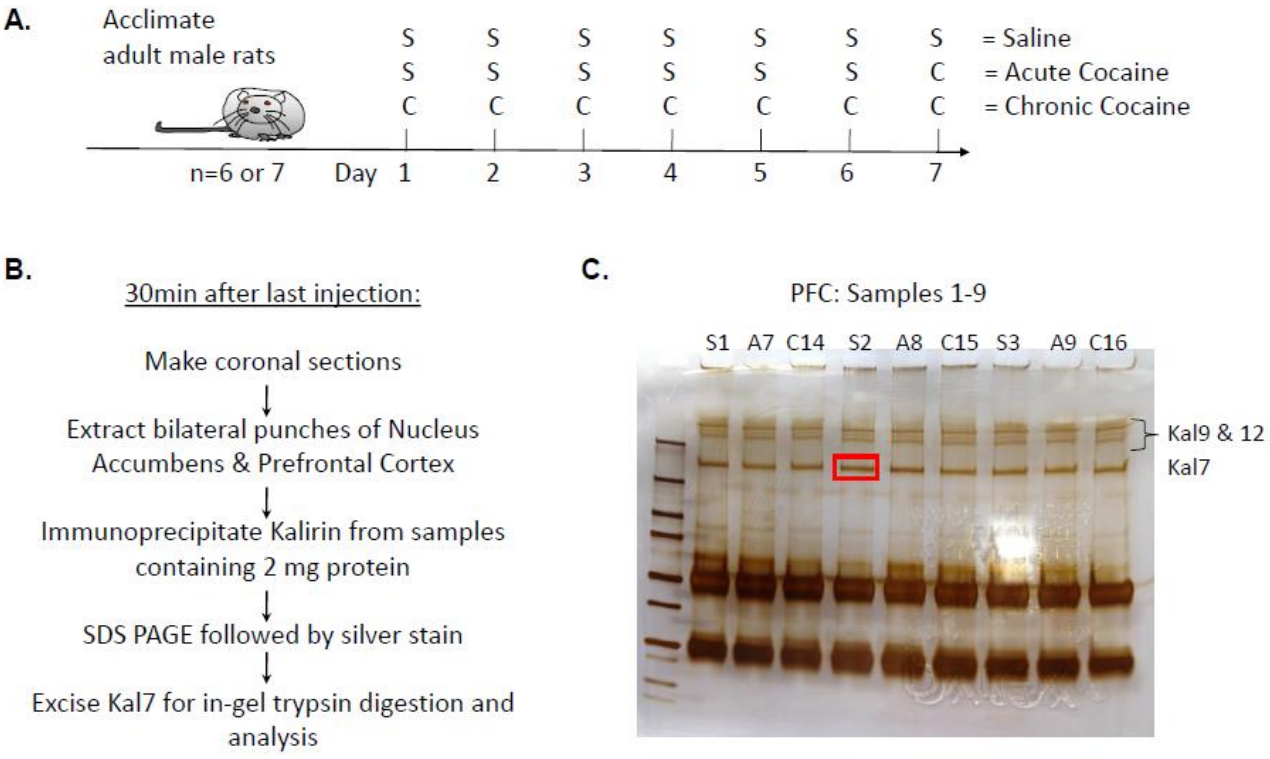

Figure 6-1. Cocaine paradigm and sample preparation. **A.** After acclimation, adult male rats were subjected to one of three treatment paradigms, as indicated. The saline group received 7 consecutive injections of saline, the chronic group received 7 consecutive injections of cocaine (20mg/kg), and the acute group received 6 saline injections, followed by a single dose of cocaine (20mg/kg) on day 7. Animals were sacrificed 30 minutes after the final injection. **B.** Prefrontal cortex (PFC) and nucleus accumbens (NAc) tissue was harvested by taking bilateral punches from coronal sections. Samples containing 2mg of total protein were then subjected to immunoprecipitation with a Kalirin antibody which recognizes the Sec14 domain (affinity purified CT302), and precipitates were separated by SDS PAGE. **C.** Protein bands were visualized by silver staining; Kal7, Kal9 and Kal12 bands are indicated. Kal7 was carefully excised from the gel and processed.

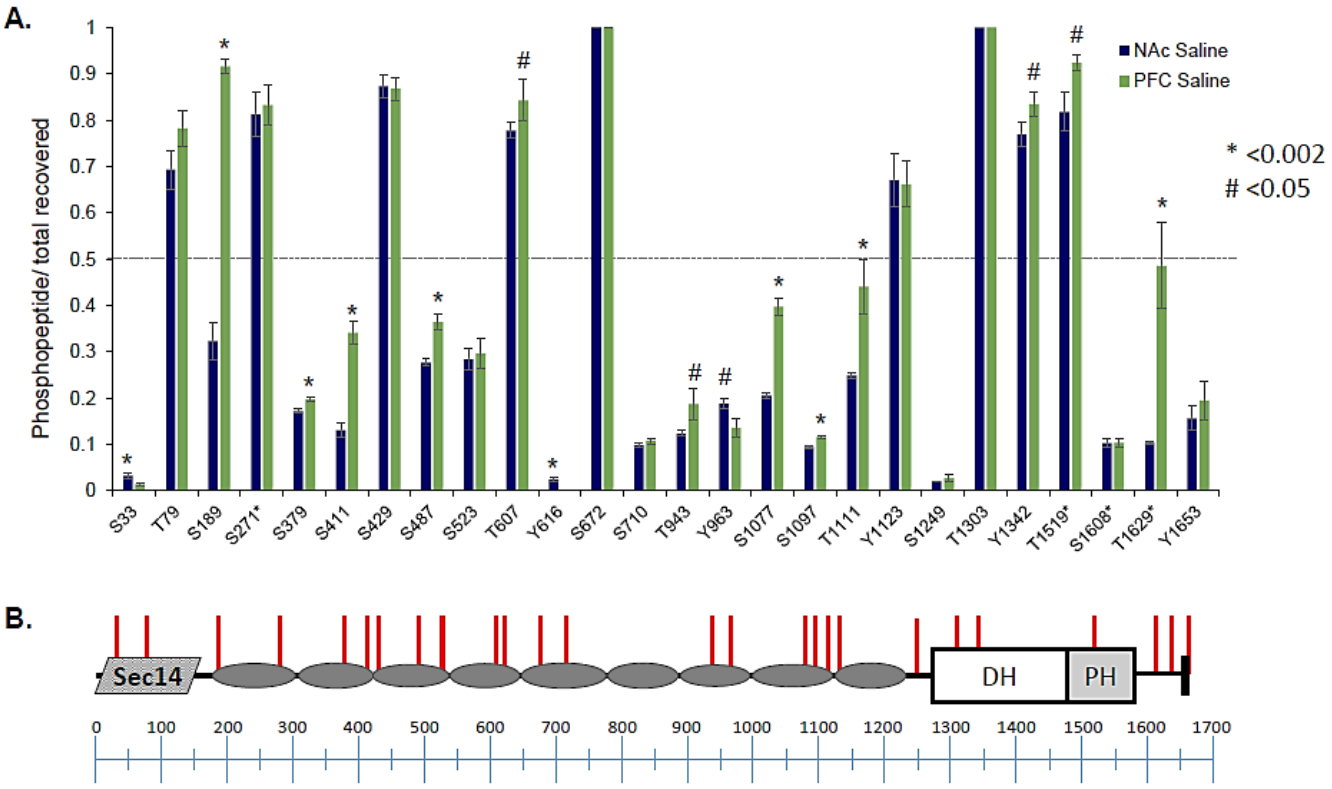

Figure 6-2. Identification of 26 phosphorylation sites in Kal7 from rat brain. **A.** Bar graph showing degree of baseline (saline) phosphorylation of each site relative to the total amount of peptide recovered. Blue and green bars show phosphorylation in the nucleus accumbens (NAc) and prefrontal cortex (PFC), respectively. Residues are indicated on the X axis; asterisks indicate indefinite residue number, as explained in the Figure 6-2 legend. The grey dashed line indicates 50% phosphorylation. Sites that are significantly different across brain regions are indicated above the bars by # ($p < 0.05$) or * ($p < 0.002$). **B.** A diagram of the Kal7 protein indicating the location of each phosphorylation site (red hashes). Residue numbers (from 0- 1,700) are indicated by the scale bar below. Protein domains starting from the N-terminus: Sec14, spectrin repeats 1-9 (grey ovals), Dbl and plextrin homology domains (DH/ PH = GEF), and a PDZ binding motif (black box), which is separated from the GEF domain by a short, unstructured linker region. Sites are numbered using AF230644_1 for rat cKal7.

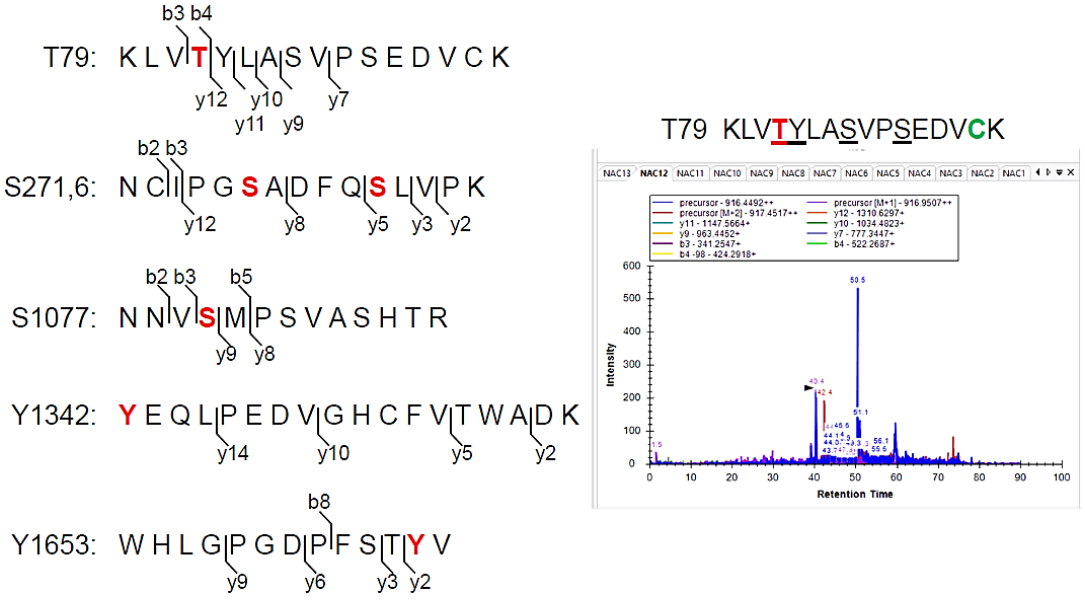

Figure 6-3. Identifying phosphorylation sites with *b* and *y* ions. **Left**, several examples of the b- and y-ions used to determine which potential phosphorylation site is used, in a tryptic peptide with a single phosphorylation (mass [+80]). As discussed in the text, all but S271/S276 are unambiguously identified by the b- and/or y-ions. Four tryptic peptides in Kal7contain more than one potential site of phosphorylation which was not resolved by the additional fragmentation, and one example of the ambiguity is shown here and discussed in the text. **Right**, the Skyline output for one of the T79 tryptic peptides from the NAc12 sample.

Highly phosphorylated residues

For nine of the observed sites, greater than 50% of the recovered peptides were phosphorylated in both tissues, and one site (Ser189) was greater than 50% phosphorylated in the PFC only (**Figs. 6-2 & 6-4, Table 6-1**). These highly phosphorylated residues cover the entire molecule, with representation in all regions except the very C-terminus. Notably, all of the recovered peptides containing Ser672 and Thr1303 were phosphorylated, suggesting that phosphorylation of these residues may be crucial for Kal7 function. Furthermore, all three of the sites located within the enzymatic region (Thr1303, Y1342 and T1519; **Fig. 6-4**) were highly phosphorylated, raising the possibility that GEF phosphorylation plays a major role in regulating enzymatic activity, as has been shown for many other GEFs (334-337). Additional sites of interest are Thr79 and Tyr1123. Thr79 is targeted by multiple PSD-localized kinases, including CaMKII, PKA, PKC and CKII, and was also identified in the mouse brain (49). Located in the Sec14 domain, Thr79 is situated just outside of the putative lipid binding pocket, and a phosphomimetic mutation of this residue (T→E) enhanced Sec14-mediated phosphoinositide binding (251). One of five tyrosine sites identified, Tyr1123 is located in SR8 (**Fig. 6-4**). Recent work from our lab has identified this site as a target of the receptor tyrosine kinase, TrkB, the major receptor for brain derived neurotropic factor (BDNF) (Yan Y. et al., 2015, in revision). The four remaining highly phosphorylated sites (Ser189, Ser271*, Ser429, Thr607) are located within the first four spectrin repeats, a region known to be crucial for the postsynaptic localization of Kal7 as well as for Kal7-mediated spine formation (251).

Highly phosphorylated residues

Site	Domain	% Phos.	Functional notes
T79	Sec14	70-80%	Affects lipid binding, identified in mouse, target of CaMKII, PKA, PKC, CKII
S189	SR1	95% in PFC	Low in NAc
S271*	SR1	80-90%	
S429	SR3	80-90%	
T607	SR4	75-85%	Not dephosphorylated
S672	SR5	100%	Not dephosphorylated
Y1123	SR8	65-75%	TrkB site
T1303	DH	100%	
Y1342	DH	75-85%	Not dephosphorylated
T1519*	PH	75-85%	PKC site; Not dephosphorylated;

Figure 6-4. Highly phosphorylated residues in Kal7. Phosphorylation sites in which the ratio of phosphopeptide to total peptide recovered was greater than 0.5. Protein domains, percent phosphorylation and relevant functional notes are also listed. Asterisks indicate indefinite residue number. Sites are indicated by red hashes on the Kal7 diagram below. "Not dephosphorylated" indicates that the site was not susceptible to phosphatase treatment in Kiraly et al., 2011 (49).

Tissue specificity

Further analysis of Kal7 tryptic peptides from saline-treated animals allowed us to identify differences in baseline phosphorylation status between the PFC and NAc. Remarkably, phosphorylation levels of 15 out of the 26 identified sites differed significantly between brain regions (**Fig. 6-3**, * and #; **Fig. 6-5**). Again, sites were distributed across the entire molecule. In most cases (12/15), phosphorylation was higher in the PFC than in the NAc, but phosphorylation of Ser33, Tyr616 and Tyr963 was higher in the NAc. Tyr616 was the only residue for which phosphorylation was identified in only one tissue (observed only in NAc). This residue was also identified as a target for the non-receptor tyrosine kinase, Abl1, and phosphorylation of recombinant KalSR4:6 by Abl1 increased its sensitivity to calpain (251). While some tissue differences were small, phosphorylation levels at five sites differed more than 2-fold between tissues, and two residues (Ser1077 and Thr1111) differed by more than 40% (check marks in **Fig. 6-4**). Three of the highly phosphorylated residues in Fig. 6-4 (Ser189, Thr607, Tyr1342 and Thr1519) also differed across brain regions (also see **Table 6-1**).

Differences between NAc and PFC (Saline)				
Site	Domain	Higher in		Functional notes
S33	Sec14	NAc	✓	
S189	SR1	PFC	✓	
S379	SR2	PFC		
S411	SR2	PFC	✓	
S487	SR3	PFC		
T607	SR4	PFC		
Y616	SR4	NAc	✓	NAc only, Abl1 site, promotes calpain cleavage
T943	SR7	PFC		
Y963	SR7	NAc		
S1077	SR8	PFC	✓	
S1097	SR8	PFC		
T1111	SR8	PFC	✓	
Y1342	DH	PFC		
T1519*	PH	PFC		
T1629*	linker	PFC	✓	

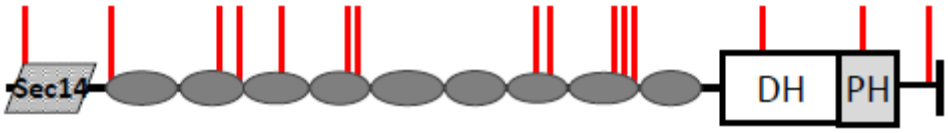

Figure 6-5. Phosphorylation differences in NAc and PFC (baseline). The extent of phosphorylation differed at 15 of 26 sites including 3 tyrosine residues, as indicated by the red or blue hash marks on the Kal7 diagram. Residues are listed along with their protein domain and the tissue in which there was more phosphorylation, red for PFC (12 sites) and blue for NAC (2 sites). Check marks indicate residues that with the largest cross-tissue differences; asterisks indicate indefinite residue number.

Cocaine regulation

We next evaluated changes in Kal7 phosphorylation levels following acute or chronic cocaine administration. We identified a small number of sites in each brain region at which the extent of phosphorylation was affected by exposure to cocaine. With the exception of one residue (Tyr1342), the sites at which phosphorylation was altered by cocaine administration in the nucleus accumbens were different from sites affected in the prefrontal cortex. Interestingly, phosphorylation at most of the cocaine sensitive sites in both tissues also differed between brain regions at baseline (**Fig. 6-5**). In order to control for any effects of handling and receiving an intraperitoneal injection, phosphorylation was evaluated 30 min after the administration of saline/cocaine.

Nucleus Accumbens

Phosphorylation levels were altered at four sites in the NAc following cocaine exposure; two of these sites were Tyr residues and all of the sites are located in the C-terminal half of the protein (**Fig. 6-6**). Though not all conditions reached statistical significance, we observed a general pattern in which phosphorylation at these four sites increased following acute cocaine, but decreased after a chronic regimen. Chronic cocaine exposure resulted in a significant decrease in phosphorylation of Tyr963, a residue in SR7 which is more highly phosphorylated in the NAc than in the PFC (**Figs. 6-3 & 6-5**). This cocaine-mediated reduction in phosphorylation was sufficient to eliminate the difference observed across tissues. Phosphorylation of Ser1608, located in the linker region between the PH domain and PDZ binding motif, was significantly higher following an acute dose of cocaine. This site was previously identified as a target for the synaptic kinase, CKII (49). When compared to the acute cocaine condition, phosphorylation of Tyr1342 (DH domain) and Thr1629 (PDZ linker) was significantly reduced by chronic cocaine administration. Significant changes are shown in **Figure 6-6**; data for all 26 sites are listed in Table 6-S1.

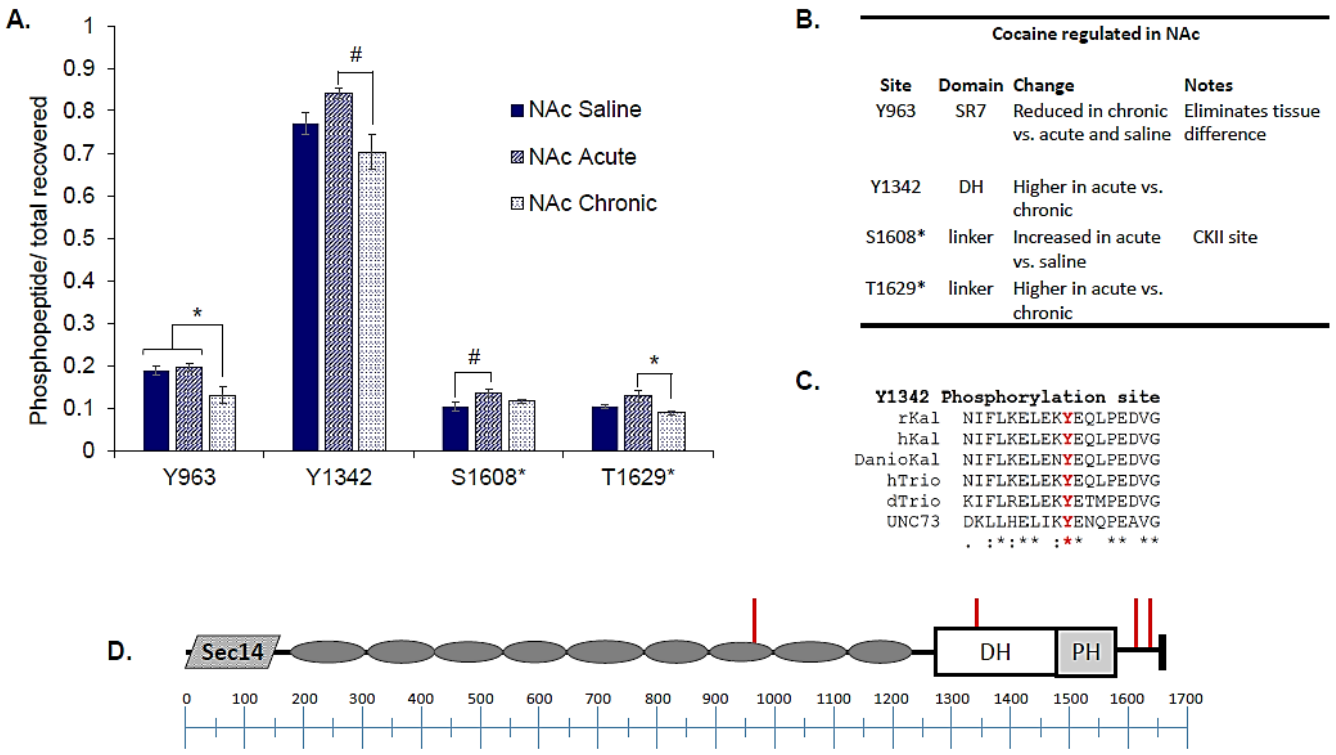

Figure 6-6. Cocaine-mediated changes in Kal7 phosphorylation in the nucleus accumbens. **A.** Bar graph showing changes in phosphorylation following acute (blue hashed bars) or chronic (blue polka-dotted bars) cocaine administration. Data are displayed as a proportion of phosphorylated peptide over the total recovered peptide. Amino acid residues are listed at the bottom; asterisks by the residue number indicate indefinite identification. Only the sites with significant changes are shown; * $p<0.005$, # $p<0.05$; see Table 6-S1 for all data. **B.** Chart lists all regulated sites as well as their associated protein domain, the observed change and functional notes of interest. **C.** Sequence alignment of Y1342 shows conservation across species and Trio orthologues. **D.** Protein diagram showing location of cocaine regulated sites in NAc (red hash marks).

Prefrontal Cortex

Cocaine treatment altered the phosphorylation of five sites in the prefrontal cortex. Interestingly, four of the five sites were located in the N-terminal quarter of the protein, a region which is crucial for synaptic localization and spine formation (251). The fact that all of the cocaine-regulated sites in the NAc were located in the C-terminal half of the protein likely reflects the presence of tissue-specific Kal7 interactors and kinases. In general, cocaine treatment decreased phosphorylation of Kal7 in the PFC. One exception was Ser33, a minor site, where phosphorylation was increased following acute exposure to cocaine (**Fig. 6-7**). Acute cocaine administration caused a decrease in phosphorylation at Ser379 and Ser411 (**Fig. 6-7**), both of which were more heavily phosphorylated in the PFC than in the NAc (**Figs. 6-2 & 6-5**). Compared with saline controls, phosphorylation of Ser429 and Tyr1342 was significantly lower following chronic cocaine exposure. The kinases used to phosphorylated recombinant Kal7 *in vitro* did not phosphorylate any of these sites.

Tyrosine 1342

Of all 26 phosphorylation sites, the only residue whose phosphorylation was affected by cocaine in both tissues was Tyr1342. This site was highly phosphorylated (75-85% of all tryptic peptides were phosphorylated) in both brain regions at baseline, with slightly more phospho-Tyr1342 observed in the PFC than NAc (**Figs. 6-2 through 6-5**). Chronic cocaine exposure reduced Tyr1342 phosphorylation in the PFC to levels comparable to that seen at baseline in the NAc (**Figs. 6-3 & 6-7**). Furthermore, Tyr1342 is one of two phosphorylation sites (a threonine and a tyrosine) identified in the catalytic Dbl homology domain. As such, this residue is highly evolutionarily conserved; it is present in *Danio rerio Kalrn*, h*TRIO* and in the single *Kalrn/Trio* homologs found in *C. elegans* (UNC-73) and *Drosophila melanogaster* (dTrio) (Clustal analysis in **Fig. 6-7**). Intriguingly, in recombinant HisMycKal7(a) isolated from transiently transfected HEK cells, phosphorylated Tyr1342 was resistant to broad-spectrum phosphatase treatment (49).

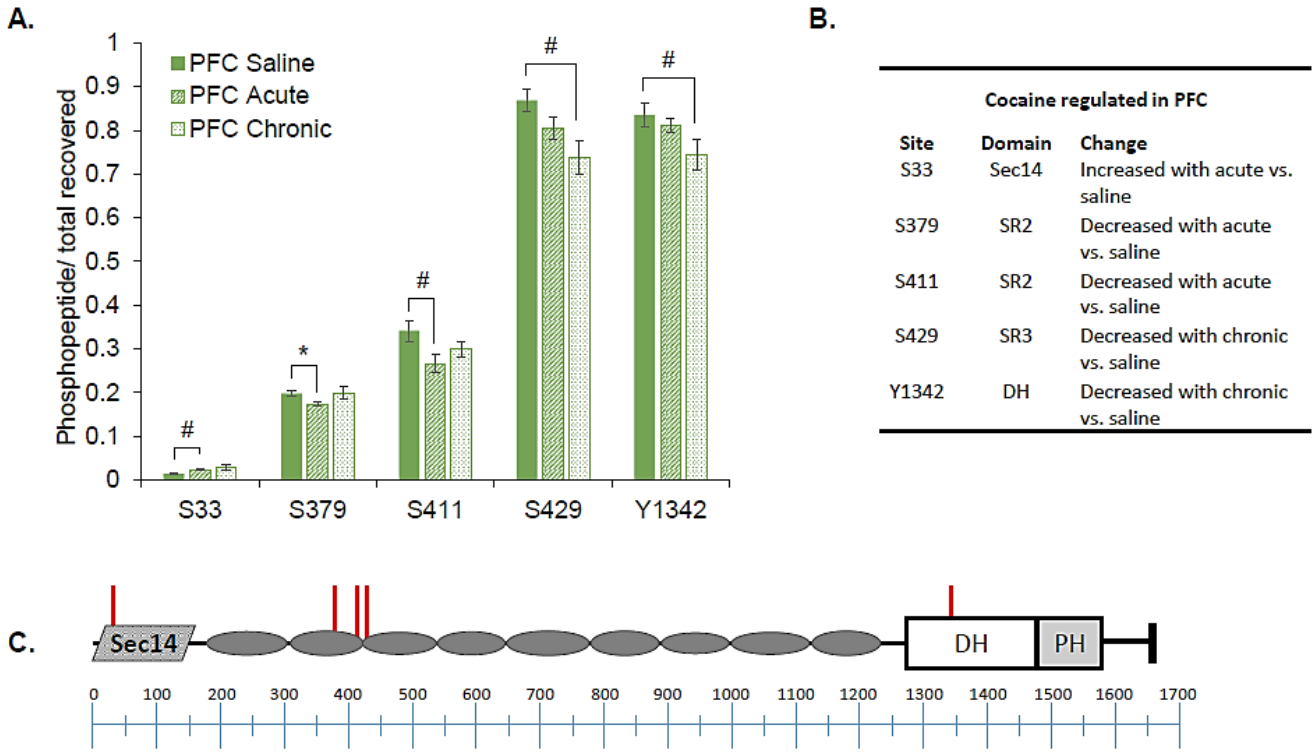

Figure 6-7. Cocaine-mediated changes in Kal7 phosphorylation in the prefrontal cortex. **A.** Bar graph showing changes in phosphorylation following acute (green hashed bars) or chronic (green polka-dots) cocaine administration. Data are displayed as a proportion of phosphorylated peptide over the total recovered peptide. Amino acid residues are listed at the bottom. Only the sites with significant changes are shown; * $p<0.005$, # $p<0.05$; see Table 6-S1 for all data. **B.** Chart lists all regulated sites, associated protein domains and observed changes. **C.** Protein diagram showing location of cocaine regulated sites in PFC (red hash marks).

Discussion

The present study confirms and extends previous results identifying Kal7 as a multiply-phosphorylated protein, implicating it as a molecular integrator of multiple signaling pathways. In addition to verifying several previously identified phosphorylation sites, we provide evidence for tissue-specific phospho-regulation of Kal7. In most tissues, Kalirin is not a major protein; Kal7, for example, accounts for only about 0.01% of the total brain protein. Reflecting its scarcity, phosphopeptides from Kalirin have been detected in global phosphoproteomic studies only when about 10,000 phosphopeptides were identified. When 10,000 phosphopeptides from cultured primary neurons were examined, one Kalirin phosphopeptide was identified; consistent with the age of the cultures being studied, the phosphopeptide identified was located near the first SH3 region, which occurs only in the longer isoforms (Kal9 and Kal12) (331). Studies in which fewer phosphopeptides were characterized failed to identify any Kalirin phosphopeptides [Wang et al.(338)– mouse phosphoproteome; 1026 phosphopeptides from 476 unique proteins; Yu et al. (333)– primary neurons; 2214 unique phosphopeptides on 1118 phosphoproteins]. Siddoway et al (339) used an antibody to P-Ser-Gln to identify the SQ phosphoproteome activated by calcium influx from L-type Ca channels; over 150 substrates whose phosphorylation was up-regulated in response to bicuculline stimulation of DIV 21 primary cortical cultures were identified, but the data set did not include any peptides from Kalirin, presumably reflecting its relatively low level of expression. Three SQ sites (Ser1608, Ser1614, Ser1629) were identified as minor sites of phosphorylation in Kal7 isolated from both NAc and PFC. In the NAc, phosphorylation of Kal7 at Ser^{1608}-Gln was up-regulated following acute exposure to cocaine, suggesting a role for PI3K-like protein kinases.

Kal7 is comprised of multiple functional domains; except for the sixth spectrin repeat, phosphorylation sites were found in each structural domain (Table 6-1). Two sites were identified in the N-terminal Sec14 domain, which binds to phosphoinositides and is crucial for normal spine formation (251). Most of the identified sites fall within one of the nine spectrin repeats (SRs), which engage in

numerous protein/protein interactions. A cluster of nine phosphorylation sites was found within the first four spectrin repeats, a region which is crucial for normal synaptic localization, potentially through an Abl1-dependent mechanism (251). Spectrin repeats 4-7 comprise the binding domains for peptidylglycine α-amidating monooxygenase, Huntingtin associated protein, inducible nitric oxide synthase, Arf6 and Disrupted in Schizophrenia-1 (52,53,67,340,341), and might be expected to be subject to regulation by phosphorylation. The catalytic DH domain contains two extensively phosphorylated sites, including Tyr1342, which is regulated by cocaine and present within an 18-residue stretch that is nearly perfectly conserved from zebrafish to humans, identical in Kalirin and Trio, and closely similar in *Drosophila* and *C.elegans*. The associated PH domain, with one extensively phosphorylated site (also highly conserved), binds directly to GluN2B, contributing to its surface expression and function (33). Lastly, three sites were identified in the unstructured region that follows the GEF domain and terminates with a PDZ binding motif. Kal7 is known to interact with multiple PDZ-domain containing proteins, including the postsynaptic scaffolds PSD95 and PICK-1 (37). Further studies will be necessary to determine the physiological importance of each of these phosphorylation sites as well as the combinatorial effects of phosphorylation at multiple sites.

Regulation of GEF activity

There are many examples of GEFs activated by phosphorylation of Tyr and Ser/Thr residues (335). The GEF activity of αPIX, which also activates Rac1, is stimulated by phosphorylation at two identified Ser residues (336), and the autoinhibition of Rabin8 (a GEF for Rab8) is relieved by ERK1/2 phosphorylation (334). Dbl, one of the first GEFs studied, is tonically inhibited; epidermal growth factor receptor activation of a Src family kinase activates Dbl at multiple Tyr residues (337). Flj00018, a Rho GEF, is activated by epidermal growth factor receptor activation of the MAPK pathway (335). In some instances, GEF activity is decreased by phosphorylation. A yeast Ras2-GEF, Cdc25p is multiply

phosphorylated, depending on nutritional status; GEF activity is markedly suppressed by increasing the phosphorylation of Cdc25p (342).

Tyrosine phosphorylation

Our data indicate that tyrosine kinases and phosphatases can be expected to play a major role in controlling Kalirin function. Global phosphoproteomic studies have consistently demonstrated that serine accounts for about 80% of the phosphorylation sites, while threonine accounts for about 18%; tyrosine consistently accounts for only about 2% of the phosphorylation sites (331-333). In Kal7, 19% (5/26) of the phosphorylation sites were tyrosine residues, with serine and threonine accounting for 54% (14/26) and 27% (7/26), respectively.

Disordered regions

Protein phosphorylation often occurs in disordered regions and in loops that are exposed; we used the Russell/Linding definition of disorder and the loop regions predicted from our structural studies of the spectrin repeat region to see whether these conclusions were valid for Kal7: the vast majority of the identified phosphorylation sites fell within a structural domain (**Fig. 6-2**). Looking more closely at the 18 phosphorylation sites identified in the nine spectrin repeats, half occur in the loops that connect the helices that form each spectrin repeat. Six other phosphorylation sites fall into disordered regions predicted at the N- and C-termini and in the linker between spectrin repeat 9 and the catalytic DH domain.

Tissue specificity

Although Kal7 may have similar functions in the PFC and NAc, we observed substantial differences in baseline phosphorylation between the brain regions. The observed differences are likely due to cell-type specific expression and control of kinases and phosphatases. Though most sites were identified in both tissues, in general, Kal7 was more heavily phosphorylated in the PFC than in the NAc.

As with most stimuli, cocaine exposure has differing effects on different cell types. For example, chronic cocaine administration causes an increase in dendritic spine density in the NAc, but decreases PFC spine density. Our data reveal changes in Kal7 phosphorylation in both brain regions following cocaine exposure, but the affected residues are mostly different, with only one overlapping site (Tyr1342). This observation suggests that Kal7 contributes to cocaine-induced changes in both tissues, but that different pathways are involved. In the NAc, all of the cocaine-mediated changes occur in the C-terminal half of Kal7, surrounding the GEF domain. Since chronic cocaine exposure mostly reduces phosphorylation at these sites, it is possible that their phosphorylation normally inhibits spine formation, and that phosphatase activity following chronic cocaine relieves a phosphorylation-dependent break on spinogenesis. This model is supported by previous work showing that normal Kal7 expression is necessary for cocaine-induced increases in NAc spine density (51). Conversely, most of the cocaine-regulated sites in the PFC occur toward the N-terminus of Kal7. Since chronic cocaine reduces phosphorylation at these sites and leads to reduced spine density in PFC, N-terminal Kal7 phosphorylation may normally promote spine formation.

Kinases and Phosphatases

Which kinases and phosphatases are at the PSD, in the position to affect synaptic transmission transiently and rapidly? The lists obtained through proteomic studies are large, but still represent only about 5% of the >500 kinases and ~200 phosphatases in the mammalian genome (343-345). Kinases and

phosphatases of varied specificity are abundant at the PSD. CamKII, which accounts for 1-2% of the protein at the PSD, is quantitatively the major kinase. An earlier report suggested that CaMKII phosphorylation of Thr95 plays an essential role in controlling Kal7 function (43); in our hands, exposure of recombinant Kal7 to purified CaMKII results in the phosphorylation of Thr79, not Thr95 (49). Importantly, for all 40 samples analyzed in this study, peptides containing Thr95 (GFT^{95}VIIDMR and RGFT^{95}VIIDMR) were abundantly recovered, but the corresponding phosphopeptides were never detected.

Specific kinases have been implicated in the regulation of Kal7. Serum-inducible, glucocorticoid-inducible kinase 1 (SGK1) mediates neuropathic pain in the spinal cord, and does so by increasing phosphorylation of Kalirin (346). Interestingly SGK1 is on the predicted list (Table 6-2) for one site only, S523 in SR3. Similarly, in a study of MAPKAPK5-deficient mice, (347) identified Kal7 as an interactor and substrate for MAPKAPK5; MAPKAPK5 is predicted to phosphorylate only two sites in Kal7, Ser487 (in SR3) and Ser1249 (between SR9 and the DH domain) (Table 6-2). Phosphorylated Ser487 was found in about 1/3 of the Kal7 recovered from both NAC and PFC, while phosphorylated Ser1249 was found in the low, but detectable range (**Fig. 6-3**).

Several web-based programs were utilized to predict phosphorylation sites in Kal7. Both PHOSPHIDA and NetPhos 2.0 failed to predict about 60% of the sites actually identified in Kal7. By comparison, GPS 3.0 (http://gps.biocuckoo.org/) (348) predicted all of the actual sites of phosphorylation except Ser33, a minor site (**Fig. 6-3**). Interestingly, the protein kinase predictions from GPS 3.0 already have significant experimental validation from *in vitro* phosphorylation assays (49): DTY10 (protein kinase C) phosphorylates T79 and S1520; CamKII phosphorylates T79 (and is not predicted to phosphorylate T95); CSNK2 (casein kinase 2) phosphorylates S1249, S1520, S1608 and S1632; and Fyn phosphorylates Y1653. In addition, 4 of the 5 sites which could not be dephosphorylated *in vitro* (T607, S672, T1519 and Y1342) (49) were found to be extensively phosphorylated *in vivo* (**Fig. 6-3**).

Kinases/phosphatases in cocaine

The PSD is made up of hundreds of proteins including dozens of kinases and phosphatases which are crucial for normal synaptic function. The large number of kinases and phosphatases vary in substrate specificity, some highly restrictive and some very promiscuous, so it is not surprising that many protein kinases are implicated in addiction (349), with the potential for disparate effects in different parts of the nervous system. For example, dendritic spine density in the orbitofrontal cortex is normally reduced following chronic cocaine exposure, but spines are non-responsive in animals lacking the non-receptor tyrosine kinase Abl2/ Arg (350). Pharmacological inhibition of Src family protein tyrosine kinases in the dorsal hippocampus impairs drug context-induced reinstatement of cocaine-seeking in rats (351). Blockade of the receptor tyrosine kinase TrkB in the infralimbic PFC impairs consolidation of conditioned place preference (CPP) for cocaine in rats, while TrkB stimulation enhances extinction of the same behavior (352). DARPP32 is a protein phosphatase inhibitor which is decreased in the NAC by chronic cocaine (353), leading to an increase in phosphatase activity after cocaine exposure.

Acknowledgements

We would like to thank Darlene D'Amato and Taylor Larese for their technical assistance and the people at the Neuroproteomics facility at Yale University for their continued collaboration.

Author Contributions

D.D.K. and R.E.M. treated animals and coordinated tissue harvest

B.A.E. oversaw sample preparation and processing; M.B.M. aided.

T.A., T.T.L. and C.C. conducted and processed Mass Spec Data

R.E.M. analyzed Mass Spec data

M.B.M., R.E.M, and B.A.E. wrote the manuscript

Y.Y. provided intellectual input and conducted biological experiments, which are not presented here but will be included in the final manuscript.

Author Institutions (if other than UConn Health Center)

D.D.K. is currently in the Department of Psychiatry, Icahn School of Medicine at Mount Sinai, New York, NY

T.T.L., T.A. and C.C. are affiliated with the W.M. Keck Facility, Yale University, New Haven, CT

Table 6-1.

Position	Protein Domain	Highly Phosph.	Regional difference	Cocaine regulation		Kiraly et al, 2011			
				NAc	PFC	Mouse brain	HEKs	in vitro	not de-P'ated
S33	Sec14		↑ NAc		Higher in acute vs. saline				
T79	Sec14	70-80%				✓		CaMKII, PKC, PKA, CKII	
S189	SR1	>90% in PFC	> 2-fold ↑ PFC			✓			
S271* (S276)	SR1	80-90%							
S379	SR2		↑ PFC		Lower in acute vs. saline	✓			
S411	SR2		> 2-fold ↑ PFC		Lower with acute vs. saline				
S429	SR3	80-90%			Lower with chronic vs. saline				
S487	SR3		↑ PFC			✓	✓		
S523	SR3								
T607	SR4	85-95%	↑ PFC			✓			✓
Y616	SR4		↑ NAc, not found in PFC						
S672	SR5	100%				✓			✓
S710	SR5					S714?	✓		

Table 6-1, continued

Position	Protein Domain	Highly Phosph.	Regional difference	Cocaine regulation		Kiraly et al, 2011			
				NAc	PFC	Mouse brain	HEKs	in vitro	not de-P'ated
T943	SR7		↑ PFC			✓			
Y963	SR7		↑ NAc	Lower with Chronic vs. Saline		✓	✓		✓
S1077	SR8		> 2-fold ↑ PFC			✓			
S1097	SR8								
T1111	SR8					✓			
Y1123	SR9	65-75%							
S1249	SR9/DH						✓	CKII	
T1303	DH	100%							
Y1342	DH	85-95%	↑ PFC	Lower with chronic vs. acute	Lower with chronic vs. saline				✓
T1519* (S1520)	PH	85-95%	↑ PFC			✓	✓	PKC, CKII	✓
S1608* (S1613, S1614)	PDZ linker			Higher with acute vs saline		✓	✓	CKII	607?
T1629* (T1625, S1626, S1632)	PDZ linker		> 2-fold ↑ PFC	Lower with chronic vs. acute		✓	✓	1632? CKII	
Y1653	PDZ motif						1652?	Fyn	

Table 6-1. Summary table of Kal7 phosphorylation in the rat brain. Results for all 26 phosphorylation sites are shown with comparisons to Kiraly et al. (49).

Table 6-2.

Position	Protein Domain	Peptide	Kinase Prediction	
			Kinase class	Candidate Kinases
S33	Sec14	R•NDGLKA**S**DVLPILK•E		-
T79	Sec14	K•LV**T**YLASVPSEDVCK•R	AGC, CAMK	DYT10(PKC), PRKD1(PKD), CHEK2, SIK1
S189	SR1	R•L**S**LEEFFNSAVHLLSR•L	AGC, STE, TKL, Other	PKN1, PRKACA(PKA), PAK4, TGFbR2
S271* (or S276)	SR1	R•NCIPG**S**ADFQ**S**LVPK•I	CAMK, AGC, CK1, Other	MARK1, CSNK1A1(CK1), CHUK, IKBKE, TBK1, NEK9, ROCK2
S379	SR2	R•L**S**EAGHYASQQIK•Q	CAMK, STE, TKL, Other	PRKD1, AURKB, EIF2AK3, MAP3K13(MLK), EIF2AK1, EIF2AK3, PAK1, MAP2K2
S411	SR2	DER•**S**TILAMSAVFHQK•A	CAMK, AGC, STE, Other, Atypical	PKD1, PKD2, AURKB, TTK, SLK, DMPK, MAP4K4, MINK1, TNIK, STK10
S429	SR3	K•AEQFL**S**GVDAWCK•M	AGC, TKL	ADRBK2, LIMK1, GRK5
S487	SR3	K•ALLDVLQRPL**S**PGNSESLTATAN YSK•A	AGC, CAMK, CMGK. TKL, Other, Atypical	PDK1, CAMK1, TTBK2, CAMK2A, CHEK1, MARK1, PIM3, CDK1, CDK2, CDK4, CDK5, DYRK1A, DYRK2, GSK3B, MAPK3(ERK1), MAPK1(ERK2), MAPK8(JNK1), NEK6, IRAK1, RPS6KB2, RPS6KA3, NUAK1, CDC28, NLK, MAPK12, EIF2AK2, ITPR1, MAPKAPK2, TGFbR2, GSK3A,MAP3K13, PRRT2(PKC), MTOR, PRKAA1(AMPK), MAPKAPK5
S523	SR3	R•LE**S**IWQHR•K	AGC, CAMK	AKT1, PRKACA, RPS6KA3(RSK), SGK1, CASK, PIM1, AKT2, PRKCI, CAMK2D, CHEK1, PIM2, PRKCQ, RPS6KB1, RPS6KA3, MARK3
T607	SR4	K•LLEAAEQLAQ**T**GECDPEEIYK•A	CAMK, STE, TKL, Other	TBK1, IRAK1, BMP2K, PRKAA1, AAK1, PAK2, MAP2K6
Y616	SR4	K•LLEAAEQLAQTGECDPEEI**Y**K•A	TK	FER, SYK, TEC, FES, FLT3, LCK, LYN, ABL1
S672	SR5	K•EVLEDVCAD**S**VDAVQELIK•Q	CK1, CAMK, AGC, STE, Other	TTBK2, BRSK2, MAP3K8, MAP3K14, BRSK1, PASK, NEK11

Table 6-2, continued

Position	Protein Domain	Peptide	Kinase Prediction	
			Kinase class	Candidate Kinases
S710	SR5	R•**S**APPSLGEPTEAR•D	AGC, CAMK, TKL	CASK, PRKCA, PRKAA2(AMPKA2), RAF1
T943	SR7	K•**T**HQSALQVQQK•A	CAMK, STE, Other	OXSR1, DAPK2, NEK6, STK39, MAP2K4
Y963	SR7	K•AEALLQAGH**Y**DADAIR•E	TK	DDR1, ABL1, CSK, DDR2
S1077	SR8	R•NNV**S**MPSVASHTR•G	AGC, CAMK, CK1, CMGC, TKL	PRKACB, CAMK2B, PRKAA2, DAPK2, CSNK1A1(CK), MAPK12(Erk3), BMPR1B
S1097	SR8	K•AIL**S**ELLQR•E	CAMK, STE, Other	DAPK1, IKBKB, EIF2AK3, PAK2, MAP2K2
T1111	SR8	R•VLHFW**T**LK•K	AGC	GRK5
Y1123	SR9	R•RLDQCQQ**Y**VVFER•S	TK	SYK, TRKB
S1249	SR9/DH	K•DLELDIIPASL**S**DR•E	CAMK, CK1, CMGC, Atypical	CHEK2, CSNK2B, MAPKAPK5, CSNK1A1
T1303	DH	R•DLHECLETYLWEM**T**SGVEEIPPGI LNK•E	STE	MAP2K6
Y1342	DH	EK•**Y**EQLPEDVGHCFVTWADK•F	TK	FGFR4, TXK, LCK
T1519* (or S1520)	PH	K•LL**TS**ELGVTEHVEGDPCK•F	AGC, CAMK, TKL, CK1, STE, Other	PRKCA, IKBKB, PRKCI, MKNK2, PASK, VRK1, EIF2AK4, MAP2K2

Table 6-2, continued

Position	Protein Domain	Peptide	Kinase Prediction	
			Kinase class	Candidate Kinases
S1608* (or S1613, S1614)	linker	R•DGVEDGD**S**QGDG**SS**QPDTISIASR•T	CAMK, STE, TKL, AGC, CK1, CMGC, Atypical, Other	CSNK1A1(CK1), SMG1(PIKK), CSNK2A1(CK2), ROCK1, ADRBK2, ATM, MAPK7(Erk5), MAPK13, IKBKB, NEK11, PLK2, TGFbR2, TTBK1, MAP2K1(MEK1), MARK1, CDK3, MAP2K1, ATR, DNAPK, PRKDC, MTOR, PRKAA2, CSNK1D, MAP3K10
T1629* (or T1625, S1626, S1632)	linker	R•**TS**QN**T**VE**S**DK•D	AGC, CAMK, STE, TKL, CMGC	MYLK3(MLCK), IRAK4, ILK, PRKCH, MAP4K4, MINK1, TNIK, CSNK2A1(CK2), CSNK2B
Y1653	PDZ motif	R•WHLGPGDPFST**Y**V	TK	ALK, CSK, EPHA2, EPHA3, EPHA4, FGFR1, FGFR2, PDGFRB, TIE1, TIE2, KDR(VEGFR), ITK, FLT1, PTK6, FYN, IGF1R, JAK3, TYK2, CSF1R

Table 6-2. Table with predicted kinases. Peptide sequences and predictions from GPS 3.0 are shown. For clarity, only mammalian enzymes and human gene names are shown.

	means						sem					
aa #	NAC Saline	NAC acute	NAC chronic	PFC Saline	PFC acute	PFC chronic	NAC Saline	NAC acute	NAC chronic	PFC Saline	PFC acute	PFC chronic
S33	0.0327	0.0262	0.0284	0.014	0.023	0.029	0.0055	0.0034	0.0043	0.0022	0.0022	0.0059
T79	0.693	0.667	0.782	0.782	0.723	0.746	0.042	0.039	0.038	0.04	0.036	0.034
S189	0.323	0.338	0.283	0.916	0.92	0.943	0.039	0.032	0.031	0.016	0.017	0.015
S271*	0.813	0.798	0.752	0.833	0.801	0.785	0.047	0.038	0.044	0.043	0.042	0.045
S379	0.172	0.168	0.164	0.198	0.174	0.199	0.0047	0.005	0.0088	0.0055	0.0061	0.015
S411	0.131	0.17	0.153	0.341	0.266	0.299	0.016	0.017	0.015	0.024	0.02	0.018
S429	0.874	0.836	0.8	0.868	0.806	0.737	0.024	0.021	0.04	0.025	0.026	0.038
S487	0.277	0.272	0.262	0.364	0.344	0.357	0.0076	0.0032	0.0067	0.018	0.007	0.0065
S523	0.284	0.3	0.329	0.296	0.28	0.242	0.022	0.023	0.02	0.032	0.0058	0.022
T607	0.778	0.789	0.723	0.843	0.848	0.879	0.017	0.016	0.049	0.045	0.021	0.036
Y616	0.024	0.043	0.032	0	0	0	0.005	0.0089	0.006			
S672	1	1	1	1	1	1	0	0	0	0	0	0
S710	0.099	0.101	0.093	0.108	0.112	0.12	0.0048	0.0047	0.0119	0.006	0.006	0.009
T943	0.124	0.129	0.114	0.187	0.203	0.193	0.006	0.006	0.0064	0.035	0.033	0.036
Y963	0.188	0.196	0.13	0.136	0.102	0.123	0.011	0.009	0.019	0.02	0.018	0.028
S1077	0.206	0.195	0.197	0.398	0.373	0.381	0.007	0.007	0.014	0.018	0.014	0.017
S1097	0.0946	0.0935	0.0839	0.116	0.11	0.11	0.0032	0.0031	0.004	0.004	0.004	0.0046
T1111	0.2496	0.259	0.248	0.441	0.326	0.299	0.0057	0.0107	0.0135	0.059	0.046	0.042
Y1123	0.671	0.694	0.643	0.662	0.53	0.652	0.056	0.038	0.042	0.049	0.037	0.046
S1249	0.0207	0.0197	0.0107	0.028	0.0216	0.0357	0.001	0.0008	0.0021	0.0065	0.0029	0.013
T1303	1	1	1	1	1	1						
Y1342	0.77	0.841	0.703	0.835	0.81	0.744	0.026	0.013	0.041	0.027	0.016	0.035
T1519*	0.818	0.771	0.804	0.924	0.877	0.892	0.042	0.046	0.055	0.018	0.037	0.028

S1608*	0.103	0.136	0.116	0.104	0.098	0.178	0.01	0.009	0.0058	0.01	0.009	0.035
T1629*	0.104	0.128	0.089	0.486	0.472	0.566	0.0039	0.0123	0.004	0.093	0.094	0.087
Y1653	0.157	0.25	0.178	0.195	0.309	0.299	0.0256	0.0418	0.0363	0.041	0.048	0.05

Table 6-S1. Cumulative data for (phosphopeptide/recovered peptide). All phosphorylation sites found with locations, mean values, sem, for all rats and for NAc and PFC.

Chapter 7

Significance and Future Directions

Beyond the GEF

To date, most studies of Kal7 function have focused on the recruitment and regulation of its GEF activity, but the GEF module is just one piece of a large, multi-domain protein. Succumbing to evolutionary pressures for greater functional complexity, multi-domain proteins arose through genetic rearrangements of ancient modules (354). Thus, by definition, the functions of these proteins are more evolved than those of their single-domain ancestors, and focusing our attention on a single, enzymatic domain is simplistic.

Modular complexity is common among GTPase regulatory proteins, and, in fact, most mammalian proteins contain more than one functional domain (354). As such, the multifaceted roles of many of these proteins have generated interest (355,356). We have shown that non-enzymatic functions of Kal7 are crucial for the protein's localization and function. N-terminal truncation of Kal7 prevents its synaptic localization and impairs its ability to promote synaptogenesis, presumably due to the loss of protein and lipid interactions mediated by the Sec14 and spectrin repeat regions [Chapter 4; (251)]. Furthermore, expression of a mutant protein which lacks GEF activity still promotes spine formation. In addition to identifying 26 phosphorylation sites in Kal7, our proteomics data revealed region-specific and cocaine-driven changes phosphorylation, suggesting that Kal7 is highly phspho-regulated (Chapter 6). Though one of the most highly regulated sites is located within the GEF domain, 23/26 are located in other domains.

Our in-depth examination of the Sec14 domain of Kalirin confirmed previous reports of phosphoinositide (PIP) binding [Chapters 3 & 4; (76,251)]. We also discovered that *Kalrn* promoter usage alters Sec14-mediated lipid interactions, suggesting that promoter switching may be a mechanism employed by cells to alter Kalirin's relationship with membranes. This idea is supported by the

observation that *Kalrn* promoter usage is strikingly developmentally regulated in the mouse brain (Chapter 5). Likewise, a phosphomimetic mutation within the Sec14 domain increases lipid binding on PIP strips (Chapter 3), revealing another regulatory mechanism for the domain's function. In addition to expanding upon our knowledge of the structure and function of Kalirin, our characterization of the KalSec14 may inform studies of the hundreds of other "Sec14 superfamily" members, which are found in eukaryotic organisms from yeast to humans.

Though not a protein domain, per se, our identification and description of a promoter-specific amphipathic helix (AH) may also be of broad interest (Chapter 4). We found that utilization of the C promoter of *Kalrn* appends an AH (Ex1C; C-helix) onto the front of the Sec14 domain. Inclusion of the C-helix enhances Sec14-mediated interactions with liposomes and drives interactions with the *trans*-Golgi Network (TGN) in a pituitary cell line. Also of interest is our discovery that the Kal-C-helix engages in a direct interaction with PI(4)P, thus acting as a lipid sensor, which requires its amphipathic nature. While Sec14 "sub-domains" have been reported [i.e. CRAL_TRIO and CRAL_TRIO_N; (263)], to our knowledge, this is the first account of a cooperative interaction between a Sec14 domain and an amphipathic helix.

Kal7 at the synapse

While at the PSD, Kal7 interacts with many other important synaptic proteins. Its PDZ binding motif interacts with PSD95 and other PDZ-containing scaffolds (37). The PH domain engages in a direct interaction with the cytoplasmic tail of GluN2B, which contributes to its surface expression, since Kal7^{KO} animals have reduced surface levels of this subunit (33). Through its GEF domain, Kal7 contributes to actin dynamics, one of the most essential components of synaptic plasticity (38,41,96). The studies presented in this dissertation reveal several novel interactions, mostly attributed to the N-terminal domains. Here, I will combine and discuss some of the key findings, placing them in the context of the synapse. An updated model of Kal7 at the synapse is shown in **Figure 7-1**.

As discussed above, the N-terminal Sec14 domain of Kalirin interacts with phosphoinositides, and this interaction is modified by both promoter usage and phosphorylation. In neurons, ΔSec14Kal7, a truncated protein which lacks only the Sec14 domain, forms the same number of spines as full-length Kal7, but the spines that form are abnormally short (Chapter 3). Fewer spines form when the Sec14 domain is expressed in isolation (aSec14-GFP), and the spines are longer than Kal7-induced spines. These experiments suggest that the Sec14 domain plays a role in determining spine morphology, but is not likely to be directly involved in initiating spine formation. This interpretation is further supported by the results of exogenous expression of bKal7 and cKal7 variants (Chapter 5). Alternate promoter usage differentially extends the N-terminus of Kalirin, with major consequences for Sec14 domain-mediated membrane interactions (Chapter 4). While both bKal7-GFP and cKal7-GFP localize to dendritic spines and promote spine formation, the spines formed by cKal7 are significantly smaller than those formed by bKal7, indicating that altered Sec14 function affects spine morphology, but not density. A potential mechanism for this is revealed by our experiments utilizing a cell-permeant peptide, Kal-C-helix-Arg9, to assess the activity of the amphipathic helix encoded by Ex1C. *In vitro*, the C-helix binds specifically to PI(4)P and enhances Sec14-mediated lipid binding (Chapter 4). In cultured rat hippocampal neurons, treatment with C-helix-Arg9 causes a net internalization of AMPA receptors with a corresponding decrease in spine length (Chapter 5). These experiments suggest that, through interactions with phosphoinositides, the N-terminal amphipathic helix in cKal7 may play a role in mediating postsynaptic receptor trafficking. The fact that reduced GluN2B surface expression was observed in $Kal7^{KO}$ animals (33) is consistent with this hypothesis. Interestingly, promoter usage is developmentally regulated, such that cKal7 expression increases around the type of synaptogenesis, with a corresponding decrease in isoforms from the B promotor (Chapter 5). This switch is particularly striking in the hippocampus.

The Sec14 domain is also phosphorylated at 2 residues in the adult rat brain, one of which (Thr79) was identified previously (49). Thr79 is one of the most highly phosphorylated sites in both the nucleus accumbens (NAc) and the prefrontal cortex (PFC; Chapter 6). Phosphorylation of the other Sec14 site, Ser33, is much less frequent, but cocaine administration increases phosphorylation at this site

in the PFC. Interestingly, a phosphomimetic mutation of Thr79 (T79E) increases aSec14-mediated lipid binding on PIP strips (Chapter 3). Furthermore, preliminary data suggest that full-length Kal7 with this mutation (aKal7-T79E) induces more spine formation than WT aKal7, while the non-phosphorylatable mutant, aKal7-T79A, forms fewer spines. Though this seems to contradict our hypothesis that the Sec14 domain contributes mostly to spine shape, not number, analysis of the same proteins with our FRET-based Rac1 activation assay reveals that aKal7-T79E also has increased GEF activity, while aKal7-T79A has less GEF activity (preliminary data; not shown). Thus, while the Sec14 domain on its own may contribute mostly to spine morphology, it may have phosphorylation-dependent influence on GEF activity which causes changes in spine number. Previous biophysical studies showed that spectrin repeat 4 is highly flexible and that full-length Kal7 may fold up on itself (264), so a direct interaction between the Sec14 and GEF domains is possible. Interestingly, very preliminary data (n = 1 experiment; not shown) suggest that *in vitro* phosphorylation (^{32}P-ATP) of recombinant cSec14 shifts lipid binding specificity from PI(4)P to PIP_3, a lipid with documented roles in AMPAR localization and plasticity (317,318). A model in which phosphorylation at Thr79 alters cKal7 lipid interactions and increases GEF activity is certainly intriguing.

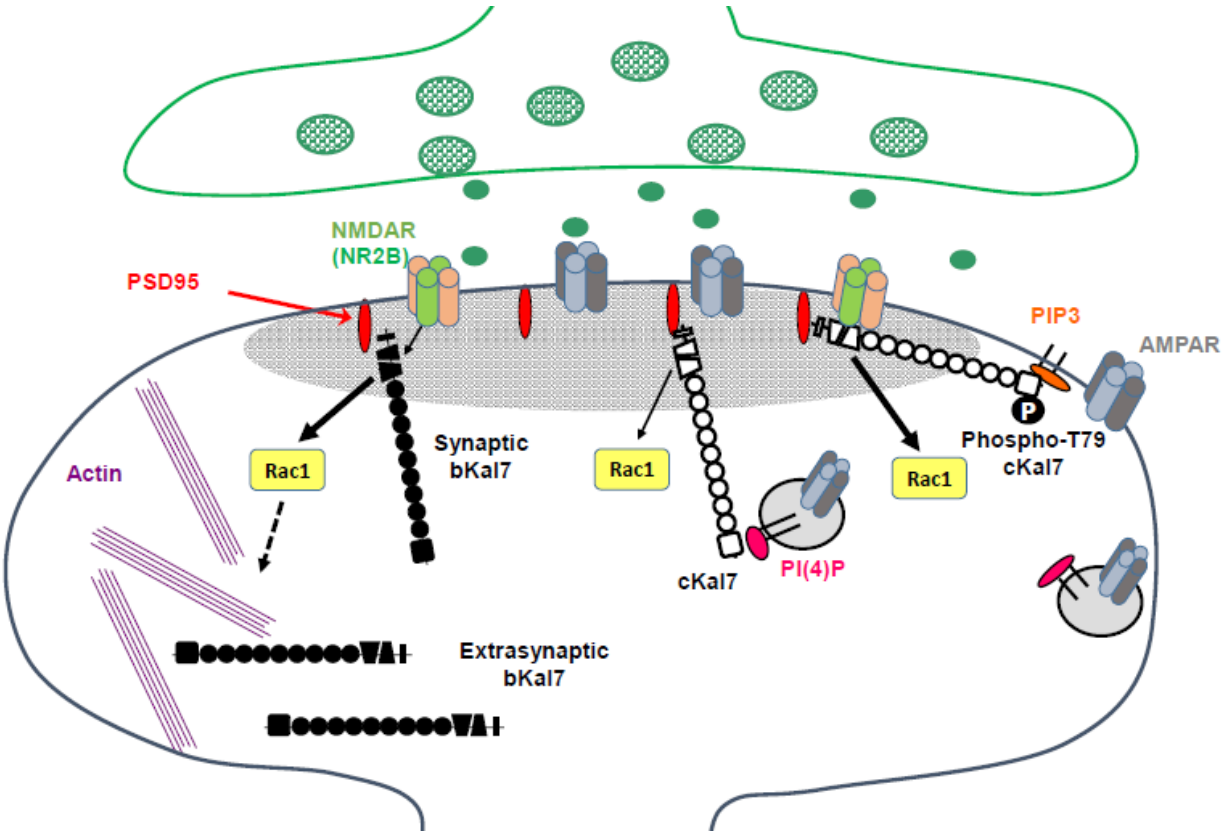

Figure 7-1. Model of Kal7 at the synapse. Two subpopulations of Kal7 are indicated, bKal7 (black fill) and cKal7 (black outline). Our data suggest a model in which bKal7 is localized both synaptically and extrasynaptically. Meanwhile cKal7 is primarily PSD-associated and has lower GEF activity than bKal7. The amphipathic helix of cKal7 interacts directly with PI(4)P and enhances Sec14-domain-mediated membrane interactions. A phosphomimetic mutation in aSec14 (T79E) increases its lipid binding ability, and preliminary data suggest that phosphorylation of cSec14 causes a shift in its specificity to PIP_3, a lipid enriched in the plasma membrane. Additionally, aKal7-T79E has increased GEF activity over wildtype aKal7. Studies with a cell-permeant C-helix peptide support a role for cKal7 in synaptic AMPAR trafficking.

Future directions

As is the nature of scientific inquiry, our progress toward understanding the function and regulation of Kal7 has raised new questions. I will discuss three of the major outstanding questions below, discussing relevant preliminary data and possible approaches along the way.

Do bKal7 and cKal7 contribute differently to synaptic physiology?

The importance of Kal7 in synaptic physiology is well-established, in part due to through electrophysiological characterization of our Kal7^{KO} animals. Acute hippocampal slices from Kal7^{KO} animals have reduced spontaneous activity (presumably due to decreased synapse/ spine formation) and significantly impaired NMDAR-dependent LTP and LTD (36,42). Further alluding to a role in receptor localization, layer 2/3 pyramidal neurons in Kal7^{KO} slices have diminished NMDA/AMPA receptor current ratios and reduced sensitivity to GluN2B inhibitors (33). The data presented in Chapter 5 suggest that alternate promoter usage gives rise to two subpopulations of Kal7 within dendritic spines: bKal7 and cKal7. Our analysis of the isoforms demonstrates that promoter usage has major influence over the localization and function of Kal7, but how this translates to synaptic physiology has not been explored. One way of investigating this is by genetically depleting each isoform and assessing the electrophysiological effects. Ideally, this would be done using Lenti-viral-packaged shRNA constructs and stereotactic injection followed by hippocampal recordings from acute slices. Alternatively, dissociated cultures or organotypic slice cultures could be used, employing chemically-induced LTP protocols to assess potential effects on plasticity. NMDA/AMPAR current ratios could be assessed in any system. Our initially developed Ex1B- and Ex1C-targeted shRNAs were unsuccessful in knocking down the exogenous protein in HEK cells, but there is room in the sequence for adjustment and additional constructs should be tried. Results from these experiments would provide enormous insight into the biological significance of the two populations of Kal7.

What role does endogenous cKal7 play in membrane trafficking at the PSD?

Experiments with the cell-permeant peptide (C-helix-Arg9) strongly suggest that the amphipathic helix of cKal7 plays a role in membrane trafficking at the PSD, but these experiments can be challenging to interpret. Again using a knockdown strategy, assessing constitutive receptor-mediated endocytosis (transferrin uptake) or stimulus-driven receptor internalization (AMPA/ NMDA stimulation) using immunostaining is fairly straightforward and would more directly address the question. Furthermore, assessing the effects of C-helix-Arg9 treatment on $Kal7^{KO}$ neurons may be informative.

What is the physiological significance of Kal7 phosphorylation?

Our identification and quantification of Kal7 phosphorylation across brain regions and in response to cocaine treatment (Chapter 6) substantiated the previous report suggesting phospho-regulation of Kal7. Though a major step in the right direction, we are a long way from understanding the biological relevance of Kal7 phosphorylation. Toward this end, phosphomimetic and non-phosphorylatable Kal7 constructs are in perpetual preparation. We have already attained interesting results from experiments evaluating the importance of several sites in spine formation and Rac1 activation, mostly conducted by Dr. Yan Yan in our lab. Moving forward, evaluating the biological role of Tyr1342, a highly regulated site in the GEF domain, will be a top priority. Additionally, mutating several residues at once may be a good strategy for evaluating cumulative effects of Kal7 phosphorylation. For instance, what happens to spine formation/morphology and GEF activity if all 4 of the sites regulated by cocaine in the NAc are mutated?

Conclusion

Kalirin was named for its likeness to the Hindu goddess, Kali, who has many arms. The studies presented here have identified several novel interactions mediated by Kalirin's N-terminal arms: a promoter-specific amphipathic helix and the N-terminal Sec14 domain interact with phosphoinositides and Abl1 phosphorylation spectrin repeat 4, all of which have physiological significance. Additionally, its 26 discrete phosphorylation sites were identified throughout the molecule, indicating that Kalirin serves as a point of kinase convergence at the PSD. In short, Kalirin lives up to its name.

References

1. Carlisle, H. J., and Kennedy, M. B. (2005) Spine architecture and synaptic plasticity. *Trends in neurosciences* **28**, 182-187
2. Park, M., Salgado, J. M., Ostroff, L., Helton, T. D., Robinson, C. G., Harris, K. M., and Ehlers, M. D. (2006) Plasticity-induced growth of dendritic spines by exocytic trafficking from recycling endosomes. *Neuron* **52**, 817-830
3. Matsuzaki, M., Honkura, N., Ellis-Davies, G. C., and Kasai, H. (2004) Structural basis of long-term potentiation in single dendritic spines. *Nature* **429**, 761-766
4. Fukazawa, Y., Saitoh, Y., Ozawa, F., Ohta, Y., Mizuno, K., and Inokuchi, K. (2003) Hippocampal LTP is accompanied by enhanced F-actin content within the dendritic spine that is essential for late LTP maintenance in vivo. *Neuron* **38**, 447-460
5. Okamoto, K., Bosch, M., and Hayashi, Y. (2009) The roles of CaMKII and F-actin in the structural plasticity of dendritic spines: a potential molecular identity of a synaptic tag? *Physiology (Bethesda)* **24**, 357-366
6. Bosch, M., and Hayashi, Y. (2011) Structural plasticity of dendritic spines. *Curr Opin Neurobiol*
7. Kasai, H., Fukuda, M., Watanabe, S., Hayashi-Takagi, A., and Noguchi, J. (2010) Structural dynamics of dendritic spines in memory and cognition. *Trends in neurosciences* **33**, 121-129
8. Holtmaat, A., and Svoboda, K. (2009) Experience-dependent structural synaptic plasticity in the mammalian brain. *Nature reviews. Neuroscience* **10**, 647-658
9. Calabrese, B., Wilson, M. S., and Halpain, S. (2006) Development and regulation of dendritic spine synapses. *Physiology (Bethesda)* **21**, 38-47
10. Bennett, M. R. (2011) Schizophrenia: susceptibility genes, dendritic-spine pathology and gray matter loss. *Progress in neurobiology* **95**, 275-300
11. Penzes, P., Cahill, M. E., Jones, K. A., VanLeeuwen, J. E., and Woolfrey, K. M. (2011) Dendritic spine pathology in neuropsychiatric disorders. *Nature neuroscience* **14**, 285-293
12. Fuhrmann, M., Mitteregger, G., Kretzschmar, H., and Herms, J. (2007) Dendritic pathology in prion disease starts at the synaptic spine. *The Journal of neuroscience : the official journal of the Society for Neuroscience* **27**, 6224-6233
13. Spires, T. L., Grote, H. E., Garry, S., Cordery, P. M., Van Dellen, A., Blakemore, C., and Hannan, A. J. (2004) Dendritic spine pathology and deficits in experience-dependent dendritic plasticity in R6/1 Huntington's disease transgenic mice. *The European journal of neuroscience* **19**, 2799-2807
14. Fiala, J. C., Spacek, J., and Harris, K. M. (2002) Dendritic spine pathology: cause or consequence of neurological disorders? *Brain research. Brain research reviews* **39**, 29-54
15. Lewis, D. A., and Gonzalez-Burgos, G. (2008) Neuroplasticity of neocortical circuits in schizophrenia. *Neuropsychopharmacology : official publication of the American College of Neuropsychopharmacology* **33**, 141-165
16. Swann, J. W., Al-Noori, S., Jiang, M., and Lee, C. L. (2000) Spine loss and other dendritic abnormalities in epilepsy. *Hippocampus* **10**, 617-625
17. Selkoe, D. J. (2002) Alzheimer's disease is a synaptic failure. *Science* **298**, 789-791
18. Robinson, T. E., and Kolb, B. (1999) Alterations in the morphology of dendrites and dendritic spines in the nucleus accumbens and prefrontal cortex following repeated treatment with amphetamine or cocaine. *The European journal of neuroscience* **11**, 1598-1604
19. Reeve, S. P., Bassetto, L., Genova, G. K., Kleyner, Y., Leyssen, M., Jackson, F. R., and Hassan, B. A. (2005) The Drosophila fragile X mental retardation protein controls actin dynamics by directly regulating profilin in the brain. *Current biology : CB* **15**, 1156-1163

20. Fifkova, E., and Morales, M. (1992) Actin matrix of dendritic spines, synaptic plasticity, and long-term potentiation. *International review of cytology* **139**, 267-307
21. Hotulainen, P., and Hoogenraad, C. C. (2010) Actin in dendritic spines: connecting dynamics to function. *The Journal of cell biology* **189**, 619-629
22. Krucker, T., Siggins, G. R., and Halpain, S. (2000) Dynamic actin filaments are required for stable long-term potentiation (LTP) in area CA1 of the hippocampus. *Proceedings of the National Academy of Sciences of the United States of America* **97**, 6856-6861
23. Tashiro, A., Minden, A., and Yuste, R. (2000) Regulation of dendritic spine morphology by the rho family of small GTPases: antagonistic roles of Rac and Rho. *Cereb Cortex* **10**, 927-938
24. Nakayama, A. Y., Harms, M. B., and Luo, L. (2000) Small GTPases Rac and Rho in the maintenance of dendritic spines and branches in hippocampal pyramidal neurons. *The Journal of neuroscience : the official journal of the Society for Neuroscience* **20**, 5329-5338
25. Tashiro, A., and Yuste, R. (2004) Regulation of dendritic spine motility and stability by Rac1 and Rho kinase: evidence for two forms of spine motility. *Molecular and cellular neurosciences* **26**, 429-440
26. Irie, F., and Yamaguchi, Y. (2002) EphB receptors regulate dendritic spine development via intersectin, Cdc42 and N-WASP. *Nature neuroscience* **5**, 1117-1118
27. Tolias, K. F., Duman, J. G., and Um, K. (2011) Control of synapse development and plasticity by Rho GTPase regulatory proteins. *Progress in neurobiology* **94**, 133-148
28. Rex, C. S., Chen, L. Y., Sharma, A., Liu, J., Babayan, A. H., Gall, C. M., and Lynch, G. (2009) Different Rho GTPase-dependent signaling pathways initiate sequential steps in the consolidation of long-term potentiation. *The Journal of cell biology* **186**, 85-97
29. Murakoshi, H., Wang, H., and Yasuda, R. (2011) Local, persistent activation of Rho GTPases during plasticity of single dendritic spines. *Nature* **472**, 100-104
30. Ridley, A. J. (2006) Rho GTPases and actin dynamics in membrane protrusions and vesicle trafficking. *Trends in cell biology* **16**, 522-529
31. Kiraly, D. D., Eipper-Mains, J. E., Mains, R. E., and Eipper, B. A. (2010) Synaptic plasticity, a symphony in GEF. *ACS chemical neuroscience* **1**, 348-365
32. Tolias, K. F., Bikoff, J. B., Kane, C. G., Tolias, C. S., Hu, L., and Greenberg, M. E. (2007) The Rac1 guanine nucleotide exchange factor Tiam1 mediates EphB receptor-dependent dendritic spine development. *Proceedings of the National Academy of Sciences of the United States of America* **104**, 7265-7270
33. Kiraly, D. D., Lemtiri-Chlieh, F., Levine, E. S., Mains, R. E., and Eipper, B. A. (2011) Kalirin binds the NR2B subunit of the NMDA receptor, altering its synaptic localization and function. *The Journal of neuroscience : the official journal of the Society for Neuroscience* **31**, 12554-12565
34. Shin, E. Y., Shin, K. S., Lee, C. S., Woo, K. N., Quan, S. H., Soung, N. K., Kim, Y. G., Cha, C. I., Kim, S. R., Park, D., Bokoch, G. M., and Kim, E. G. (2002) Phosphorylation of p85 beta PIX, a Rac/Cdc42-specific guanine nucleotide exchange factor, via the Ras/ERK/PAK2 pathway is required for basic fibroblast growth factor-induced neurite outgrowth. *The Journal of biological chemistry* **277**, 44417-44430
35. Miller, M. B., Yan, Y., Eipper, B. A., and Mains, R. E. (2013) Neuronal Rho GEFs in synaptic physiology and behavior. *Neuroscientist* **19**, 255-273
36. Ma, X. M., Kiraly, D. D., Gaier, E. D., Wang, Y., Kim, E. J., Levine, E. S., Eipper, B. A., and Mains, R. E. (2008) Kalirin-7 is required for synaptic structure and function. *The Journal of neuroscience : the official journal of the Society for Neuroscience* **28**, 12368-12382
37. Penzes, P., Johnson, R. C., Sattler, R., Zhang, X., Huganir, R. L., Kambampati, V., Mains, R. E., and Eipper, B. A. (2001) The neuronal Rho-GEF Kalirin-7 interacts with PDZ domain-containing proteins and regulates dendritic morphogenesis. *Neuron* **29**, 229-242

38. Penzes, P., Johnson, R. C., Kambampati, V., Mains, R. E., and Eipper, B. A. (2001) Distinct roles for the two Rho GDP/GTP exchange factor domains of kalirin in regulation of neurite growth and neuronal morphology. *J. Neurosci.* **21**, 8426-8434
39. Ma, X. M., Johnson, R. C., Mains, R. E., and Eipper, B. A. (2001) Expression of kalirin, a neuronal GDP/GTP exchange factor of the trio family, in the central nervous system of the adult rat. *J. Comp. Neurol.* **429**, 388-402
40. Hansel, D. E., Quinones, M. E., Ronnett, G. V., and Eipper, B. A. (2001) Kalirin, a GDP/GTP exchange factor of the Dbl family, is localized to nerve, muscle, and endocrine tissue during embryonic rat development. *J. Histochem. Cytochem.* **49**, 833-844
41. Penzes, P., Beeser, A., Chernoff, J., Schiller, M. R., Eipper, B. A., Mains, R. E., and Huganir, R. L. (2003) Rapid induction of dendritic spine morphogenesis by trans-synaptic ephrinB-EphB receptor activation of the Rho-GEF kalirin. *Neuron* **37**, 263-274
42. Lemtiri-Chlieh, F., Zhao, L., Kiraly, D. D., Eipper, B. A., Mains, R. E., and Levine, E. S. (2011) Kalirin-7 is necessary for normal NMDA receptor-dependent synaptic plasticity. *BMC Neurosci* **12**, 126
43. Xie, Z., Srivastava, D. P., Photowala, H., Kai, L., Cahill, M. E., Woolfrey, K. M., Shum, C. Y., Surmeier, D. J., and Penzes, P. (2007) Kalirin-7 controls activity-dependent structural and functional plasticity of dendritic spines. *Neuron* **56**, 640-656
44. Xie, Z., Photowala, H., Cahill, M. E., Srivastava, D. P., Woolfrey, K. M., Shum, C. Y., Huganir, R. L., and Penzes, P. (2008) Coordination of synaptic adhesion with dendritic spine remodeling by AF-6 and kalirin-7. *J. Neurosci.* **28**, 6079-6091
45. Wang, X., Cahill, M. E., Werner, C. T., Christoffel, D. J., Golden, S. A., Xie, Z., Loweth, J. A., Marinelli, M., Russo, S. J., Penzes, P., and Wolf, M. E. (2013) Kalirin-7 mediates cocaine-induced AMPA receptor and spine plasticity, enabling incentive sensitization. *J. Neurosci.* **33**, 11012-11022
46. Jones, K. A., Srivastava, D. P., Allen, J. A., Strachan, R. T., Roth, B. L., and Penzes, P. (2009) Rapid modulation of spine morphology by the 5-HT2A serotonin receptor through kalirin-7 signaling. *Proc. Natl. Acad. Sci. U. S. A.* **106**, 19575-19580
47. Cahill, M. E., Remmers, C., Jones, K. A., Xie, Z., Sweet, R. A., and Penzes, P. (2013) Neuregulin1 signaling promotes dendritic spine growth through kalirin. *J. Neurochem.* **126**, 625-635
48. Cahill, M. E., Jones, K. A., Rafalovich, I., Xie, Z., Barros, C. S., Muller, U., and Penzes, P. (2012) Control of interneuron dendritic growth through NRG1/erbB4-mediated kalirin-7 disinhibition. *Mol. Psychiatry* **17**, 1, 99-107
49. Kiraly, D. D., Stone, K. L., Colangelo, C. M., Abbott, T., Wang, Y., Mains, R. E., and Eipper, B. A. (2011) Identification of kalirin-7 as a potential post-synaptic density signaling hub. *Journal of proteome research* **10**, 2828-2841
50. Lemtiri-Chlieh, F., Zhao, L., Kiraly, D. D., Eipper, B. A., Mains, R. E., and Levine, E. S. (2011) Kalirin-7 is necessary for normal NMDA receptor-dependent synaptic plasticity. *BMC neuroscience* **12**, 126
51. Kiraly, D. D., Ma, X. M., Mazzone, C. M., Xin, X., Mains, R. E., and Eipper, B. A. (2010) Behavioral and morphological responses to cocaine require kalirin7. *Biol. Psychiatry* **68**, 249-255
52. Hayashi-Takagi, A., Takaki, M., Graziane, N., Seshadri, S., Murdoch, H., Dunlop, A. J., Makino, Y., Seshadri, A. J., Ishizuka, K., Srivastava, D. P., Xie, Z., Baraban, J. M., Houslay, M. D., Tomoda, T., Brandon, N. J., Kamiya, A., Yan, Z., Penzes, P., and Sawa, A. (2010) Disrupted-in-Schizophrenia 1 (DISC1) regulates spines of the glutamate synapse via Rac1. *Nat. Neurosci.* **13**, 327-332
53. Colomer, V., Engelender, S., Sharp, A. H., Duan, K., Cooper, J. K., Lanahan, A., Lyford, G., Worley, P., and Ross, C. A. (1997) Huntingtin-associated protein 1 (HAP1) binds to a Trio-like polypeptide, with a rac1 guanine nucleotide exchange factor domain. *Hum. Mol. Genet.* **6**, 1519-1525

54. Ikeda, M., Aleksic, B., Kinoshita, Y., Okochi, T., Kawashima, K., Kushima, I., Ito, Y., Nakamura, Y., Kishi, T., Okumura, T., Fukuo, Y., Williams, H. J., Hamshere, M. L., Ivanov, D., Inada, T., Suzuki, M., Hashimoto, R., Ujike, H., Takeda, M., Craddock, N., Kaibuchi, K., Owen, M. J., Ozaki, N., O'Donovan, M. C., and Iwata, N. (2011) Genome-wide association study of schizophrenia in a Japanese population. *Biological psychiatry* **69**, 472-478
55. Ikram, M. A., Seshadri, S., Bis, J. C., Fornage, M., DeStefano, A. L., Aulchenko, Y. S., Debette, S., Lumley, T., Folsom, A. R., van den Herik, E. G., Bos, M. J., Beiser, A., Cushman, M., Launer, L. J., Shahar, E., Struchalin, M., Du, Y., Glazer, N. L., Rosamond, W. D., Rivadeneira, F., Kelly-Hayes, M., Lopez, O. L., Coresh, J., Hofman, A., DeCarli, C., Heckbert, S. R., Koudstaal, P. J., Yang, Q., Smith, N. L., Kase, C. S., Rice, K., Haritunians, T., Roks, G., de Kort, P. L., Taylor, K. D., de Lau, L. M., Oostra, B. A., Uitterlinden, A. G., Rotter, J. I., Boerwinkle, E., Psaty, B. M., Mosley, T. H., van Duijn, C. M., Breteler, M. M., Longstreth, W. T., Jr., and Wolf, P. A. (2009) Genomewide association studies of stroke. *N. Engl. J. Med.* **360**, 1718-1728
56. Lesch, K. P., Timmesfeld, N., Renner, T. J., Halperin, R., Roser, C., Nguyen, T. T., Craig, D. W., Romanos, J., Heine, M., Meyer, J., Freitag, C., Warnke, A., Romanos, M., Schafer, H., Walitza, S., Reif, A., Stephan, D. A., and Jacob, C. (2008) Molecular genetics of adult ADHD: converging evidence from genome-wide association and extended pedigree linkage studies. *J Neural Transm* **115**, 1573-1585
57. Krug, T., Manso, H., Gouveia, L., Sobral, J., Xavier, J. M., Albergaria, I., Gaspar, G., Correia, M., Viana-Baptista, M., Simoes, R. M., Pinto, A. N., Taipa, R., Ferreira, C., Fontes, J. R., Silva, M. R., Gabriel, J. P., Matos, I., Lopes, G., Ferro, J. M., Vicente, A. M., and Oliveira, S. A. (2010) Kalirin: a novel genetic risk factor for ischemic stroke. *Hum. Genet.* **127**, 513-523
58. Youn, H., Jeoung, M., Koo, Y., Ji, H., Markesbery, W. R., Ji, I., and Ji, T. H. (2007) Kalirin is under-expressed in Alzheimer's disease hippocampus. *Journal of Alzheimer's disease : JAD* **11**, 385-397
59. Hill, J. J., Hashimoto, T., and Lewis, D. A. (2006) Molecular mechanisms contributing to dendritic spine alterations in the prefrontal cortex of subjects with schizophrenia. *Mol. Psychiatry* **11**, 557-566
60. Rossman, K. L., Der, C. J., and Sondek, J. (2005) GEF means go: turning on RHO GTPases with guanine nucleotide-exchange factors. *Nature reviews. Molecular cell biology* **6**, 167-180
61. Schiller, M. R. (2006) Coupling receptor tyrosine kinases to Rho GTPases--GEFs what's the link. *Cellular signalling* **18**, 1834-1843
62. Bouquier, N., Vignal, E., Charrasse, S., Weill, M., Schmidt, S., Leonetti, J. P., Blangy, A., and Fort, P. (2009) A cell active chemical GEF inhibitor selectively targets the Trio/RhoG/Rac1 signaling pathway. *Chemistry & biology* **16**, 657-666
63. Rabiner, C. A., Mains, R. E., and Eipper, B. A. (2005) Kalirin: a dual Rho guanine nucleotide exchange factor that is so much more than the sum of its many parts. *The Neuroscientist : a review journal bringing neurobiology, neurology and psychiatry* **11**, 148-160
64. Mandela, P., and Ma, X. M. (2012) Kalirin, a key player in synapse formation, is implicated in human diseases. *Neural Plast* **2012**, 728161
65. Penzes, P., and Jones, K. A. (2008) Dendritic spine dynamics--a key role for kalirin-7. *Trends in neurosciences* **31**, 419-427
66. Debant, A., Serra-Pages, C., Seipel, K., O'Brien, S., Tang, M., Park, S. H., and Streuli, M. (1996) The multidomain protein Trio binds the LAR transmembrane tyrosine phosphatase, contains a protein kinase domain, and has separate rac-specific and rho-specific guanine nucleotide exchange factor domains. *Proceedings of the National Academy of Sciences of the United States of America* **93**, 5466-5471

67. Alam, M. R., Caldwell, B. D., Johnson, R. C., Darlington, D. N., Mains, R. E., and Eipper, B. A. (1996) Novel proteins that interact with the COOH-terminal cytosolic routing determinants of an integral membrane peptide-processing enzyme. *J. Biol. Chem.* **271**, 28636-28640
68. McPherson, C. E., Eipper, B. A., and Mains, R. E. (2002) Genomic organization and differential expression of Kalirin isoforms. *Gene* **284**, 41-51
69. Ma, X. M., Huang, J. P., Eipper, B. A., and Mains, R. E. (2005) Expression of Trio, a member of the Dbl family of Rho GEFs in the developing rat brain. *The Journal of comparative neurology* **482**, 333-348
70. Peng, Y. J., He, W. Q., Tang, J., Tao, T., Chen, C., Gao, Y. Q., Zhang, W. C., He, X. Y., Dai, Y. Y., Zhu, N. C., Lv, N., Zhang, C. H., Qiao, Y. N., Zhao, L. P., Gao, X., and Zhu, M. S. (2010) Trio is a key guanine nucleotide exchange factor coordinating regulation of the migration and morphogenesis of granule cells in the developing cerebellum. *The Journal of biological chemistry* **285**, 24834-24844
71. McPherson, C. E., Eipper, B. A., and Mains, R. E. (2005) Multiple novel isoforms of Trio are expressed in the developing rat brain. *Gene* **347**, 125-135
72. Liebl, E. C., Forsthoefel, D. J., Franco, L. S., Sample, S. H., Hess, J. E., Cowger, J. A., Chandler, M. P., Shupert, A. M., and Seeger, M. A. (2000) Dosage-sensitive, reciprocal genetic interactions between the Abl tyrosine kinase and the putative GEF trio reveal trio's role in axon pathfinding. *Neuron* **26**, 107-118
73. Awasaki, T., Saito, M., Sone, M., Suzuki, E., Sakai, R., Ito, K., and Hama, C. (2000) The Drosophila trio plays an essential role in patterning of axons by regulating their directional extension. *Neuron* **26**, 119-131
74. Bateman, J., Shu, H., and Van Vactor, D. (2000) The guanine nucleotide exchange factor trio mediates axonal development in the Drosophila embryo. *Neuron* **26**, 93-106
75. Xin, X., Rabiner, C. A., Mains, R. E., and Eipper, B. A. (2009) Kalirin12 interacts with dynamin. *BMC neuroscience* **10**, 61
76. Schiller, M. R., Ferraro, F., Wang, Y., Ma, X. M., McPherson, C. E., Sobota, J. A., Schiller, N. I., Mains, R. E., and Eipper, B. A. (2008) Autonomous functions for the Sec14p/spectrin-repeat region of Kalirin. *Experimental cell research* **314**, 2674-2691
77. Williams, S. L., Lutz, S., Charlie, N. K., Vettel, C., Ailion, M., Coco, C., Tesmer, J. J., Jorgensen, E. M., Wieland, T., and Miller, K. G. (2007) Trio's Rho-specific GEF domain is the missing Galpha q effector in C. elegans. *Genes & development* **21**, 2731-2746
78. Chan, J. P., Hu, Z., and Sieburth, D. (2012) Recruitment of sphingosine kinase to presynaptic terminals by a conserved muscarinic signaling pathway promotes neurotransmitter release. *Genes & development* **26**, 1070-1085
79. McMullan, R., Anderson, A., and Nurrish, S. (2012) Behavioral and immune responses to infection require Galphaq- RhoA signaling in C. elegans. *PLoS pathogens* **8**, e1002530
80. Luo, L. (2000) Trio quartet in D. (melanogaster). *Neuron* **26**, 1-2
81. Astigarraga, S., Hofmeyer, K., Farajian, R., and Treisman, J. E. (2010) Three Drosophila liprins interact to control synapse formation. *The Journal of neuroscience : the official journal of the Society for Neuroscience* **30**, 15358-15368
82. Ball, R. W., Warren-Paquin, M., Tsurudome, K., Liao, E. H., Elazzouzi, F., Cavanagh, C., An, B. S., Wang, T. T., White, J. H., and Haghighi, A. P. (2010) Retrograde BMP signaling controls synaptic growth at the NMJ by regulating trio expression in motor neurons. *Neuron* **66**, 536-549
83. Lutz, S., Shankaranarayanan, A., Coco, C., Ridilla, M., Nance, M. R., Vettel, C., Baltus, D., Evelyn, C. R., Neubig, R. R., Wieland, T., and Tesmer, J. J. (2007) Structure of Galphaq-p63RhoGEF-RhoA complex reveals a pathway for the activation of RhoA by GPCRs. *Science* **318**, 1923-1927

84. Rojas, R. J., Yohe, M. E., Gershburg, S., Kawano, T., Kozasa, T., and Sondek, J. (2007) Galphaq directly activates p63RhoGEF and Trio via a conserved extension of the Dbl homology-associated pleckstrin homology domain. *The Journal of biological chemistry* **282**, 29201-29210
85. O'Brien, S. P., Seipel, K., Medley, Q. G., Bronson, R., Segal, R., and Streuli, M. (2000) Skeletal muscle deformity and neuronal disorder in Trio exchange factor-deficient mouse embryos. *Proceedings of the National Academy of Sciences of the United States of America* **97**, 12074-12078
86. Briancon-Marjollet, A., Ghogha, A., Nawabi, H., Triki, I., Auziol, C., Fromont, S., Piche, C., Enslen, H., Chebli, K., Cloutier, J. F., Castellani, V., Debant, A., and Lamarche-Vane, N. (2008) Trio mediates netrin-1-induced Rac1 activation in axon outgrowth and guidance. *Molecular and cellular biology* **28**, 2314-2323
87. Mandela, P., Yankova, M., Conti, L. H., Ma, X., Grady, J., Eipper, B. A., and Mains, R. E. (2012) Kalrn plays key roles within and outside of the nervous system. *BMC neuroscience* **13**, 136
88. Xie, Z., Cahill, M. E., Radulovic, J., Wang, J., Campbell, S. L., Miller, C. A., Sweatt, J. D., and Penzes, P. (2011) Hippocampal phenotypes in kalirin-deficient mice. *Molecular and cellular neurosciences* **46**, 45-54
89. May, V., Schiller, M. R., Eipper, B. A., and Mains, R. E. (2002) Kalirin Dbl-homology guanine nucleotide exchange factor 1 domain initiates new axon outgrowths via RhoG-mediated mechanisms. *The Journal of neuroscience : the official journal of the Society for Neuroscience* **22**, 6980-6990
90. Wu, J. H., Fanaroff,A. C., Sharma, K.C., Zhang, L., Smith, L. S., Brian, L., Eipper, B. A., Mains, R. E., Freedman, N. J. . (2012) Kalirin Promotes Neointimal Hyperplasia by Activating Rac in Smooth Muscle Cells. *Arterioscler Thromb Vasc Biol.* **In press**
91. Cahill, M. E., Xie, Z., Day, M., Photowala, H., Barbolina, M. V., Miller, C. A., Weiss, C., Radulovic, J., Sweatt, J. D., Disterhoft, J. F., Surmeier, D. J., and Penzes, P. (2009) Kalirin regulates cortical spine morphogenesis and disease-related behavioral phenotypes. *Proceedings of the National Academy of Sciences of the United States of America* **106**, 13058-13063
92. Kushima, I., Nakamura, Y., Aleksic, B., Ikeda, M., Ito, Y., Shiino, T., Okochi, T., Fukuo, Y., Ujike, H., Suzuki, M., Inada, T., Hashimoto, R., Takeda, M., Kaibuchi, K., Iwata, N., and Ozaki, N. (2012) Resequencing and association analysis of the KALRN and EPHB1 genes and their contribution to schizophrenia susceptibility. *Schizophrenia bulletin* **38**, 552-560
93. Wang, L., Hauser, E. R., Shah, S. H., Pericak-Vance, M. A., Haynes, C., Crosslin, D., Harris, M., Nelson, S., Hale, A. B., Granger, C. B., Haines, J. L., Jones, C. J., Crossman, D., Seo, D., Gregory, S. G., Kraus, W. E., Goldschmidt-Clermont, P. J., and Vance, J. M. (2007) Peakwide mapping on chromosome 3q13 identifies the kalirin gene as a novel candidate gene for coronary artery disease. *Am J Hum Genet* **80**, 650-663
94. Ma, X. M., Huang, J. P., Xin, X., Yan, Y., Mains, R. E., and Eipper, B. A. (2012) A role for kalirin in the response of rat medium spiny neurons to cocaine. *Mol. Pharmacol.* **82**, 738-745
95. Mains, R. E., Kiraly, D. D., Eipper-Mains, J. E., Ma, X. M., and Eipper, B. A. (2011) Kalrn promoter usage and isoform expression respond to chronic cocaine exposure. *BMC Neurosci* **12**, 20
96. Ma, X. M., Wang, Y., Ferraro, F., Mains, R. E., and Eipper, B. A. (2008) Kalirin-7 is an essential component of both shaft and spine excitatory synapses in hippocampal interneurons. *The Journal of neuroscience : the official journal of the Society for Neuroscience* **28**, 711-724
97. Li, W., Li, Q. J., and An, S. C. (2010) Preventive effect of estrogen on depression-like behavior induced by chronic restraint stress. *Neuroscience bulletin* **26**, 140-146
98. Habets, G. G., Scholtes, E. H., Zuydgeest, D., van der Kammen, R. A., Stam, J. C., Berns, A., and Collard, J. G. (1994) Identification of an invasion-inducing gene, Tiam-1, that encodes a protein with homology to GDP-GTP exchangers for Rho-like proteins. *Cell* **77**, 537-549

99. Michiels, F., Habets, G. G., Stam, J. C., van der Kammen, R. A., and Collard, J. G. (1995) A role for Rac in Tiam1-induced membrane ruffling and invasion. *Nature* **375**, 338-340
100. Ehler, E., van Leeuwen, F., Collard, J. G., and Salinas, P. C. (1997) Expression of Tiam-1 in the developing brain suggests a role for the Tiam-1-Rac signaling pathway in cell migration and neurite outgrowth. *Molecular and cellular neurosciences* **9**, 1-12
101. Tolias, K. F., Bikoff, J. B., Burette, A., Paradis, S., Harrar, D., Tavazoie, S., Weinberg, R. J., and Greenberg, M. E. (2005) The Rac1-GEF Tiam1 couples the NMDA receptor to the activity-dependent development of dendritic arbors and spines. *Neuron* **45**, 525-538
102. Chiu, C. Y., Leng, S., Martin, K. A., Kim, E., Gorman, S., and Duhl, D. M. (1999) Cloning and characterization of T-cell lymphoma invasion and metastasis 2 (TIAM2), a novel guanine nucleotide exchange factor related to TIAM1. *Genomics* **61**, 66-73
103. Malliri, A., van der Kammen, R. A., Clark, K., van der Valk, M., Michiels, F., and Collard, J. G. (2002) Mice deficient in the Rac activator Tiam1 are resistant to Ras-induced skin tumours. *Nature* **417**, 867-871
104. Gerard, A., van der Kammen, R. A., Janssen, H., Ellenbroek, S. I., and Collard, J. G. (2009) The Rac activator Tiam1 controls efficient T-cell trafficking and route of transendothelial migration. *Blood* **113**, 6138-6147
105. Woodcock, S. A., Rushton, H. J., Castaneda-Saucedo, E., Myant, K., White, G. R., Blyth, K., Sansom, O. J., and Malliri, A. (2010) Tiam1-Rac signaling counteracts Eg5 during bipolar spindle assembly to facilitate chromosome congression. *Current biology : CB* **20**, 669-675
106. Yoo, S., Kim, Y., Lee, H., Park, S., and Park, S. (2012) A gene trap knockout of the Tiam-1 protein results in malformation of the early embryonic brain. *Molecules and cells* **34**, 103-108
107. Hoshino, M., Sone, M., Fukata, M., Kuroda, S., Kaibuchi, K., Nabeshima, Y., and Hama, C. (1999) Identification of the stef gene that encodes a novel guanine nucleotide exchange factor specific for Rac1. *The Journal of biological chemistry* **274**, 17837-17844
108. Goto, A., Hoshino, M., Matsuda, M., and Nakamura, T. (2011) Phosphorylation of STEF/Tiam2 by protein kinase A is critical for Rac1 activation and neurite outgrowth in dibutyryl cAMP-treated PC12D cells. *Mol Biol Cell* **22**, 1780-1790
109. Kunda, P., Paglini, G., Quiroga, S., Kosik, K., and Caceres, A. (2001) Evidence for the involvement of Tiam1 in axon formation. *J Neurosci* **21**, 2361-2372
110. Chiou, T. T., Bonhomme, B., Jin, H., Miralles, C. P., Xiao, H., Fu, Z., Harvey, R. J., Harvey, K., Vicini, S., and De Blas, A. L. (2011) Differential regulation of the postsynaptic clustering of gamma-aminobutyric acid type A (GABAA) receptors by collybistin isoforms. *The Journal of biological chemistry* **286**, 22456-22468
111. Zhang, H., and Macara, I. G. (2006) The polarity protein PAR-3 and TIAM1 cooperate in dendritic spine morphogenesis. *Nature cell biology* **8**, 227-237
112. Matsuo, N., Terao, M., Nabeshima, Y., and Hoshino, M. (2003) Roles of STEF/Tiam1, guanine nucleotide exchange factors for Rac1, in regulation of growth cone morphology. *Mol Cell Neurosci* **24**, 69-81
113. Montenegro-Venegas, C., Tortosa, E., Rosso, S., Peretti, D., Bollati, F., Bisbal, M., Jausoro, I., Avila, J., Caceres, A., and Gonzalez-Billault, C. (2010) MAP1B regulates axonal development by modulating Rho-GTPase Rac1 activity. *Molecular biology of the cell* **21**, 3518-3528
114. Terawaki, S., Kitano, K., Mori, T., Zhai, Y., Higuchi, Y., Itoh, N., Watanabe, T., Kaibuchi, K., and Hakoshima, T. (2010) The PHCCEx domain of Tiam1/2 is a novel protein- and membrane-binding module. *The EMBO journal* **29**, 236-250
115. Miyamoto, Y., Yamauchi, J., Tanoue, A., Wu, C., and Mobley, W. C. (2006) TrkB binds and tyrosine-phosphorylates Tiam1, leading to activation of Rac1 and induction of changes in cellular

morphology. *Proceedings of the National Academy of Sciences of the United States of America* **103**, 10444-10449
116. Lai, K. O., Wong, A. S., Cheung, M. C., Xu, P., Liang, Z., Lok, K. C., Xie, H., Palko, M. E., Yung, W. H., Tessarollo, L., Cheung, Z. H., and Ip, N. Y. (2012) TrkB phosphorylation by Cdk5 is required for activity-dependent structural plasticity and spatial memory. *Nat Neurosci* **15**, 1506-1515
117. Abe, H., Okazawa, M., and Nakanishi, S. (2012) Gene regulation via excitation and BDNF is mediated by induction and phosphorylation of the Etv1 transcription factor in cerebellar granule cells. *Proceedings of the National Academy of Sciences of the United States of America* **109**, 8734-8739
118. Mendoza-Naranjo, A., Gonzalez-Billault, C., and Maccioni, R. B. (2007) Abeta1-42 stimulates actin polymerization in hippocampal neurons through Rac1 and Cdc42 Rho GTPases. *Journal of cell science* **120**, 279-288
119. Ma, Q. L., Yang, F., Calon, F., Ubeda, O. J., Hansen, J. E., Weisbart, R. H., Beech, W., Frautschy, S. A., and Cole, G. M. (2008) p21-activated kinase-aberrant activation and translocation in Alzheimer disease pathogenesis. *The Journal of biological chemistry* **283**, 14132-14143
120. Vigil, D., Cherfils, J., Rossman, K. L., and Der, C. J. (2010) Ras superfamily GEFs and GAPs: validated and tractable targets for cancer therapy? *Nat Rev Cancer* **10**, 842-857
121. Welch, H. C., Coadwell, W. J., Ellson, C. D., Ferguson, G. J., Andrews, S. R., Erdjument-Bromage, H., Tempst, P., Hawkins, P. T., and Stephens, L. R. (2002) P-Rex1, a PtdIns(3,4,5)P3- and Gbetagamma-regulated guanine-nucleotide exchange factor for Rac. *Cell* **108**, 809-821
122. Hill, K., Krugmann, S., Andrews, S. R., Coadwell, W. J., Finan, P., Welch, H. C., Hawkins, P. T., and Stephens, L. R. (2005) Regulation of P-Rex1 by phosphatidylinositol (3,4,5)-trisphosphate and Gbetagamma subunits. *The Journal of biological chemistry* **280**, 4166-4173
123. Donald, S., Hill, K., Lecureuil, C., Barnouin, R., Krugmann, S., John Coadwell, W., Andrews, S. R., Walker, S. A., Hawkins, P. T., Stephens, L. R., and Welch, H. C. (2004) P-Rex2, a new guanine-nucleotide exchange factor for Rac. *FEBS letters* **572**, 172-176
124. Donald, S., Humby, T., Fyfe, I., Segonds-Pichon, A., Walker, S. A., Andrews, S. R., Coadwell, W. J., Emson, P., Wilkinson, L. S., and Welch, H. C. (2008) P-Rex2 regulates Purkinje cell dendrite morphology and motor coordination. *Proceedings of the National Academy of Sciences of the United States of America* **105**, 4483-4488
125. Yoshizawa, M., Kawauchi, T., Sone, M., Nishimura, Y. V., Terao, M., Chihama, K., Nabeshima, Y., and Hoshino, M. (2005) Involvement of a Rac activator,P-Rex1, in neurotrophin-derived signaling and neuronal migration. *The Journal of neuroscience : the official journal of the Society for Neuroscience* **25**, 4406-4419
126. Waters, J. E., Astle, M. V., Ooms, L. M., Balamatsias, D., Gurung, R., and Mitchell, C. A. (2008) P-Rex1 - a multidomain protein that regulates neurite differentiation. *Journal of cell science* **121**, 2892-2903
127. Mayeenuddin, L. H., McIntire, W. E., and Garrison, J. C. (2006) Differential sensitivity of P-Rex1 to isoforms of G protein betagamma dimers. *The Journal of biological chemistry* **281**, 1913-1920
128. Hernandez-Negrete, I., Carretero-Ortega, J., Rosenfeldt, H., Hernandez-Garcia, R., Calderon-Salinas, J. V., Reyes-Cruz, G., Gutkind, J. S., and Vazquez-Prado, J. (2007) P-Rex1 links mammalian target of rapamycin signaling to Rac activation and cell migration. *The Journal of biological chemistry* **282**, 23708-23715
129. Urano, D., Nakata, A., Mizuno, N., Tago, K., and Itoh, H. (2008) Domain-domain interaction of P-Rex1 is essential for the activation and inhibition by G protein betagamma subunits and PKA. *Cellular signalling* **20**, 1545-1554
130. Balamatsias, D., Kong, A. M., Waters, J. E., Sriratana, A., Gurung, R., Bailey, C. G., Rasko, J. E., Tiganis, T., Macaulay, S. L., and Mitchell, C. A. (2011) Identification of P-Rex1 as a novel Rac1-

guanine nucleotide exchange factor (GEF) that promotes actin remodeling and GLUT4 protein trafficking in adipocytes. *The Journal of biological chemistry* **286**, 43229-43240
131. Jackson, C., Welch, H. C., and Bellamy, T. C. (2010) Control of cerebellar long-term potentiation by P-Rex-family guanine-nucleotide exchange factors and phosphoinositide 3-kinase. *PloS one* **5**, e11962
132. Welch, H. C., Condliffe, A. M., Milne, L. J., Ferguson, G. J., Hill, K., Webb, L. M., Okkenhaug, K., Coadwell, W. J., Andrews, S. R., Thelen, M., Jones, G. E., Hawkins, P. T., and Stephens, L. R. (2005) P-Rex1 regulates neutrophil function. *Current biology : CB* **15**, 1867-1873
133. Feig, L. A. (2011) Regulation of Neuronal Function by Ras-GRF Exchange Factors. *Genes & cancer* **2**, 306-319
134. Chen, L., Zhang, L. J., Greer, P., Tung, P. S., and Moran, M. F. (1993) A murine CDC25/ras-GRF-related protein implicated in Ras regulation. *Developmental genetics* **14**, 339-346
135. Fernandez-Medarde, A., and Santos, E. (2011) The RasGrf family of mammalian guanine nucleotide exchange factors. *Biochimica et biophysica acta* **1815**, 170-188
136. Farnsworth, C. L., Freshney, N. W., Rosen, L. B., Ghosh, A., Greenberg, M. E., and Feig, L. A. (1995) Calcium activation of Ras mediated by neuronal exchange factor Ras-GRF. *Nature* **376**, 524-527
137. Baouz, S., Jacquet, E., Bernardi, A., and Parmeggiani, A. (1997) The N-terminal moiety of CDC25(Mm), a GDP/GTP exchange factor of Ras proteins, controls the activity of the catalytic domain. Modulation by calmodulin and calpain. *The Journal of biological chemistry* **272**, 6671-6676
138. de Hoog, C. L., Fan, W. T., Goldstein, M. D., Moran, M. F., and Koch, C. A. (2000) Calmodulin-independent coordination of Ras and extracellular signal-regulated kinase activation by Ras-GRF2. *Molecular and cellular biology* **20**, 2727-2733
139. Krapivinsky, G., Krapivinsky, L., Manasian, Y., Ivanov, A., Tyzio, R., Pellegrino, C., Ben-Ari, Y., Clapham, D. E., and Medina, I. (2003) The NMDA receptor is coupled to the ERK pathway by a direct interaction between NR2B and RasGRF1. *Neuron* **40**, 775-784
140. Norum, J. H., Methi, T., Mattingly, R. R., and Levy, F. O. (2005) Endogenous expression and protein kinase A-dependent phosphorylation of the guanine nucleotide exchange factor Ras-GRF1 in human embryonic kidney 293 cells. *The FEBS journal* **272**, 2304-2316
141. Li, S., Tian, X., Hartley, D. M., and Feig, L. A. (2006) Distinct roles for Ras-guanine nucleotide-releasing factor 1 (Ras-GRF1) and Ras-GRF2 in the induction of long-term potentiation and long-term depression. *The Journal of neuroscience : the official journal of the Society for Neuroscience* **26**, 1721-1729
142. Yang, H., Cooley, D., Legakis, J. E., Ge, Q., Andrade, R., and Mattingly, R. R. (2003) Phosphorylation of the Ras-GRF1 exchange factor at Ser916/898 reveals activation of Ras signaling in the cerebral cortex. *The Journal of biological chemistry* **278**, 13278-13285
143. Mattingly, R. R. (1999) Phosphorylation of serine 916 of Ras-GRF1 contributes to the activation of exchange factor activity by muscarinic receptors. *The Journal of biological chemistry* **274**, 37379-37384
144. Mattingly, R. R., and Macara, I. G. (1996) Phosphorylation-dependent activation of the Ras-GRF/CDC25Mm exchange factor by muscarinic receptors and G-protein beta gamma subunits. *Nature* **382**, 268-272
145. Brambilla, R., Gnesutta, N., Minichiello, L., White, G., Roylance, A. J., Herron, C. E., Ramsey, M., Wolfer, D. P., Cestari, V., Rossi-Arnaud, C., Grant, S. G., Chapman, P. F., Lipp, H. P., Sturani, E., and Klein, R. (1997) A role for the Ras signalling pathway in synaptic transmission and long-term memory. *Nature* **390**, 281-286

146. d'Isa, R., Clapcote, S. J., Voikar, V., Wolfer, D. P., Giese, K. P., Brambilla, R., and Fasano, S. (2011) Mice Lacking Ras-GRF1 Show Contextual Fear Conditioning but not Spatial Memory Impairments: Convergent Evidence from Two Independently Generated Mouse Mutant Lines. *Frontiers in behavioral neuroscience* **5**, 78
147. Giese, K. P., Friedman, E., Telliez, J. B., Fedorov, N. B., Wines, M., Feig, L. A., and Silva, A. J. (2001) Hippocampus-dependent learning and memory is impaired in mice lacking the Ras-guanine-nucleotide releasing factor 1 (Ras-GRF1). *Neuropharmacology* **41**, 791-800
148. Fasano, S., D'Antoni, A., Orban, P. C., Valjent, E., Putignano, E., Vara, H., Pizzorusso, T., Giustetto, M., Yoon, B., Soloway, P., Maldonado, R., Caboche, J., and Brambilla, R. (2009) Ras-guanine nucleotide-releasing factor 1 (Ras-GRF1) controls activation of extracellular signal-regulated kinase (ERK) signaling in the striatum and long-term behavioral responses to cocaine. *Biological psychiatry* **66**, 758-768
149. Rubino, T., Vigano, D., Premoli, F., Castiglioni, C., Bianchessi, S., Zippel, R., and Parolaro, D. (2006) Changes in the expression of G protein-coupled receptor kinases and beta-arrestins in mouse brain during cannabinoid tolerance: a role for RAS-ERK cascade. *Molecular neurobiology* **33**, 199-213
150. Fernandez-Medarde, A., Barhoum, R., Riquelme, R., Porteros, A., Nunez, A., de Luis, A., de Las Rivas, J., de la Villa, P., Varela-Nieto, I., and Santos, E. (2009) RasGRF1 disruption causes retinal photoreception defects and associated transcriptomic alterations. *Journal of neurochemistry* **110**, 641-652
151. Fernandez-Medarde, A., Esteban, L. M., Nunez, A., Porteros, A., Tessarollo, L., and Santos, E. (2002) Targeted disruption of Ras-Grf2 shows its dispensability for mouse growth and development. *Molecular and cellular biology* **22**, 2498-2504
152. Tonini, R., Franceschetti, S., Parolaro, D., Sala, M., Mancinelli, E., Tininini, S., Brusetti, R., Sancini, G., Brambilla, R., Martegani, E., Sturani, E., and Zippel, R. (2001) Involvement of CDC25Mm/Ras-GRF1-dependent signaling in the control of neuronal excitability. *Molecular and cellular neurosciences* **18**, 691-701
153. Tian, X., and Feig, L. A. (2006) Age-dependent participation of Ras-GRF proteins in coupling calcium-permeable AMPA glutamate receptors to Ras/Erk signaling in cortical neurons. *The Journal of biological chemistry* **281**, 7578-7582
154. Zhang, G. C., Hoffmann, J., Parelkar, N. K., Liu, X. Y., Mao, L. M., Fibuch, E. E., and Wang, J. Q. (2007) Cocaine increases Ras-guanine nucleotide-releasing factor 1 protein expression in the rat striatum in vivo. *Neuroscience letters* **427**, 117-121
155. Rubino, T., Forlani, G., Vigano, D., Zippel, R., and Parolaro, D. (2005) Ras/ERK signalling in cannabinoid tolerance: from behaviour to cellular aspects. *Journal of neurochemistry* **93**, 984-991
156. Parelkar, N. K., Jiang, Q., Chu, X. P., Guo, M. L., Mao, L. M., and Wang, J. Q. (2009) Amphetamine alters Ras-guanine nucleotide-releasing factor expression in the rat striatum in vivo. *European journal of pharmacology* **619**, 50-56
157. Fasano, S., Bezard, E., D'Antoni, A., Francardo, V., Indrigo, M., Qin, L., Dovero, S., Cerovic, M., Cenci, M. A., and Brambilla, R. (2010) Inhibition of Ras-guanine nucleotide-releasing factor 1 (Ras-GRF1) signaling in the striatum reverts motor symptoms associated with L-dopa-induced dyskinesia. *Proceedings of the National Academy of Sciences of the United States of America* **107**, 21824-21829
158. Kins, S., Betz, H., and Kirsch, J. (2000) Collybistin, a newly identified brain-specific GEF, induces submembrane clustering of gephyrin. *Nature neuroscience* **3**, 22-29
159. Harvey, K., Duguid, I. C., Alldred, M. J., Beatty, S. E., Ward, H., Keep, N. H., Lingenfelter, S. E., Pearce, B. R., Lundgren, J., Owen, M. J., Smart, T. G., Luscher, B., Rees, M. I., and Harvey, R. J.

(2004) The GDP-GTP exchange factor collybistin: an essential determinant of neuronal gephyrin clustering. *The Journal of neuroscience : the official journal of the Society for Neuroscience* **24**, 5816-5826

160. Papadopoulos, T., Korte, M., Eulenburg, V., Kubota, H., Retiounskaia, M., Harvey, R. J., Harvey, K., O'Sullivan, G. A., Laube, B., Hulsmann, S., Geiger, J. R., and Betz, H. (2007) Impaired GABAergic transmission and altered hippocampal synaptic plasticity in collybistin-deficient mice. *The EMBO journal* **26**, 3888-3899
161. Kneussel, M., Engelkamp, D., and Betz, H. (2001) Distribution of transcripts for the brain-specific GDP/GTP exchange factor collybistin in the developing mouse brain. *The European journal of neuroscience* **13**, 487-492
162. Tyagarajan, S. K., Ghosh, H., Harvey, K., and Fritschy, J. M. (2011) Collybistin splice variants differentially interact with gephyrin and Cdc42 to regulate gephyrin clustering at GABAergic synapses. *Journal of cell science* **124**, 2786-2796
163. Jedlicka, P., Papadopoulos, T., Deller, T., Betz, H., and Schwarzacher, S. W. (2009) Increased network excitability and impaired induction of long-term potentiation in the dentate gyrus of collybistin-deficient mice in vivo. *Molecular and cellular neurosciences* **41**, 94-100
164. Krug, T., Manso, H., Gouvela, L., Sobral, J., Xavier, J. M., and Oliveira, S. A. (2010) Kalirin: a novel genetic risk factor for ischemic stroke. *Hum. Genet.* **127**, 513-523
165. Kushima, I., Nakamura, Y., Aleksic, B., Ikeda, M., Ito, Y., Shiino, T., Okochi, T., Fukuo, Y., Ujike, H., Suzuki, M., Inada, T., Hashimoto, R., Takeda, M., Kaibucchi, K., Iwata, N., and Ozaki, N. (2012) Resequencing and association analysis of the KALRN and EPHB1 genes and their contribution to schizophrenia susceptibility. *Schizo.Bull.* **38**, 552-560
166. Lesch, K. P., Timmesfeld, N., Renner, T. J., Halperin, Roser, C., Nguyen, T. T., Craig, D. W., Romanos, J., Heine, M., Meyer, J., Freitag, C., Warnke, A., Romanos, M., Schafer, H., Walita, S., Reif, A., Stephan, D. A., and Jacob, C. (2008) Molecular genetics of adult ADHD: converging evidence from genome-wide association and extended pedigree linkage studies. *J.Neural Tran* **115**, 1573-1585
167. Wang, L., Hauser, E. R., Shah, S. H., Pericak-Vance, M. A., Haynes, C., Crossman, D., Seo, D., Gregory, S. G., Kraus, W. E., Goldschmidt-Clermont, P. J., and Vance, J. M. (2007) Peakwide mapping on chromosome 3q13 identifies the kalirin gene as a novel candidate gene for coronary artery disease. *Am.J.Hum.Genet.* **80**, 650-663
168. Ma, X. M., Huang, J. P., Kim, E. J., Zhu, Q., Kuchel, G. A., Mains, R. E., and Eipper, B. A. (2011) Kalirin-7, an important component of excitatory synapses, is regulated by estradiol in hippocampal neurons. *Hippocampus* **21**, 661-677
169. Cahill, M. E., Jones, K. A., Rafalovich, I., Xie, Z., Barros, C. S., Muller, U., and Penzes, P. (2011) Control of interneuron dendritic growth through NRG1/erbB4-mediated kalirin-7 disinhibition. *Mol. Psychiatry* **doi:10.1038/mp.2011.35**, 1-9
170. Ma, X. M., Huang, J., Wang, Y., Eipper, B. A., and Mains, R. E. (2003) Kalirin, a multifunctional Rho guanine nucleotide exchange factor, is necessary for maintenance of hippocampal pyramidal neuron dendrites and dendritic spines. *J.Neurosci.* **23**, 10593-10603
171. Ma, X. M., Kiraly, D. D., Gaier, E. D., Wang, Kim, E. J., Levine, E. S., Eipper, B. A., and Mains, R. E. (2008) Kalirin-7 is required for synaptic structure and function. *J.Neurosci.* **28**, 12368-12382
172. Penzes, P., Beeser, A., Chernoff, J., Schiller, M. R., Eipper, B. A., Mains, R. E., and Huganir, R. L. (2003) Rapid induction of dendritic spine morphogenesis by trans-synaptic ephrinB-EphB receptor activation of the Rho-GEF kalirin. *Neuron* **37**, 263-274
173. Xie, Z., Photawala, H., Cahill, M. E., Srivastava, D. P., Woolfrey, K. M., Shum, C. Y., Huganir, R. L., and Penzes, P. (2008) Coordination of synaptic adhesion with dendritic spine remodeling by AF-6 and kalirin-7. *J.Neurosci.* **28**, 6079-6091

174. Murray, P. S., Kirkwood, C. M., Gray, M. C. I. M. D., Paljug, W. R., Abrahamson, E. E., Henteleff, R. A., Hamilton, R. L., Kofler, J. K., Klunk, W. E., Lopez, O. L., Penzes, P., and Sweet, R. A. (2012) beta-Amyloid 42/40 ratio and kalirin expression in Alheimer disease with psychosis. *Neurobiol.Aging* **33**, 2807-2816
175. Youn, H., Jeoung, M., Koo, Y., Ji, H., Markesbery, W. R., Ji, I., and Ji, T. H. (2007) Kalirin is under-expressed in Alzheimer's disease hippocampus. *J.Alzheimers Dis.* **11**, 385-397
176. Schiller, M. R., Ferraro, F., Wang, Y., Ma, X. M., McPherson, C. E., Sobota, J. A., Schiller, N. I., Mains, R. E., and Eipper, B. A. (2008) Autonomous functions for the Sec14p/spectrin-repeat region of Kalirin. *Exp.Cell Res.* **314**, 2674-2691
177. Debant, A., Serra-Pages, C., Seipel, K., O'Brien, S., Tang, M., Park, S. H., and Streuli, M. (1996) The multidomain protein Trio binds the LAR transmembrane tyrosine phosphatase, contains a protein kinase domain, and has separate rac-specific and rho-specific guanine nucleotide exchange factor domains. *Proc.Natl.Acad.Sci.U.S.A.* **93**, 5466-5471
178. McPherson, C. E., Eipper, B. A., and Mains, R. E. (2005) Multiple novel isoforms of Trio are expressed in the developing rat brain. *Gene* **347**, 125-135
179. van Rijssel, J., and van Buul, J. D. (2012) The many faces of the guanine-nucleotide exchange factor trio. *Cell Adh.Migr* **6**
180. Ishikawa, K., Toru, S., Tsunemi, T., Li, M., Kobayashi, K., Yokata, T., and others. (2005) An autosomal dominant cerebellar ataxia linked to chromosome 16q22.1 is associated with a single nucleotide substitution in the 5' untranslated region of the gene encoding a protein with spectrin repeat and rho guanine-nucleotide exchange-factor domains. *Am.J.Hum.Genet.* **77**, 280-296
181. Kostenko, E. V., Mahon, G. M., Cheng, L., and Whitehead, I. P. (2005) The Sec14 homology domain regulates the cellular distribution and transforming activity of the Rho-specific guanine nucleotide exchange factor Dbs. *J Biol.Chem.* **280**, 2807-2817
182. Ueda, S., Kataoka, T., and Satoh, T. (2004) Role of the Sec14-like domain of Dbl family exchange factors in the regulation of Rho family GTPases in different subcellular sites. *Cell. Signal.* **16**, 899-906
183. Mousley, C. J., Tyeryar, K. R., Ryan, M. M., and Bankaitis, V. A. (2006) Sec14p-like proteins regulate phosphoinositide homeostasis and intracellular protein and lipid trafficking in yeast. *Biochem. Soc. Trans.* **34**, 346-350
184. Saito, K., Tautz, L., and Mustelin, T. (2007) The lipid-binding SEC14 domain. *Biochim.Biophys.Acta* **1771**, 719-726
185. Schaaf, G., Ortlund, E. A., Tyeryar, K. R., Mously, C. J., Ile, K. E., Garrett, T. A., Ren, J., Woolls, M. J., Raetz, C. R. H., Redinbo, M. R., and Bankaitis, V. A. (2008) Functional anatomy of phospholipid binding and regulation of phosphoinositide homeostasis by proteins of the Sec14 superfamily. *Mol.Cell* **29**, 191-206
186. Vishwanatha, K. S., Wang, Y., Keutmann, H. T., Mains, R. E., and Eipper, B. A. (2012) Structural organization of the nine spectrin repeats of kalirin. *Biochemistry (Mosc).* **51**, 5663-5673
187. Alam, M. R., Caldwell, B. D., Johnson, R. C., Darlington, D. N., Mains, R. E., and Eipper, B. A. (1996) Novel Proteins That Interact with the COOH-terminal Cytosolic Routing Determinants of an Integral Membrane Peptide-processing Enzyme. *J.Biol.Chem.* **271**, 28636-28640
188. Colomer, V., Engelender, S., Sharp, A. H., Duan, K., Cooper, J. K., Lanahan, A., Lyford, G., Worley, P., and Ross, C. A. (1997) Huntingtin-associated protein 1 (HAP1) binds to a Trio-like polypeptide, with a rac1 guanine nucleotide exchange factor domain. *Hum. Mol. Genet.* **6**, 1519-1525
189. Hayashi-Takagi, A., Takaki, M., Graziane, N., Seshadri, S., Murdoch, H., Dunlop, A. J., Makino, Y., Seshadri, A., Ishizuka, K., Srivastava, D. P., Xie, Z., Baraban, J. M., Houslay, M. D., Tomoda, T.,

Brandon, N. J., Kamiya, A., Yan, Z., Penzes, P., and Sawa, A. (2010) Disrupted-in-Schizophrenia 1 (DISC1) regulates spines of the glutamate synapse via Rac1. *Nature Neurosci.* **13**, 327-332

190. Koo, T. H., Eipper, B. A., and Donaldson, J. G. (2007) Arf6 recruits the Rac GEF Kalirin to the plasma membrane facilitating Rac activation. *BMC Cell Biol.* **8**, 29
191. Ratovitski, E. A., Alam, M. R., Quick, R. A., McMilan, A., Bao, C., Kozlovsky, C., Hand, T. A., Johnson, R. C., Mains, R. E., Eipper, B. A., and Lowenstein, C. J. (1999) Kalirin Inhibition of Inducible Nitric-oxide Synthase. *J.Biol.Chem.* **274**, 993-999
192. Giorgi, M., Cianci, C. D., Gallagher, P. G., and Morrow, J. S. (2006) Spectrin Oligomerization is Cooperatively Coupled to Membrane Assembly: A Linkage Targeted by Many Hereditary Hemolytic Anemias? *Exptl Mol Pathology* **70**, 215-230
193. Ipsaro, J. J., and Mondragon, A. (2010) Structural basis for spectrin recognition by ankyrin. *Blood* **115**, 4093-4101
194. Sheetz, M. P., Sable, J. E., and Dobereiner, H. G. (2006) Continuous Membrane-Cytoskeleton Adhesion Requires Continuous Accommodation to Lipid and Cytoskeleton Dynamics. *Annu.Rev.Biophys.Biomol.Struct.* **35**, 417-434
195. Nicolas, G., Fournier, C. M., Galand, C., Malbert-Colas, L., Bournier, O., Kroviarski, Y., Bourgeois, M., Camonis, J. H., Dhermy, D., Grandchamp, B., and Lecomte, M. C. (2002) Tyrosine Phosphorylation Regulates AlphaII Spectrin Cleavage by Calpain. *Mol.Biol.Cell* **22**, 3527-3536
196. Siminovic, M., Zhang, Z., Cianci, C. D., Steitz, T. A., and Morrow, J. S. (2006) Structure of the calmodulin alphaII-spectrin complex provides insight into the regulation of cell plasticity. *J Biol.Chem* **281**, 34333-34340
197. Zadran, S., Jourdi, H., Rostamiani, K., Qin, Q., Bi, X., and Baudry, M. (2009) Brain-Derived Neurotrophic Factor and Epidermal Growth Factor Activate Neuronal m-Calpain via Mitogen-Activated Protein Kinase-Dependent Phosphorylation. *J.Neurosci.* **30**, 1086-1095
198. Nedrelow, J. H., Cianci, C. D., and Morrow, J. S. (2003) c-Src Binds aII Spectrin's Src Homology 3 (SH3) Domain and Blocks Calpain Susceptibility by Phosphorylating Tyr 1176 *J Biol.Chem* **278**, 7735-7741
199. Jones, K. A., Srivastava, D. P., Allen, J. A., Strachan, R. T., Roth, B. L., and Penzes, P. (2009) Rapid modulation of spine morphology by the 5-HT2A serotonin receptor through kalirin-7 signaling. *Proc.Natl.Acad.Sci.U.S.A.* **106**, 19575-19580
200. Wu, J. H., Fanaroff, A. C., Sharma, K. C., Smith, L. S., Brian, L., Eipper, B. A., Mains, R. E., Freedman, N. J., and Zhang, L. (2013) Kalirin promotes neointimal hyperplasia by activating Rac in smooth muscle cells. *Arterioscler. Thromb. Vasc. Biol.* **33**, 702-708
201. Kiraly, D. D., Stone, K. L., Colangelo, C. M., Abbott, T., Wang, Y., Mains, R. E., and Eipper, B. A. (2011) Identification of kalirin-7 as a potential post-synaptic density signaling hub. *J.Proteome Res.* **10**, 2828-2841
202. Bateman, J., Shu, H., and Van Vactor, D. (2000) The Guanine Nucleotide Exchange Factor Trio Mediates Axonal Development in the Drosophila Embryo. *Neuron* **26**, 93-106
203. Liebl, E. C., Forsthoefel, D. J., Franco, L. S., Sample, S. H., Hess, J. E., Cowger, J. A., Chandler, M. P., Shupert, A. J., and Seeger, M. A. (2000) Dosage-Sensitive, Reciprocal Genetic Interactions between the Abl Tyrosine Kinase and the Putative GEF trio Reveal trio's Role in Axon Pathfinding. *Neuron* **26**, 107-118
204. Mains, R. E., Kiraly, D. D., Eipper-Mains, J. E., Ma, X. M., and Eipper, B. A. (2011) Kalrn promoter usage and isoform expression respond to chronic cocaine exposure. *BMC Neurosci* **12**, 1471-2202/1412/1420
205. Mandela, P., Yankova, M., Conti, L. H., Ma, X. M., Grady, J., Eipper, B. A., and Mains, R. E. (2012) Kalrn plays key roles within and outside of the nervous system. *BMC Neurosci* **13**, 136

206. McPherson, C. E., Eipper, B. A., and Mains, R. E. (2002) Genomic organization and differential expression of Kalirin isoforms. *Gene* **284**, 41-50
207. Chen, L. Y., Rex, C. S., Casale, M. S., Gall, C. M., and Lynch, G. (2007) Changes in Synaptic Morphology Accompany Actin Signaling during LTP. *J.Neurosci.* **27**, 5363-5372
208. Hotulainen, P., and Hoogenraad, C. C. (2010) Actin in dendritic spines: connecting dynamics to function. *J.Cell Biol.* **189**, 619-629
209. McMahon, S. A., and Diaz, E. (2011) Mechanisms of excitatory synapse maturation by trans-synaptic organizing complexes. *Curr.Op.Neurobiol.* **21**, 221-227
210. Ma, X. M., Wang, Y., Ferraro, F., Mains, R. E., and Eipper, B. A. (2008) Kalirin-7 Is an Essential Component of both Shaft and Spine Excitatory Synapses in Hippocampal Interneurons. *J.Neurosci.* **28**, 711-724
211. Penzes, P., Johnson, R. C., Sattler, R., Zhang, X., Huganir, R. L., Kambampati, V., Mains, R. E., and Eipper, B. A. (2001) The neuronal Rho-GEF Kalirin-7 interacts with PDZ domain-containing proteins and regulates dendritic morphogenesis. *Neuron* **29**, 229-242
212. McPherson, C. E., Eipper, B. A., and Mains, R. E. (2004) Kalirin Expression Is Regulated by Multiple Promoters. *J. Mol. Neurosci.* **22**, 51-62
213. Aravind, L., Neuwald, A. F., and Ponting, C. P. (1999) Sec14p-like domains in NF1 and Dbl-like proteins indicate lipid regulation of Ras and Rho signaling. *Curr.Biol.* **9**, 195-197
214. Colicelli, J. (2010) ABL Tyrosine Kinases: Evolution of Function, Regulation, and Specificity. *Sci Signaling* **3**, DOI: 10.1126/scisignal.3139re1126
215. Greuber, E. K., Smith-Pearson, P., Wang, J., and Pendergast, A. M. (2013) Role of ABL family kinases in cancer: from leukaemia to solid tumours. *Nature Reviews Cancer* **13**, 559-571
216. Koleske, A. J. (2013) Molecular mechanisms of dendrite stability. *Nature Rev Neurosci* **14**, 536-550
217. Beazely, M. A., Weerapura, M., and MacDonald, J. F. (2008) Abelson tyrosine kinase links PDGFbeta receptor activation to cytoskeletal regulation of NMDA receptors in CA1 hippocampal neurons. *Mol Brain* **1**, doi:10.1186/1756-6606-1181-1120
218. Baudry, M., Chou, M. M., and Bi, X. (2013) Targeting calpain in synaptic plasticity. *Expert Opin.Ther.Targets* **17**, 579-592
219. Chamma, I., Heubl, M., Chevy, Q., Renner, M., Moutkine, I., Eugene, E., Poncer, J. C., and Levi, S. (2013) Activity-Dependent Regulation of the K/Cl Transporter KCC2 Membrane Diffusion, Clustering, and Function in Hippocampal Neurons. *J.Neurosci.* **33**, 15488-15503
220. Wu, H. Y., and Lynch, D. R. (2006) Calpain and Synaptic Function. *Mol. Neurobiol.* **33**, 215-236
221. Penzes, P., Johnson, R. C., Alam, M. R., Kambampati, V., Mains, R. E., and Eipper, B. A. (2000) An Isoform of Kalirin, a Brain-Specific GDP-GTP Exchange Factor, Is Enriched in the Post-synaptic Density Fraction. *J.Biol.Chem.* **275**, 6395-6403
222. Araya, R., Jiang, J., Eisenthal, K. B., and Yuste, R. (2006) The spine neck filters membrane potentials. *Proc.Natl.Acad.Sci.U.S.A.* **103**, 17961-17966
223. Bloodgood, B. L., and Sabatini, B. L. (2005) Neuronal activity regulates diffusion across the neck of dendritic spines. *Science* **310**, 866-869
224. Nestor, M. W., Cai, X., Stone, M. R., Block, R. J., and Thompson, S. M. (2011) The Actin Binding Domain of b1-Spectrin Regulates the Morphological and Functional Dynamics of Dendritic Spines. *PLOS* **6**, e16197
225. Yuste, R. (2013) Electrical compartmentalization in dendritic spines. *Annu. Rev. Neurosci.* **36**, 429-449
226. Gupta, A. B., Wee, L. E., Zhou, Y. T., Hortsch, M., and Low, B. C. (2012) Cross-Species Analyses Identify the B NIP-2 and C dc42GAP H omology (BCH) Domain as a Distinct Functional Subclass of the CRAL_TRIO/Sec14 Superfamily. *PloS one* **7**, e33863

227. Maeda, K., Anand, K., Chiapparino, A., Kumar, A., Poletto, M., Kaksonen, M., and Gavin, A. C. (2013) Interactome map uncovers phosphatidylserine transport by oxysterol-binding proteins. *Nature* **501**, 257-261
228. Abe, N., Inoue, T., Galvez, T., Klein, L., and Meyer, T. (2008) Dissecting the role of PtdIns(4,5)P 2 in endocytosis and recycling of the transferrin receptor. *J Cell Sci.* **121**, 1488-1494
229. Arendt, K. L., Rovo, M., Fernandez-Monreal, M., Knafo, S., Petrok, C. N., Martens, J. R., and Esteban, J. A. (2010) PIP3 controls synaptic function by maintaining AMPA receptor clustering at the postsynaptic membrane. *Nature Neurosci.* **13**, 36-44
230. Cuesto, G., Enriquez-Barreto, L., Carames, C., Cantarero, M., Gasull, X., Sandi, C., Ferrus, A., Acebes, A., and Morales, M. (2011) Phosphoinositide-3-kinase activation controls synaptogenesis and spinogenesis in hippocampal neurons. *J.Neurosci.* **31**, 2721-2733
231. Papa, M., and Segal, M. (1996) Morphological plasticity in dendritic spines of cultured hippocampal neurons. *Neuroscience* **71**, 1005-1011
232. Segal, M. (1995) Morphological alterations in dendritic spines of rat hippocampal neurons exposed to N-methyl-D-aspartate. *Neurosci.Lett.* **193**, 73-76
233. Cheadle, L., and Biederer, T. (2012) The novel synaptogenic protein Farp1 links postsynaptic cytoskeletal dynamics and transsynaptic organization. *J.Cell Biol.* **199**, 985-1001
234. Beique, J. C., Lin, D. T., Kang, M. G., Aizawa, H., Takamiya, K., and Huganir, R. L. (2006) Synapse-specific regulation of AMPA receptor function by PSD-95. *Proc.Natl.Acad.Sci.U.S.A.* **103**, 19535-19540
235. Wyszynski, M., Lin, J., Rao, A., Nigh, E., Beggs, A. H., Craig, A. M., and Sheng, M. (1997) Competitive binding of a-actinin aand calmodulin to the NMDA receptor. *Nature* **385**, 438-442
236. Nakagawa, T., Engler, J. A., and Sheng, M. (2004) The dynamic turnover and functional roles of a-actinin in dendritic spines. *Neuropharm* **47**, 734-745
237. Xie, Y., Vessey, J. P., Konecna, A., Dahm, R., Macchi, P., and Kiebler, M. A. (2007) The GTP-Binding Protein Septin 7 Is Critical for Dendrite Branching and Dendritic-Spine Morphology. *Curr.Biol.* **17**, 1746-1751
238. Brand, F., Schumacher, S., Kant, S., Menon, M. B., Simon, R., Turgeon, B., Britsch, S., Meloche, S., Gaestel, M., and Kotlyarov, A. (2012) The Extracellular Signal-Regulated Kinase 3 (Mitogen-Activated Protein Kinase 6 [MAPK6])-MAPK-Activated Protein Kinase 5 Signaling Complex Regulates Septin Function and Dendrite Morphology. *Mol. Cell. Biol.* **32**, 2467-2478
239. Lin, M. Z., and Greenberg, M. E. (2000) Orchestral Maneuvers in the Axon: Trio and the Control of Axon Guidance. *Cell* **101**, 239-242
240. Perez de Arce, K., Varela-Nallar, L., Farias, O., Cifuentes, A., Bull, P., Couch, B. A., Koleske, A. J., Inestrosa, N. C., and Alvarez, A. R. (2010) Synaptic Clustering of PSD-95 Is Regulated by c-Abl through Tyrosine Phosphorylation. *J.Neurosci.* **30**, 3728-3738
241. Amini, M., Ma, C. l., Farazifard, R., Zhu, G., Zhang, Y., Vanderluit, J., Zoltewica, J. S., Hage, F., Savitt, J. M., Lagace, D. C., Slack, R. S., Beique, J. C., Baudry, M., Greer, P. A., Bergeron, R., and Park, D. S. (2013) Conditional Disruption of Calpain in the CNS Alters Dendrite Morphology, Impairs LTP, and Promotes Neuronal Survival following Injury. *J.Neurosci.* **33**, 5772-5784
242. Lynch, G., Rex, C. S., and Gall, C. M. (2006) LTP consolidation: Substrates, explanatory power, and functional significance. *Neuropharmacology* **52**, 12-23
243. Francone, V. P., Ifrim, M. F., Rajagopal, C., Leddy, C. J., Wang, Y., Carson, J. H., Mains, R. E., and Eipper, B. A. (2010) Signaling from the Secretory Granule to the Nucleus: Uhmk1 and PAM. *Mol.Endo.* **24**, 1543-1558
244. Liu, B., and Krieger, M. (2002) Highly purified scavenger receptor class B, type I reconstituted into phosphtidylcholine/cholesterol liposomes mediates high affinity high density lipoprotein binding and selective lipid uptake. *J.Biol.Chem.* **277**, 34125-34135

245. Sreerama, N., and Woody, R. W. (2003) Structural composition of betaI- and betaII-proteins. *Protein Sci.* **12**, 384-388
246. MacLean, B., Tomazela, D. M., Shulman, N., Chambers, M., Finney, G. L., Frewen, B., Kern, R., Tabb, D. L., Liebler, D. C., and MacCoss, M. J. (2010) Skyline: an open source document editor for creating and analyzing targeted proteomics experiments. *Bioinformatics* **26**, 966-968
247. Penzes, P., Johnson, R. C., Alam, M. R., Kambampati, V., Mains, R. E., and Eipper, B. A. (2000) An isoform of kalirin, a brain-specific GDP/GTP exchange factor, is enriched in the postsynaptic density fraction. *J. Biol. Chem.* **275**, 6395-6403
248. Yan, Y., Eipper, B. A., and Mains, R. E. (2014) Kalirin-9 and Kalirin-12 Play Essential Roles in Dendritic Outgrowth and Branching. *Cereb. Cortex*
249. Huang, S., Eleniste, P. P., Wayakanon, K., Mandela, P., Eipper, B. A., Mains, R. E., Allen, M. R., and Bruzzaniti, A. (2014) The Rho-GEF Kalirin regulates bone mass and the function of osteoblasts and osteoclasts. *Bone* **60**, 235-245
250. Wu, J. H., Fanaroff, A. C., Sharma, K. C., Smith, L. S., Brian, L., Eipper, B. A., Mains, R. E., Freedman, N. J., and Zhang, L. (2013) Kalirin promotes neointimal hyperplasia by activating Rac in smooth muscle cells. *Arterioscler. Thromb. Vasc. Biol.* **33**, 702-708
251. Ma, X. M., Miller, M. B., Vishwanatha, K. S., Gross, M. J., Wang, Y., Abbott, T., Lam, T. T., Mains, R. E., and Eipper, B. A. (2014) Nonenzymatic domains of Kalirin7 contribute to spine morphogenesis through interactions with phosphoinositides and Abl. *Mol. Biol. Cell* **25**, 1458-1471
252. Curwin, A. J., Fairn, G. D., and McMaster, C. R. (2009) Phospholipid transfer protein Sec14 is required for trafficking from endosomes and regulates distinct trans-Golgi export pathways. *J. Biol. Chem.* **284**, 7364-7375
253. Hama, H., Schnieders, E. A., Thorner, J., Takemoto, J. Y., and DeWald, D. B. (1999) Direct involvement of phosphatidylinositol 4-phosphate in secretion in the yeast Saccharomyces cerevisiae. *J. Biol. Chem.* **274**, 34294-34300
254. Schaaf, G., Ortlund, E. A., Tyeryar, K. R., Mousley, C. J., Ile, K. E., Garrett, T. A., Ren, J., Woolls, M. J., Raetz, C. R., Redinbo, M. R., and Bankaitis, V. A. (2008) Functional anatomy of phospholipid binding and regulation of phosphoinositide homeostasis by proteins of the sec14 superfamily. *Mol. Cell* **29**, 191-206
255. Saito, K., Tautz, L., and Mustelin, T. (2007) The lipid-binding SEC14 domain. *Biochim. Biophys. Acta* **1771**, 719-726
256. Kono, N., Ohto, U., Hiramatsu, T., Urabe, M., Uchida, Y., Satow, Y., and Arai, H. (2013) Impaired alpha-TTP-PIPs interaction underlies familial vitamin E deficiency. *Science* **340**, 1106-1110
257. He, X., Lobsiger, J., and Stocker, A. (2009) Bothnia dystrophy is caused by domino-like rearrangements in cellular retinaldehyde-binding protein mutant R234W. *Proc. Natl. Acad. Sci. U. S. A.* **106**, 18545-18550
258. Nile, A. H., Bankaitis, V. A., and Grabon, A. (2010) Mammalian diseases of phosphatidylinositol transfer proteins and their homologs. *Clin Lipidol* **5**, 867-897
259. Sirokmany, G., Szidonya, L., Kaldi, K., Gaborik, Z., Ligeti, E., and Geiszt, M. (2006) Sec14 homology domain targets p50RhoGAP to endosomes and provides a link between Rab and Rho GTPases. *J. Biol. Chem.* **281**, 6096-6105
260. Ueda, S., Kataoka, T., and Satoh, T. (2004) Role of the Sec14-like domain of Dbl family exchange factors in the regulation of Rho family GTPases in different subcellular sites. *Cell. Signal.* **16**, 899-906
261. Sha, B., Phillips, S. E., Bankaitis, V. A., and Luo, M. (1998) Crystal structure of the Saccharomyces cerevisiae phosphatidylinositol-transfer protein. *Nature* **391**, 506-510

262. D'Angelo, I., Welti, S., Bonneau, F., and Scheffzek, K. (2006) A novel bipartite phospholipid-binding module in the neurofibromatosis type 1 protein. *EMBO Rep* **7**, 174-179
263. Gupta, A. B., Wee, L. E., Zhou, Y. T., Hortsch, M., and Low, B. C. (2012) Cross-species analyses identify the BNIP-2 and Cdc42GAP homology (BCH) domain as a distinct functional subclass of the CRAL_TRIO/Sec14 superfamily. *PloS one* **7**, e33863
264. Vishwanatha, K. S., Wang, Y. P., Keutmann, H. T., Mains, R. E., and Eipper, B. A. (2012) Structural organization of the nine spectrin repeats of Kalirin. *Biochemistry (Mosc).* **51**, 5663-5673
265. Spijker, S., Smit, A. B., Eipper, B. A., Malik, A., Mains, R. E., and Geraerts, W. P. (1999) A molluscan peptide alpha-amidating enzyme precursor that generates five distinct enzymes. *FASEB J.* **13**, 735-748
266. Manneville, J. B., Leduc, C., Sorre, B., and Drin, G. (2012) Studying in vitro membrane curvature recognition by proteins and its role in vesicular trafficking. *Methods Cell Biol.* **108**, 47-71
267. Steveson, T. C., Zhao, G. C., Keutmann, H. T., Mains, R. E., and Eipper, B. A. (2001) Access of a membrane protein to secretory granules is facilitated by phosphorylation. *J. Biol. Chem.* **276**, 40326-40337
268. Sobota, J. A., Ferraro, F., Back, N., Eipper, B. A., and Mains, R. E. (2006) Not all secretory granules are created equal: Partitioning of soluble content proteins. *Mol. Biol. Cell* **17**, 5038-5052
269. Milgram, S. L., Kho, S. T., Martin, G. V., Mains, R. E., and Eipper, B. A. (1997) Localization of integral membrane peptidylglycine alpha-amidating monooxygenase in neuroendocrine cells. *J. Cell Sci.* **110 (Pt 6)**, 695-706
270. Bonnemaison, M., Back, N., Lin, Y., Bonifacino, J. S., Mains, R., and Eipper, B. (2014) AP-1A controls secretory granule biogenesis and trafficking of membrane secretory granule proteins. *Traffic* **15**, 1099-1121
271. Zhou, A., Paquet, L., and Mains, R. E. (1995) Structural elements that direct specific processing of different mammalian subtilisin-like prohormone convertases. *J. Biol. Chem.* **270**, 21509-21516
272. Wenk, M. R., and De Camilli, P. (2004) Protein-lipid interactions and phosphoinositide metabolism in membrane traffic: insights from vesicle recycling in nerve terminals. *Proc. Natl. Acad. Sci. U. S. A.* **101**, 8262-8269
273. Di Paolo, G., and De Camilli, P. (2006) Phosphoinositides in cell regulation and membrane dynamics. *Nature* **443**, 651-657
274. Back, N., Rajagopal, C., Mains, R. E., and Eipper, B. A. (2010) Secretory granule membrane protein recycles through multivesicular bodies. *Traffic* **11**, 972-986
275. van Meer, G., Voelker, D. R., and Feigenson, G. W. (2008) Membrane lipids: where they are and how they behave. *Nat Rev Mol Cell Biol* **9**, 112-124
276. Orci, L., Montesano, R., Meda, P., Malaisse-Lagae, F., Brown, D., Perrelet, A., and Vassalli, P. (1981) Heterogeneous distribution of filipin--cholesterol complexes across the cisternae of the Golgi apparatus. *Proc. Natl. Acad. Sci. U. S. A.* **78**, 293-297
277. Wang, Y. J., Wang, J., Sun, H. Q., Martinez, M., Sun, Y. X., Macia, E., Kirchhausen, T., Albanesi, J. P., Roth, M. G., and Yin, H. L. (2003) Phosphatidylinositol 4 phosphate regulates targeting of clathrin adaptor AP-1 complexes to the Golgi. *Cell* **114**, 299-310
278. Milgram, S. L., and Mains, R. E. (1994) Differential effects of temperature blockade on the proteolytic processing of three secretory granule-associated proteins. *J. Cell Sci.* **107 (Pt 3)**, 737-745
279. Antonny, B., Beraud-Dufour, S., Chardin, P., and Chabre, M. (1997) N-terminal hydrophobic residues of the G-protein ADP-ribosylation factor-1 insert into membrane phospholipids upon GDP to GTP exchange. *Biochemistry (Mosc).* **36**, 4675-4684

280. Vanni, S., Vamparys, L., Gautier, R., Drin, G., Etchebest, C., Fuchs, P. F., and Antonny, B. (2013) Amphipathic lipid packing sensor motifs: probing bilayer defects with hydrophobic residues. *Biophys. J.* **104**, 575-584
281. Drin, G., and Antonny, B. (2010) Amphipathic helices and membrane curvature. *FEBS Lett.* **584**, 1840-1847
282. Martin, T. F. (2014) PI(4,5)P-binding effector proteins for vesicle exocytosis. *Biochim. Biophys. Acta*
283. Niu, Y., Zhang, C., Sun, Z., Hong, Z., Li, K., Sun, D., Yang, Y., Tian, C., Gong, W., and Liu, J. J. (2013) PtdIns(4)P regulates retromer-motor interaction to facilitate dynein-cargo dissociation at the trans-Golgi network. *Nat Cell Biol* **15**, 417-429
284. Cunningham, C. C., Vegners, R., Bucki, R., Funaki, M., Korde, N., Hartwig, J. H., Stossel, T. P., and Janmey, P. A. (2001) Cell permeant polyphosphoinositide-binding peptides that block cell motility and actin assembly. *J. Biol. Chem.* **276**, 43390-43399
285. Eberhard, D. A., Cooper, C. L., Low, M. G., and Holz, R. W. (1990) Evidence that the inositol phospholipids are necessary for exocytosis. Loss of inositol phospholipids and inhibition of secretion in permeabilized cells caused by a bacterial phospholipase C and removal of ATP. *Biochem. J.* **268**, 15-25
286. Hay, J. C., Fisette, P. L., Jenkins, G. H., Fukami, K., Takenawa, T., Anderson, R. A., and Martin, T. F. (1995) ATP-dependent inositide phosphorylation required for Ca(2+)-activated secretion. *Nature* **374**, 173-177
287. Milosevic, I., Sorensen, J. B., Lang, T., Krauss, M., Nagy, G., Haucke, V., Jahn, R., and Neher, E. (2005) Plasmalemmal phosphatidylinositol-4,5-bisphosphate level regulates the releasable vesicle pool size in chromaffin cells. *J. Neurosci.* **25**, 2557-2565
288. Gong, L. W., Di Paolo, G., Diaz, E., Cestra, G., Diaz, M. E., Lindau, M., De Camilli, P., and Toomre, D. (2005) Phosphatidylinositol phosphate kinase type I gamma regulates dynamics of large dense-core vesicle fusion. *Proc. Natl. Acad. Sci. U. S. A.* **102**, 5204-5209
289. Di Paolo, G., Moskowitz, H. S., Gipson, K., Wenk, M. R., Voronov, S., Obayashi, M., Flavell, R., Fitzsimonds, R. M., Ryan, T. A., and De Camilli, P. (2004) Impaired PtdIns(4,5)P2 synthesis in nerve terminals produces defects in synaptic vesicle trafficking. *Nature* **431**, 415-422
290. Hille, B., Dickson, E. J., Kruse, M., Vivas, O., and Suh, B. C. (2014) Phosphoinositides regulate ion channels. *Biochim. Biophys. Acta*
291. Prosser, D. C., Tran, D., Schooley, A., Wendland, B., and Ngsee, J. K. (2010) A novel, retromer-independent role for sorting nexins 1 and 2 in RhoG-dependent membrane remodeling. *Traffic* **11**, 1347-1362
292. Collins, M. O., Husi, H., Yu, L., Brandon, J. M., Anderson, C. N., Blackstock, W. P., Choudhary, J. S., and Grant, S. G. (2006) Molecular characterization and comparison of the components and multiprotein complexes in the postsynaptic proteome. *J. Neurochem.* **97 Suppl 1**, 16-23
293. Peng, J., Kim, M. J., Cheng, D., Duong, D. M., Gygi, S. P., and Sheng, M. (2004) Semiquantitative proteomic analysis of rat forebrain postsynaptic density fractions by mass spectrometry. *J. Biol. Chem.* **279**, 21003-21011
294. Kiraly, D. D., Nemirovsky, N. E., LaRese, T. P., Tomek, S. E., Yahn, S. L., Olive, M. F., Eipper, B. A., and Mains, R. E. (2013) Constitutive knockout of kalirin-7 leads to increased rates of cocaine self-administration. *Mol. Pharmacol.* **84**, 582-590
295. Mandela, P., Yan, Y., LaRese, T., Eipper, B. A., and Mains, R. E. (2014) Elimination of Kalrn expression in POMC cells reduces anxiety-like behavior and contextual fear learning. *Horm. Behav.* **66**, 430-438

296. Johnson, R. C., Penzes, P., Eipper, B. A., and Mains, R. E. (2000) Isoforms of kalirin, a neuronal Dbl family member, generated through use of different 5'- and 3'-ends along with an internal translational initiation site. *J. Biol. Chem.* **275**, 19324-19333
297. Borjigin, J., and Nathans, J. (1994) Insertional mutagenesis as a probe of rhodopsin's topography, stability, and activity. *J. Biol. Chem.* **269**, 14715-14722
298. Das, S., Yin, T., Yang, Q., Zhang, J., Wu, Y. I., and Yu, J. (2015) Single-molecule tracking of small GTPase Rac1 uncovers spatial regulation of membrane translocation and mechanism for polarized signaling. *Proc. Natl. Acad. Sci. U. S. A.* **112**, E267-276
299. Gaier, E. D., Miller, M. B., Ralle, M., Aryal, D., Wetsel, W. C., Mains, R. E., and Eipper, B. A. (2013) Peptidylglycine alpha-amidating monooxygenase heterozygosity alters brain copper handling with region specificity. *J. Neurochem.* **127**, 605-619
300. Francone, V. P., Ifrim, M. F., Rajagopal, C., Leddy, C. J., Wang, Y., Carson, J. H., Mains, R. E., and Eipper, B. A. (2010) Signaling from the secretory granule to the nucleus: Uhmk1 and PAM. *Mol. Endocrinol.* **24**, 1543-1558
301. Boudreau, A. C., and Wolf, M. E. (2005) Behavioral sensitization to cocaine is associated with increased AMPA receptor surface expression in the nucleus accumbens. *J. Neurosci.* **25**, 9144-9151
302. Landry, J. R., Mager, D. L., and Wilhelm, B. T. (2003) Complex controls: the role of alternative promoters in mammalian genomes. *Trends Genet.* **19**, 640-648
303. Shabalina, S. A., Ogurtsov, A. Y., Spiridonov, N. A., and Koonin, E. V. (2014) Evolution at protein ends: major contribution of alternative transcription initiation and termination to the transcriptome and proteome diversity in mammals. *Nucleic Acids Res* **42**, 7132-7144
304. Kimura, K., Wakamatsu, A., Suzuki, Y., Ota, T., Nishikawa, T., Yamashita, R., Yamamoto, J., Sekine, M., Tsuritani, K., Wakaguri, H., Ishii, S., Sugiyama, T., Saito, K., Isono, Y., Irie, R., Kushida, N., Yoneyama, T., Otsuka, R., Kanda, K., Yokoi, T., Kondo, H., Wagatsuma, M., Murakawa, K., Ishida, S., Ishibashi, T., Takahashi-Fujii, A., Tanase, T., Nagai, K., Kikuchi, H., Nakai, K., Isogai, T., and Sugano, S. (2006) Diversification of transcriptional modulation: large-scale identification and characterization of putative alternative promoters of human genes. *Genome Res.* **16**, 55-65
305. Davuluri, R. V., Suzuki, Y., Sugano, S., Plass, C., and Huang, T. H. (2008) The functional consequences of alternative promoter use in mammalian genomes. *Trends Genet.* **24**, 167-177
306. Baek, D., Davis, C., Ewing, B., Gordon, D., and Green, P. (2007) Characterization and predictive discovery of evolutionarily conserved mammalian alternative promoters. *Genome Res.* **17**, 145-155
307. Tasic, B., Nabholz, C. E., Baldwin, K. K., Kim, Y., Rueckert, E. H., Ribich, S. A., Cramer, P., Wu, Q., Axel, R., and Maniatis, T. (2002) Promoter choice determines splice site selection in protocadherin alpha and gamma pre-mRNA splicing. *Mol. Cell* **10**, 21-33
308. Liu, S. (2010) Increasing alternative promoter repertories is positively associated with differential expression and disease susceptibility. *PloS one* **5**, e9482
309. Timmusk, T., Palm, K., Metsis, M., Reintam, T., Paalme, V., Saarma, M., and Persson, H. (1993) Multiple promoters direct tissue-specific expression of the rat BDNF gene. *Neuron* **10**, 475-489
310. Parsons, M. J., D'Souza, U. M., Arranz, M. J., Kerwin, R. W., and Makoff, A. J. (2004) The -1438A/G polymorphism in the 5-hydroxytryptamine type 2A receptor gene affects promoter activity. *Biol. Psychiatry* **56**, 406-410
311. Boroumand, M., Ziaee, S., Zarghami, N., Anvari, M. S., Cheraghi, S., Abbasi, S. H., Jalali, A., and Pourgholi, L. (2014) The Kalirin Gene rs9289231 Polymorphism as a Novel Predisposing Marker for Coronary Artery Disease. *Laboratory medicine* **45**, 302-306
312. Horne, B. D., Hauser, E. R., Wang, L., Muhlestein, J. B., Anderson, J. L., Carlquist, J. F., Shah, S. H., and Kraus, W. E. (2009) Validation study of genetic associations with coronary artery disease on

chromosome 3q13-21 and potential effect modification by smoking. *Ann. Hum. Genet.* **73**, 551-558
313. Nicholson, D. A., Cahill, M. E., Tulisiak, C. T., Geinisman, Y., and Penzes, P. (2012) Spatially restricted actin-regulatory signaling contributes to synapse morphology. *J. Neurochem.* **121**, 852-860
314. Frost, N. A., Shroff, H., Kong, H., Betzig, E., and Blanpied, T. A. (2010) Single-molecule discrimination of discrete perisynaptic and distributed sites of actin filament assembly within dendritic spines. *Neuron* **67**, 86-99
315. Honkura, N., Matsuzaki, M., Noguchi, J., Ellis-Davies, G. C., and Kasai, H. (2008) The subspine organization of actin fibers regulates the structure and plasticity of dendritic spines. *Neuron* **57**, 719-729
316. Park, M., Penick, E. C., Edwards, J. G., Kauer, J. A., and Ehlers, M. D. (2004) Recycling endosomes supply AMPA receptors for LTP. *Science* **305**, 1972-1975
317. Arendt, K. L., Benoist, M., Lario, A., Draffin, J. E., Munoz, M., and Esteban, J. A. (2014) PTEN counteracts PIP3 upregulation in spines during NMDA-receptor-dependent long-term depression. *J. Cell Sci.* **127**, 5253-5260
318. Arendt, K. L., Royo, M., Fernandez-Monreal, M., Knafo, S., Petrok, C. N., Martens, J. R., and Esteban, J. A. (2010) PIP3 controls synaptic function by maintaining AMPA receptor clustering at the postsynaptic membrane. *Nat. Neurosci.* **13**, 36-44
319. Gong, L. W., and De Camilli, P. (2008) Regulation of postsynaptic AMPA responses by synaptojanin 1. *Proc. Natl. Acad. Sci. U. S. A.* **105**, 17561-17566
320. Murphy, E. J., Schapiro, M. B., Rapoport, S. I., and Shetty, H. U. (2000) Phospholipid composition and levels are altered in Down syndrome brain. *Brain Res.* **867**, 9-18
321. Gupta, A. R., Pirruccello, M., Cheng, F., Kang, H. J., Fernandez, T. V., Baskin, J. M., Choi, M., Liu, L., Ercan-Sencicek, A. G., Murdoch, J. D., Klei, L., Neale, B. M., Franjic, D., Daly, M. J., Lifton, R. P., De Camilli, P., Zhao, H., Sestan, N., and State, M. W. (2014) Rare deleterious mutations of the gene EFR3A in autism spectrum disorders. *Molecular autism* **5**, 31
322. Voronov, S. V., Frere, S. G., Giovedi, S., Pollina, E. A., Borel, C., Zhang, H., Schmidt, C., Akeson, E. C., Wenk, M. R., Cimasoni, L., Arancio, O., Davisson, M. T., Antonarakis, S. E., Gardiner, K., De Camilli, P., and Di Paolo, G. (2008) Synaptojanin 1-linked phosphoinositide dyshomeostasis and cognitive deficits in mouse models of Down's syndrome. *Proc. Natl. Acad. Sci. U. S. A.* **105**, 9415-9420
323. Koob, G. F., and Volkow, N. D. (2010) Neurocircuitry of addiction. *Neuropsychopharmacology* **35**, 217-238
324. Wolf, M. E. (1998) The role of excitatory amino acids in behavioral sensitization to psychomotor stimulants. *Prog. Neurobiol.* **54**, 679-720
325. Kalivas, P. W. (2009) The glutamate homeostasis hypothesis of addiction. *Nature reviews. Neuroscience* **10**, 561-572
326. van Huijstee, A. N., and Mansvelder, H. D. (2014) Glutamatergic synaptic plasticity in the mesocorticolimbic system in addiction. *Frontiers in cellular neuroscience* **8**, 466
327. Gipson, C. D., Kupchik, Y. M., and Kalivas, P. W. (2014) Rapid, transient synaptic plasticity in addiction. *Neuropharmacology* **76 Pt B**, 276-286
328. Nestler, E. J. (2013) Cellular basis of memory for addiction. *Dialogues in clinical neuroscience* **15**, 431-443
329. MacLean, B., Tomazela, D. M., Shulman, N., Chambers, M., Finney, G. L., Frewen, B., Kern, R., Tabb, D. L., Liebler, D. C., and MacCoss, M. J. (2010) Skyline: an open source document editor for creating and analyzing targeted proteomics experiments. *Bioinformatics* **26**, 966-968

330. Baucum, A. J., Shonesy, B. C., Rose, K. L., and Colbran, R. J. (2015) Quantitative proteomics analysis of CaMKII phosphorylation and the CaMKII interactome in the mouse forebrain. *ACS chemical neuroscience*
331. Liao, L., Sando, R. C., Farnum, J. B., Vanderklish, P. W., Maximov, A., and Yates, J. R. (2012) 15N-labeled brain enables quantification of proteome and phosphoproteome in cultured primary neurons. *Journal of proteome research* **11**, 1341-1353
332. Gnad, F., Ren, S., Cox, J., Olsen, J. V., Macek, B., Oroshi, M., and Mann, M. (2007) PHOSIDA (phosphorylation site database): management, structural and evolutionary investigation, and prediction of phosphosites. *Genome biology* **8**, R250
333. Yu, P., Pisitkun, T., Wang, G., Wang, R., Katagiri, Y., Gucek, M., Knepper, M. A., and Geller, H. M. (2013) Global analysis of neuronal phosphoproteome regulation by chondroitin sulfate proteoglycans. *PloS one* **8**, e59285
334. Wang, J., Ren, J., Wu, B., Feng, S., Cai, G., Tuluc, F., Peranen, J., and Guo, W. (2015) Activation of Rab8 guanine nucleotide exchange factor Rabin8 by ERK1/2 in response to EGF signaling. *Proc. Natl. Acad. Sci. U. S. A.* **112**, 148-153
335. Sato, K., Sugiyama, T., Nagase, T., Kitade, Y., and Ueda, H. (2014) Threonine 680 phosphorylation of FLJ00018/PLEKHG2, a Rho family-specific guanine nucleotide exchange factor, by epidermal growth factor receptor signaling regulates cell morphology of Neuro-2a cells. *J. Biol. Chem.* **289**, 10045-10056
336. Llavero, F., Urzelai, B., Osinalde, N., Galvez, P., Lacerda, H. M., Parada, L. A., and Zugaza, J. L. (2015) Guanine nucleotide exchange factor alphaPIX leads to activation of the Rac 1 GTPase/Glycogen phosphorylase pathway in Interleukin (IL)-2-stimulated T cells. *J. Biol. Chem.*
337. Gupta, M., Qi, X., Thakur, V., and Manor, D. (2014) Tyrosine phosphorylation of Dbl regulates GTPase signaling. *J. Biol. Chem.* **289**, 17195-17202
338. Wang, F., Blanchard, A. P., Elisma, F., Granger, M., Xu, H., Bennett, S. A., Figeys, D., and Zou, H. (2013) Phosphoproteome analysis of an early onset mouse model (TgCRND8) of Alzheimer's disease reveals temporal changes in neuronal and glia signaling pathways. *Proteomics* **13**, 1292-1305
339. Siddoway, B., Hou, H., Yang, H., Petralia, R., and Xia, H. (2014) Synaptic activity bidirectionally regulates a novel sequence-specific S-Q phosphoproteome in neurons. *J. Neurochem.* **128**, 841-851
340. Koo, T. H., Eipper, B. A., and Donaldson, J. G. (2007) Arf6 recruits the Rac GEF Kalirin to the plasma membrane facilitating Rac activation. *BMC cell biology* **8**, 29
341. Ratovitski, E. A., Alam, M. R., Quick, R. A., McMillan, A., Bao, C., Kozlovsky, C., Hand, T. A., Johnson, R. C., Mains, R. E., Eipper, B. A., and Lowenstein, C. J. (1999) Kalirin inhibition of inducible nitric-oxide synthase. *J. Biol. Chem.* **274**, 993-999
342. Jian, D., Aili, Z., Xiaojia, B., Huansheng, Z., and Yun, H. (2010) Feedback regulation of Ras2 guanine nucleotide exchange factor (Ras2-GEF) activity of Cdc25p by Cdc25p phosphorylation in the yeast Saccharomyces cerevisiae. *FEBS Lett.* **584**, 4745-4750
343. Cheng, D., Hoogenraad, C. C., Rush, J., Ramm, E., Schlager, M. A., Duong, D. M., Xu, P., Wijayawardana, S. R., Hanfelt, J., Nakagawa, T., Sheng, M., and Peng, J. (2006) Relative and absolute quantification of postsynaptic density proteome isolated from rat forebrain and cerebellum. *Molecular & cellular proteomics : MCP* **5**, 1158-1170
344. Husi, H., Ward, M. A., Choudhary, J. S., Blackstock, W. P., and Grant, S. G. (2000) Proteomic analysis of NMDA receptor-adhesion protein signaling complexes. *Nat. Neurosci.* **3**, 661-669
345. Sacco, F., Perfetto, L., Castagnoli, L., and Cesareni, G. (2012) The human phosphatase interactome: An intricate family portrait. *FEBS Lett.* **586**, 2732-2739

346. Peng, H. Y., Chen, G. D., Lai, C. Y., Hsieh, M. C., and Lin, T. B. (2013) Spinal serum-inducible and glucocorticoid-inducible kinase 1 mediates neuropathic pain via kalirin and downstream PSD-95-dependent NR2B phosphorylation in rats. *J. Neurosci.* **33**, 5227-5240
347. Brand, F., Schumacher, S., Kant, S., Menon, M. B., Simon, R., Turgeon, B., Britsch, S., Meloche, S., Gaestel, M., and Kotlyarov, A. (2012) The extracellular signal-regulated kinase 3 (mitogen-activated protein kinase 6 [MAPK6])-MAPK-activated protein kinase 5 signaling complex regulates septin function and dendrite morphology. *Mol. Cell. Biol.* **32**, 2467-2478
348. Xue, Y., Liu, Z., Cao, J., Ma, Q., Gao, X., Wang, Q., Jin, C., Zhou, Y., Wen, L., and Ren, J. (2011) GPS 2.1: enhanced prediction of kinase-specific phosphorylation sites with an algorithm of motif length selection. *Protein engineering, design & selection : PEDS* **24**, 255-260
349. Lee, A. M., and Messing, R. O. (2008) Protein kinases and addiction. *Ann. N. Y. Acad. Sci.* **1141**, 22-57
350. Gourley, S. L., Olevska, A., Warren, M. S., Taylor, J. R., and Koleske, A. J. (2012) Arg kinase regulates prefrontal dendritic spine refinement and cocaine-induced plasticity. *J. Neurosci.* **32**, 2314-2323
351. Xie, X., Arguello, A. A., Wells, A. M., Reittinger, A. M., and Fuchs, R. A. (2013) Role of a hippocampal SRC-family kinase-mediated glutamatergic mechanism in drug context-induced cocaine seeking. *Neuropsychopharmacology* **38**, 2657-2665
352. Otis, J. M., Fitzgerald, M. K., and Mueller, D. (2014) Infralimbic BDNF/TrkB enhancement of GluN2B currents facilitates extinction of a cocaine-conditioned place preference. *J. Neurosci.* **34**, 6057-6064
353. Eipper-Mains, J. E., Kiraly, D. D., Duff, M. O., Horowitz, M. J., McManus, C. J., Eipper, B. A., Graveley, B. R., and Mains, R. E. (2013) Effects of cocaine and withdrawal on the mouse nucleus accumbens transcriptome. *Genes, brain, and behavior* **12**, 21-33
354. Vogel, C., Bashton, M., Kerrison, N. D., Chothia, C., and Teichmann, S. A. (2004) Structure, function and evolution of multidomain proteins. *Curr. Opin. Struct. Biol.* **14**, 208-216
355. Stalder, D., and Antonny, B. (2013) Arf GTPase regulation through cascade mechanisms and positive feedback loops. *FEBS Lett.* **587**, 2028-2035
356. Bertagnolo, V., Brugnoli, F., Grassilli, S., Nika, E., and Capitani, S. (2012) Vav1 in differentiation of tumoral promyelocytes. *Cell. Signal.* **24**, 612-620